Universidade de Aveiro Departamento de Geociências
2011

Sérgio Carreiras Esperancinha

Embasamento Fracturado da Bacia de SEAL – Desafiando o Paradigma de Exploração

SEAL Basin Fractured Basement – Challenging the Exploration Paradigm

Universidade de Aveiro Departamento de Geociências
2011

Sérgio Carreiras Esperancinha

Embasamento Fracturado da Bacia de SEAL – Desafiando o Paradigma de Exploração

SEAL Basin Fractured Basement – Challenging the Exploration Paradigm

Dissertação apresentada à Universidade de Aveiro para cumprimento dos requisitos necessários à obtenção do grau de Mestre em Geomateriais e Recursos Geológicos, realizada sob a orientação científica do Doutor Duncan Alistair Lockhart, Geólogo Chefe da Galp Exploração e Produção, S.A. e do Prof. Doutor Luís Menezes Pinheiro, Professor Associado do Departamento de Geociências da Universidade de Aveiro. Esta tese foi realizada no âmbito de um projecto de colaboração entre a Galp Exploração e Produção S.A. e o Departamento de Geociências da Universidade de Aveiro.

This thesis was presented to University of Aveiro as part of the requirement for obtaining the degree in the Master of Science (Geo-materials and Geological Resources. It was tutored by Doctor Duncan Alistair Lockhart, Chief Geologist of Galp Exploration & Production, S.A. and Doctor Luís Menezes Pinheiro, Associated Professor of the Geosciences Department, University of Aveiro. This thesis was elaborated as part of a cooperation project between Galp Exploration and Production, S.A. and the Geosciences Department of University of Aveiro.

Agradecimentos

Esta tese é o culminar de uma etapa que se iniciou quando em Agosto de 2006 embarquei rumo a Aracajú, a capital do Estado de Sergipe na Bacia de Sergipe-Alagoas. Nessa altura não poderia imaginar o quão importante aquele momento seria para os anos seguintes – talvez porque nunca antes tivesse ouvido falar de Aracajú ou da Bacia de Sergipe-Alagoas. No entanto esse momento foi decisivo e o Brasil, em particular a Bacia de Sergipe-Alagoas, fizeram parte da minha vida diária nos anos que se seguiram. Durante este tempo várias pessoas contribuíram directa ou indirectamente para esta conquista. Tentando não esquecer ninguém, os meus agradecimentos:

Ao meu orientador, Duncan Lockhart sem o qual esta tese concerteza não seria a mesma. Não há palavras que descrevam a minha gratidão por me ter ensinado, corrigido e guiado ao longo deste tempo. Melhor era impossível. Muito obrigado!

Ao meu orientador, Prof. Luís Menezes Pinheiro por todas as ideias que apresentou para o enriquecimento deste trabalho, pela disponibilidade, e pela enorme paciência em ler e reler todo o trabalho. A sua ajuda foi crucial para levar este projecto a bom porto.

Ao *Exploration Manager* da GALP Exploração, Roland Muggli, por ter depositado em mim a sua confiança e me ter apoiado em todos os momentos.

Aos colegas da UNL, U. Aveiro e UALG (Filipa, Leonardo, Hugo, Prof. José António Almeida, Prof. Carlos Kullberg, Prof. Conceição Neves), cujo trabalho foi a base desta tese.

Ao Dr. Rui Baptista por me ter dado a oportunidade de entrar para o desafiante mundo que é a indústria petrolífera e para a GALP Energia, quando em 2006 me convenceu a aceitar a bolsa de estudo, que me levou até Sergipe.

Ao João Afonso. O *wingman*, o irmão ("vocês são irmãos?"), que embarcou comigo nesta aventura brasileira e que me entende como muito poucos, mesmo em silêncio e à distância.

À Carolina por existir perto de mim e ser o fiel da balança.

Aos colegas da GALP Exploração & Produção com quem todos os dias partilho o espaço e que são, sem dúvida, uma espectacular equipa de trabalho. Não nomeio ninguém em particular pois todos contribuíram para que esta tese visse a luz do dia.

A todos na Petrogal Brasil, em particular ao Carlão, ao Manuel Peres, ao Torres, ao Cohen, ao Flávio e ao Allyson com quem passei muitas horas e muitos dias na DF-02 e 06 e sempre me fizeram sentir como parte da equipa, ensinando-me quase tudo o que hoje sei sobre geologia/engenharia de sonda e tantas outras coisas que me fizeram crescer. Ao Kléber, ao Alcimar e à Dulce Cid.

Ao João Antunes e à Vera Lourenço. A comida, o calor, o pó e a lama, as mutucas, o barulho e as noites mal dormidas, são tudo parte da experiência que passámos juntos, que tenho a certeza nunca esqueceremos e de que, quem sabe, um dia até teremos saudades.

Ao Douglas, o verdadeiro Master Yoda, e ao Carlos Gonçalves, um professor sempre disposto a ajudar. Talvez agora o *Outlook* tenha descanso…

Ao Professor Antônio Garcia, por ter acolhido da melhor forma em Aracajú um jovem inexperiente e apreensivo, e por ter sido um professor e amigo em doses certas.

Ao Dr. João Pacheco pelo exemplo de vida e pelos conselhos. É assim que quero ser quando crescer.

Às equipas da Drillfor-02, que me mostraram o que é ter uma vida dura e ainda assim saber rir e ser feliz; e à equipa da CWA com quem passei muitas horas nos vários poços: Leonardo, Samir, Jetro, Allany, Tales, Leandro e muitos outros que nunca deixaram perder uma amostra de calha ou passar um indício de hidrocarboneto.

À galera do Brasil. Aos amigos da UFS, que acolheram "o Portuga" e me fizeram sentir verdadeiramente em casa: Bero, Luana, Jamyle, Aline, Bira, Laiany, Pel, Ulisses, Humberto. Um obrigado especial à minha amiga de sempre e à sua família, Shauane. Ao colega Cristiano Rancan, um geólogo brilhante cujo entusiasmo todos contagiava. Às Julianas que me ensinaram a gostar de Recife, *visse*!

Aos que tiveram paciência para me ouvir falar incessantemente deste trabalho nos últimos meses, compreenderam a minha ausência em muitas ocasiões, e me apoiaram. Os amigos: Gonçalo, Levi, Bernardo, Pedro, JP, B. Cunha, Rita T., Pudinzinho, Firmino. E a família: Tia Lélé, Tia Mimi, Avó Emilia, Avó Maria, Leonor.

Aos que partiram mas que tenho a certeza sentiriam orgulho nas minhas pequenas conquistas: Chico, Artur e Carlos.

Finalmente, aos meus pais que me incutiram o gosto pela geologia e pelo conhecimento. Ensinaram-me a questionar o mundo, a pensar e a viver, e apoiaram-me incondicionalmente mesmo quando as minhas escolhas me enviaram para longe. São o meu maior orgulho.

Resumo

A bacia onshore de Sergipe-Alagoas, onde a GALP Energia detém dois blocos exploratórios, possui um exemplo provado de um Reservatório Naturalmente Fracturado no soco cristalino (Embasamento na terminologia brasileira utilizada nesta tese). Nestes blocos, sete poços verticais foram completados com sucesso, e em todos, o Embasamento Fracturado (cujas características foram provadas através do uso da ferramenta de imagem – *Formation Micro Imager* ou FMI – e de testes a poço aberto – *Drill Stem Tests* ou DST) foi o intervalo que apresentou os melhores resultados.

Nesta tese, foi feita uma análise extensiva da estratégia exploratória, desde a aquisição sísmica aos resultados e procedimentos dos poços, e uma Estratégia de Exploração alternativa foi apresentada como conclusão. Esta análise integrou dados provenientes dos sete poços realizados com dados do Projecto de Modelação do Embasamento Fracturado (uma parceria entre GALP e uma equipa composta por elementos da Universidade de Aveiro, Universidade Nova de Lisboa, Universidade do Algarve e Instituto Superior Técnico). Neste projecto as equipas utilizaram dados sísmicos (planos de falhas interpretados manualmente) e dados de FMI (a partir dos quais as principais orientações de fracturação foram extraídas) para simular um elemento geométrico correspondente ao Embasamento. A essa rede foram aplicados princípios de geomecânica juntamente com modelação DFN (*Density Fracture Network*), permitindo simular a permeabilidade de fractura para cada uma das famílias extraídas dos dados de FMI. Estes dados permitiram ao autor calcular o volume de hidrocarbonetos presentes e simular um poço direccional para ser que deverá ser efectuado em alternativa os poços verticais perfurados até agora.

Acknowledgements

This thesis is the closure of a stage that began when; in August 2006 I embarked towards Aracajú, the capital of Sergipe State in Sergipe-Alagoas Basin, Brazil. At that time, I was far from imagining how important that moment would be for the following years – maybe because ever before I had heard about Aracajú or the Sergipe-Alagoas Basin. However, that moment was decisive, and Brasil, and in particular this Basin, were part of my daily life in the years that followed. During this time several people directly or indirectly contributed to this achievement. Trying not to forget anyone, I thank to:

My tutor Doctor Duncan Lockhart, without whom this thesis would not exist in this form. There are no words to describe my gratitude for having taught me, guided and corrected me during this time. I could not ask for better. Thank you very much!

Prof. Luís Menezes Pinheiro for all the ideas presented for the enrichment of this work, the availability that always demonstrated, and the patience of reading it again and again even when time urged. His help was crucial to sail this boat into a safe harbour.

To GALP E&P Exploration Manager, Roland Muggli, for the trust and support.

To the colleagues from UNL, U. Aveiro and UALG (Filipa, Leonardo, Hugo, Prof. José António Almeida, Prof. Carlos Kullberg and Prof. Conceição Neves), whose work was the base of this thesis.

To Dr. Rui Baptista for giving me the opportunity of entering the exciting world of the oil industry and to GALP Energia, when in 2006 convinced me to accept the scholarship that took me to Sergipe.

To João Afonso, the *wingman*, the brother ("are you guys brothers?"), that sailed with me in this Brazilian adventure and that understands me like few, even in silence and at a distance.

To Carolina, for existing at my side.

To my colleagues in GALP E&P, with whom I share the working space and, without any doubt are a wonderful team! As everyone as contributed in its own way so that this thesis could see daylight, I won't mention any names...That's because we are a team!

To everyone in Petrogal Brasil, but more specifically to Carlão, Manuel Peres, Torres, Cohen, Flávio and Allyson with whom I spent many hours and many days in DF-02/06 and have always made me feel as part of the team. They taught me almost everything I know about drilling engineering/geology, and so many other things that made me grow! To Kéber, Alcimar and Dulce Cid.

To João Antunes and Vera Lourenço. The food, the heat, the dust and mud, the *mutucas*, the loud noise and the bad nights are all part of the experience that we've spent together and that I'm sure we will never forget. Who knows if one day we won't miss it…
To Douglas, the real Master Yoda and to Carlos Gonçalves, a teacher always there to help - maybe now I'll give your Outlook a rest.

To Professor Antônio Garcia, for welcoming an apprehensive and inexperienced young man the best way, and for being a teacher and a friend in the right proportions.

To Dr. João Pacheco, for the fantastic example of how to live and for the advices he gave. That's how I want to be when I grow up.

To the teams of Drillfor-02 rig, who showed me how to face a real hard life with a smile on your face; and to the CWA team with whom I spent many hours in several wells: Leonardo, Samir, Jetro, Allany, Tales, Leandro and many others that have never lost a cutting or have left an HC show undetected.

To the Brazilian "galera". The friends in UFS, who have welcomed "o Portuga" and made me feel truly at home: Bero, Luana, Jamyle, Aline, Bira, Laiany, Pel, Ulisses, Humberto. To my friend Shauane and her family a special thank you. My colleague from Petrobrás, Cristiano Rancan, a brilliant geologist. The "Julianas" for teaching me how to love Recife, *visse*!

To those who had the patience for hearing me talking incessantly about this work over the last few months and accepted my absence in many occasions. Friends: Gonçalo, Levi, Bernardo, Pedro, JP, B. Cunha, Rita T., Pudinzinho, Firmino. Family: Lélé, Mimi, Grandmother Emilia, Grandmother Maria and Leonor.

To those who are gone but I'm sure would be proud of my small achievements: Chico, Artur and Carlos.

Finally, to my dear parents, who instigated in me the love for geology and knowledge. They have taught me to question the world, to think, to live and have unconditionally supported me even when my choices took me to distant places. You are my greatest pride.

Abstract

The Sergipe-Alagoas, onshore Basin, where GALP Energia holds two exploration blocks, has an example of a proven Naturally Fractured Basement Reservoir. In these blocks seven vertical wells were successfully drilled, and in all seven, fractured Basement (which was proven by the use of Formation Micro Imaging – FMI – tool and the results of the Drill Stem Tests - DST) presented the best results.

In this thesis an extensive analysis of the exploration strategy, ranging from seismic acquisition to drilling /testing results and procedures, was made, and an alternative Exploration Workflow was presented as a conclusion. This analysis integrated data from the study of the drilling and testing procedures, with data from the Fractured Basement Project (a joint project with Universidade de Aveiro, Universidade Nova de Lisboa, Universidade do Algarve and Instituto Superior Técnico). In this project the team used seismic data (mainly interpreted fault surfaces) and FMI data (from which fracture families were extracted), and by applying geomechanical principles together with Density Fracture Network (DFN) modelling created permeability maps per fracture family. This allowed the author to calculate the Hydrocarbons Initially in Place (HIIP) and simulate a directional well to be drilled as an alternative to the vertical wells drilled so far.

key-words: Sergipe-Alagoas Basin, basement, fractures, Naturally Fractured Reservoirs, Drill Stem Test, Formation Micro Imager, whole-core Ant-Tracking, seismic attributes, wide-azimuth acquisition, directional drilling, underbalanced driling.

Contents

List of Figures

List of Tables

1. EXECUTIVE SUMMARY

Basement rocks (any metamorphic or igneous rocks, regardless of age, which are unconformably overlain by a sedimentary sequence) are not usually seen by the oil industry as having the capacity to hold hydrocarbons (HC) in sufficient quantity to be considered a profitable reservoir. Their lithological characteristics, with matrix porosity usually close to zero (or inexistent) causes storage space to be given only by fractures, placing Basement reservoirs in the category of Naturally Fractured Reservoirs, having for that reason very specific exploration strategies (full diameter coring, directional and underbalanced drilling as well as detailed geological field studies are crucial) . All this leads most to exploration wells reaching their total depth (TD) when the basement rock is intersected, hence not fully evaluating the basement potential for HC storage. This procedure is common despite many successful examples of Basement reservoirs around the world, of which Bach Ho field in Vietnam, Mara Field in Venezuela and Habban Field in Yemen, are probably the most prominent.

The Sergipe-Alagoas, onshore Basin, where GALP Energia holds two exploration blocks, has an example of a proven Naturally Fractured Basement Reservoir. In these blocks seven vertical wells were successfully drilled, and in all seven, fractured Basement (which was proven by the use of the Formation Micro Imaging – FMI – tool and the results of the Drill Stem Tests - DST) presented the best results.

In this thesis an extensive analysis of the exploration strategy, ranging from seismic acquisition to drilling /testing results and procedures, was made, and an alternative Exploration Workflow was presented as a conclusion. This analysis integrated data from the study of the drilling and testing procedures, with data from the Fractured Basement Project (a joint project with Universidade de Aveiro, Universidade Nova de Lisboa, Universidade do Algarve and Instituto Superior Técnico). In this project the team used seismic data (mainly interpreted fault surfaces) and FMI data (from which fracture families were extracted), and by applying geomechanical principles together with Discrete Fracture Network (DFN) modelling created permeability maps per fracture family. This allowed the author to calculate the Hydrocarbons Initially in Place (HIIP) and simulate a directional well to be drilled as an alternative to the vertical wells drilled so far.

In the alternative Exploration Workflow, this author recommends that the following exploration procedures should be executed in the future:

- Detailed geological field studies over the Basement outcrops that are present in the Basin, in order to better understand the fracture system.
- Wide-Azimuth Seismic acquisition.
- Pre-stack seismic processing with detailed velocity analysis.
- Full-diameter cores to be taken from at least one well.
- Drill-Stem Tests to be executed equally in all the wells. Testing the same intervals and having the same mechanical procedures is crucial to understand how the fracture system behaves during production.
- Image logs to be run equally in all the wells and to TD.

If the option of drilling another exploration well is taken, then this thesis demonstrates that it should be drilled aiming for a specific family of fractures (Family A), which was ranked as the best fracture family in terms of density, permeability and porosity relative to two other families (Family B and B1). This well should have a 30º inclination and should be drilled in the direction of the 240º azimuth in order to perpendicularly intersect the N22ºW/60ºNE Family A fractures. Underbalanced drilling should be considered as a valid option as it became proven by the economic simulation, where the increment in cost for drilling a directional and underbalanced well was not significant (close to $600K). The benefits of using such techniques are proven by worldwide analogues, such as Ninotsiminda Field, where a directional well drilled in 2003 increased daily production by as much as ten times; or by the more than 100 successfully drilled underbalanced wells in Canada (Lunan, B, 1995).

The lack of accurate data (no geological field studies, no coring data and vertical wells mean that the fracture system is not fully evaluated) may be considered as a handicap in the way that the SEAL Fractured Basement was evaluated, and consequently a weakness of the Workflow. Even tough, and considering that to the present a considerable amount of funds have been spent without relevant results, this author believes that this methodology will allow for an optimisation of procedures, with the equation cost vs. results to be favourable to GALP.

2. THE SERGIPE ALAGOAS BASIN

2. 1 INTRODUCTION

The Sergipe-Alagoas Basin (SEAL) (Figure 2-1), is located in the north-eastern coast of Brazil between the parallels 11 and 9.30. Its onshore part corresponds to a narrow band of about 35 km wide, stretching for about 350 km in the direction N45ºE. The boundary of the basin to the sea is not well defined, but it certainly extends beyond the isobathic line of 2000 m, corresponding to an approximate area of 45,960 km^2, of which around 13.200 km^2 are emerged.

Figure 2-1: Brazil's sedimentary basins (http://ri.ogx.com.br/images/bacias_sedimentares_eng.gif)

The SEAL basin is one of the sedimentary basins along the Brazilian coast, formed during the opening of the South Atlantic in the late Jurassic and Cretaceous, crossing various tectonic compartments of the Pre-Cambrian basement. Much of this basement belongs to the Province

Borborema (Almeida et.al.1977), represented in the basin by the Sergipe Fold Belt and the Pernambuco-Alagoas Massif, which will be presented in detail ahead.

This basin presents the most complete stratigraphic sequence of all of the Brazilian Eastern Margin Basins (Figure 2-2), with 5 sequences, mostly separated by regional unconformities.

(unfold next page)

Figure 2-2: Sergipe Sub-basin Litho-stratigraphic Column (Campos Neto *et al.*, 2007).

Structurally, the basin is a half graben dipping to SE (Figure 2-3), and can be divided into four sub-basins: sub-basins of Jacuípe, Sergipe, Alagoas and the Cape sub-basin, with different histories and distinct tectono-sedimentary infills. The Rio Real River high separates the sub-basin of Sergipe from Jacuípe sub-basin. The sub-basins of Sergipe and Alagoas are separated by Japoatã and Penedo highs, along the São Francisco River, while the Maragogi high separates the Alagoas sub-basin from the Cape sub-basin (formerly considered the southern portion of Pernambuco-Paraíba basin).

2.2 TECTONOSTRATIGRAPHIC SEQUENCES

For locating the following stages and corresponding sedimentary in the stratigraphic record, please refer to Figure 2-2.

Stage I: this stage is represented by sediments that were deposited in large depressions associated with intracratonic basins. These depressions that extended from West Africa to NE Brazil, allowed the preservation of part of the Paleozoic sedimentary record. In the SEAL basin the Aracaré Fm. (desert, deltaic and shallow marine Permian sediments) and the Batinga Fm. (glacial, alluvial-deltaic Carboniferous sediments) are examples of such depositional systems.

Stage II (Pré-Rift): This stage, which occurred from Late Jurassic to Early Cretaceous, is characterized by crustal doming as a response to the heating caused by *hotspots* presence in the central Gondwana. This doming created a series of shallow peripheral depressions that were filled

by continental deposits such as red-beds, in fluvial-lacustrine and eolian environments, during Tithonian times. The Candeeiro Fm. (fluvial sandstones), Bananeiras Fm. (lacustrine red-beds), and Serraria Fm. (fluvial sandstones), are the examples of such depositional conditions.

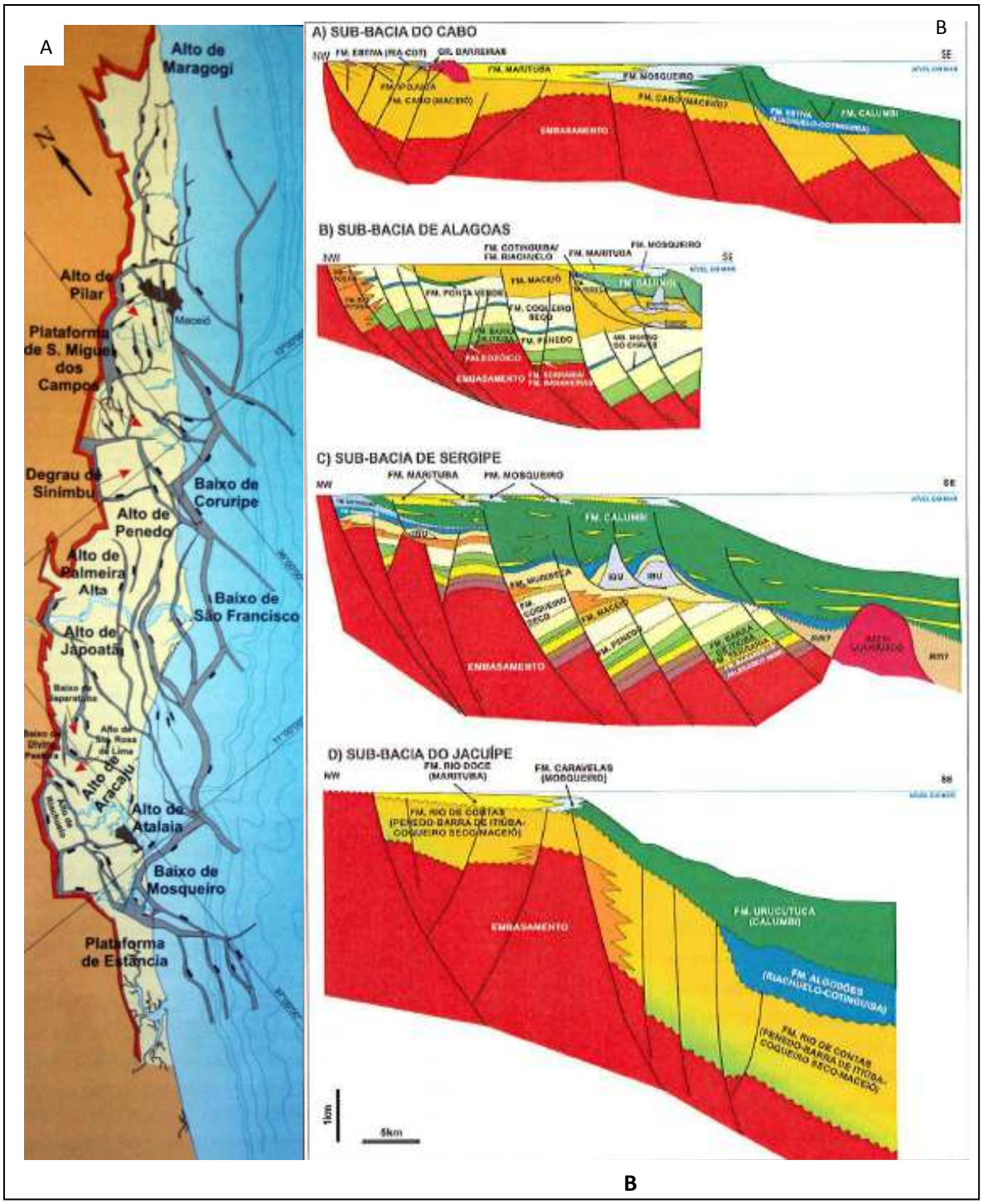

Figure 2-3: A - schematic representation of the structural setting of SEAL basin (Modified from Falkenheim,1986); B - schematic geological sections of the SEAL sub-basins. (A) Cabo Sub-basin; (B) Alagoas Sub-basin; (C) Sergipe Sub-basin; (D) Jacuípe Sub-basin (Souza Lima, 2006).

Stage III (Rift): The evolution of the continental break-up was conditioned by the predominant structural directions in the cratons and fold belts that formed the Basement of the newly formed sedimentary basins. Thus, from the most southern margin to the region of the Camamu basin, the break-up was influenced mainly by the lineaments inherited from the Brasilian Orogeny (late Proterozoic), of NE-SW orientation, and created a long and narrow rift. In the region of the SEAL basin these structural lineaments - of which the Pernambuco lineament is a good example - were perpendicular to the later. This caused the subsidence to be much slower than the adjacent regions, limiting the crustal extension, and causing this region to be one of the last to detach from Africa – while the rifting was already happening in Berriasian/Valanginian in the southern areas, it only occurred in the Albian, in the equatorial basins.

The predominant sedimentary processes were of siliciclastic origin in several depositional environments: alluvial, fluvial, deltaic and lacustrine. These were controlled by the normal faults that bordered the basin. At the base of the Rift sequence and deposited during the Valanginian are the deltaic-lacustrine shales with interbedded sandstones of the Feliz Deserto Fm. This interval is limited at the top by the Pre-Aratu unconformity.

From the Pre-Aratu unconformity to the end of the Rift stage, the alluvial/fluvial conglomerates of the Rio Pitanga Fm. were deposited in the proximal areas of the basin. Distally, however, two different intervals can be defined. From Hauterivian to Barremian times, the Rio Pitanga Fm. grades laterally to the alluvial/fluvial sandstones of the Penedo Fm., and the lacustrine/deltaic shales with interbedded sandstones of the Barra Itiúba Fm. From Barremian to Aptian times the Rio Pitanga Fm. grades laterally to the Morro do Chaves Fm. coquinas, and the alluvial-deltaic and lacustrine sandstones and shales of the Coqueiro Seco Fm. At the top of the sequence, the Rio Pitanga Fm. grades laterally to the lacustrine-deltaic shales and sandstones of the Maceió Fm.

Stage IV (Transitional): the separation between the South American and African plates, allowed the intermittent entrance of sea water in the elongated gulf created during the *rift* stage. This event marks the beginning of the Transitional stage, and started between the Aptian and the Cenomanian depending on the location.

The influx of sea water was controlled by a transversal structural feature between South America and Africa – the Rio-Grande Walvis Sea mounts chain – which worked has a barrier for the water circulation between the proto-ocean that was forming and the Austral Atlantic already developed (Figure 2-4). This controlled water influx plus the high evaporation rates – these events were

happening at a particularly warm climate and near the equator – contributed for the accumulation of evaporites in the gulf.

This stage is represented by the Muribeca Fm. that has three Members:

- The basal alluvial-fluvial and deltaic siliciclastics of the Carmópolis Mb., which correspond to a Lowstand and Transgressive System Tracts (LST and TST) and were deposited over the Pre-Muribeca unconformity.
- The shallow marine evaporites, microbial carbonates and shales of the Ibura Mb., deposited over the Carmópolis siliciclastics corresponding to a Highstand System Tract.
- The carbonates and shales of the Oiteirinhos Mb. that were deposited at the top of the sequence in the Highstand System Tract.

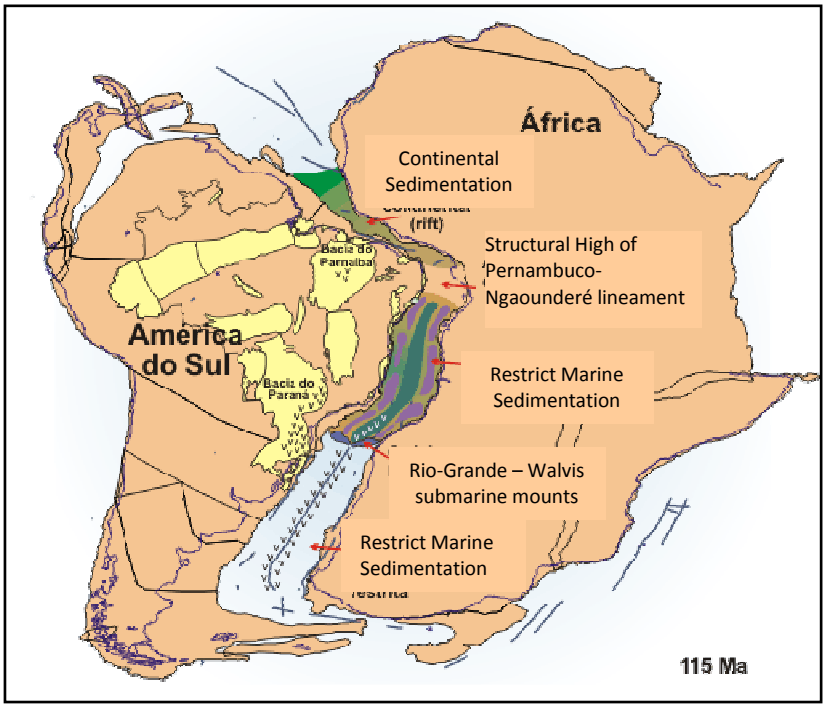

Figure 2-4: Paleogeographic reconstruction of the South Atlantic during the Late Aptian. Note the position of Rio Grande- Walvis sea mounts that conditioned the sedimentation on the marginal basins.

Stage V (Drift): With the continuous separation of both land masses, the Rio Grande Walvis Sea Mount lost its influence in controlling the sea water influx, which now became definitive. From the Albian to the Late Cenomanian, the deposition of the predominatly marine sediments, of the Riachuelo Fm. occurs (In proximal areas the deltaic sandstones of the Ângico Mb. were deposited, varying to the shallow marine oolitic carbonates of the Maruim Mb., and the mudstones and shales of the Taquari Mb.). From the late Cenomanian to the Coniacian, a major transgressive event occurred allowing the deposition of the ramp carbonates of the Cotinguiba Fm. The

continuous drifting modified the climate and inhibited carbonate sedimentation, leading to the evolution of a predominantly siliciclastic system and the deposition of the Marituba Fm. sandstones in the platform and shales with interbedded turbiditic sands of the Calumbi Fm. in the slope and basin floor.

2.3 STRUCTURAL MODELS

In terms of structural setting, SEAL basin is associated with a system of NE and SW trending normal faults and subsidiary E-W and NW-SE transfer faults (e.g. Mohriak et al., 1998). There are several theories for the evolution of the rifting process, but all agree that the structural evolution of the basin occurred in several phases of extension. The three main hypotheses are:

- Lana and Milani (1983): according to these authors the basin evolved in two main stages: the initial stage through N45^{o}E sinistral transtension where en-echelon N-S normal faults, N30^{o}E and N30^{o}W strike-slip faults develop and a second stage characterized by NW-SE extension where the N30^{o}E faults were reactivated as normal faults.
- Falkenhein et al. (1985): this author considers that the basin has undergone three main stages of rifting corresponding to different stress regimes: (1) a normal faulting regime dominated by E-W extension, (2) a strike-slip regime in which NNW-SSE strike-slip faults developed and N-S faults were reactivated, and (3) a normal faulting regime dominated by NW-SE extension.
- Chagas et al. (1983) (Figure 2-5): The Chagas theory is presently the most accepted hypothesis. Through regional mapping these authors concluded that the main extensional faults, i.e. the ones that created the large depocenters along their strike, were oriented in two directions – NS and NE-SW – which indicated two different stress regimes. Associated with the large normal faults others occurred - transversally or orthogonally - which were interpreted as transfer faults. Hence, this model considers that there was an initial, purely extensional, stage of EW direction that generated N-S normal faults and E-W transfer faults; and a second stage of NW-SE extension that created NE-SW and NNW-SSE normal and transfer faults respectively (Figure 2-5). The rifting process occurred transversally to the pre-Cambrian basement structures, which acted as a barrier for the propagation of the normal faults that have been deviated or interrupted. At the same time, these pre-existing

structures contributed for the development of the transfer faults that exerted a very strong influence on the rift development.

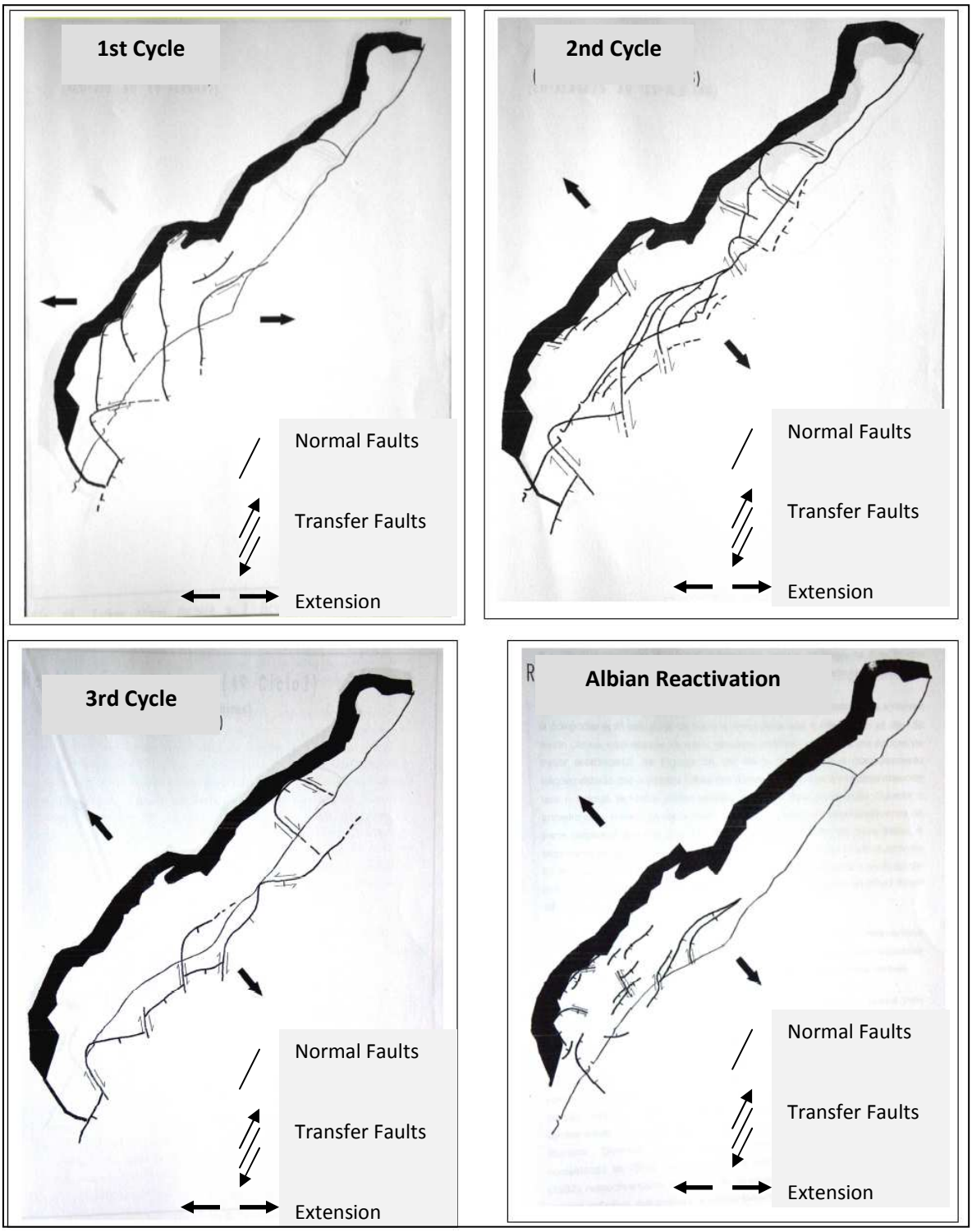

Figure 2-5: Chagas cycles for the structural evolution of the SEAL basin (Chagas, 1996).

2.4 THE BASEMENT IN SEAL BASIN

The SEAL basin basement is formed by a great variety of lithologies ranging from low grade metamorphosed sedimentary rocks to high grade metamorphic rocks with acid and basic intrusions. These are the product of a very complex geological evolution that goes back to Proterozoic ages. Because the focus of this thesis is on Hydrocarbon (HC) exploration on the metamorphic basement rocks of SEAL basin, a brief description of its evolution is presented here.

In order to understand the evolution of SEAL basin basement rocks we have to go back 1500 Million years to the Greenville Orogeny. The Grenville Orogeny was a long-lived Mesoproterozoic mountain-building event associated with the assembly of the supercontinent Rodinia. Its record is a prominent orogenic belt which spans a significant portion of the North American continent, from Newfoundland to Mexico, as well as to Scotland (Figure 2-6).

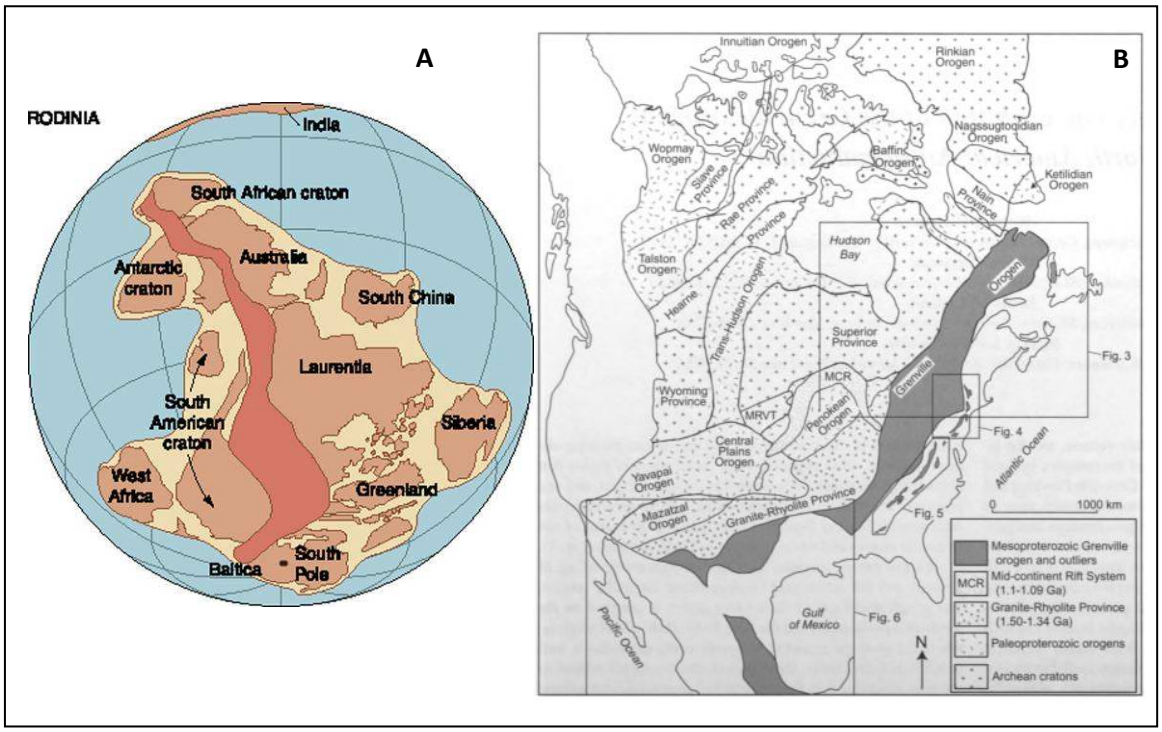

Figure 2-6: (A): Highlighted in brown is the location of the Grenville Orogen in the Rodinia Supercontinent (Levin, 2007); (B): Generalized map showing the location of the Grenville Orogen, including both its subsurface extent and the location of exposed outliers occuring within the Appalachians and its continuation in Texas and Mexico, in relation to other principal Precambrian lithotectonic elements of North America. MCR- Mid-continent Rift System; MRVT- Minnesota River Valley terrane. Map modified from Rankin et al. (1990), Wheeler et. al. (1996), Rivers (1997), Card and Poulsen (1998), and Davidson (1998).

The Grenville Orogeny is thought to have given origin to the Supercontinent Rodinia (Figure 2-7) which, according to present day plate tectonic reconstructions, existed between 1100 and 750 million years ago, in the Neoproterozoic era. Its configuration is still very controversial, but its breakup is fairly well understood and believed to have started around 750 million years ago.

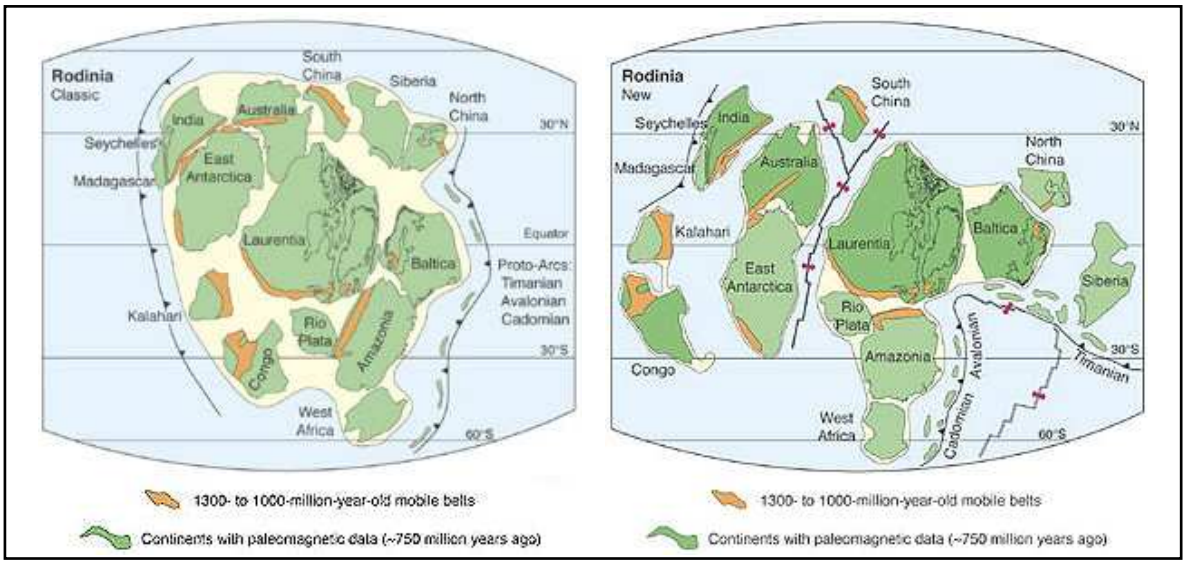

Figure 2-7: Alternative Neoproterozoic configurations for the supercontinent Rodinia (after Torsvik, 2003)

As early as 850 and 800 million years ago, a rift developed between the continental masses of present-day Australia, eastern Antarctica, India and the Congo and Kalahari cratons on one side, and later Laurentia, Baltica, Amazonia and the West African and Rio de la Plata cratons on the other (Figure 2-7). The first group of cratons would eventually, around 550 million years ago (on the boundary between the Ediacaran and Cambrian), fuse again with Amazonia, West Africa and the Rio de la Plata cratons in what is called the Pan-African orogeny (Brasilian Orogeny in south america context), creating a configuration of continents that would remain stable for hundreds of millions of years in the form of the continent Gondwana (Figure 2-8). It is in the fragmentation and the subsequent collision of the continental masses that lays the key for understanding the SEAL basin basement rocks.

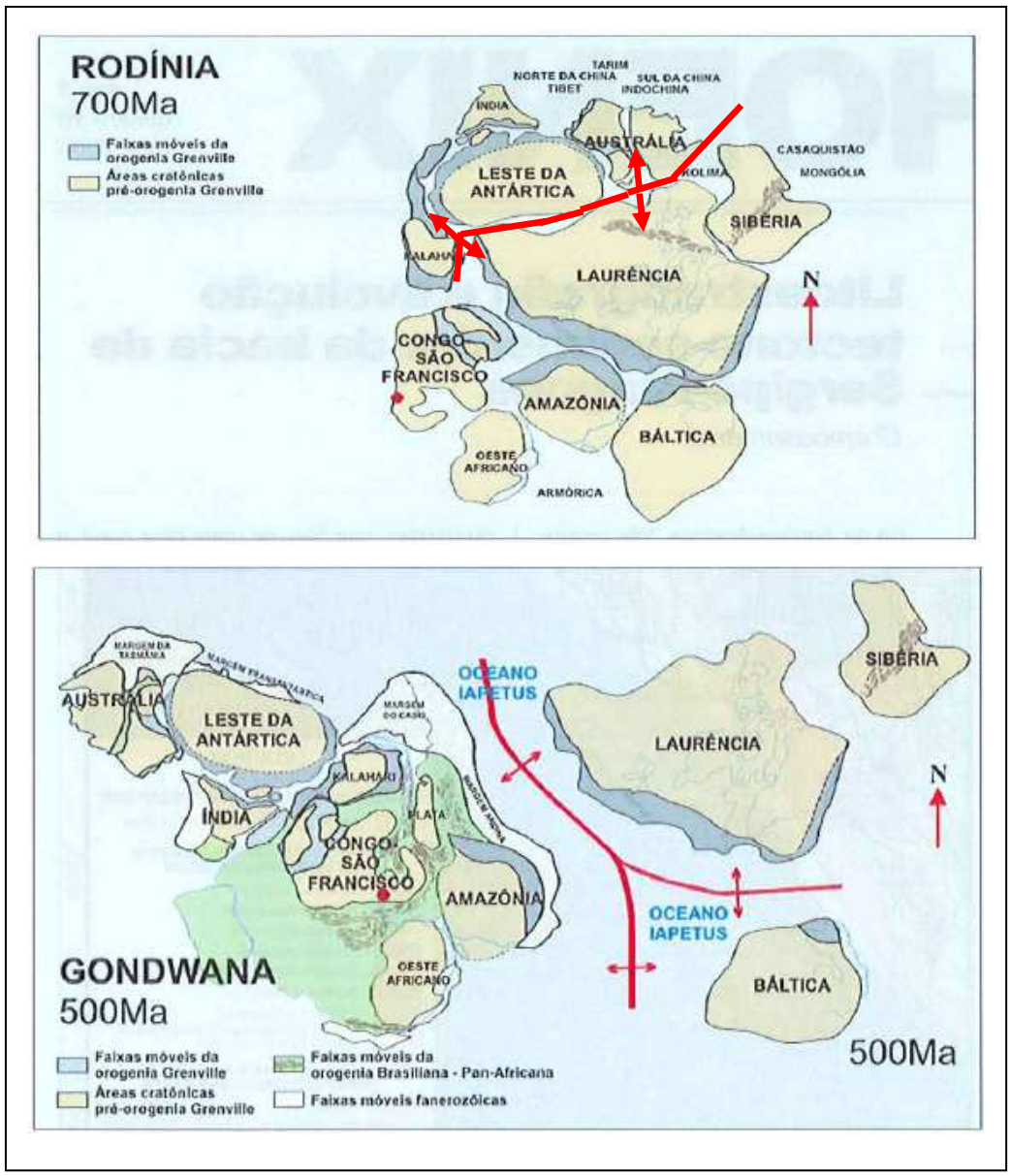

Figure 2-8: paleogeographic reconstruction of the fragmentation of the supercontinent Rodinia and subsequent amalgamation in the Gondwana supercontient (Souza-Lima, 2006; modified from Hoffman, 1991).

The landmasses of the Congo-São Francisco Craton and the West African Craton that collided during the Pan-African/Brasilian Orogeny mentioned above, generated what are today the basement rocks in the SEAL basin. Locally, these are divided in three provinces which are the remnants of the cratonic masses:

- **Borborema Province**: the south-american remnant of the West African Craton.
- **São Francisco Craton**: the south-american counterpart of the Congo craton.

- **Sergipano Fold Belt:** a triangle shaped orogenic belt lying between the Borborema Province (represented here by the Pernambuco-Alagoas massif) and the São Francisco Craton. It is the southern segment of a Brasiliano-age (≈600 Ma) continental collision zone which extends over NE Brazil and continues into Central Africa as the North Equatorial Fold Belt

It is this last province that forms the basement in the studied area. For this reason it will be discussed ahead with more detail.

2.4.1 The Sergipano Fold Belt

The Sergipano Fold Belt (SFB) borders the NE rim of the São Francisco Craton (Figure 2-9). It represents a small southern part of a complex collision zone of much larger proportions. The SFB is one of the few places in NE Brazil where probable Late Proterozoic low-grade metasediments are preserved, the main part of the deformed zone being high-grade gneisses or older metasediments. Humphrey & Allard (1968), Allard (1969), Allard & Hurst (1969) were pioneers in suggesting its continuation to the African continent, and presently the Sergipano Fold Belt is regarded as the central part of a megaorogen connecting the Oubangides Belt (or North Equatorial Belt) of Africa, with the Rio Preto Belt in Brazil (Davison & Santos, 1989; Trompette, 1994) throughout the Riacho do Pontal Belt (Jardim de Sa *et al.,* 1992; Jardim de Sá, 1994). This megaorogen stretches for more than 2000 Km and is a key element for global reconstructions whereby the northern margin of the São Francisco- Congo Craton faced a continuous ocean, the closure of which was part of the final amalgamation of western Gondwana about 500Ma ago (cf. Hoffman, 1991; Dalziel, 1992) (Figure 2-9).

The tectonic evolution of the SFB is interpreted as result of a half graben inversion by a low angle décollement of a listric fault system, in the continental crust (Figure 2-10). This evolution occurred between 670 and 600 Ma Rb/Sr (D'el-Rey Silva, 1995) or between 630-600 Ma U/Pb (Oliveira *et. al.*, 2006), as a consequence of the frontal to oblique collision between the São Francisco-Congo Craton and the Pernambuco Alagoas Massif (West African Craton), as mentioned above. This author considers that structurally, the evolution of the SFB can be simplified by the analysis of the structural model of D'el-Rey Silva for the Itabaiana Dome area, which is represented in Figure 2-11.

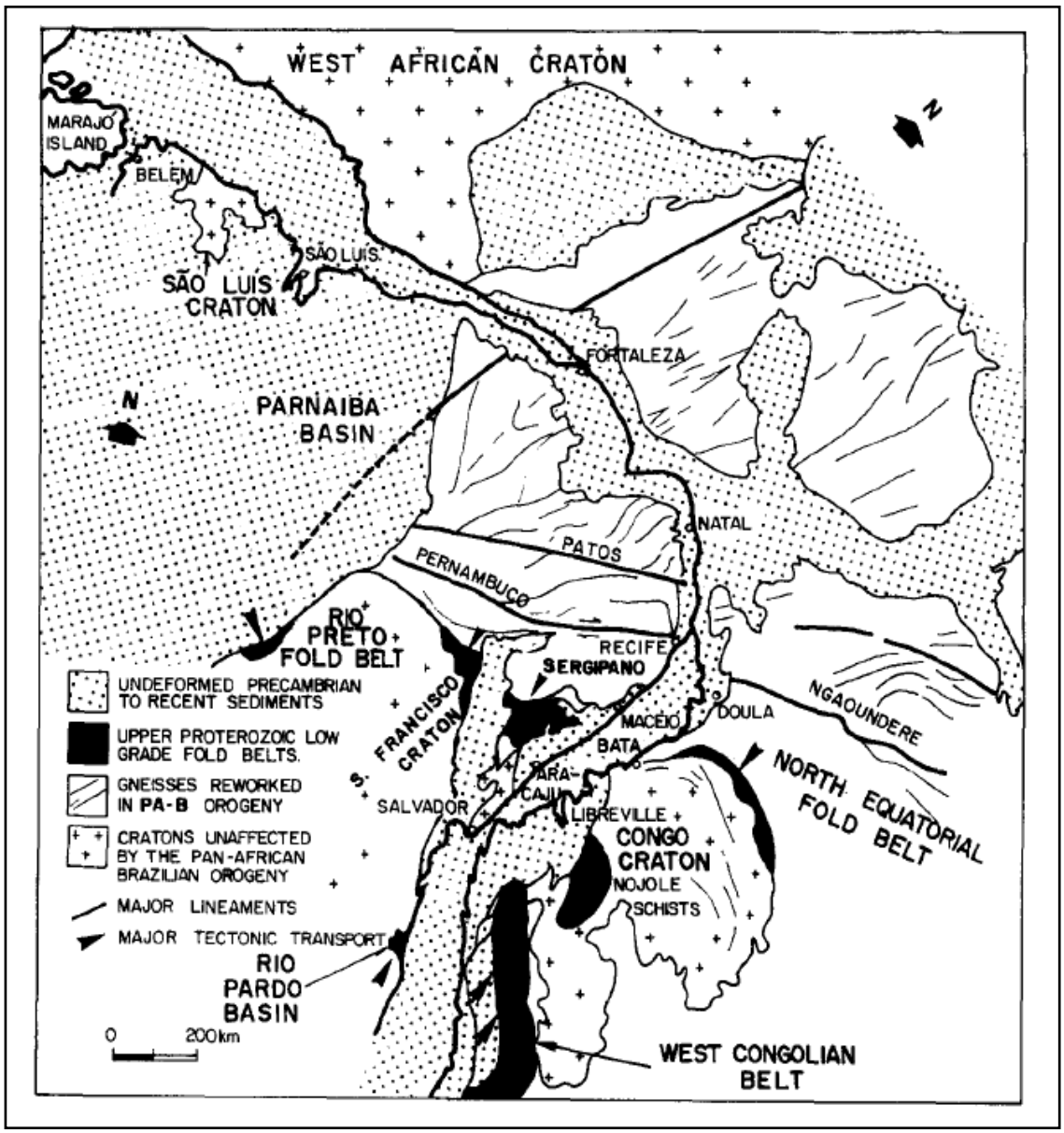

Figure 2-9: Pre-drift reconstruction of NE Brazil and West Africa, showing the continuity of the Sergipano Fold Belt with North Equatorial Fold Belt. The West Congolian Fold Belt was a separate arm which can be correlated with the Rio Pardo Basin, in Brazil. Pre-drift reconstruction taken from Rabinowitz and Labecque (1979). Geological data from Allard and Hurst (1969), Coward (1981), Shobbenhaus (1984), Karmann (1987), Silva (1987) and Nzenti et al. (1988). Source: Davison & Santos (1999).

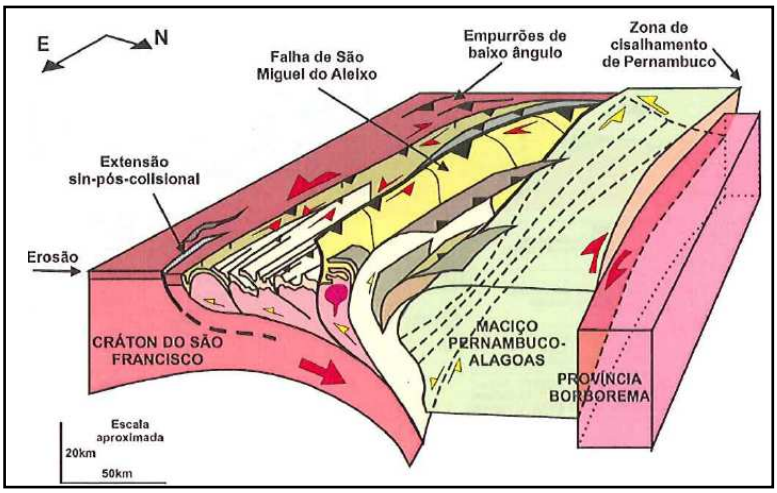

Figure 2-10: Tectonic evolution of the SFB (Souza-Lima, 2006b; modified from D'el-Rey Silva, 1992), interpreted as a half-graben inversion, by a low angle *décollement* of a listric fault system in the continental crust (Rancan, 2009).

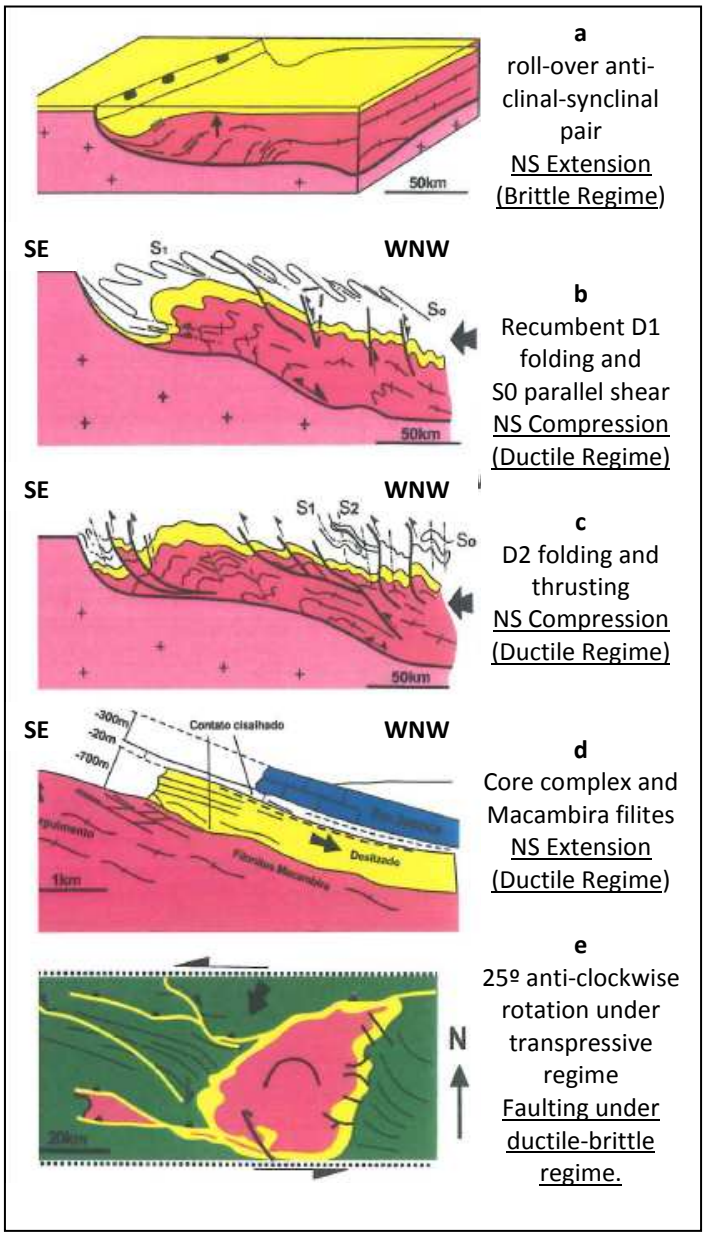

a
roll-over anti-clinal-synclinal pair
NS Extension
(Brittle Regime)

b
Recumbent D1 folding and S0 parallel shear
NS Compression
(Ductile Regime)

c
D2 folding and thrusting
NS Compression
(Ductile Regime)

d
Core complex and Macambira filites
NS Extension
(Ductile Regime)

e
25º anti-clockwise rotation under transpressive regime
Faulting under ductile-brittle regime.

Figure 2-11: Structural evolution of the SFB in the Itabaiana Dome area (Rancan, 2009; modified from D'el-Rey Silva, 1995)

a) Synsedimentary initial state, with E-W extensional faults related to N-S extension.

b) N-S compressive binary reversed E-W faults in sub horizontal thrust faults (D1 phase)

c) the second deformation phase (D2) shows a compressive binary which was initially parallel to the frist and later it rotated (NNE-SSW) resulting in SSW subvertical thrust fault belts and E-W sinistral transpressional faults.

d) during the end of D2 phase, Itabaiana Dome was rotated by NNW-SSE major faults. D3 deformation phase is a late D2 event, characterized by interfoliation slump in ductile for brittle progressive deformation

e) final effect in map. Itabaiana dome presents a porphyroblastic texture, being the dome itself the porphyroblast and the metassedimentary rocks of Vaza-Barris Domain the lepidoblastic

The Sergipano Fold Belt is cross-cut by the Phanerozoic Sergipe-Alagoas and Tucano-Jatobá sedimentary basins and, according to its structural and metamorphic features, may be divided longitudinally, from north to south, into an internal, an intermediate, an external and a cratonic zone, whereas its lithotypes have been grouped by Santos et al. (1988), Davison and Santos (1989) and Silva Filho (1998) into seven lithotectonic domains, named Sul-Alagoas, Canindé , Poço Redondo, Marancó, Macururé, Vaza Barris and Estância. These domains are all bounded by high-angle thrusts associated with sinistral and dextral sense strike-parallel movement, respectively, to the east and west of the Tucan-Jatobá basin (Jardim de Sá et al.,1986; D'el-Rey Silva, 1992, 1995a) (Figure 2-12 and 2-13).

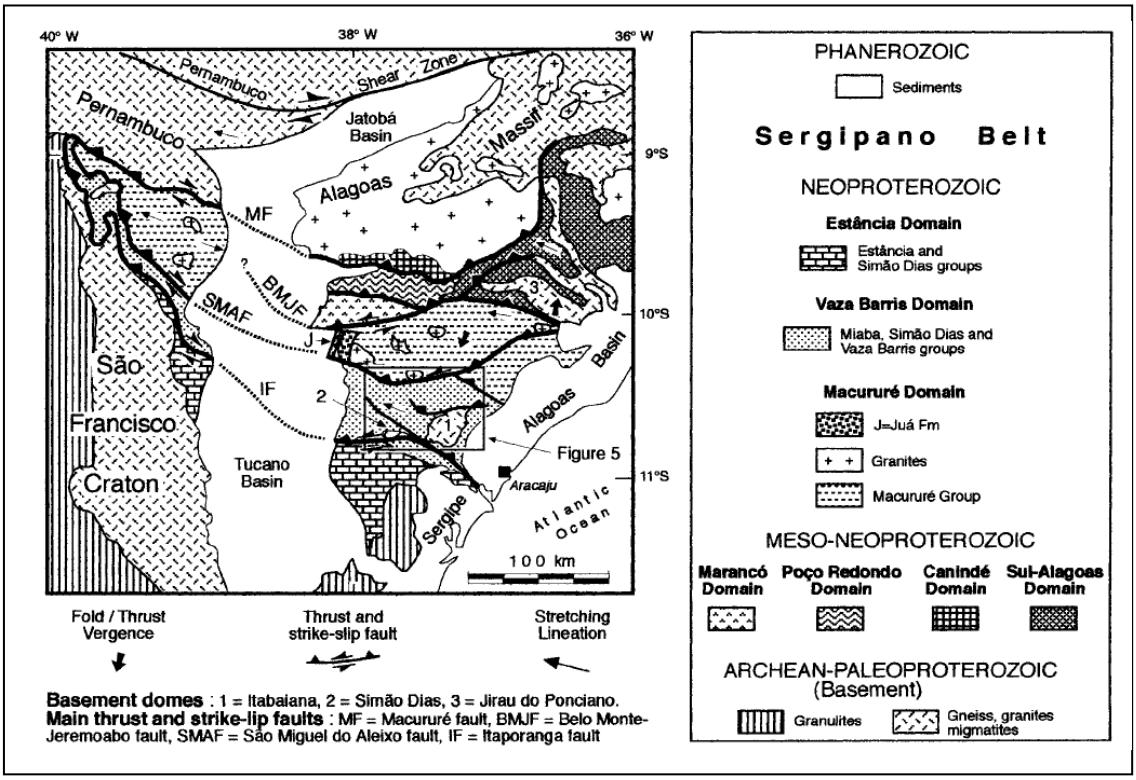

Figure 2-12: Simplified geological map of the Sergipano Belt. Modified from D'el-Rey Silva (1992). The Belo Monte-Jeremoabo fault (BMJF) stretches up to the border of the Sergipe-Alagoas basin, and separates the internal zone (to the north) from the intermediate, external and cratonic zones (to the south). The internal zone stands for a Meso-Neoproterozoic Andean-type margin. The other zones stand for a deformed passive continental margin (D'el-Rey Silva, 1999).

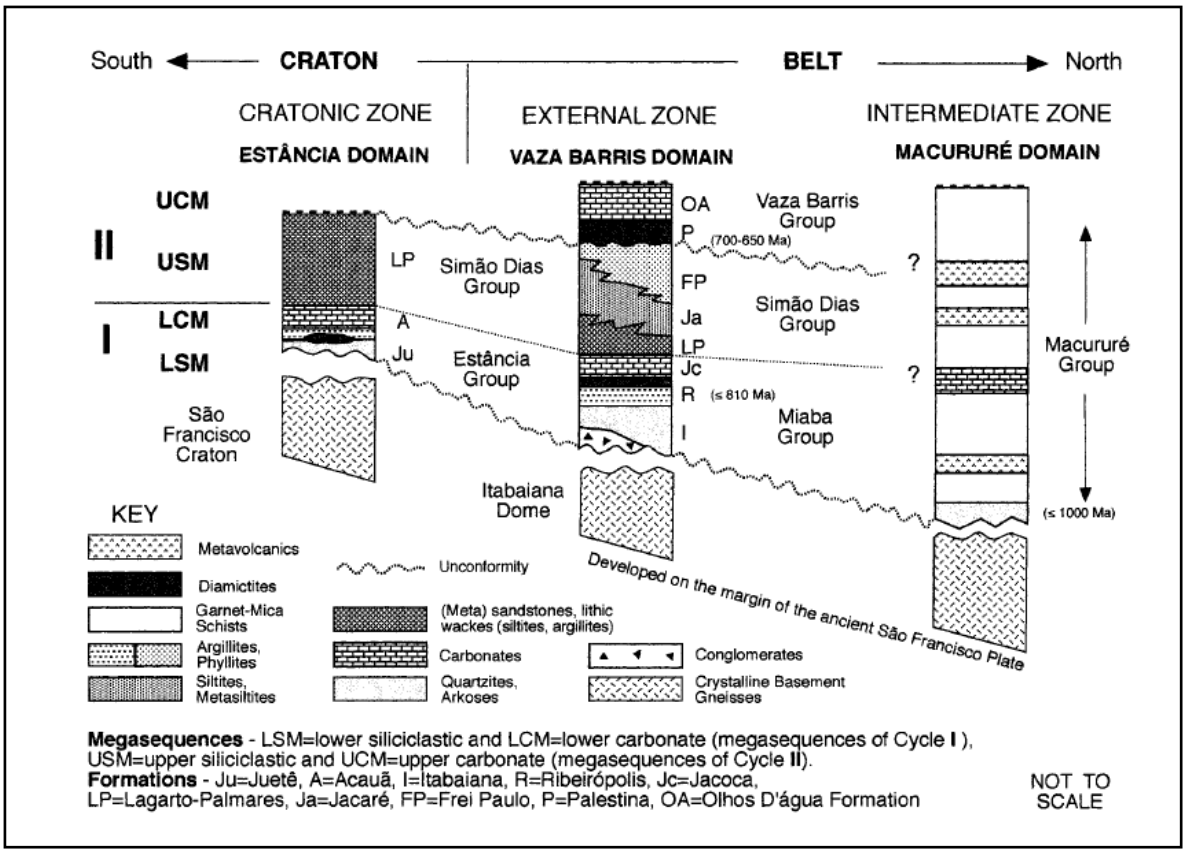

Figure 2-13: Summary stratigraphy of the Itabaiana-Carira dome area, based on D'el-Rey Silva (1992, 1995b) and D'el-Rey Silva and McClay (1995). Sedimentation lasted from ≤1.0 Ga (U±Pb zircon data in metavolcanics of the Marancó domain (Brito Neves et al., 1993)) to possibly 0.65 Ga. New U±Pb data from zircons in volcaniclastics indicate an older age of 810 Ma for the Ribeirópolis Formation (D'el-Rey Silva, 1999).

Based on age determinations in Brito Neves et al. (1993), Van Schmus et al. (1995), and on is own work, Silva Filho (1998) proposes a sub-division into 6 main domains (Figure 2-12, 2-13 and 2-14):

- **Marancó and Canindé Domains:** intraoceanic arcs consisting respectively of metasediments and metavolcanics displaying zircon U±Pb ages of 10452±20 Ma and 10072±10 Ma, along with a 1940 Ma suite of juvenile gabbros and associated metasediments/metavolcanics. Both domains exhibit deformed S-type granites with 1715 Ma U±Pb zircon ages;

- **Poço Redondo Domain**: consists of tonalitic migmatites and paragneisses;

• **Sul-Alagoas Domain:** comprises lithotypes typical of an accretionary prism, as well as the Jirau do Poncian basement dome that is overlain by a sillimanite-bearing quartzite formation all intruded by tonalitic granitoids displaying a Rb±Sr age of 966214 Ma.

• **Macururé Domain:** a <13 km-thick wedge comprising the Macururé Group (siliciclastic and carbonate metasediments and metavolcanics of eugeoclinal affinities), a suite of syn- to post-tectonic calc-alkaline granites, also found in the internal zone, as well as in the Pernambuco-Alagoas Massif (Giuliani and Santos, 1988; Fujimori, 1989; Silva Filho et al., 1992), and the Juá Formation: undeformed psephites derived from rocks of the Marancó domain and infilling a small graben (Silva Filho et al., 1978a; Santos et al., 1988).

• **Vaza Barris Domain:** a 1 to 4 km-thick wedge of platformal (miogeoclinal), shallow marine siliciclastic and carbonate metasediments and minor volcanic rocks occurring around basement domes and divided into the Miaba, Simão Dias, and Vaza Barris groups.

• **Estância Domain**: a 1±3 km-thick blanket of continental to shallow marine siliciclastic and carbonate sediments resting unconformably on the São Francisco Craton and divided into the Estancia and Simão Dias groups.

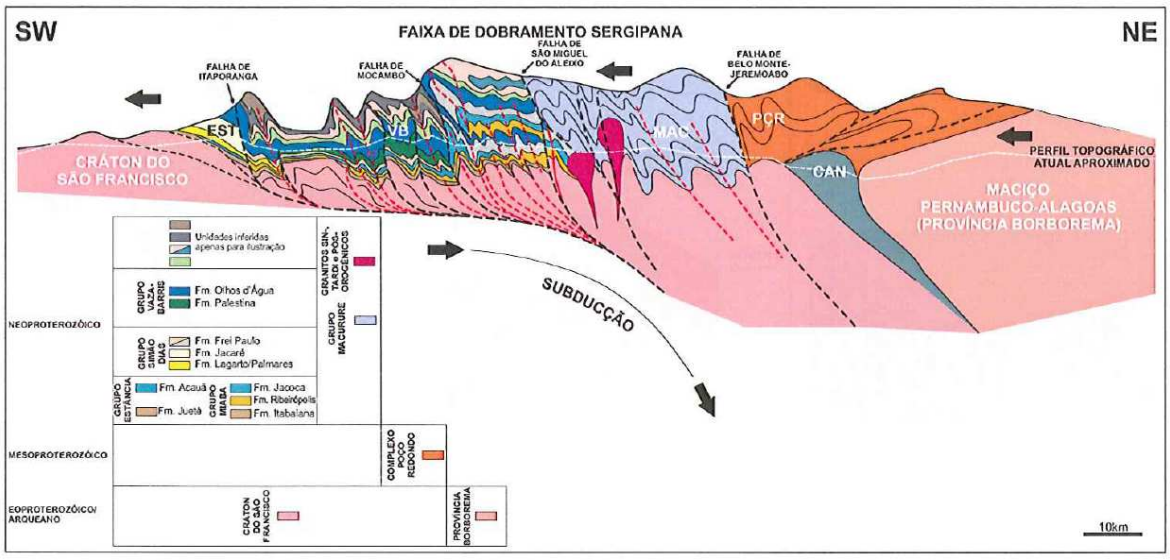

Figure 2-14: schematic geological section, showing an hypothetic reconstruction illustrating the collision of São Francisco-Congo craton and West African craton (Pernambuco-Alagoas Massif) and the lithotectonic domains. EST- Estância; VB- Vaza-Barris; MAC-Macururé; PCR-Poço Redondo; CAN-Canindé (Souza-Lima, Wagner, 2006; from Silva, 1999).

2.5 PETROLEUM SYSTEMS

2.5.1 Sources and Migration

For locating the Formations referred in t in the stratigraphic record, please refer to Figure 2-2.

The main source for the SEAL Basin is the Maceió Fm. (Aptian) – Figure 2-2 - black shales, with type II Organic Matter (OM) and average Total Organic Carbon (TOC) content of 3.5%. The hydrocarbon generation started between 108 and 67 Ma, and lasts to present day. This source rock is not present in the entire basin and in most onshore areas charge depends on medium to long distance migration. Typically, migration occurs through normal faults to the Carmópolis Mb. sandstones, and then laterally to structural highs.

Other proved source rocks are the Barra de Itiúba shales, with hydrocarbon generation starting 115 Ma and lasting to the present day, and the Coqueiro Seco lacustrine shales. It is generally considered that the Ibura Mb shales and the Aracaré Fm. black shales are potential source rocks in some areas. The migration for all the sources in the Pre-Rift and Rift stages is similar to the one that occurs for the Maceió Fm. source.

2.5.2 Reservoir and Seal Pairs

The main reservoirs for the basin are the Carmópolis Mb. sandstones, sealed by the Ibura Mb. evaporites and shales, and the Calumbi Fm. turbidite sands, sealed by the encasing shales.

The secondary reservoirs are the Serraria Fm. Sandstones, sealed by the basal shales of the Barra de Itiúba Fm., and the fractured and porous carbonates of the Riachuelo and Cotinguiba Formations, both sealed by intra-formational shales. Ahead it will be demonstrated that the Basement, which is sealed by the Ibura Mb., evaporites should also be considered a reservoir.

2.5.3 Trap Styles

For the fractured Basement and reservoirs of the Pre-Rift and Rift stages, traps are structural. The Carmópolis Mb. accumulations occur in mostly stratigraphic traps related with the Pre-Muribeca unconformity. Traps in the remaining Transitional stage intervals, as well as early Drift stage, are structural, mainly rotated fault blocks or structures associated with salt displacement. Finally, the Calumbi Fm. accumulations occur in stratigraphic or mixed traps.

2.6 EXPLORATION HISTORY

1935 – Geophysics and drilling of 2-AL-1 well in Northern Alagoas.

1957 – 1st commercial oil discovery with TM-1-AL well.

1960's – Most of the discoveries were made in this decade. Exploration begun in the continental shelf.

1963 – Carmópolis field discovery. It's the largest oil accumulation in the onshore Sergipe sub-basin with more than 1.6 BBO of original oil in place.

1968 – Guaricema field. First offshore oil discovery in Brazil.

Up-to-Date Information

Wells: 996 exploratory and 3,582 development (total of 4,578) – Figure 2-15;

Seismic: 39.927 km 2D onshore, 82.642 km 2D offshore, 4.523 km² 3D onshore and 27.930 km² 3D offshore.

Fields: 44 under development/production/evaluation and 13 turned.

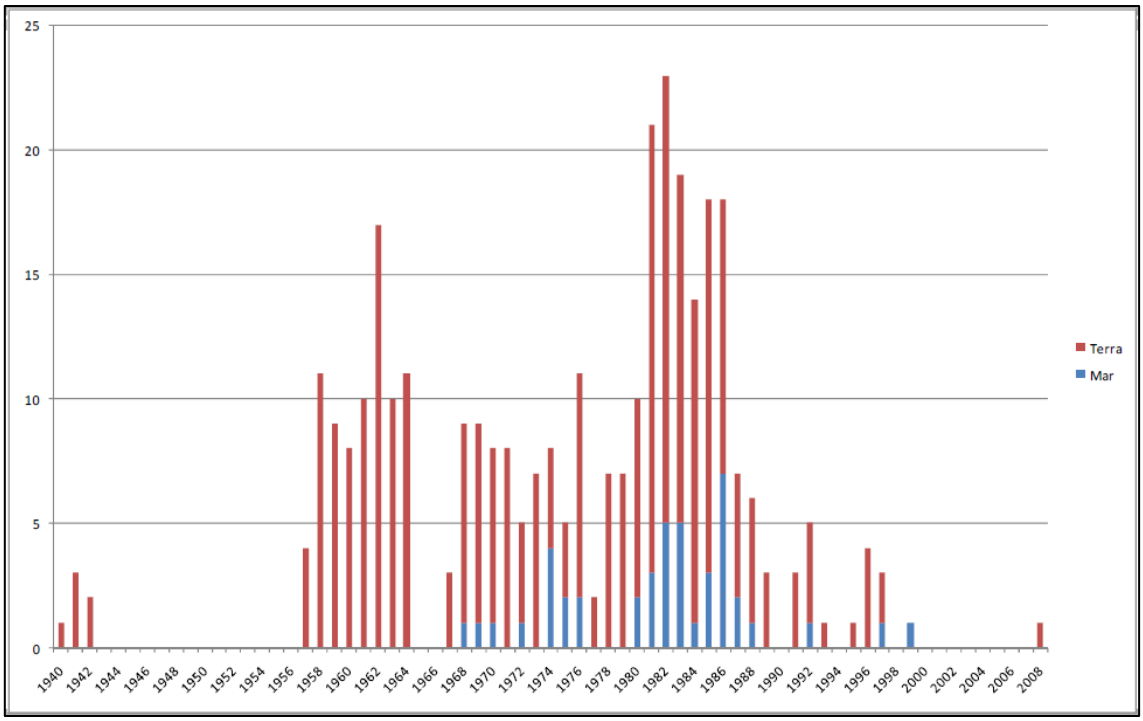

Figure 2-15: Number of wells drilled since the beginning of the exploration in the SEAL basin. Source: ANP.

3. ASSESSMENT OF THE PROBLEM

In 2005, GALP acquired a set of exploration blocks located in Sergipe-Alagoas Basin – Sergipe Sub-Basin. Four exploration wells were drilled in these blocks, all with the Ibura Member carbonates as the primary objective and the intercalated sandstones of the Calumbi Formation as the secondary objective. The results of the first well demonstrated the potential of the fractured Basement play and by the time of the fourth well it had become the primary objective. The results of the four wells proved that the fractured Basement – together with the similarly fractured Ibura Member carbonates– should become the primary objective for future drilling campaigns in the area.

The second drilling campaign, executed in 2010, confirmed the results of the previous campaign. Three wells were drilled, and in all three, fractured metamorphic basement rock presented the best results in the cuttings and when Drill Stem Tested. The results of the two drilling campaigns in the area had clearly proven the presence of a Naturally Fractured Reservoir, and in particular a fractured metamorphic basement rock.

As a consequence of these findings, GALP created a joint team from Universidade de Aveiro, Universidade Nova de Lisboa, Universidade do Algarve and Instituto Superior Técnico to structurally characterize the Basement rock and as a final product create a Discrete Fracture Network and simulate 3D permeability maps. The objective of this project was to provide GALP with a better understanding of this complex reservoir, and allow future drilling campaigns to be planned in a manner which would best exploit the potential petroleum resources of the area. This thesis integrates all the data and results that the project team has gathered and the analysis of the drilling and testing procedures with the final objective of providing a technically supported recommendation on how future exploration operations in this area should be run, by presenting an A to Z Exploration Workflow for Naturally Fractured Reservoirs, using SEAL's Basement as a case-study.

In order to achieve the objective described above the following strategy was used:

- Re-interpretation of the available seismic, focussing primarily on the Ibura Member and Basement horizons, with detailed fault interpretation in order to achieve a better understanding of the structural setting;
- Creation of new structural maps of the Basement horizon based on the re-interpretation;

- Detailed analysis of the well results: drilling and testing procedures (focussing on the fractured Basement);
- Analysis of the *Fractured Basement Project* results in light of the present day knowledge on Naturally Fractured Reservoirs, so that they may be integrated into an overall petroleum exploration strategy, and provide a technically supported recommendation for drilling locations, along with the optimal azimuth and angle for future directional exploration wells;
- Use of world analogues to demonstrate how different exploration strategies (compared to the traditional approach on typical reservoirs) can improve the results and optimize the resources.
- Economic analysis of Traditional Methodologies VS Fractured Reservoirs Exploration Strategies.

4. NATURALLY FRACTURED RESERVOIRS – AN OMNIPRESENT REALITY

4.1 INTRODUCTION

Taking into account all the outcrops of sedimentary rocks that a geologist observes along the years, it is not likely to find any that is unfractured – exceptions made to those extremely ductile rocks, such as salt or certain shales. This happens because; unfractured rocks do not exist! It has also been demonstrated that the vast majority of fractures observed in outcrop are not solely the result of surface conditions, which means that the fractures that one can observe in outcrop can also exist in the subsurface. Therefore, it follows that hydrocarbon reservoirs in sedimentary rock s(and also in metamorphosed sedimentary rocks) all contain fractures and many are fractured enough to be treated as fractured reservoirs.

Despite this, the practice of treating reservoirs as fractured rock masses is not a standard industry practice. Why?! This author considers that there are several reasons for this:

1. As stated, virtually all reservoirs contain at least some natural fractures. However, the effect of these fractures on fluid flow is in most cases negligible and the reservoir can be treated, from a geological and reservoir engineering perspective, as a “conventional” reservoir.
2. Most common naturally fractured reservoirs are characterized as hard rock of low porosity and permeability but still having most of the fluids stored in the matrix rock. The fractures are only providing the flow paths for those fluids. This means that, for most fractured reservoirs, the rock matrix accounts for the bulk of the reserves, and that an important part of the exploration strategy - and hence for the selection of prospective drilling locations - is the identification of fractured intervals with sufficient matrix porosity. In such cases it is more common that the traditional exploration approach is followed. Exceptions made for those cases where it is needed to intersect the fractures in order to assure flow.
3. Almost all fractured reservoirs respond in a manner unique to that specific reservoir. That is, despite the existence of a good, working fractured reservoir classification, each fractured reservoir responds in its own distinctive way. As a consequence, applying general rules of thumb to specific fractured reservoirs can be misleading.

From this comes that, due to the desire of simplifying technical work and reducing cycle times in exploration and production, geologists and engineers tend to fall into the fracture denial paradigm. It is true that fractured reservoirs are more complicated than matrix reservoirs, and that they require more time and money to be evaluated correctly, but the problems with this denial or avoidance can be serious and include: 1) irreparable loss of recovery factor; 2) primary recovery patterns that are inappropriate for secondary recovery; 3) inefficient capital expenditure during development; 4) drilling of unnecessary in-fill wells; and 5) improper assessment of economic opportunities. To avoid this it is important to determine the effect of natural fractures on the reservoir that we are analysing, so that the exploration strategy can be adequate from day one.

This thesis has the objective of providing a technically supported recommendation on how future exploration operations should be run, by presenting an A to Z Exploration Workflow for Naturally Fractured Reservoirs (NFR), using SEAL's Basement as a case-study. As it will be shown ahead, this basement rock is a naturally fractured reservoir and therefore traditional exploration approaches do not work well here. The present chapter has the objective of presenting the geological and engineering aspects of Naturally Fractured Reservoirs.

4.2 DEALING WITH NATURALLY FRACTURED RESERVOIRS

Before any other consideration is made, it is important to define *fracture* and *fractured reservoir.* Because this work is dealing with the effect of naturally occurring fractures on reservoir rock, the definition will be restricted to this context. Hence, *a reservoir fracture* is a macroscopic planar discontinuity that results from stresses (due to deformation or physical diagenesis) that exceeds the rupture strength of the rock. Natural fractures may have either a positive or negative effect on fluid flow within the rock (Nelson, 2001).

If the definition of a reservoir fracture is broad, the definition of *fractured reservoir* even more so: a *fractured reservoir* is defined as a reservoir in which naturally occurring fractures either have, or are *predicted* to have, a significant effect on reservoir fluid flow either in the form of increased reservoir permeability and/or reserves, or increased permeability anisotropy (Nelson, 2001).

Having these definitions in mind, we can now approach the way of how to deal with a fractured reservoir. It is of paramount importance to know what we are looking for and what we have found in terms of reservoir properties. For this reason most authors consider that, despite the fact that each fractured reservoir has its particularities, a general set of information has to be gathered to evaluate any Naturally Fractured Reservoir: fracture origin, fracture properties affecting reservoir properties, fracture/matrix interaction and reservoir typing. Ultimately this information has the objective of supplying a well location. To gather this information the geologist can use several sources at different times during the exploration workflow, but if a logical sequence is followed, this process will be less time and money consuming and results will improve. Figure 4-1 represents the exploration workflow suggested by this author for the SEAL Basement Naturally Fractured Reservoir (NFR), but that can be applied for other similar situations.

(unfold next page)

Figure 4-1 (unfold next page): Proposed workflow for the present study. Inside the green squares are the key points of the workflow: the identification of the fracture system and its properties (origin, properties affecting reservoir performance, fracture-matrix interaction), classification of the reservoir type, well design, well results and Pre- and Post-Drill volumes calculation. This method involves several sources of information, gathered at different times during the Exploration process.
It is first important to assess if there is the possibility of the presence of fractures. If it is, then the geologist should understand the Fracture System properties. To do that, he can use old well data, outcrop data, regional geology and, if available, seismic. Old well data and outcrop analysis will give information on the lithology, orientation of fracture patterns and on rock mechanical properties, which will allow the geologist to derive the Fracture Properties Affecting Reservoir Performance and how Fractures and Matrix Interact. Regional geology, in its turn, will supply the regional tectonic regimes and the structural setting of the area, which allows for the classification of the Fracture System Origin. Together, data from these three sources will constrain the Geomechanical Models that allow the creation of Discrete Fracture Network (DFN) models to simulate the Fracture System Properties (fracture and permeability distribution) leading ultimately to the classification of the Reservoir Type. If seismic is not available in the first phase, the analysis of the other data can help on the decision on whether it should or not be acquired and on the parameters to do so. Seismic interpretation - especially fault interpretation - of the available seismic will also help on the understanding of the fracture patterns and will be an input for any reservoir models that are created. Notice that emphasis is also given on processing, as complex settings as NFR's (especially in Basement contexts) require special processing steps.
All these have the ultimate objective of finding a suitable well location. Prior to drilling there is the need of calculating hydrocarbon (HC) volumes in place. This will be based on the properties simulated by the models, and using parameters given by the previous analysis. Well design will be subjected to the fracture system properties (orientation and permeability distribution), in terms of orientation as in most cases NFR's wells are drilled directional and underbalanced. The evaluation of the wells will give more information about the reservoir properties and consequently help readjusting the models previously created as well as accessing Post-Drill Volumetrics. This is an iterative workflow. The following paragraphs will analyse the workflow in more detail.

4.2.1 Fracture System Identification

The identification of the presence of fractures in the area of interest prior to the realisation of wells is of paramount importance as it will influence much of the future exploration strategy. Presently, some of the available methods allow the geologists to identify not only the presence of fractures, but in many cases – depending on the quality of the available data – their distribution and orientation in the rock volume. This section will describe the data that can be used to accomplish this objective.

Well Data: The analysis of well data from past drilling campaigns is very important, as the presence of fractures might have gone unnoticed due to a lack of awareness of the geologists and engineers at the time. Well data includes cuttings, well logs, image logs, core data and production tests results. Some situations might indicate the presence of fractures (Nelson, 2001):

- Mud losses might be associated with natural fractures, vugs, underground caverns or induced fractures and penetration rates can increase significantly while drilling all types of secondary porosity.
- If from cores the permeability of a formation is 0.1 md, and the well produces 1,000 Bbl/day (Bbl = Barrels) in an Extended Well Test (EWT), it can be inferred that the rate is the result of some type of secondary porosity, including fractures.
- Consider also the situation where a rock was described by the mudlogger as a crystalline rock – hence with no primary porosity – and good oil shows were detected. Some kind of secondary porosity should be inferred and image logs may help clarifying this.

The analysis of this data also allows for the early calculation of parameters such as fracture porosity, permeability and fracture density, helping the geologist to plan future data acquisition and/or drilling campaigns (Nelson, 2001). Emphasis on how to use Drill Stem Test's and Image logs information is presented in the Appendix of this thesis.

Outcrops: A properly conducted outcrop study can probably provide the most useful information on the relation between fractures and the host rock. In other words, outcrops supply valuable information for the calculation of most rock parameters that need to be assessed when characterizing a NFR – fracture and matrix permeability, fracture density and fracture system

orientation. The use of outcrops is obviously conditioned to one very simple factor – their existence. Assuming that outcrops are available, the geologist can face two different situations:

1) the outcrop is the exact same formation as the one that is being targeted
2) the outcrop can be used as an analogue for the targeted formation

It is obvious that the first situation is much more convenient as it makes the gathered information more reliable, but if the correct analogue is chosen, the geologist can extrapolate the data collected from that analysis to his own situation.

Outcrop studies should be conducted with care, taking into account the fact that the exposed rock was subjected to the effect of lithospheric unloading (creating joints) and weathering that altered many of the rock properties, relative to the same rock in burial conditions.

Regional Geology: as in any other geosciences study, the regional geological context where our object of study is inserted is of paramount importance. It is the regional geological context that will determine some of the properties of the rock mass to be analysed. Information on the lithologies encountered, fault patterns, stress fields (present and past), geodynamic evolution, and the relations between all of this will allow for fracture system classification in terms of origin – which in turn will determine most of the fracture properties such as spacing, length, width and orientation. This knowledge can be used as an input in geomechanical modelling for prediction on fracture distribution.

The facture properties mentioned, fracture morphology, fracture width and permeability, fracture spacing, origin of the fracture system, the interaction between matrix and the fractures and the reservoir classification will be discussed in detail ahead.

Seismic Information: If seismic is available, the geologist can use it to obtain valuable information on the structural context of the area – by mapping horizons and faults – and even on fracture patterns - by extracting attributes from the seismic volume or by detailed azimuthal velocity analysis on pre-stack data. Both can also be used as an input to constrain any geomechanical modelling that is done. If seismic is not available, the analysis of the previous data will help in deciding if it should or should not be acquired. Seismic acquisition and processing for Naturally Fractured Reservoirs (NFR) will be described ahead.

Fractures can interfere with the propagation of the seismic waves and cause low P and S-wave velocities (Vp and Vs), and lower seismic frequency and quality factor (Q). These characteristics help the interpreter to identify fractures in the seismic record.

- Low Vp and Vs: Fractures lower seismic P and S-wave velocity due to the rock's secondary porosity that was caused by the fractures. As fracture density increases, P-wave velocity decreases. A plausible explanation for this is that, as fracture density increases, the overall velocity becomes increasingly more sensitive to the fracture properties and less sensitive to the intact rock properties (Boadu, 1997). But if the fractures are filled with minerals (not fluid), the changes in Vp and Vs are dependent on the elastic properties of the minerals which filled the fractures. At the same time, Hilterman (1977) states that the compressional wave velocity (Vp) for hydrocarbon filled fractures is lower than brine filled fractures. The Vs of hydrocarbon filled fractures will be slightly higher than brine filled fractures.
- Fractures also lower seismic frequency and quality factor (Q). The fractures cause a time delay in the propagating waveform and act as filter by attenuating the high frequency components in the spectrum of the waveform (Boadu, 1997)- Figure 4-2.

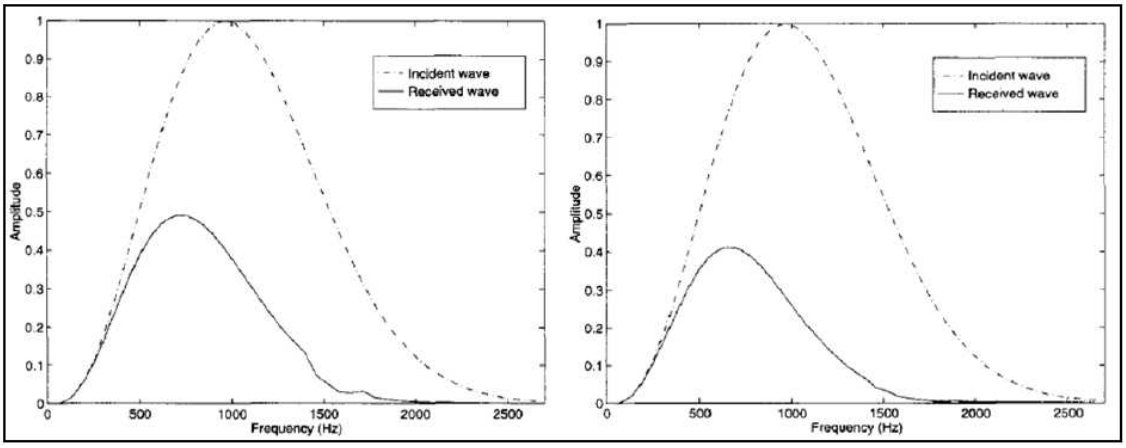

Figure 4-2: Amplitude spectra of incident and received waveforms (P-wave) for a model that consists of four vertically aligned fractures (left) and for a model that consists of seven vertically aligned fractures (right) (Boadu, 1997). As the number of fractures increases, the amplitude of the received waveforms is significantly reduced and there is also a shift in the peak amplitude towards lower frequency. Source: Sugiri, O. I. (2010).

Surface seismic data has long been used for detecting faults and large fractures, but recent developments in seismic attribute analysis have shown promise in identifying groups of closely spaced fractures or interconnected fracture networks. These significant advances in 3D seismic

technology allow in many cases the interpreters to determine fracture orientation, anisotropy and fracture density. One of the greatest strengths of 3D seismic is the dense, regular sampling of data over the region of interest, providing images that accurately represent the areal extent of the features. Among the various geophysical techniques available for characterizing faults and fractures, 3D seismic attributes have proven to be some of the most useful, in particular those that are sensitive to reservoir impedance, thickness, or geomorphology. Although there are a few hundred seismic attributes that are in common use today, post-stack attributes such as dip-magnitude, dip-azimuth, coherence and curvature, are the most useful, and proven to work, for fault/fracture detection.

According to Chopra (2009), the benefits of using these discontinuity seismic attributes are:

1. Easier recognition of detailed geology within a 3D seismic dataset.
2. Interpretation of higher resolution faults/fractures in any orientation without interpretation bias.
3. Clearer stratigraphic features for more accurate interpretations
4. Features imaged in a consistent three-dimensional manner
5. Suitable comparison with log data allows confident interpretation of faults/fractures
6. Reduction of exploration and development risk by providing a more accurate understanding of subsurface geologic features recorded by 3D seismic data.
7. Reduces interpretation cycle time and costs by providing a clearer picture of the subsurface
8. Added value to existing 3D seismic investment by exploiting the data to its fullest.
9. Represent a small percentage of the total seismic cost.

The main attributes which have proven efficient for fault /fracture detection are, *dip-magnitude, dip-azimuth, coherence and curvature.* Notice that the quality of these attributes is directly proportional to the quality of the input seismic data. So, for extracting more accurate information from seismic attributes, the input seismic data needs to be cleared of all distortion effects, whether near-surface or amplitude/phase related. Curvature and coherence attributes are presently considered to be the most powerful tools to detect fractures. For that reason they will be given emphasis here.

Dip-Magnitude: computes, for each trace, the best fit plane (3D) or line (2D) between its immediate neighbour traces on a horizon and outputs the magnitude of dip (gradient) of that plane or line measured in degrees – Figure 4-3.

Dip-Azimuth: computes, for each trace, the best fit plane (3D) between its immediate neighbour traces on a horizon and outputs the direction of maximum slope (dip direction) measured in degrees, clockwise from North- Figure 4-3.

Coherence (Figure 4-4): measures the continuity between seismic traces in a specified window along a picked horizon. Similar traces are mapped with high coherence coefficients, while discontinuities have low coefficients. Regions of seismic traces cut by faults, for example, result in sharp discontinuities of trace-to-trace coherence, resulting in delineation by low coherence along fault planes. It is essentially a cube of coherence coefficients generated from the input 3D seismic data volume that portrays faults and other stratigraphic anomalies clearly, on time or horizon slices. An advantage of the coherence cube is that it gives an unbiased view of the features in the seismic volume. No interpretation is required for viewing them.

Curvature (Figure 4-5): A group of post-stack attributes that are computed from the curvature of a specified horizon or seismic volume. The concept of curvature applied to a specific task is illustrated in Figure 4-5. There are many curvature measurements that can be computed, but the most-positive and most-negative curvature measures are the most useful in that they tend to be most easily related to geological structures.

Presently, curvature attributes can be computed using the full seismic volume instead of a specific horizon. As the name implies, horizon-based curvature is computed directly from a picked seismic horizon which in general requires that the data quality be good and that the horizon of interest corresponds to a prominent impedance contrast. Horizons picked on noisy surface seismic data or picked through regions where no continuous surface exists can produce misleading curvature measures. A way of addressing such problems is to spatially filter the horizon picks, with the objective of removing the noise and retaining the features of geologic interest (Bergbauer et al., 2003; Chopra et al., 2006). Volumetric curvature begins by first computing dip and azimuth using a small analysis window (9 traces by +/-10 ms for the examples shown in the figures that follow) for every point in the 3D volume. By using a vertical analysis window and the analytic (original trace and its Hilbert transform) rather than just the original trace, volumetric estimates of dip and azimuth are in general more robust than horizon-based estimates.

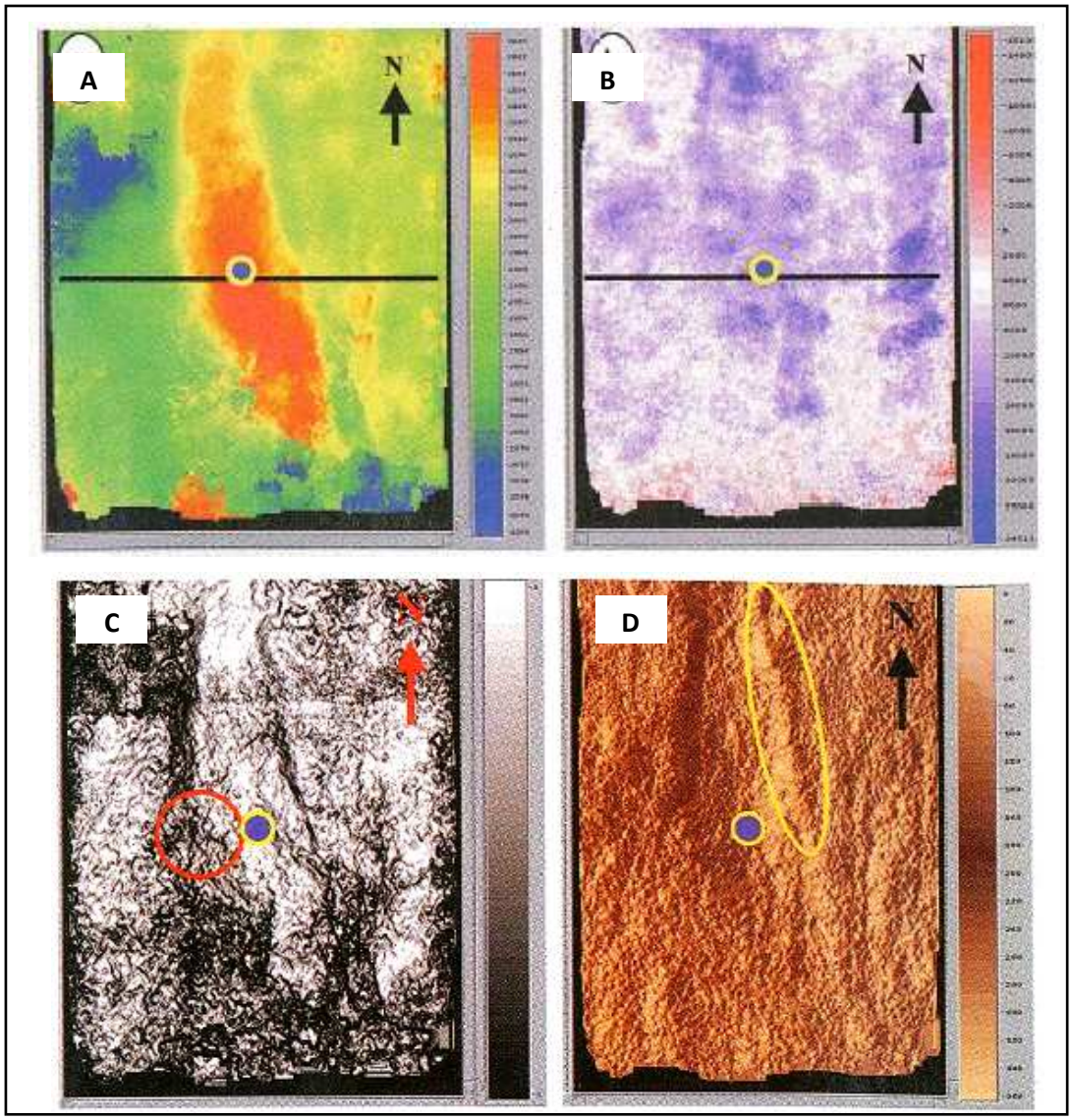

Figure 4-3: a) time-structure map of top reservoir (colour scale is two-way travel time in miliseconds). The map shows the existence of faults bounding the large red areas. b) Amplitude map at top reservoir (colour scale is maximum seismic amplitude). Note that there is no clear indication of fracturing that could be extracted confidently from these two traditional attribute maps. Dip (c) and azimuth (d) map calculated from the time values of b). Note that the full extent of the east flank of the fault block (circled in yellow) is better delineated by the azimuth attribute, whereas an indication of a possible fractured zone (highlighted in red) is better inferred from the dip attribute. Colour scales for dip (1-7) and azimuth (0-360) are both in degrees. Area of the figure is about 18 x 15 km. The blue circle represents the well that was used for calibrating the models (Neves,2004).

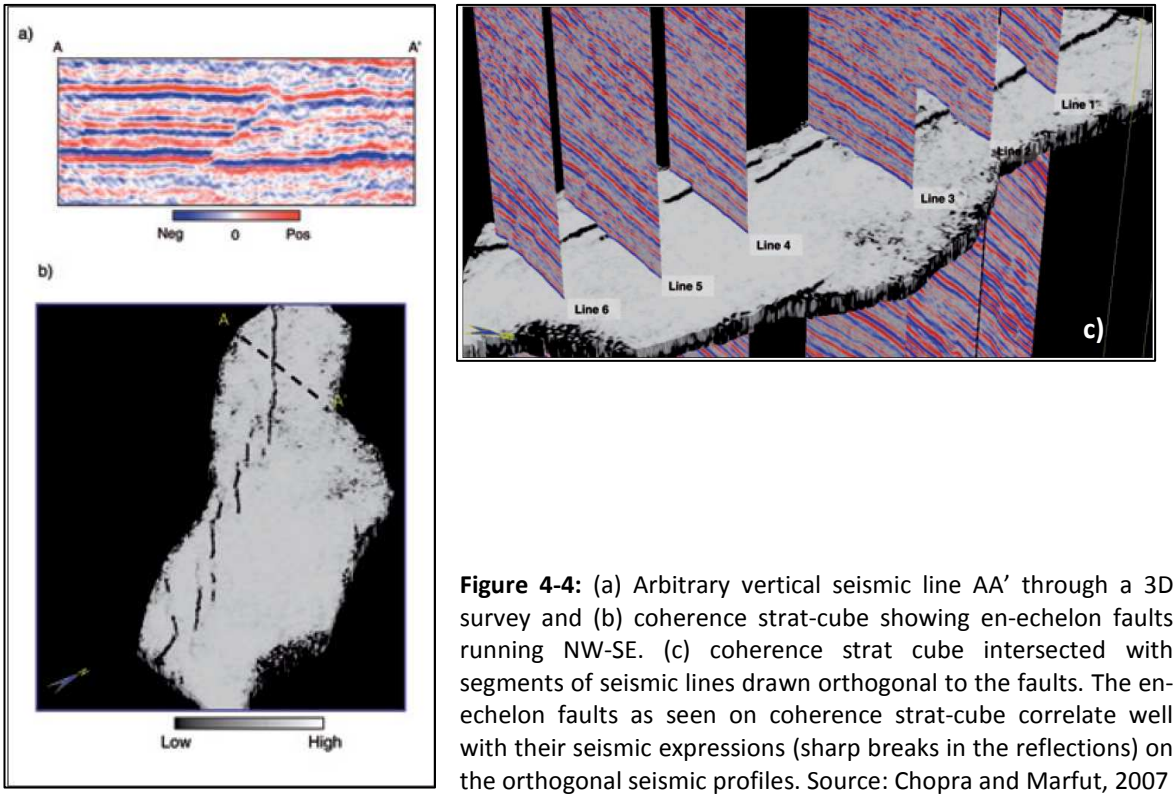

Figure 4-4: (a) Arbitrary vertical seismic line AA' through a 3D survey and (b) coherence strat-cube showing en-echelon faults running NW-SE. (c) coherence strat cube intersected with segments of seismic lines drawn orthogonal to the faults. The en-echelon faults as seen on coherence strat-cube correlate well with their seismic expressions (sharp breaks in the reflections) on the orthogonal seismic profiles. Source: Chopra and Marfut, 2007

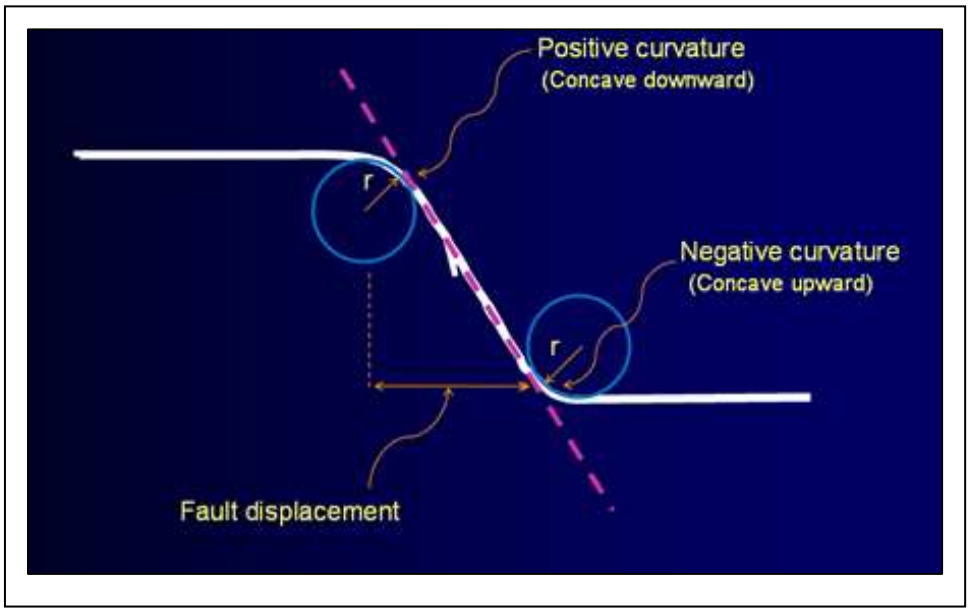

Figure 4-5: Curvature concept for detection of fault features. The up-thrown side of the fault has a downward concave shape so it is considered to have a positive curvature; similarly the down-thrown side of the fault has an upward concave shape and it is considered as a negative curvature. The positive and negative curvature attribute displays will be seen as separate lineaments, each corresponding to one side of the fault. The distance between them is proportional to the horizontal fault displacement. Source: Chopra, 2009.

At the same time, curvature computations with different wavelengths (Multispectral) enhance geologic features having different scales. Tight (short-wavelength) curvature often delineates details within intense, highly localized fracture systems. Broad (long wavelength) curvature often enhances subtle flexures on the scale of 100-200 traces that are difficult to see in conventional seismic, but are frequently correlated to fracture zones that are below seismic resolution, as well as to collapse features and diagenetic alterations (Figure 4-6).

There are two possible explanations why the coherence image of Figure 4-4 b) does not provide as much detail as the curvature images. The first reason is geological: the faults can progressively lose throw and eventually become simple flexures; alternatively, there may be sediment drag along some of the faults that make them appear to be flexures. The second reason is geophysical: either the fault has insufficient throw to be resolved as a discontinuity or the velocities are inaccurate such that the faults are somewhat smeared and therefore only *appear* to be flexures. Be they faults or flexures, we might anticipate increased presence of natural fractures near these lineaments. We also note synthetic folds indicated by white arrows that are nearly perpendicular to the en echelon reverse fault system.

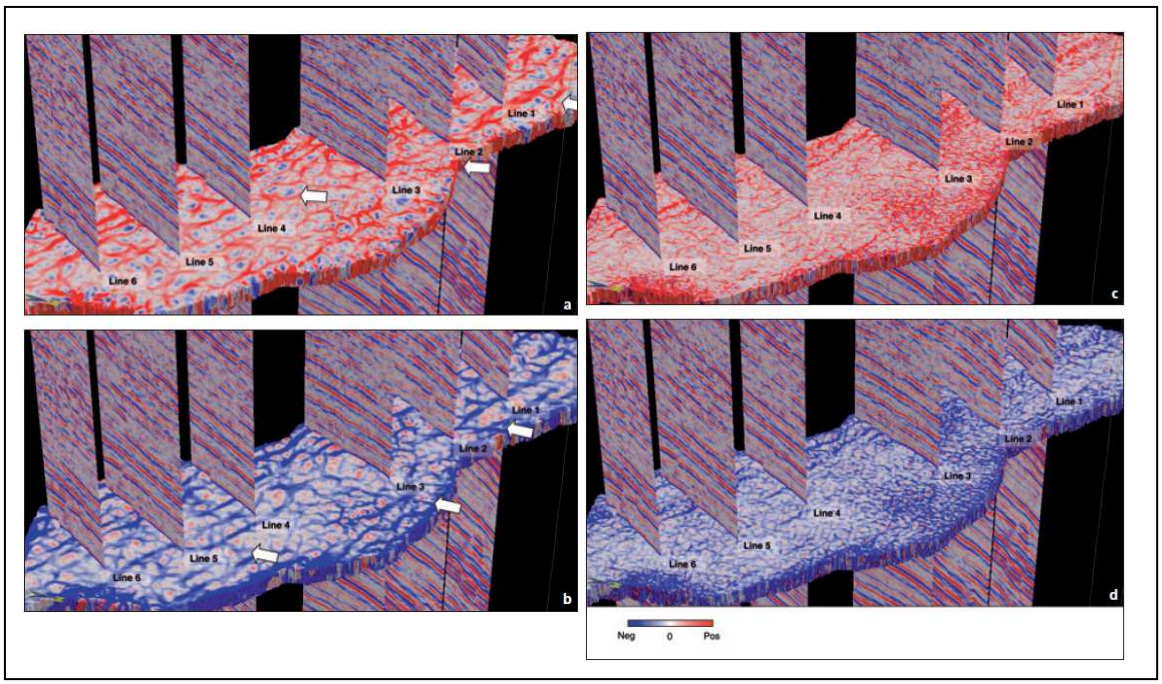

Figure 4-6: Long-wavelength (a) most-positive and (b) most-negative curvature and short-wavelength (c) most-positive and (d) most-negative curvature strat-cubes corresponding to the coherence strat-cube shown in Figure 4-4 (b). The fault/ fracture/flexure lineaments seen on these four images extend and augment the patterns seen in the coherence image in Figure 4-4 (c) (Chopra and Marfut, 2007).

Curvature attributes exhibit detailed patterns for fracture networks that can be correlated with image logs and production data to confirm their authenticity. To do this correlation, the interpreter can manually pick the lineaments seen on the curvature displays for a localized area around the borehole, and then transform these lineaments into rose diagrams comparing them with similar rose diagrams obtained from image logs. Another way is to generate automated 3D rose diagrams from seismic attributes and correlate them with other lineaments seen on the coherence attribute, for example.
If by using these attributes the interpreter establishes fracture orientation and distribution, it is possible to make conclusions about the fracture system origin (the next step in this evaluation sequence), and save resources evaluating logs and cores.

By using these information sources, the geologist is now prepared to make conclusions on the fracture system itself. These are relative to the fracture system origin and the properties that influence the reservoir performance. In the following sections these topics will be discussed in detail.

4.2.2 Fracture System Origin

Understanding the origin of the fracture system has the objective of allowing the interpreter to predict how fractures will be distributed in the rock volume. The input data for this consists of fracture dip, morphology, strike, relative abundance, aperture, and the angular relationships between fracture sets. Full-diameter cores (oriented or conventional), borehole imaging logs (Dipmeter, FMI, CMI), or other less oriented logging tools, can supply this information, which can then be applied to one of the existent geological fracture models allowing the extrapolation and interpolation of fracture distribution. Geological fracture models, which are postulated from the combination of geological and rock mechanics approaches, classify fractures as being: tectonic (fold and/or fault related), regional, contractional (diagenetic) or surface related (Aguilera, 1998; Stearns and Friedman 1972; Nelson 1979). These models assume that natural fracture patterns depict the local state of stress at the time of fracturing, and that subsurface rocks fracture in a manner qualitatively similar to equivalent rocks in laboratory tests performed at analogous environmental conditions. This way, natural fracture patterns are interpreted in light of the laboratory-derived fracture patterns (Handin and Hager, 1957) and in terms of postulated paleo-

stress fields and strain distributions at the time of fracturing. In general, any physical or mathematical model of deformation that depicts stress or strain fields can, by various levels of extrapolation, be used as a fracture distribution model (Hafner, 1951; Ode, 1957; and Lorenz and others, 1993).

Nelson (2001) presents an alternative version to the Stearns and Friedman (1979) model who divides fractures into those observed in laboratory experiments and those observed in outcrop and subsurface settings (Table 4-1).

Table 4-1 – Experimental and Natural Fracture Classification (Nelson, 2001, adapted from Stearns and Friedman, 1979).

Experimental and Natural Fracture Classification
Experimental Fracture Classification
1. Shear fractures 2. Extension fractures 3. Tensile fractures
Naturally Occurring Fracture Classification
1. Tectonic fractures (due to surface forces) 2. Regional fractures (due to surface forces or body forces) 3. Contractional fractures (due to body forces) 4. Surface-related fractures (due to body forces)

The following definitions are simplified from Nelson, 2001 according to Table 4-1. A detailed structural description of each type of fractures will not be made, as this is not the objective of the present work. Emphasis will be given on the occurrence of each type in terms of hydrocarbon production.

Experimental Fracture Classification

1. Shear Fractures: Shear fractures form when all three principal stresses are compressive having a sense of displacement parallel to the fracture plane. They form at some acute angle to the maximum compressive principal stress direction (σ_1) and at an obtuse angle to the minimum compressive stress direction (σ_3) within the rock sample. Potentially, two shear fracture orientations can develop in every laboratory fracture experiment, one on either side of, and oriented at the same angle to σ_1. This is predicted by the Mohr-Coulomb Shear Stress theory.

2. Extension Fractures: These fractures also form when all three principal stresses are compressive and have a sense of displacement perpendicular to and away from the fracture plane. They form parallel to σ_1 and σ_2 and perpendicular to σ_3 (Figure 4-7). In laboratory fracture experiments, extension fractures can and often do form synchronously with shear fractures.

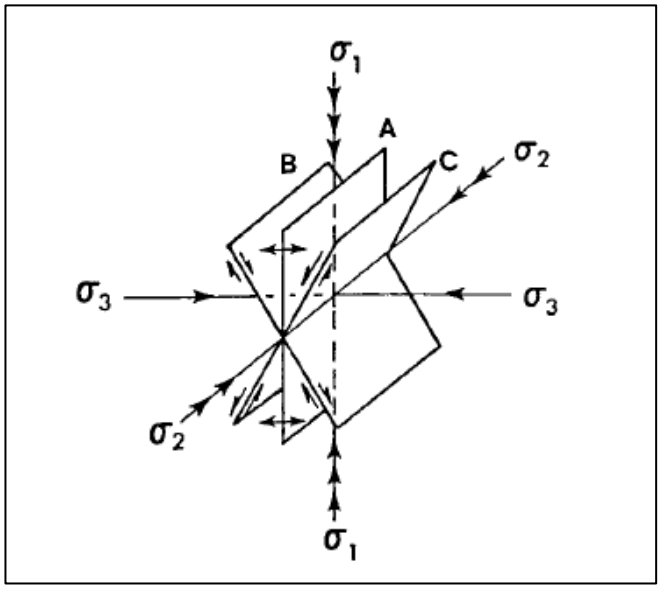

Figure 4-7: Potential fracture planes developed in laboratory compression tests. Extension fractures (A) and shear fractures (B and C) are shown (Nelson, 2001).

3. Tension fractures: Tension fractures also have a sense of displacement perpendicular to and away from the fracture plane and form parallel to σ_1 and σ_2. In terms of orientation of σ_1 and sense of displacement, these fractures resemble extension fractures. However, to form a tension fracture, at least one principal stress (σ_3) must be negative (tensile) while to form an extension fracture, all three principal stresses must be positive (compressive). The distinction between the two is important because rocks have a much lower (10 to 50 times lower) fracture strength in tension tests than they do in extension tests, an observation that becomes important in mathematical prediction of subsurface fracturing. Also, it is likely that true tensile fractures only occur in near subsurface environment, while extension fractures can occur in all low mean stress subsurface conditions.

Geological Fracture Classification

As stated, the geological fracture classification is based on the assumptions that natural fracture patterns (conjugate shear and extension or tensile fractures) reliably depict the local state of stress at the time of fracturing and that subsurface rocks and equivalent laboratory samples fracture in a manner that is qualitatively similar, when tests are performed at analogous environmental conditions. This means that one can consider that natural fracture patterns reflect the same geometry with respect to applied loads as do fractures generated in laboratory experiments and naturally occurring fractures can be classified on the basis of the origin the forces that caused them as determined from laboratory data and fracture system geometry (Table 4–1).

Tectonic Fractures: Tectonic fractures are those whose origin can, on the basis of orientation, distribution, and morphology, be attributed to or associated with a local tectonic event. They are formed by the application of surface forces and form in networks with specific spatial relationships to folds and faults. Historically, most hydrocarbon production has been obtained from tectonic fractures.

a) Fault Related Tectonic Fractures**:** Fault planes are, by definition, planes of shear motion. The majority of fractures developed in relation with faults are the result of the same stress field that caused the fault. These are shear fractures parallel or conjugate to the fault or extension fractures bisecting the acute angle between these two shear directions (Figure 4-8). The intensity of fracturing associated with faulting appears to be a function of lithology, distance from the fault plane, amount of displacement along the fault, total strain in the rock mass, depth of burial, and possibly the type of fault (thrust, growth, etc.) (Nelson, 2001). Which of these parameters will dominate fracture intensity varies from fault to fault.

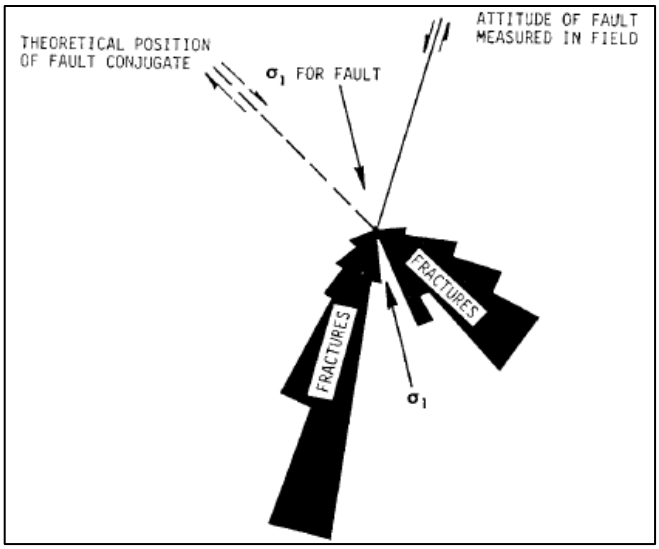

Figure 4-8: Rose diagram of shear fractures associated with normal displacement (Nelson, 2001; after Stearns, 1968b).

b) Fold Related Tectonic Fractures: these types of fractures are very complex, because the way stress and strain act in folds is not as linear as in faults. The best way to present the total fracture geometry is by using Stearns (1964, 1968a, 1968b) work, resumed in Table 4-2.

Table 4-2: Fracture geometry of Folds (Nelson 2001; after Stearns, 1968)

Fracture Geometry of Folds			
Type Set	σ_1	σ_2	σ_3
I	parallel to dip direction parallel to bedding	perpendicular to bedding	parallel to bedding
II	perpendicular to dip direction parallel to bedding	perpendicular to bedding	parallel to bedding
III	(a) perpendicular to bedding	parallel to bedding strike	parallel to dip direction
	(b) parallel to dip direction	parallel to bedding strike	perpendicular to bedding
IV	parallel to bedding	parallel to bedding strike	perpendicular to bedding
V	at an angle to bedding plane (dihedral angle)	parallel to bedding strike	at an angle to bedding plane (90° – dihedral angle)

I associated with bending in strike section
II associated with bending dip section
III associated with bending in cross-section: a. extensional, b. compressional
IV associated with fold-related thrusting
V associated with bedding plan slip

Regional Fractures: regional fractures are developed over large areas of the earth's crust with relatively little change in orientation, show no evidence of offset across the fracture plane, and are always perpendicular to major bedding surfaces (Stearns, 1968a, 1968b, 1972; and Nelson and Stearns, 1977). They differ from tectonic fractures in that they are developed in a consistent and simple geometry, have a relatively large spacing, and are developed over an extremely large area crosscutting local structures. The origin of regional fractures is still dubious but theories ranging from plate tectonics to earth tides (fatigue) have been proposed; however, none have proven conclusive. Presently they are considered as a result of the application of external or surface forces (refer to Lorenz et al., 1993; Engelder and Geiser, 1980 for details).
Regional fracture systems produce hydrocarbons in numerous fields; examples of such are the Big Sandy Field in Kansas and the Altamont-Blue Bell in Uinta Basin, Utah.

Contractional Fractures: This class is a collection of tension or extension fractures associated with a general bulk volume reduction throughout the rock and are a result of: desiccation; syneresis; thermal gradients; or mineral phase changes. Details of these processes are not going to be described as cases of HC production from contractional fractures are not very common except for thermal contraction fractures, which allow storage in rocks such as basalts (ex.: West Rozel Field, Salt Lake, Utah).

Surface Related Fractures: these fractures have not proven to be important in hydrocarbon production to date in other than weathering surfaces. This class includes fractures developed during unloading, release of stored stress and strain, creation of free surfaces or unsupported boundaries, and weathering in general. Surface-related fractures are often developed due to the application of body forces.

4.2.3 Fracture Properties Affecting Reservoir Performance

After determining the origin of the fracture system, it is necessary to understand if they represent an advantage or handicap to the reservoir performance. To do this we need to address the petrophysical properties of the rock-fracture system. The four petrophysical determinations most useful in this evaluation are, in order of increasing difficulty of calculation: fracture permeability;

fracture porosity; fluid saturations within the fractures and the recovery factor expected from the fracture system. These properties are directly dependent on three fracture properties:

- fracture morphology,
- fracture width and permeability,
- fracture spacing.

For determining these, core analysis, well tests and image logs are the best methods. Core analysis is used to determine reservoir quality and performance by summing the individual small-scale elements of the reservoir. Well testing, on the other hand, is used to determine the bulk response of a relatively large volume of the reservoir and is a summary of the relative contribution of all its individual parts. Image log analysis has been used successfully to delineate fracture occurrence and distribution in the wellbore. The quantification of the subsurface reservoir properties such as porosity and permeability of fracture systems by image logs is, however, much more uncertain. For this reasons most authors agree that cores represent the most important source of information.

4.2.3.1 Fracture Morphology

An important factor that determines fracture porosity and permeability is the morphology of the fracture planes, which can be observed in core and outcrop and inferred from some well logs. There are four Basic types of natural fracture plane morphology (Nelson, 2001):

1. Open fractures
2. Deformed fractures
    a. Gouge-filled fractures
    b. Slickensided fractures
3. Mineral-filled fractures
4. Vuggy fractures

1. Open Fractures**:** When the natural fractures are open and have a negligible amount of secondary mineralization the hydrocarbons move from the matrix to the fractures in an unrestricted way. As the name implies, open fractures virtually possess no deformational or diagenetic material filling the width between the walls of the fracture. Permeability of open fractures is a function of:

- the initial fracture width;
- the roughness of the fracture walls;
- the contact area of the fracture walls

} Function of the grain size distribution of the host material

- the *in situ* effective stress component normal to the fracture plane;

In general, open fractures greatly increase reservoir permeability parallel to the fracture plane but will have little or no effect on fluid flow perpendicular to the fracture plane (Figure 4-9).

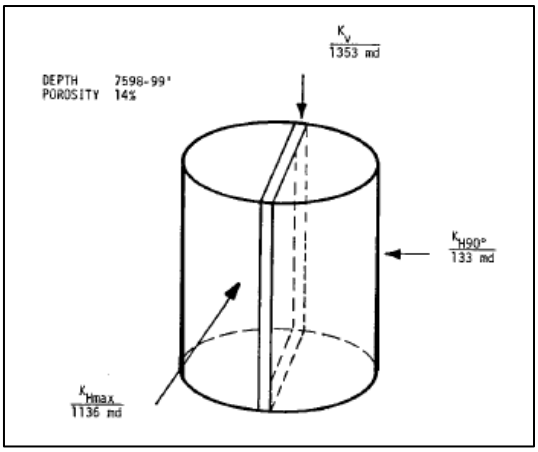

Figure 4-9: Example of 3-D whole-core permeability associated with an open fracture. K= permeability in mili-darcys (md). Notice that K_{Hmax} is parallel to the fracture plane (Nelson, 2001).

2. Deformed Fractures: formed as a relative ductile shear zone or initially open and subsequently physically altered by tectonic shear motions; deformed fractures create strong anisotropy within the reservoir. Two types are considered: gouge-filled (Figure 4-10 and 4-12) (deformation bands) and slickensided (Figure 4-11 and 4-13). Both types reduce the permeability of the fracture.

3. Mineral Filled Fractures: these fractures have been filled or constricted by secondary or diagenetic mineralization. This secondary cement is usually quartz, carbonate, or both. Its effect on permeability depends on the mineralization grade which can be complete or incomplete depending on the diagenetic history of the material (Figure 4-14 and 4-15).

4. Vuggy Fractures: vuggy fractures can have very large porosities and several darcies of permeability. They form when fluid in disequilibrium with the rock matrix enters a low-permeability rock along fracture planes. This causes dissolution, and vugs to form along and

adjacent to the fractures. These vugs are usually restricted to a narrow zone surrounding the fracture channel. Vuggy fractures exist in all types of lithologies. Examples of which are the Bach Ho Field, offshore Vietnam (hydrothermally altered and fractured granitic basement) and the carbonate reservoirs of Iran.

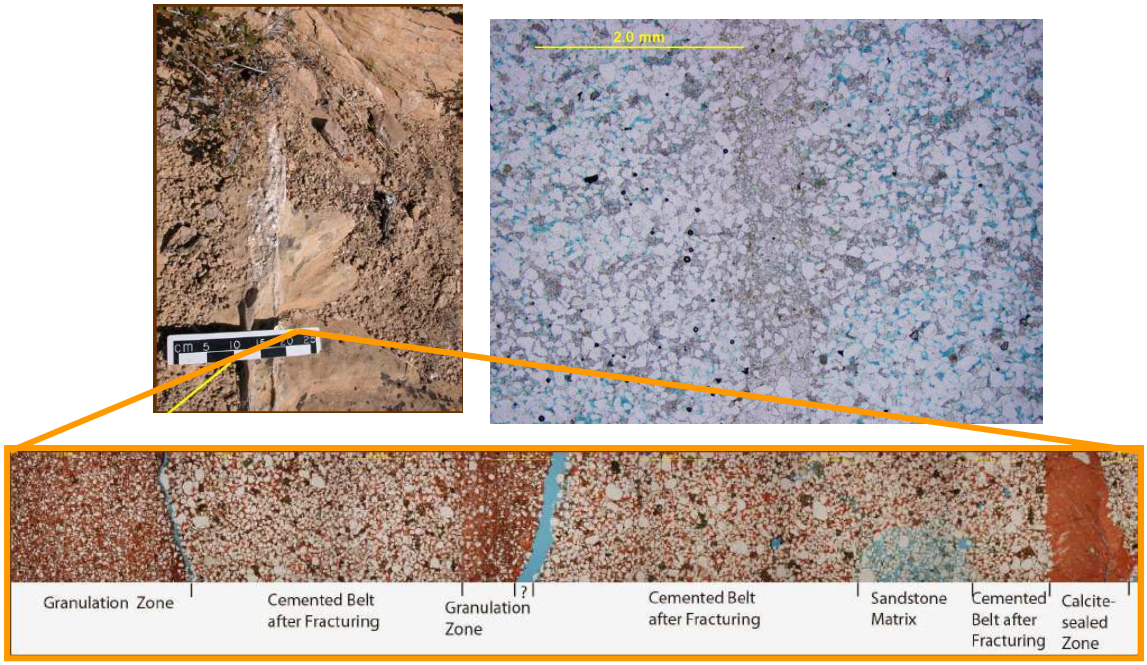

Figure 4-10: Gouge-filled fractures in the Tensleep Sandstones, Wyoming, USA. Source: Peigui Yin & Shaochang Wo, Enhanced Oil Recovery Institute University of Wyoming, http://www.uwyo.edu/eori/_files/misc_download/AAPG-2007-Yin.pdf.

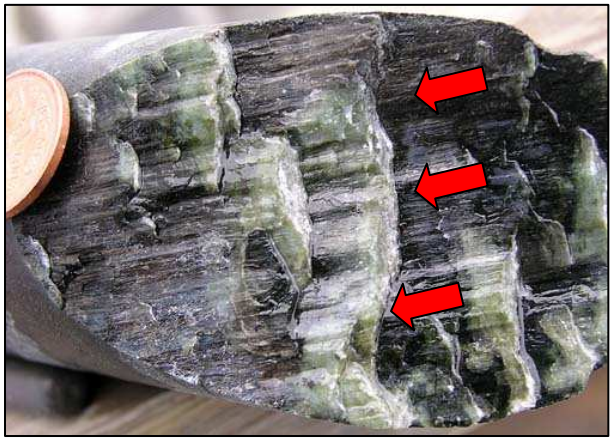

Figure 4-11: sample of diamond-drill core of a peridotite body with slickensided fractures. Source: http://www.turnstone.ca/rom82.htm

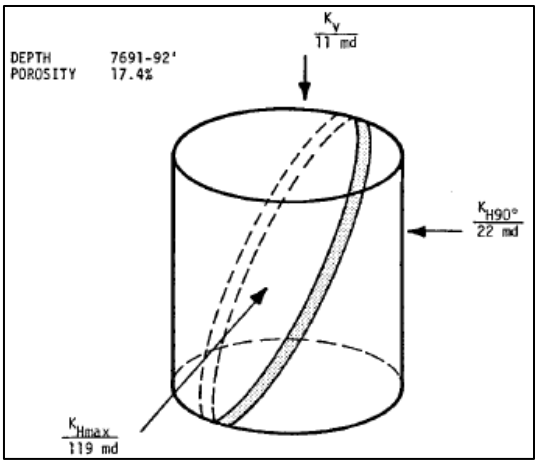

Figure 4-12: Example of 3-D whole-core permeability associated with a gouge-filled fracture. K= permeability in mili-darcys (md). Notice that K_y and $K_{h90º}$ are the lowest values of permeability (Nelson, 2001).

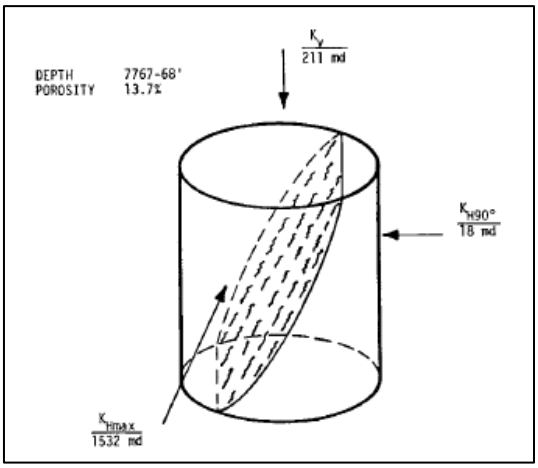

Figure 4-13: Example of 3-D whole-core permeability associated with a slickensided fracture. K= permeability in mili-darcys (md). Notice that $K_{h90º}$ is the lowest value of permeability (Nelson, 2001)

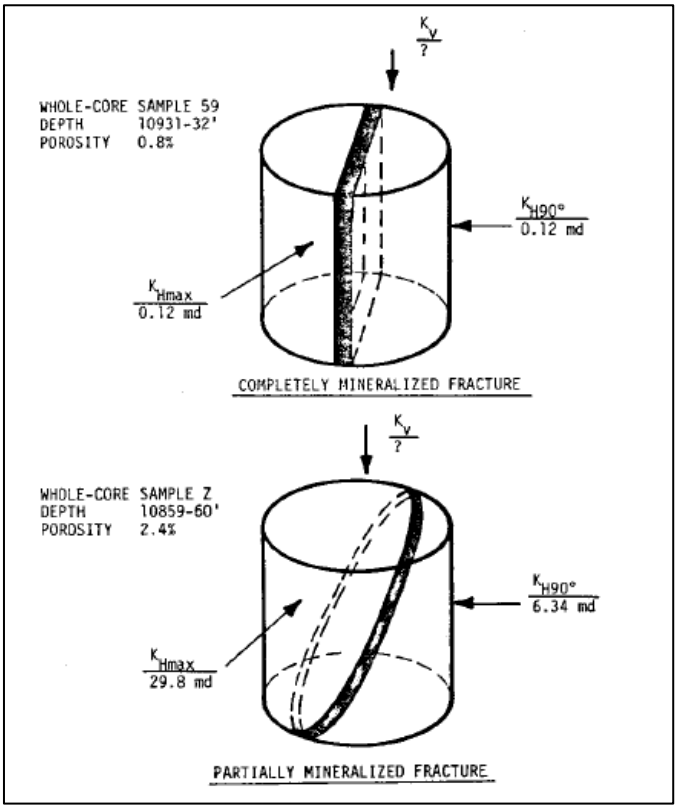

Figure 4-14: Example of 3-D whole-core permeability associated with mineralized fractures. K= permeability in mili-darcys (md). Notice that on the completely mineralized fractures permeability is close to zero in any direction while in partially filled fractures there is some permeability especially in the direction parallel to fracture plane (Nelson, 2001).

Figure 4-15: examples of mineralized fractures. Fibrous mineral growths in fractures generally indicate the direction in which the fracture walls opened with respect to each other. Source: Mineralization and fibers in fractures; University of Oregon Website; http://darkwing.uoregon.edu/~millerm/fiberfracs.html

To summarise, fracture morphology influences the directional permeability of the host rock:

- Open Fractures: increase permeability parallel to fracture plane. Permeability across the open fracture is identical to normal matrix permeability in that direction.
- Gouge-filled Fracture: reduces reservoir permeability across the fracture.
- Slickensided Fracture: creates the largest permeability anisotropy, of all fracture morphologies by increasing permeability parallel to the fracture and decreasing it across the fracture.
- Vuggy: similar to open fractures if diagenetic alteration of the vug walls doesn't occur.

4.2.3.2 Fracture Width and Permeability

The effect of individual fractures on fluid flow is dependent on the character and morphology of the fracture plane. This means that fractures do not always enhance permeability, as in some cases they may act as a barrier to fluid flow.

Despite not being an easy task, there are some indicators that can give the geologist or engineer clues if the fractures present in a rock, play or not an important role in fluid production:

- Direct observation of oil-stained or "bleeding" fracture planes in core samples can indicate fracture control.
- High permeability derived from flow tests in zones of relatively low pressure plug (core-derived) permeability can indicate flow control by natural fractures.

- Fluid flow control can also be revealed by three-directional whole-core permeability analysis (K_{hmax}, K_h90^o, K_v) as explained in the previous section.

The first and general equation for a quantitative description of fluid flow was formulated by Darcy (1856). This equation was derived for laminar, incompressible, single-phase, Newtonian flow in a continuous, homogeneous, porous material. To summarise, Darcy's law is a simple proportional relationship between the instantaneous discharge rate through a porous medium, the viscosity of the fluid and the pressure drop over a given distance (Figure 4-16).

Despite being a good approximation for fluid flow across a porous medium, Darcy's law could not be applied to flow along a fracture. Therefore, the theory of parallel flow was developed. Here, flow is assumed to occur between two smooth parallel plates separated by a distance *e* (Figure 4-17).

The next logical step was to combine both equations (Darcy's and parallel plates fluid flow), which was made by Parsons (1996). The resulting equation is resumed in Figure 4-18, and it is considered to be a good approximation of total reservoir flow for subsurface reservoirs prior to production (Nelson, 2001 and Jones, 1975). This equation assumes that flow across the fracture/matrix surface does not alter the flow of either system, which is true for rocks of either high or near nonexistent matrix permeability. This means that, if matrix permeability is high, that same matrix will respond individually to the overall pressure gradient rather than to the relative pressure drop of the fracture. If, alternatively, the matrix permeability is close to being null, cross-flow becomes unimportant. In a rock of relatively low or intermediate matrix permeability, cross-flow becomes more important and Parsons Equation becomes a poorer approximation of the total flow. There are alternative approximations, but their complexity and the fact that Parson's Equation has shown successful in laboratory experiments leads to the conclusion that it is an apt semi-quantitative representation of fractured reservoir flow for use in exploration.

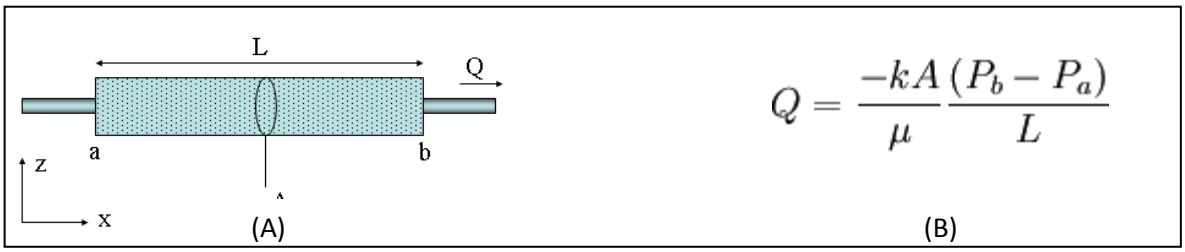

Figure 4-16: Diagram (A) and formula (B) of Darcy's Law (1856) which states that the total discharge, Q (units of volume per time, e.g., m^3/s) is equal to the product of the permeability of the medium, k, the cross-sectional area to flow, *A* (units of area, e.g., m^2), and the pressure drop (Pb-Pa), all divided by the viscosity, μ (Pa.s) and the length over which the pressure drop is taking place over. The negative sign in *k* is essential because fluids flow from high pressure to low pressure. So if the change in pressure is negative (where $P_a > P_b$) then the flow will be in the positive 'x' direction.

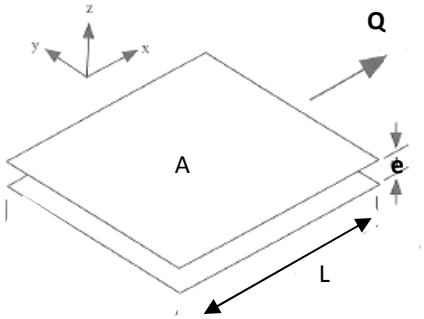

$$\frac{Q}{A} = \frac{e^3}{12D}\frac{dh}{dl}\cdot\frac{\rho g}{\mu}$$

Figure 4-17: formula and diagram for parallel plate flow. Where: Q= total discharge (m^3/s); A= cross sectional area to flow (m^2); e = distance between plates (mm, cm, etc.); dh/dl = (Pb-Pa)/L = pressure drop over the length pressure drop is taking place; D= fracture distance, the average distance between parallel regularly spaced fractures (mm, cm, etc.); ρ= fluid density (g/cm^3); g= acceleration gravity; μ= fluid viscosity (Pa·s =kg/(s·m)).

$$k_{fr} = k_r + \frac{e^e \cos^2\alpha}{12D} \qquad k_f = \frac{e^2}{12}\cdot\frac{\rho g}{\mu}$$

(A) (B)

Figure 4-18: Parsons equations for fluid flow in a fractured rock (Parsons, 1966). (A): Equation for permeability of the fracture plus intact rock system, $k_{fr.}$ (B): equation for permeability of a fracture, k_f. This equation assumes that flow is laminar between smooth, non-moving, parallel plates, that fluid flow across any fracture/matrix surface does not alter the flow of either system, and that the fractures are homogeneous with respect to orientation, width, and spacing. Where:
e = distance between plates or aperture (mm, cm, etc.); D= fracture distance, the average distance between parallel regularly spaced fractures (mm, cm, etc.); ρ= fluid density (g/cm^3); g= acceleration gravity; μ= fluid viscosity (Pa·s =kg/(s·m)); kr = permeability of the intact-rock; α = angle between the axis of the pressure gradient and the fracture planes

4.2.3.3 Fracture Spacing

Fracture spacing can be directly quantified by observation of outcrops, wellbore and cores and does not change when the reservoir is perturbed. However, the quantification is complicated due to the small size of subsurface sampling methods (core and wellbore observations) with respect to the fracture spacing or matrix block size.

The definition which is mostly used in theoretical fracture permeability equations, considers that fracture spacing is defined as the average distance between regularly spaced fractures measured perpendicular to a parallel set of fractures of a given orientation (Parsons, 1966). This definition allows the calculation of fracture spacing by counting the number of fractures along a line of some given length perpendicular to the fracture set of interest, for each of the fracture sets present and dividing by the length of measurement line (Nelson, 2001). This calculation is similar to what modern FMI tools automatically operate.The effect of fracture spacing on both fracture porosity and permeability is shown in Figures 4-19, 4-20 and 4-21.

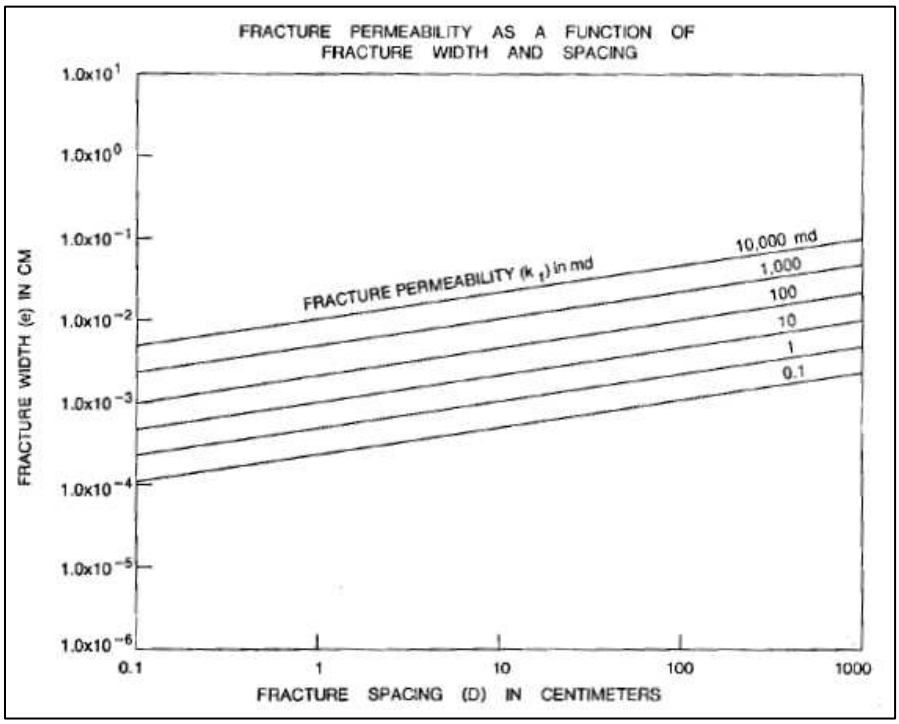

Figure 4-19: Fracture permeability as a function of fracture width and fracture spacing. Notice that for a given spacing, permeability increases with fracture width (Nelson, 2001)

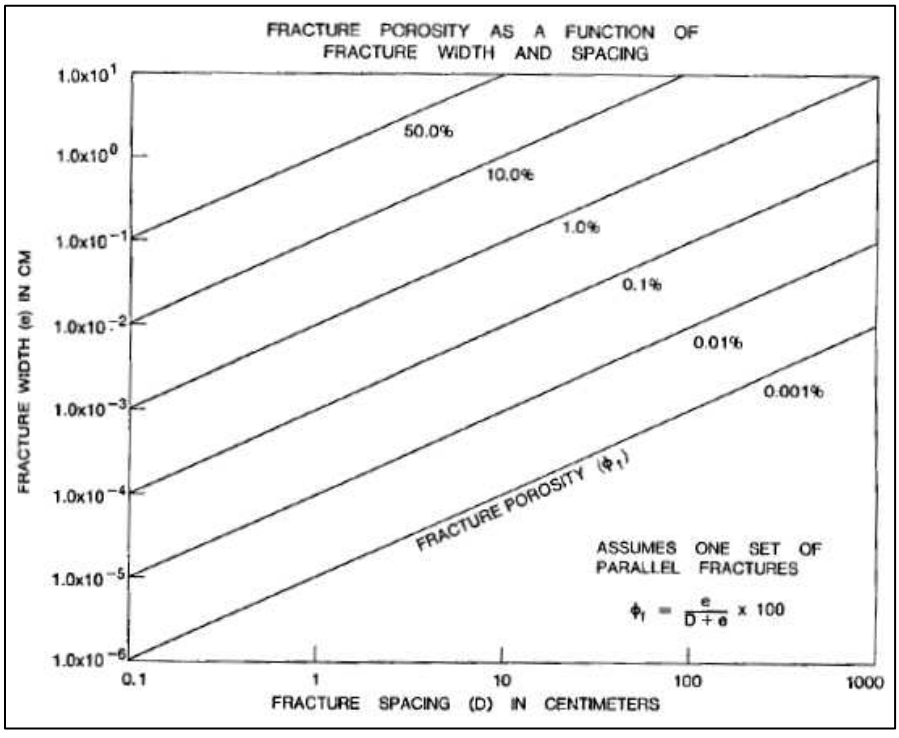

Figure 4-20: Fracture porosity as a function of fracture width and fracture spacing. Notice that for a given spacing, porosity increases with fracture width (Nelson, 2001)**.**

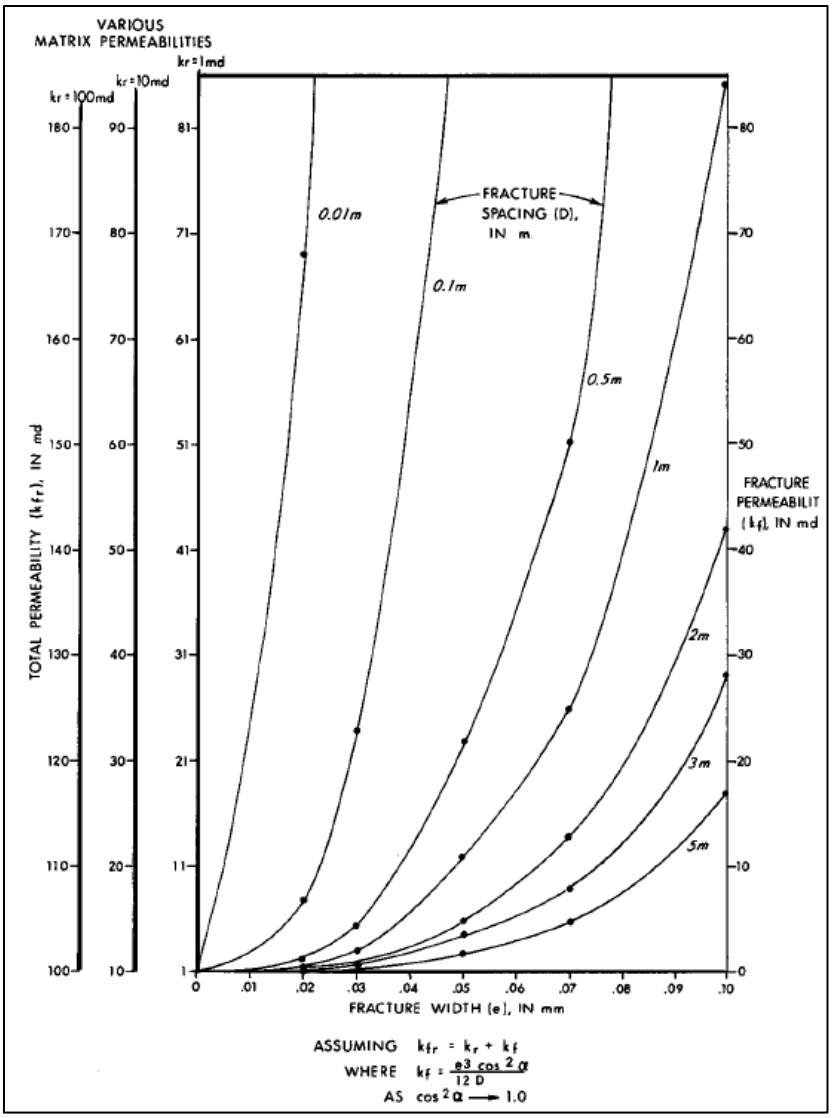

Figure 4-21: Graphic of Parsons equation, which depicts total formation permeability as a function of fracture width, fracture spacing, and matrix permeability. Nelson, 2001

4.2.4 Fracture and Matrix Interaction – Porosity Communication

Reservoirs in which fractures play a significant role must be treated as a dual-porosity system – one system is the rock matrix, and the other the fractures. What is important to understand is the relation between these two systems, i.e. how flow communication between the fractures and the matrix occurs and how it will condition reservoir productivity. Like matrix porosity, fracture porosity is the percentage of a particular void volume in a rock mass compared to its total volume. The difference lies in the fact that in fracture porosity only those voids occurring between the walls of fractures are considered. Matrix porosity, on the contrary, accounts for all voids within a

rock other than those within fractures. The two basic relationships used to calculate fracture porosity and matrix porosity are presented below (Figure 4-22):

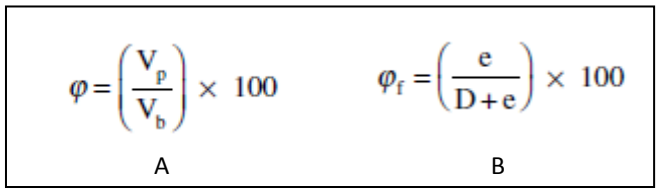

Figure 4-22: mathematical formulas for matrix (A) and fracture (B) porosity calculation. Where: V- volume of pores (other than fractures; Vb- bulk volume; D- average spacing between parallel fractures; e-average effective width of fractures.

Some characteristics of fracture porosity are:

- Relative small increases in fracture porosity have great influence in permeability parallel to fracture because of the high interconnectivity of fractures.
- Fractures compress or reduce in porosity and permeability much more readily than the matrix when subjected to external stress increases (below the yield point) due to either increasing depth of burial or reservoir depletion.
- Fracture porosity is generally a small number compared to “normal” matrix porosity. Most fractured reservoirs have fracture porosities less than 1% (Nelson, 2001).

Fracture porosity estimations can be made by:

1. Core analysis
2. kf/φf relationship
3. Field determinations
4. Logs
5. Multiple well tests

Only core analysis, logs and well tests will be approached here in more detail. For further reading please refer to Nelson, 2001.

Core analysis: despite the fact that larger volumes of rock are sampled when whole cores are taken, fracture porosity calculation is determined by the orientation and spacing of the fractures

relative to the direction and diameter of the core. For that reason it is important to try to determine general fracture orientation before collecting a whole core.

Logs: There is no direct method for calculating fracture porosity from well logs. Several authors have developed methods to detect natural fracture systems through logs (Aguilera and van Poollen, 1977; and Aguilera, 1995), but none can calculate φ_f directly. Presently, the image tools allow for this calculation by recording not only the fractures orientation but also their aperture and intensity (density) which can be used for fracture porosity calculation. However, as the tools have a limited radius of investigation within the formation, fracture porosity values cannot be considered absolute. See the Appendix for more details.

Well Test Analysis: Pulse tests and transient pressure analysis (see Appendix for details), can be used for φ_f calculation. However, they require close-spaced wells for testing and are usually only applicable in well-developed areas where production can be ceased in several wells long enough to perform the tests. Well test analysis is further discussed ahead.

Note: Modeling for NFR's will be presented in Section 5 as part of the implementation of the workflow for SEAL Basement Fractured Reservoir.

4.2.5 Reservoir Classification

Once fracture origin, fracture properties affecting reservoir performance and fracture/matrix interaction has been defined, we can classify the reservoir which we are dealing with. This classification is done on the basis of what positive effects the fracture system provides to overall reservoir quality. Nelson (2001), based on Hubbert and Willis (1955) classification proposes the following classification (Figure 4-23):

- **Type 1:** Fractures provide the essential reservoir porosity and permeability.
- **Type 2:** Fractures provide the essential reservoir permeability.
- **Type 3:** Fractures assist permeability in an already producible reservoir.
- **Type 4:** Fractures provide no additional porosity or permeability but create significant reservoir anisotropy (barriers).

From these four types of reservoir, those classified as Type 1, are those where fractures play the most important role, by providing both porosity and permeability. For this reason an early

calculation of fracture porosity or fracture volume existent per well is essential, so that total reserves are calculated, and to predict if initially high flow rates will be maintained or will drop rapidly with time.

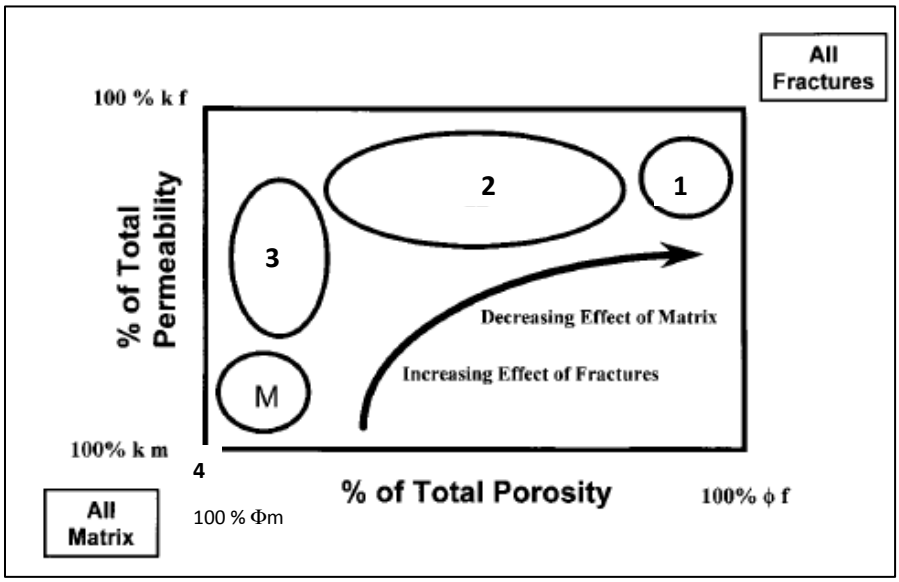

Figure 4-23: A schematic cross plot of percent reservoir porosity versus percent reservoir permeability (percent due to matrix versus percent due to fractures) for the fractured reservoir classification used by Nelson, 2001. Reservoir type IV is outside the box because fractures provide no additional porosity or permeability but create significant reservoir anisotropy. M = matrix.

For these estimations, fracture width and fracture spacing values are crucial. For reservoirs of Type 2 and 3 accurate fracture porosity calculations are much less important because the fracture system only provides permeability (porosity or storage volume is given by the matrix). In these later cases, the matrix pore volume is usually several orders of magnitude greater than fracture volume and overshadows it so much that early calculations of fracture porosity are not important. However it is important to understand how fractures and matrix interact to predict if the fluids stored in the matrix porosity can be drained through the fractures. Each of these categories has its particularities, which are better described if we use a table, where examples of each reservoir type are also shown – Figure 4-24 and Tables 4-3 and 4-4.

One characteristic of fractured reservoirs is that each is a particular case, meaning that even if they are of the same Type, they can have very different exploration and production stories. One example of such difference is the Edison Field in California and Big Sandy in Kentucky (Nelson, 2001). Both are Type 1 reservoirs, but in Edison Field the fractured Jurassic schist has a 395 m thick section of producing tectonic fractures formed over a structural high, over an area of 28

km^2; while Big Sandy Devonian shale, despite having variable thickness, is spread over an area of 2600 km^2 and the fracture system is believed to be of regional origin. As it can be seen from Table 4-4, the difference in reserves between these two shallow, low-pressure fields is dramatic. The explanation for such difference is in the horizontal area of the fractured reservoir and in the type of fractures found. In Edison, fractures are related to the development of the structural high. As such, the fractures are restricted to the size of that structure (7,090 acres). At Big Sandy, however, the regional fractures crosscut numerous structures and consequently the area of fracture development is very large (650,000 acres). Regional fractures will by definition be developed over much larger areas than tectonic fractures, thus giving the potential for larger reserves in Type 1 fractured reservoirs.

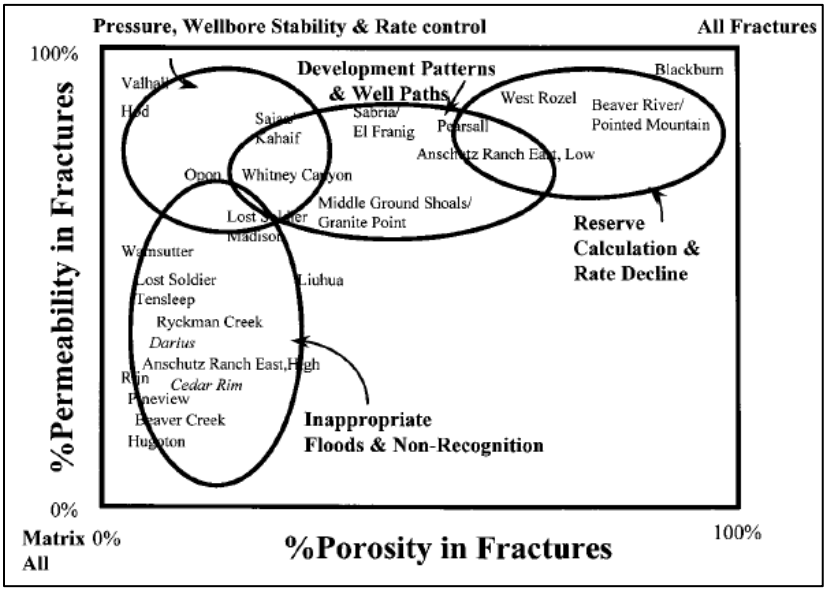

Figure 4-24: Visual representation of the fractured reservoirs classification, with the fractured reservoirs presented in Table 4-3 displayed. Also shown are production and evaluation problems encountered as a function of fractured reservoir type and relative position on this diagram (Nelson, 2001).

Table 4-3: positive attributes and potential problems of fractured reservoirs by reservoir type. Notice that each reservoir Type has its own particularities, due to the different relation between fractures and the matrix (adapted from Nelson, 2001).

Reservoir	Fracture/Matrix Interaction	Positive Reservoir Attributes	Pontential Problems
Type 1	Fractures Provide Essential Porosity and Permeabilily	Drainage areas per well are large Few wells needed in development (in-fill for rate acceleration only) Good correlation between well rates and well reservoirs Best wells are often early Generally high Initial Potentials (IPs) Can produce from nonstandard and nonreservoir quality rocks	Often a rapid decline curve Possible early water encroachment Size and shape of drainage area is difficult to determine Reserve calculations difficult to constrain Many development wells add rate but not additional reserves
Type 2	Fractures Provide Essential Permeability	Can develop low permeability rocks Often higher than anticipated well rates Hydrocarbon charge often facilitated by fractures	Poor fracture and matrix porosity communication leads to poor matrix recovery and disastrous secondary recovery Possible early water encroachment (production rates may need to be controlled) Fracture intensity and dip critical Development pattern must be tailored to the reservoir Recovery factor difficult to determine and quite variable Fracture closure in overpressured reservoirs may occur
Type 3	Fractures Provide a Permeability Assist	Reserves dominated by matrix properties Reserve distribution fairly homogeneous High sustained well rates Great reservoir continuity	Highly anisotropic permeability Often unusual response in secondary recovery Drainage areas often highly elliptical Often interconnected reservoirs Correlation between log/core analysis and well test/performance often poor
Type 4	Fractures Create Flow Barriers		Reservoir compartmentalization Wells underperform compared to matrix capabilities Recovery factor highly variable across the field Permeability anisotropy opposite to other adjacent fractured reservoirs of other fracture types

Table 4-4: Examples of producing oil and gas fields by reservoir type. MMBO= million of barrels of oil. Notice that the largest reserves stand in Type 3 reservoirs that account for some of the largest fields in the world. Fractures here give the voluminous flow rates, which make these fields so economic (flow rates often in excess of 100,000 barrels of oil per day [BOPD]). Type 2 reservoirs have also large reserves when compared to Type 1, which reflects the larger storage volume associated with matrix porosity (up to 20–30 percent in the matrix as opposed to up to 1–2 percent in the fractures). The smallest volumes of HC are encountered in Type 1 reservoirs, being the largest known field of this type, the Amal field in Lybia. Here the reserves are substantial due to its large thickness and very large aerial extent (100,000 acres, 800 ft. thick), as the fracture porosity is close to 1.7% and the matrix has no porosity. Adapted from Nelson,2001.

Reservoir	Example Fields	Location	Reserves (MMBO)	Age and Lithology	Formation
Type 1	Amal	Libya	1700	Cambrian quartzite	Amal Fm.
	Ellenburger Fields	Texas	107.8	Devonian dolomite	-
	Edison	Califórnia	42	Jurassic basement Schist	-
	Wolf Springs	Montana	5.4	Pennsilvanian cherts and dolomites	Amsden Fm.
	Big Sandy	Kentucky/West Virgínia	3 (TCF)	Devonian shale	Big Sandy Fm.
Type 2	Agha Jari	Iran	9500	Miocene/Pliocene clastics	Agha Jhari Fm.
	Haft Kel	Iran	2660	Oligocene limestones	Asmari Fm.
	Rangeley	Colorado	600	Cretaceous sand bodies within a shaly formation	Mancos Fm.
	Spraberry	Texas	447	Siltstones	Bone Spring/Wolfcamp Fms.
	Altamont-Bluebell	Utah	250	Eocene Siltstones	Green River Fm.
	Sooner Trend	Oklahoma	70	-	-
	La Paz/Mara	Venezuela	800	Basement igneous and metamorphic rocks	-
Type 3	Kirkuk	Iraq	15000	Oligocene limestones	Asmari Fm.
	Gachsaran	Iran	8000	Oligocene, Campanian and Albian limestones	Asmari, Khami Fms.
	Hassi Messaoud	Algeria	6000	Cambrian Sanstones	Hassi Messaoud Fm.
	Dukhan	Qatar	4570	-	-
	Cottonwood Creek	Wyoming	182	Permian sandstones	Phosphoria Fm.
	Lacq	France	8.8 (TCF)	Turonian to Aptian limestones	-

4.2.6 Seismic Acquisition for Fractured Reservoirs

During a 3D seismic survey, the main objective is that every subsurface point at the target is properly illuminated and has reflected seismic energy with a uniform distribution of source receiver offsets, azimuths and incidence angles. Similar to a photographic session in a studio, several light sources are required to fully illuminate the subject being photographed so that an unblemished and uniformly high resolution image may be possible to capture. The big difference between a photographic session and seismic acquisition is that in the later there is a continuously variable medium in all directions – Earth. This causes energy not to propagate equally in all directions and in many cases the effects of the Earth's materials cause such influence in wave propagation that targets cannot be imaged coherently.

Fractured reservoirs are an example of a rock medium that causes directional differences in the velocity, amplitude, reflection waveform as well as in the phase of the seismic energy. If a normal seismic acquisition campaign (Narrow-Azimuth) is implemented, and the inline direction is about parallel to the direction of the faults or fractures for example, the final image can be poor. To try to solve that problem most surveys try to adjust the inline direction perpendicularly to the main structural direction, i.e. perpendicularly to the main faults strike or to the fold hinges. The problem arises when those directions are not clearly known or when there are several structural trends caused by differently oriented stresses. In such cases Wide-Azimuth seismic acquisition might be a solution.

The distinction between narrow and wide azimuth surveys is made on the basis of the aspect ratio of the recording patch. The aspect ratio is defined as the cross-line dimension of the patch divided by the in-line dimension. Recording patches with an aspect ratio of less than 0.5 are considered narrow azimuth, while recording patches with an aspect ratio of greater than 0.5 are wide azimuth (Figure 4-25). Wide-Azimuth acquisition is considered superior to narrow-azimuth in the aspects of image resolution, coherent noise attenuation as well as in other characteristics mentioned below, and that are directly related to fracture imaging (Cordsen and Galbraith, 1999):

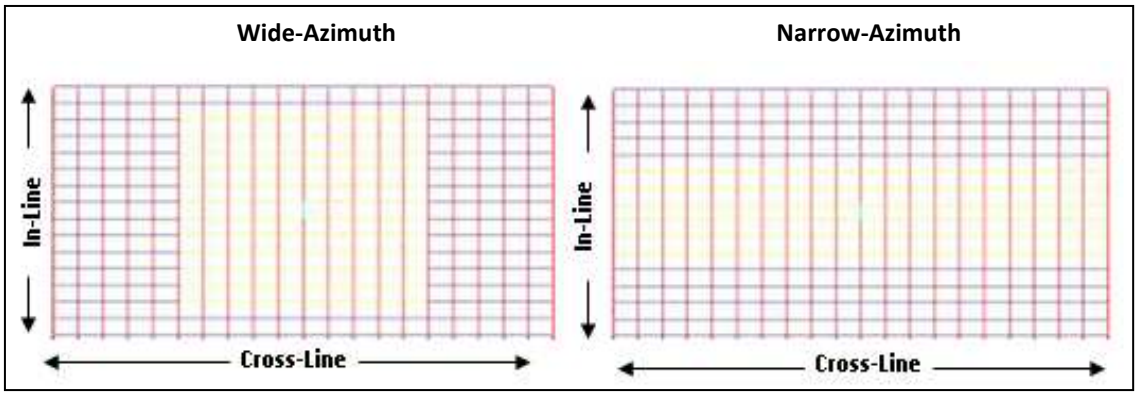

Figure 4-25: Example of Wide-Azimuth VS Narrow- Azimuth patches. Wide-Azimuth patch consists of 12 lines with 60 stations per line, and Narrow-Azimuth patch of 6 lines with 120 stations each (Cordsen and Galbraith, 1999).

Imaging: By using single fold 3D data sets with limited extent (e.g. a cross-spread or a shot gather) Vermeer, 1999, proved that the resolution was dependent on the position of the output point with respect to the centre of the data set. This way, by limiting the extent in one direction (cross-line) it was possible to obtain different resolutions in the in-line and cross-line directions. Combining such data sets did not change these resolution properties. The final combined result therefore shows variations in resolution that depend on the period of overlap of the data sets and the in-line and cross-line offsets of the basic data set (e.g. shot). Clearly the best results are obtained from a square patch (equal in-line and cross-line offsets), which is the configuration closer to the wide-azimuth patch. Spatial continuity can be enhanced by maximizing the extent of the basic data set in all directions.

Another consideration is that a 3-D shot recorded by a wide patch receives more widespread signal (specular reflections) than a narrow patch. Thus for areal geometries, a wide patch forms more consistent (artifact free) images than a narrow

Azimuths: The azimuth dependent trace count proves the more even distribution of source receiver pairs for the wide patch (Figure 4-26). The rose diagram (Figure 4-27), where colour indicates the multiplicity of the occurrence of a particular source–receiver pair (in offset and azimuth distribution), is extremely focused for the narrow azimuth patch, and shows that for the wide patch the source-receiver pairs are much more distributed.

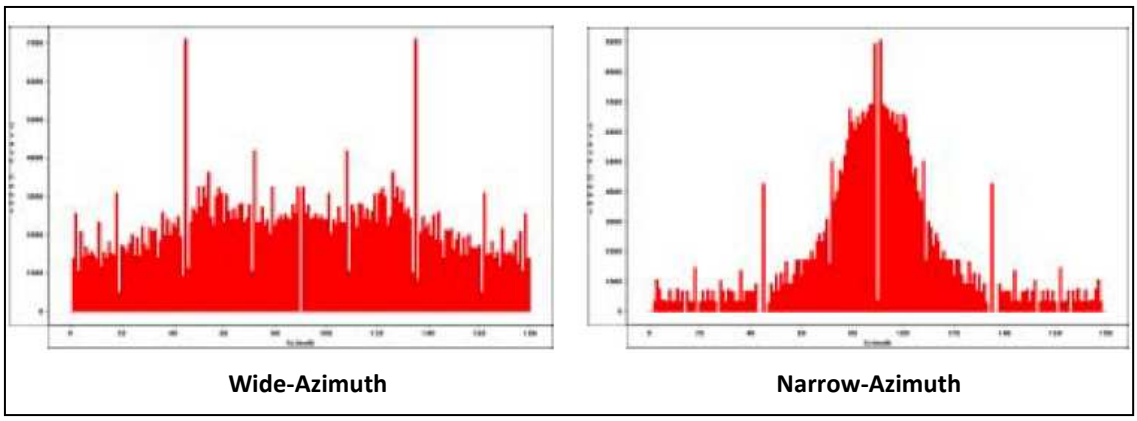

Figure 4-26: distribution of traces relative to the azimuths. Notice the more even distribution of source receiver pairs for the wide patch (Cordsen and Galbraith, 1999).

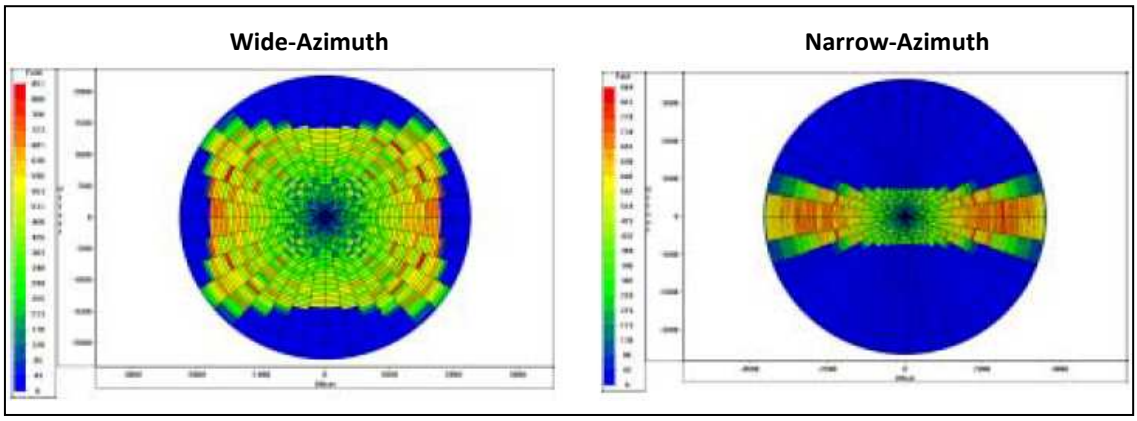

Figure 4-27 rose diagrams showing how the wide-azimuth acquisition covers a larger range of azimuths than narrow-azimuth (Cordsen and Galbraith, 1999).

AVO: If azimuthal anisotropy is present in an AVO response, for example in a fractured rock (with variable oriented fractures) a narrow patch would merely give consistent AVO measurements in one direction of the survey and not measure the anisotropy in other azimuths. Therefore anisotropy (which means AVO response due to some fractures with certain orientations) might go undetected with a narrow azimuth patch. These cases of anisotropical AVO's may require higher fold so that there is sufficient fold in each azimuth slice for reliable AVO estimation. Only a wide patch would allow such operation.

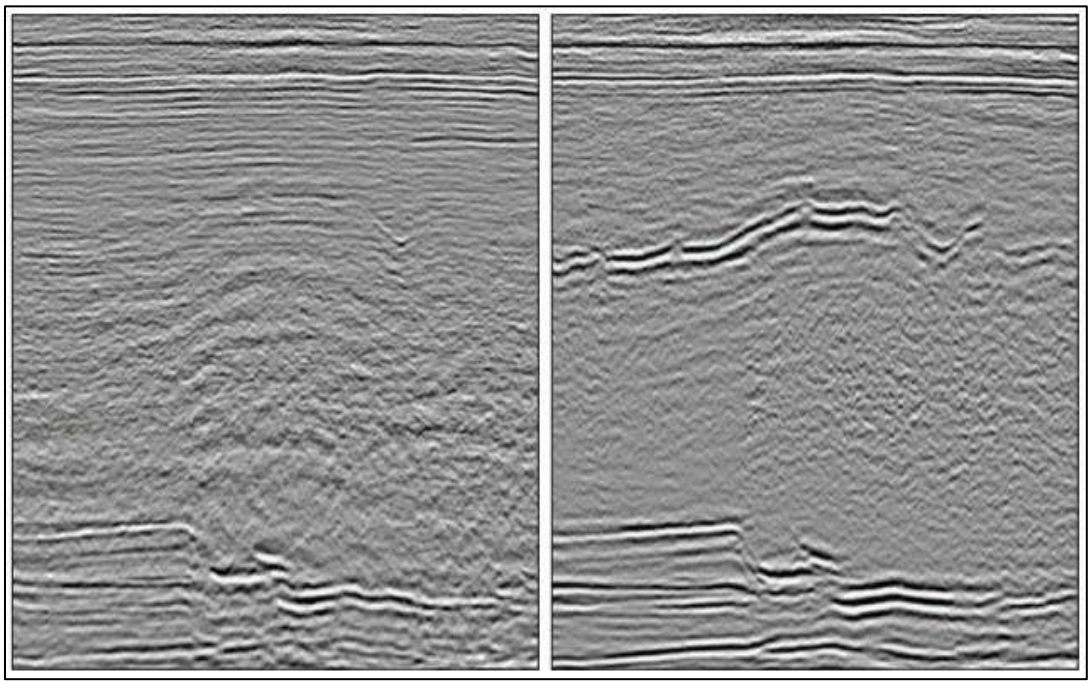

Figure 4-28: Southern Oman narrow-azimuth acquisition with recent reprocessing (left) compared to new-generation high-density wide-azimuth acquisition, processed with the latest true-3D WAZ algorithms (right). This enormous improvement in image quality has allowed new prospects to be identified in the carbonates (bottom of section) and the top of salt to be clearly interpreted (middle of section). Source: CGG Veritas

Wide-Azimuth for fracture detection

It is widely known that in naturally fractured reservoirs, permeability and therefore production can be controlled by fracture networks. These fractures are typically small, sub-vertical and well below the resolution of the seismic, so they are not directly observable (SEAL case). However, the cumulative effect of these small aligned fractures is measurable through the azimuthal variation of seismic attributes. Attributes, such as amplitude, velocity and impedance, can be correlated with available fracture data from wells. Literature often mentions the direct relationship between the magnitude of azimuthal anisotropy, fracture intensity and permeability. This can be used to derive seismic based fracture intensity estimates across fields. As it was stated previously, only wide-azimuth seismic is capable of dealing with situations like these. Seismic azimuthal anisotropy analysis can either be performed for specific horizons, or volumetrically for a much larger subsurface interval. The results can be visualized in a number of ways, and displays using anisotropy vectors are particularly intuitive, making them a powerful tool for interpretation (Figure 4-29).

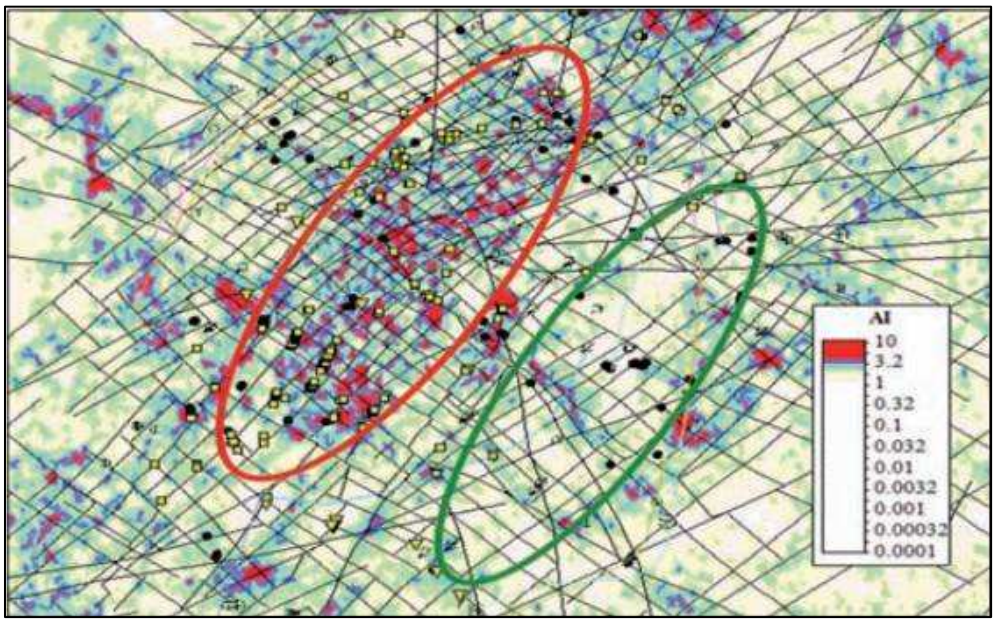

Figure 4-29: Normalized azimuthal amplitude anisotropy intensity map (left) with overlay of interpreted faults in black. Well data is shown with the mud-loss points in yellow indicative of permeable fracture zones. Outlined in red is the known conductive fracture corridor which correlates with high anisotropy intensity values and in green an area of low fracture intensity. Without the use of Wide-Azimuth acquisition it would not have been possible to produce such map. Source: CGG Veritas.

Despite allowing for better imaging (Figure 4-28) it is true that a wide-azimuth survey is more expensive than a narrow azimuth due to all of the acquisition structure that is needed to do it. But it is also true that it will add much new information. This means that the information VS cost equation needs to be considered having in mind that any information is only useful if its value is greater than its cost. There is always pressure on saving money but this must be balanced against the need to solve the problem. It is also important to remember that acquisition costs are greater than processing costs, and that technical advances in processing can get more out of the data. However processing does not make miracles. If the data is not acquired properly and imaging is not good, not even the best processing technology will solve the problem. At the end the reality is that "the most expensive 3-D seismic acquisition is one that does not meet its objectives" (Cordsen and Galbraith, 1999).

4.2.7 Seismic Processing For Fractured Reservoirs

Seismic acquisition is not a zero-offset operation, i.e. source and receivers are at different locations, rock layers are not flat and, unlike sonar, the seismic energy is not directed in the Earth. Hence, when a geophysicist views the recorded energy from the receiver, he can only view the energy that was recorded at that location, but has no way of determining where it came from in the subsurface. Because of this, seismic data needs to be processed to create an accurate image of the subsurface. Apart from the processing steps to suppress noise and enhance signal and resolutuin, such as filtering and deconvolution, there is the need to geometrically correct the data, i.e., geometrically reposition the returning signals to show an event where it is being hit by the seismic wave rather than where it is being recorded– this process is called migration. Migration improves the spatial disposition of the reflecting layers and hence achieves 'Imaging'. There are two main types of migration: Post-Stack Migration and Pre-Stack Migration.

Post-Stack Migration: Post-stack migration is the migration done on stacked section (traces are stacked before migration) as indicated by its name. This migration is based on the idea that all data elements represent either primary reflection or diffractions. This is done by using an operation involving the rearrangement of seismic information so that reflections and diffractions are plotted at their true locations.

Pre-Stack Migration: When the subsurface structure is complex, with significant dip variations, and velocity variation is also complex, reflection events are not hyperbolic and the stacking process does not work very well. Therefore, post stack migration will not give clear results. Pre-stack migration, as the name suggests, is done on pre stack data i.e. on CMP gathers and can be done in time or depth domain.

Pre-stack migration is applied only when the layers being observed have complicated velocity and dip profiles, or when the structures are just too complex to see with post-stack migration. It is an important tool in modelling salt diapirs because of their complexity and this has immediate benefits if the resolution can pick up any hydrocarbons trapped by diapirs.

Pre-stack migration is applied to avoid amplitude distortions due to CMP smearing and non-hyperbolic move out. Hence, Pre-stack Time or Depth migration is a valuable tool in imaging seismic data. In the past, the main constraints on prestack migration were the computation

requirement the time and skill required to construct velocity model within a reasonable time. Advances in computing technology and formation of new migration algorithms have eased these constraints.

Pre-Stack Migration VS Post-Stack Migration – Fractured Basement Case

When the subsurface structures are simple, post-stack migration works well. But post-stack migration is not faithful in areas with complex geology and complex variations in velocities. Pre-stack migration is a better imaging tool which works quite well in areas with complex structures and complex velocities.

Relative to the Fractured Basement in Cuu Long Basin, Vietnam, Huy Ngoc and Quoc QuanThe (2011), state that applying state of the art "*acquisition and processing technology such as Kirchhoff and Beam Anisotropic Pre-stack Depth Migration could provide good imaging not only for top of the basement but also for faults inside the basement".* Also in the website of Japan Oil, Gas and Metals National Corporation (http://www.jogmec.go.jp), it is clearly stated that "*PSDM is a model-based seismic imaging methodology that works well for complex geological structures such as subsalt layers and basement fractures".*

The above examples prove that using Pre-Stack Migration, especially in Depth domain largely improves seismic imaging for Fractured Basement contexts.

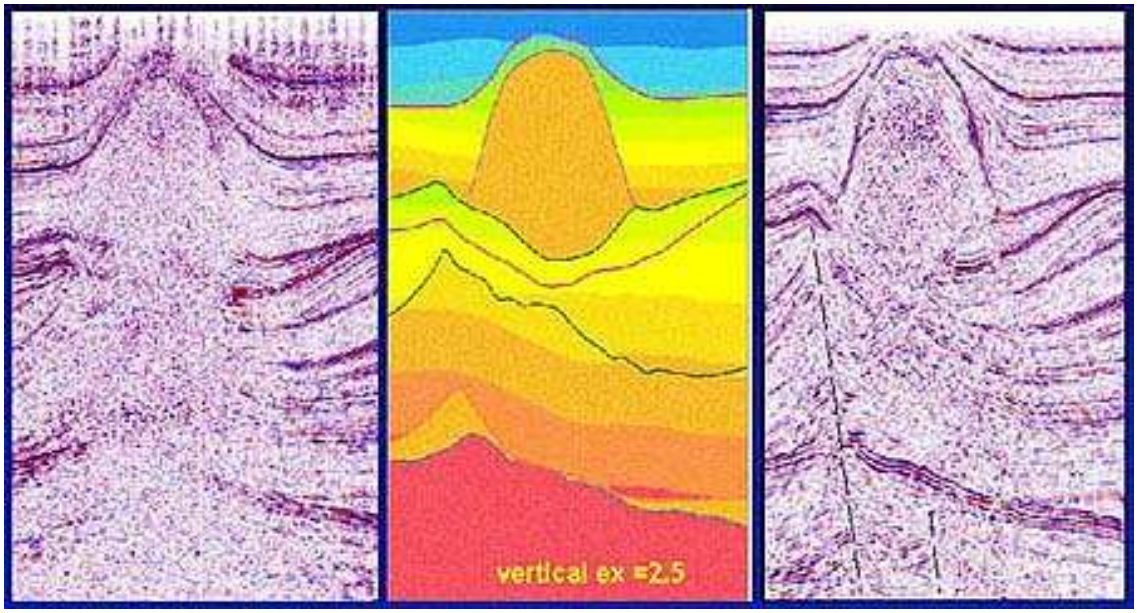

Figure 4-30: comparison between post-stack migration a (left) and pre-stack migration (right); model in the centre. Notice that the pre-stack seismic allowed the interpreter to identify more geological features than when post-stack migration seismic was used. Source: CGG Veritas.

4.2.8 Drilling Strategies in Naturally Fractured Reservoirs

4.2.8.1 Directional Drilling

Traditional exploration drilling practices are based on three premises: targeting the structural crest; maintain a vertical borehole; and drilling over-balanced for safety reasons. All three drilling practices may threaten success in naturally fractured reservoirs simply because well and reservoir flow depends on flow through natural fractures (Ehlig-Economides and Mohamed Taha, 2000).

The vertical stress from the overburden represents the largest of the three present day *in situ* stress directions (the minimum being one of the horizontal directions), which means that most horizontal, or near horizontal fractures will tend to close (an example of such are those generated by thrust faulting), and most open – and therefore most productive –natural fractures have their planes perpendicular to the minimum stress direction, i.e. they are vertical or sub-vertical. Thus, what are the probabilities of intercepting a vertical fracture with a vertical well? Very slim, simply because a vertical well trajectory will be parallel to most of those fractures, and hence productivity will be low. A very simple example is shown in Figure 4-30.

If the reservoir we are dealing is of Type 3 or 4 – where most of the storage volume is in the rock matrix – although not the best option, a vertical well would probably still be able to present a reasonable productivity. But if we face a Type 1 or 2 reservoir – where fractures supply the porosity and permeability in Type 1 and permeability paths in Type 2 – drilling directional wells at an angle from vertical in a direction normal to fracture planes and parallel to the minimum *in situ* stress, where most fractures can be intersected is the recommend strategy by most authors (e.g. Nelson, 2001; Aguilera, 1995, Ehlig-Economides, 2000). In terms of wellbore stability, directional wells should not be a problem in most basins, because the borehole will be encircled by approximately balanced stresses from the overburden and the maximum horizontal stress (scenario for relaxed basins).

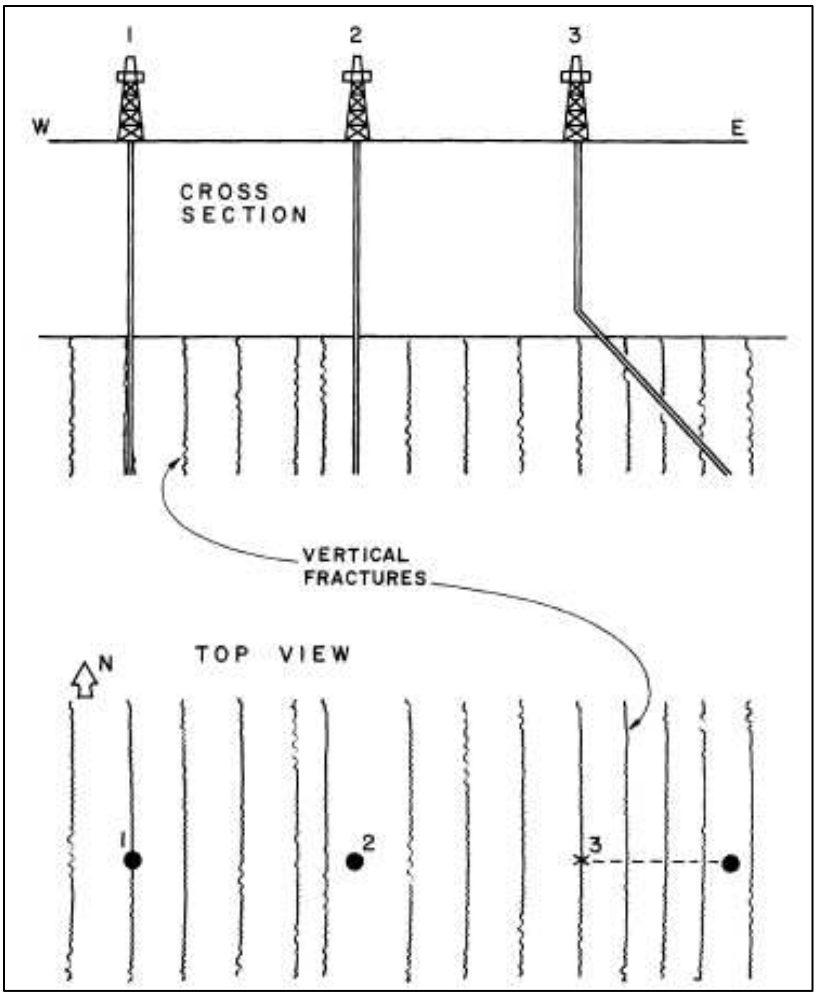

Figure 4-31: Schematic representation of an hypothetical set of wells in a fractured reservoir context. Notice that both Well 1 and 2 were done vertically, but only Well 1 intercepted a fracture (probably by a very lucky strike). Well 3, in its turn was deviated when reached the reservoir interval, and consequently intersected a much larger area of fractures (Aguilera, 1983).

4.2.8.2 Underbalanced Drilling

In traditional drilling procedures, the usual practice is to maintain the weight of the mud at such value that the hydrostatic pressure of the mud column exceeds the pressure of the fluids in the penetrated formations. This differential pressure towards the formation prevents formation fluids to flow into the wellbore, potentially causing a blow-out. This drilling practice usually alters the fluid content of the formation near the wellbore, due to the dislocation of the original fluids in the pores by the filtrate in a process known as invasion.

Most water base muds contain solids in suspension, apart from chemicals in solution. When the mud tries to flow into the pores of the wellbore rock, usually only the filtrate enters, leaving a deposit – the mud cake – on the face of the rock. In fractured formations this may not be true. Literature frequently mentions that when natural fractures are encountered in an overbalanced drilling condition, drilling fluids, including solids, penetrate deep into the most open fractures – the most productive – and the drilling fluid filtrate penetrates the matrix rock facing the invaded fractures. Besides the danger of losing well control due to lost circulation, the main sources of productivity are damaged, possibly permanently. An alternative to this method is to drill at balanced or underbalanced conditions, with better results achieved with the second method.
In underbalanced drilling the pressure exerted on the well is less than, or equal to, that of the reservoir. It is performed with a light-weight drilling mud that applies less pressure than formation pressure preventing the mud to penetrate the formation and avoiding formation damage. This negative differential pressure between the reservoir and the wellbore induces production of formation fluids and gases, i.e. flow from the reservoir is driven into the wellbore rather than away from it in contrast to conventional drilling (Figure 4-31).

There are four main techniques to achieve "underbalance" while drilling a well (http://www.rigzone.com):

Lightweight drilling fluids: This is the simplest way to reduce wellbore pressure. Fluids such as fresh water, diesel and lease crude are used instead of the heavy mud. However, in most reservoirs the pressure in the wellbore cannot be reduced enough to achieve "underbalance" by this technique.

Injecting gas down the drillpipe: this involves adding air or nitrogen to the drilling fluid that is pumped directly down the drillpipe. This technique can be used in wells not specifically designed for underbalanced drilling and improves penetration rates. On the other hand, there is a risk of overbalance conditions during shut-in and very specific tools of measurement while drilling (MWD) have to be used which may increase the costs.

Note: In air drilling a faster *up hole* volume is needed because cuttings will fall faster down the annulus when the compressors are taken off the hole compared to having a higher viscosity fluid in the hole, at the same time, because air is compressible, Measure While Drilling (MWD) tools which require an incompressible fluid cannot work. Common

technologies used to eliminate this problem are either electromagnetic MWD tools or wireline MWD tools which are less common and more expensive.

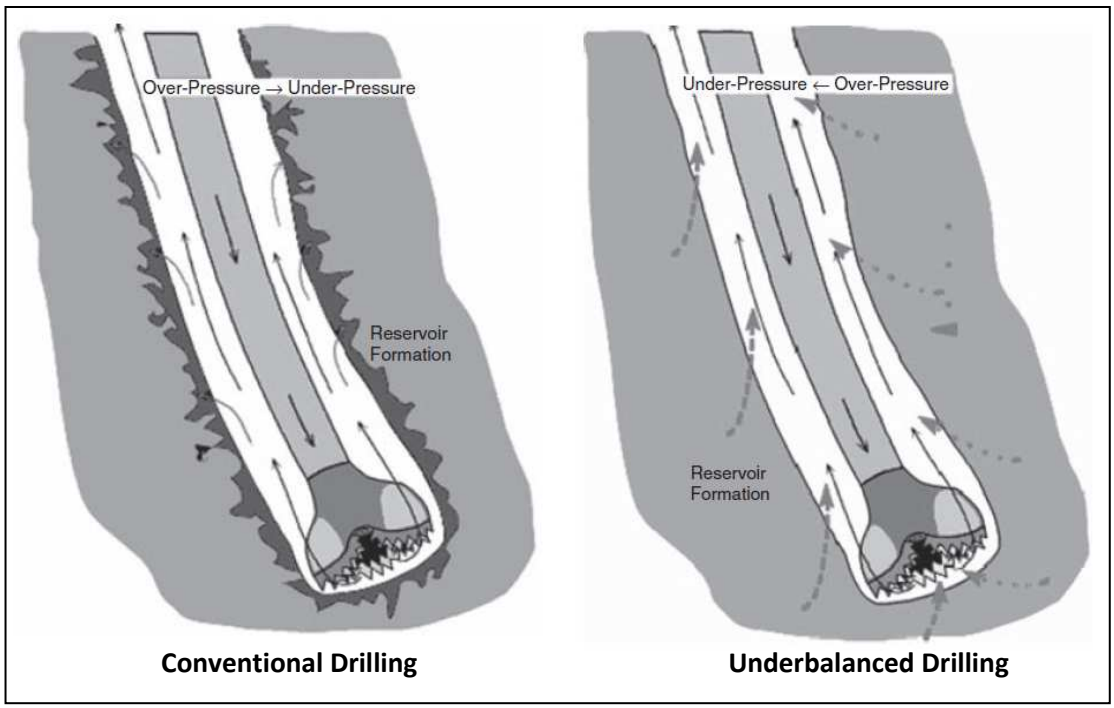

Figure 4-32: Conventional drilling, with drilling fluid and fines flowing into the reservoir VS. Underbalanced drilling, with formation fluids flowing from the reservoir (Lyons, 2009).

Gas injection via parasite string: here, a second pipe is run outside of the intermediate casing. This increases both the drilling costs and the time it takes to drill the well. However this technique applies constant bottom-hole pressure and requires no operational differences or unique MWD systems.

Nitrogen foam: this method is less damaging to formations that exhibit water sensitivities, and the safety index is much greater when compared to other methods (nitrogen is inert and eliminating the possibility of down-hole fires). The problem resides in the additional nitrogen needed to generate stable foam, which makes this technique very costly. At the same time it can only be used in wells measuring less than 3600m deep due to temperature limitations.

In sum, Underbalanced Drilling has two main objectives (Leading Edge Training Manual, 2002):

1. Maximising hydrocarbon recovery
2. Minimising drilling problems

1. Maximising hydrocarbon recovery

- **Reduced formation damage:** there is no invasion of solids or mud filtrate into the reservoir formation, which means that the lithological characteristics of geological formations will be preserved
- **Early production:** Well is producing as soon as the reservoir is penetrated with a bit which could be a disadvantage if hydrocarbon production cannot be handled or stored on site or if the required export lines are not available, but if the correct procedures are executed then this will avoid doing post-drill evaluation tests such as Drill Stem Tests (DST's – See Appendix) and save funds.
- **Reduced Stimulation:** Stimulation procedures such as acid wash are proved to reduce the productivity of the reservoir. In underbalanced drilling, as there is no filtrate or solids invasion, the need for reservoir stimulation is eliminated.
- **Enhanced recovery:** The combined effect of the higher productivity of underbalanced wells with the ability to drill infill wells in depleted fields, makes possible the recovery of bypassed hydrocarbons, which can significantly extend the life of a field.

2. Minimising drilling problems

- **Higher rate of penetration**: with less pressure at the bottom of the wellbore, it is easier for the drill bit to cut and remove rock.
- **Reduced probability of lost circulation**: when the well is drilled underbalanced, mud will not enter the formation and the problem can be avoided.
- **Elimination of differential sticking**: differential sticking is when the drill pipe is pressed against the wellbore wall so that part of its circumference will see only reservoir pressure, while the rest will continue to be pushed by wellbore pressure. As a result the pipe becomes stuck to the wall, and can require thousands of pounds of force to remove, which may prove impossible. Because the reservoir pressure is greater than the wellbore pressure in UBD, the pipe is pushed away from the walls, eliminating differential sticking.
- **Extending the life of the drill bit:** drilling gases cool the bit while quickly removing cuttings allowing for a longer usage.

In terms of costs, underbalanced drilling is always more expensive than a regular overbalanced well. The costs vary with the complexity of the reservoir and the consequent sophistication of the equipment required on the surface separation and data acquisition system. The reservoir fluids dictate the required separation equipment and the reservoir pressure dictate the pressure control equipment requirements as well as the gas lift requirements (Leading Edge Advantage, 2002).

Leading Edge Advantage (2002) considers that a value of 10% of the well cost is the additional cost required for underbalanced drilling by comparing a number of operations in Europe, Canada and the middle East. They also define a rule of thumb to easily evaluate if the costs will be high or low: *if the well is expensive because of the complex reservoir geometry, it is likely that the underbalanced drilling equipment will also have to be suited to the complex drilling systems required. If a simple vertical well is required in a homogeneous reservoir then the well costs as well as the UBD costs can be low.*

In terms of productivity, they consider that *if a multi-well development can be drilled successfully underbalanced the reduction in well count* (the number of wells drilled to achieve a certain productivity) *could be as high as 25% as a result of the increased productivity. This benefit outweighs the obstacles and cost of underbalanced drilling significantly.*

5. NATURALLY FRACTURED BASEMENT RESERVOIRS A PROVEN WORLDWIDE PLAY

Naturally fractured reservoirs are often ignored due to the increased difficulty in exploration techniques. This is even more evident when the cases are basement reservoirs. Despite being known within the hydrocarbon industry for many years, naturally fractured basement reservoirs are generally regarded as non-productive and they have failed to draw the attention of the explorationist. These reservoirs are often seen as 'of no economic potential', and their investigation by exploratory drilling has been left to chance. This section is dedicated to demonstrate that these types of reservoirs have an underexplored potential, even though they are commonly distributed in various petroliferous regions throughout the world with many successful cases.

Before any consideration is made on how to explore Basement reservoirs, it is important to define the concept of *Basement:*

Berkley University Geological Glossary: *The oldest rocks in a given area; a complex of metamorphic and igneous rocks that underlies the sedimentary deposits. Usually Precambrian or Paleozoic in age.*

Wikipedia: *rocks below a sedimentary platform or cover, or more generally any rock below sedimentary rocks or sedimentary basins that are metamorphic or igneous in origin.*

Landes (1960): *basement rocks are considered as any metamorphic or igneous rocks (regardless of age) which are unconformably overlain by a sedimentary sequence.*

P'na (1982): considers two definitions of basement related to HC exploration:

1) *metamorphic and igneous rocks (regardless of age) that are unconformably overlain by a younger oil-generating formation (source rock). The oil, which is generated from the overlying sediments, is stored in the older metamorphic and igneous rocks.*
2) *any rock that unconformably underlies oil generating or oil-bearing formations.*

Aguilera (1980, 1995): *does not consider sandstones and carbonates as basement rock, even if they conformably underlie oil-bearing or oil-generating formations.*

North (1990): *considers basement rocks to include those of sedimentary origin, if they have essentially little or no matrix porosity. He states that 'basement' should not be compared with 'Precambrian' and that basement rock may have considerable fracture porosity due to deformation, weathering or both.*

From the above paragraphs, we can conclude that the definition of basement rock is very broad, and like most other definitions it depends on the objective and scientific context of the author who is giving the definition. Some authors consider basement rock only if it's not of sedimentary origin (igneous or metamorphic), but others also include sedimentary rocks if they have little or no matrix porosity. From this it is obvious that the essential characteristic that a rock must have to be considered basement, is the inexistence or the very low matrix porosity. Adding to this it forms an unconformity with the above sedimentary sequence and it may or not be of Precambrian or Paleozoic age. In SEAL, the basement is a metamorphic rock, unconformably lying below a sedimentary sequence and dated from the Pre-Cambrian. For this reason this author considers Landes definition as the most accurate for the present study.

Commercial, naturally fractured basement oil deposits have been found largely by accident, when looking for other types of reservoir (Aguilera, 1980; Landes et al, 1960). The proof of this accidental success is that in the Western countries, all the oil fields that produce from crystalline basements were discovered when aiming for other formations. Furthermore, most naturally fractured reservoirs (sandstones, carbonates, cherts, shales and not just basement reservoirs) were discovered by accident (Aguilera, 1995, Russell, 1995). In Russia and in other countries from the former USSR however, drilling into crystalline basements has been carried out intentionally (Kenney et al., 1996) for a long time.

Landes et al.; (1960) considers that basement rock oil accumulations shouldn't be considered rarities to be found solely by chance but are normal concentrations of hydrocarbons obeying the rules of origin, migration and entrapment. Therefore, in areas of not too deep basement, oil deposits should be sought with the same professional skill and zeal as accumulations in the overlying sediments.

5.1 FAVOURABLE CONDITIONS FOR HC ACCUMULATION IN BASEMENT ROCKS

Like in any other HC reservoir, there a number of favourable conditions that a basement rock reservoir should have and that are mentioned by several authors (Gutmanis et al., 2005; Aguilera, several articles; Landes et al., 1960):

Regional Unconformity: because basement rock is not a reservoir rock by nature, i.e. it usually has low porosity and permeability; the hydrocarbons have to be present in a typical reservoir rock (clastic, carbonate) or in the source rock itself before migrating into the basement. For this reason basement reservoirs have to underlie a regional unconformity. All basement reservoirs known comply with this and almost all lie on an uplift or high. This uplift or high was generally continuously uplifted for long periods of geologic time and was subject to a long period of weathering and erosion, which sculptured hills in the basement rock and created the differential geomorphology. Younger sediments, which act as hydrocarbon sources, either flank or directly overlie basement providing the opportunity for entrapment of oil in the basement rock. These younger sediments may either be a reservoir rock to where HC have migrated, or even the source rock as in Yemen, where in the Habban field, Khulan Formation intraformational shales provide the source of the HC.

Seal: It is important that the reservoir is overlain by a seal. In most cases the cap rock for basement accumulations is a relatively tight sedimentary rock (Sergipe-Alagoas case, where the seal is formed by Ibura Mb. anhydrite). However, at the Mara field in Venezuela, a tight zone within the basement rock may act as the seal. At the other extreme is the situation in several California fields where a thick oil column extends from an oil-water interface within the basement rock upward through a continuous reservoir, which includes such permeable material as wash and basal sandstone, until a tight rock is reached somewhere above the base of the sedimentary section, Landes et al (1960).

Migration: As in any other reservoir, a migration path as to exist. As most basement rocks are hard and brittle with very low matrix permeability, the migration route occurs through higher permeability sedimentary units, active faults and the basement/sedimentary cover interface, into the basement (Figure 5-1). There are three most common possible sources for oil accumulation in basement reservoirs:

1. Overlying organic rock from which oil is expelled downward during compaction.

2. Lateral, off-the-basement, but topographically lower, organic rock. The oil is then squeezed from this rock, into an underlying carrier bed through which it migrates up dip into the basement rock, or directly into the Basement
3. Lower, lateral reservoirs from which earlier trapped oil is spilled due to tilting or overfilling.

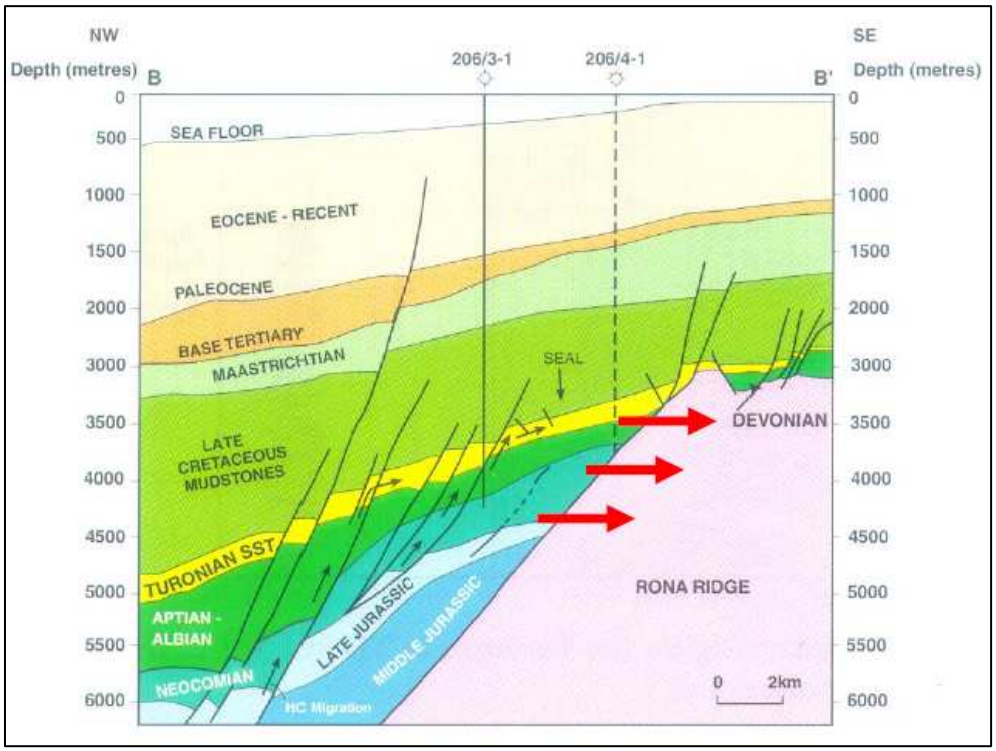

Figure 5-1: probable basement migration routes at the Rona Ridge, West of Shetland, and UKCS. Notice the lateral migration of the HC (signed by the red arrows) from the sedimentary sequence that unconformably lies over and at the sides of the Basement (Gutmanis, 2009; modified from Grant et al., 1999)

Reservoir: Reservoir space is also needed. In most basement rocks matrix porosity is close to zero, and reservoir quality depends on the development of secondary porosity, which in most cases is given by the fractures. The degree of reservoir space, i.e. fracture porosity, depends on the mechanical properties of the host rock and on the applied stress over that rock.

5.2 WORLDWIDE EXAMPLES OF FRACTURED BASEMENT RESERVOIRS

There are examples of Fractured Basement reservoirs all around the globe. Most reservoirs are granitic, volcanic or gneissic; rocks with brittle behaviour which contributes for the formation of fractures. Below are some examples that this author considers important due to their similarity to the SEAL Basin Fractured Basement, to their good production rates or operational procedures. It is important to highlight however that SEAL Basement rock is described as being a micashist, which, by its semi-ductile behaviour, is less prone to fracturing than brittle rocks. For a more complete list of Fractured Basement reservoirs please refer to Gutmanis and Batchelor, 2005; from where these examples were taken.

China

Yaerxia Oil Field: located in the Jiuxi Basin it was the first basement reservoir in China. The production comes from fractures in the Quannaogou Formation, a Paleozoic hard phylite, slate and meta-sandstone. The production from the wells ranged from around 70 bbl/day to 1050 bbl/day.

Dong Sheng Pu Buried Hill Reservoir: it is a metamorphic basement rock which started to produce in 1983 with a production of aroud 1300 bbls/day. By December 1987, there were 14 active producers and one observation well with cumulative volumes of oil and gas of around 7 MMbo and 2.3 Bcf respectively. With water injection, oil production rates varied between 7300 bbl/day and 11500 bbl/day which relates to an estimated cumulative oil production, at the end of the field's production life, of 160 MMbo.

Georgia

Ninotsiminda Field*:* Located 25 km east of Tbilisi, and discovered in 1979, the Ninotsminda Field represents the largest remaining oil accumulation in Georgia. It is an anticlinal trap, with production mainly from the fractured Middle Eocene volcaniclastics. The reservoir is underpressured at 0.38 psi/ft, and is dominated by sub-vertical micro and macro fractures that concentrate mainly in the hinge area of the fold.

In 2000, a vertical well was drilled into the oil producing formation, with production tests stabilising at a flow of 200 bbl/day. In 2003 an appraisal horizontal well was drilled in 2003, this increasing the production to 2200 bbl/day. The area is being extensively developed by the NOC

(Ninotsminda Oil Company), with a 5 well prospect likely to increase production from 2000 to 4500 bbl/d (Durglishvili et al., 2004).

Libya

Nafoora-Augila Field: this is one of the main giant fields in the Sirte Basin, and on of the primary oil producing reservoirs is the basement granite. This reservoir is said to produce at rates that range from 1200 bbl/day to 14,000 bbl/day.

Hungary

In Hungary, hydrocarbon reservoirs within fractured and weathered zones of crystalline basements are of great importance, as the majority of hydrocarbon reserves found in recent years have come from this type of reservoirs. These metamorphic hydrocarbon-bearing formations are generally characterised by complex lithology, low porosity and a heterogeneous distribution of pore sizes and fractures (Kiss & Tóth, 1985).

Thailand

Sirikit Oil Field: The Sirikit field lies in the Phitsanulok Basin, one of a series of Tertiary rift-related structures in central and northern Thailand. About 14 wells had been drilled into the pre-Tertiary basement to 1995. Many had oil shows and two have been placed under production. The Field has produced about 1.17 MMbo of oil from basement so far (November 1998). Smitt, 1998, has presented a fracture simulation model using Frame and Poly3D sofwares to predict the fracture patterns in the basement. No information on how this impacted the reservoir production was found.

Venezuela

Mara Oil Field: lying Northeast of La Paz, Mara oil field used to be considered, the “champion” of Basement producers (Landes, 1959). The complex basement is composed of metamorphic and igneous rocks, with hydrocarbon storage exclusively in fractures (Landes, 1959). By 1956, the Mara field was producing from 29 wells in the basement reservoir at na average depth of 1,190 ft (363 m). Initial production was about 2,700 bbl/day but one well produced 17,000 bbl/day from the basement (Landes et al, 1960).

Vietnam - Cuu Long Basin

Vietnam is one of the countries where oil and gas production from basement reservoirs are most important. Cuu Long Basin is estimated to contain 30% of the country's hydrocarbon reserves, and presently it represents 95% of production, with 85% being produced from the fractured basement (Figure 5-2).

Bach Ho Field: Vietnam's most important offshore asset is the Bach Ho field which generated over 50 MMbbo in 1996 (Anon, 1997). This field is at a depth of 5,000 m, of which 4,000 m is fractured basement granite with a pay zone interval of 1,000 m (Russell, 1997). Production rates are listed at 202,000 bbl/day in September 2004 (see PES.GB, Jan. 2005). The volume in place has been recently calculated at 1.59 billion barrels of oil, with around 95% of this amount contained within the fractured basement.

Dai Hung Field: was discovered in 1988, and is now operated by Vietsovpetro following transfer of ownership from BHP Billiton in 2000. The field contains significant accumulations of oil and gas in a fractured granitic basement (up to 730 MMbo of oil), sourcing from lacustrine shales. Current production is 22.9 MMbo/day of gas and 1385 bbl/day of oil.

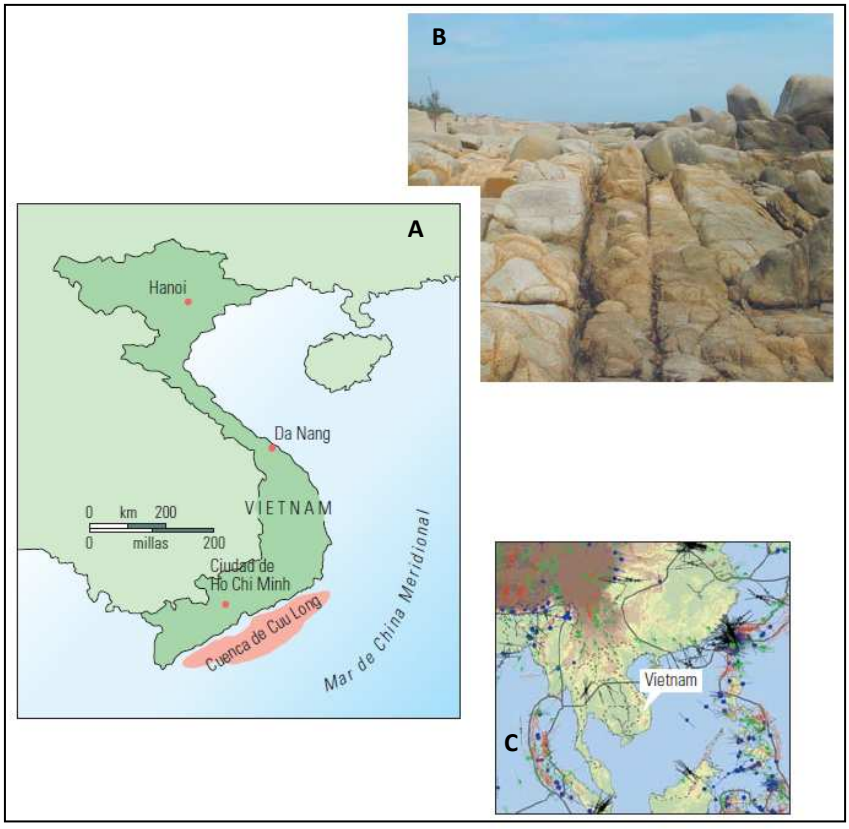

Figure 5-2: (A) Location of Cuu Long basin in offshore Vietnam. (B) Fractures in a granitic outcrop in Long Hai beach, which are used as an analogue for Bach Ho field. (C) World map of tensions. Notice the lack of data in Vietnam area. In order to understand and predict the distribution of fractures it would be important to acquire such data. *Unknown source*

Yemen

With hydrocarbons being discovered in both conventional and unconventional reservoirs, Yemen has attracted the interest of the oil industry in the last few years.

SOCO is currently developing the East Shabwa Block 10/10A, with four deviated appraisal wells having been drilled since August 2004. The primary drilling target was the fractured basement, with secondary targets lying in the overlying sedimentary sequence. Current production of the East Shabwa Development Area is 27,800 bbl/day, with around 30% of this figure being produced from the basement.

DNO have also had significant successes in onshore Block 43. The Nabrajah wells have primarily targeted both the Qishn Formation sandstone and the Kohlan Formation dolomite, however significant hydrocarbons have also been discovered in the basement. Production tests carried out in the basement resulted in 5800 bbl/day of 38.6^{o} API crude and 4162 Mscf/day of gas using an ESP. Following a pressure build-up test, flow was 2812 bbl/day of 41.9^{o} API crude, and 3054 Mscf/day of gas with no pumping. Oil is also being produced from the basement in the neighbouring Blocks 10 and 14 (operated by TotalFinaElf and Nexen respectively) (see DNO press-release, 13/04/05).

OMV is operating Block 2, Block S2 and Block 29 in the onshore Yemen. Block S2, located in Sab'atayn basin had major discoveries in the fractured basement, which gave origin to the Habban Field.

5.3 SEAL BASEMENT FRACTURED RESERVOIR

SEAL Basement fractured reservoir complies with most of the above conditions:

Presence of a regional unconformity: The Basement rock in the SEAL basin is of Pre-Cambrian age (see Section 4 for details), and unconformably underlies a Mesozoic sedimentary sequence, as it can be seen by the analysis of the seismic lines (Figures 6-4 and 6-20).

Proven presence of sedimentary reservoir rock with stored HC flanking and/or overlying the Basment rock: Carmopolis Mb. from Muribeca Fm. is an alluvial fan deposit and it is the main producing horizon in the area. Block-B is cut by the south part of Carmópolis Oil field which proves the presence of this sedimentary unit in the area.

Presence of an effective migration path and sealing effectiveness: the presence of the Ibura Mb. in the seven drilled wells and the positive results of those wells – with HC presence in all of them – prove that there is an effective sealing capacity and that HC are migrating into the Basement rock.

Reservoir space: the presence of open fractures, registered by the FMI, and the fact that the best results from the seven wells were registered in the Basement rock – a micashist with very low to inexistent matrix porosity and permeability – proves that this rock possesses reservoir space. Even though the fact that direct measurements of this reservoir space (porosity and permeability assessment) were not possible to make, quantifying it becomes an imprecise task.

It is important to stress for future reference that this author considers that SEAL Basment Fractured Reservoir should be classified as a Type 1 reservoir, as no evidence of matrix porosity was found in the data acquired to the present.

6. APPLICATION OF THE NFR WORKFLOW ON SEAL FRACTURED BASEMENT

In 2005 GALP acquired a set of exploration blocks located in Sergipe-Alagoas Basin – Sergipe Sub-Basin. What started to be a traditional exploration campaign, revealed the presence of a Naturally Fractured Reservoir (NFR), and in particular a fractured metamorphic basement rock, when, after drilling seven wells, the best results were registered in this formation. This Section is dedicated to the analysis of the SEAL Fractured Basement Play, using the worlflow presented in the previous section as a guideline.

6.1 FRACTURE SYSTEM PROPERTIES

As shown in Section 4, identifying the fracture system can be done by using several sources of information: well data, outcrops, regional geology and seismic. These will then give information on the properties that affect the reservoir performance and on the fracture system origin, which will lead ultimately to the classification of the reservoir type – Figure 6-1.

(unfold next page)

Figure 6-1: Initial part of the workflow dedicated to the identification of the Fracture System and to extract information about its properties from the available sources (Well Data, Outcrops, Regional Geology and Seismic). Seismic processing and Acquisition are not listed here, because in the present case Seismic was available for use. As it will be seen ahead, the available seismic may not be the most adequate for the study of a NFR such as this, and acquisition and/or processing of new seismic should be considered. Volumes calculation and Well design are also excluded as they are going to be considered individually in another section.

6.1.1 Outcrop Study

Despite the fact that several outcrops are present in the area none was studied for the present work.

By its close geographical location relative to the areas of Block-A and Block-B, probably the Itabaiana Dome (Section 2) would have been a good area to collect information on lithology of the host rock and on fractures. As stated in the previous section, outcrop studies have to be conducted with care as most outcropping rocks will be altered by weathering, and probably more fractured than the same rock in burial conditions. However they supply very important information as a larger volume of rock is available, and apart from cores (which are much more expensive), are the only direct contact that the geologist can have with the fractured rock.

This author considers that in the future some time should be dedicated to the study of the outcrops in Itabaiana Dome as they could clarify some doubts that remain unclear, even after the present study was conducted.

6.1.2 Regional Geology

The information that can be taken from the analysis of the regional geology is available in the literature, and it was presented in Section 2. From there we can conclude on the stress regimes that the Basin was subjected to – Figure 6-2. Presently the most accepted theory was proposed by Chagas, 1996. This was the premise used for geomechanical modelling which will be presented ahead.

Lana and Milani		
Stress Direction	**Faulting/Regime**	
NE-SW	NS	normal
	N30E	strike-slip
	N30W	
NW-SE	N30E	normal

Falkenhein		
Stress Direction	**Faulting**	
E-W	NS	normal
stike-slip	NNW-SSE	strike-slip
	NS	strike-slip
NW-SE	NW	normal

Chagas		
Stress Direction	**Faulting**	
E-W	NS	normal
	E-W/ENE-WSW	transfer faults
NW-SE	NW-SW	normal
	NNW-SSE	transfer faults

Figure 6-2: Structural regimes in SEAL basin according to different authors.

By the analysis of the local geological maps, using the information available in the literature about the SEAL basement and the information from the wells (where lithology is described as phylite) this author considers that the studied blocks are located over the Vaza Barris Domain – see Figure 2-12.

6.1.3 Seismic

The work previously developed for this area had the objective of assessing the blocks' potential and recommend prospects to be drilled. As a result, the wells Alpha, Bravo, Charlie and Delta were drilled on Phase I and then, after an evaluation of their results, Phase II was conducted with Echo, Fox and Golf wells being drilled. For the present work the interpretation of Phase I will not be described because Phase II re-interpretation replaced it and is considered to be more accurate. At the same time all the analysis made over the seismic volume for this work was done using the Phase II re-interpretation.

Interpretation Workflow

An analysis of the existing interpretation (Phase I interpretation) was carried out to determine what needed to be re-interpreted. Apart from the problem of the horizons that had been picked on the wrong seismic attributes it was also recognised that, after the drilling of Alpha, Bravo, Charlie, and in particular of Delta well, the top of Basement interpretation could be changed so that in the structural lows, this formation could be deeper than previously thought, allowing the deposition of Carmópolis sandstones in the paleo-valeys. The importance of this formation for this play was described in Section 2. The current interpretation does not contemplate this formation as it is unclear as to what seismic reflector it is represented by. This is due to its low thickness which causes it to be below seismic resolution. Probably with better quality data, Spectral Decomposition would allow us to detect it.

At this time, Basement was considered as the main objective, and as a result of this analysis and of time constraints, it was decided to re-interpret only the top of the Ibura Mb. and the top of Basement. At a later stage, the base of the Calumbi Fm. horizon was interpreted for depth conversion purposes only, with the objective of giving another control for the velocity model. However, this horizon has some interpretation problems, especially in the area of the Bravo well. The faults were extensively reviewed.

Interpretation followed the regular workflow and it was undertaken in Seisworks®: faults were interpreted initially followed by the horizon interpretation over the time volume. Inevitably, some faults were reviewed or interpreted during the horizon interpretation. A Structure Cube (Figure 6-6) was created and used only as a guide for fault interpretation due to the low S/N ratio (Figure 6-3) of the seismic data which lead the interpretation to take longer than expected.

The horizon interpretation started around the wells area, where a good well-tie was achieved and then expanded to the whole area. The Auto-tracking mode was preferentially used relative to other tracking options, although this was always limited to reflector continuity. This interpretation took longer than initially estimated mainly due to the poor quality data (Figure 6-4),

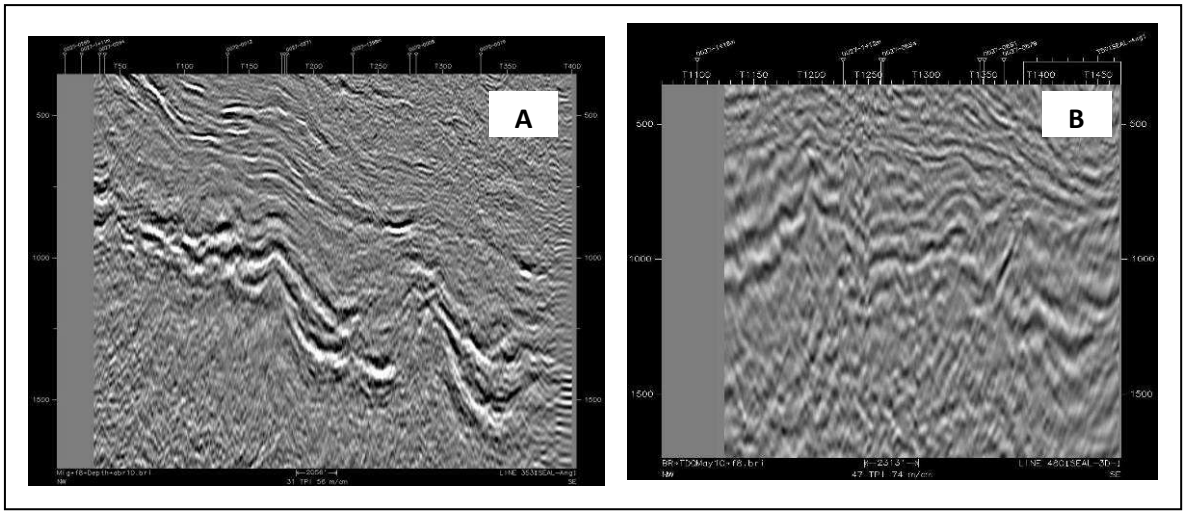

Figure 6-3: (A) seismic line in Depth for Block SEAL-T-A (C) seismic line in Depth for Block SEAL-T-B. Notice the bad seismic quality and the low S-N ratio.

Time-Depth Conversion

The depth conversion was carried out using the DepthTeam Express® application from Landmark, which allows the simultaneous use of seismic velocity cubes, well velocity functions, well picks, and corresponding time surfaces (Figure 6-5). The 3D seismic, horizons and faults were converted to depth, and maps were then created using the depth converted horizons.

Attributes Extraction

As stated, the S/N ratio of the available seismic was very low. This conditioned the use of seismic attributes for detecting structural features such as faults and fractures. Even though, as part of the previously recommend workflow, Coherence, Dip-Azimuth and Dip-Magnitude attributes were run. The Coherence attribute is not available in-house.

1. Coherence

In Seisworks ® coherence is called structure cube. This attribute was run, and the result is presented in Figure 6-6. As it can be seen, the low S/N ratio of the seismic caused the identification of lineaments to be very difficult. Some faults can be identified when using seismic sections together with the structure cube, but no fracture patterns can be identified.

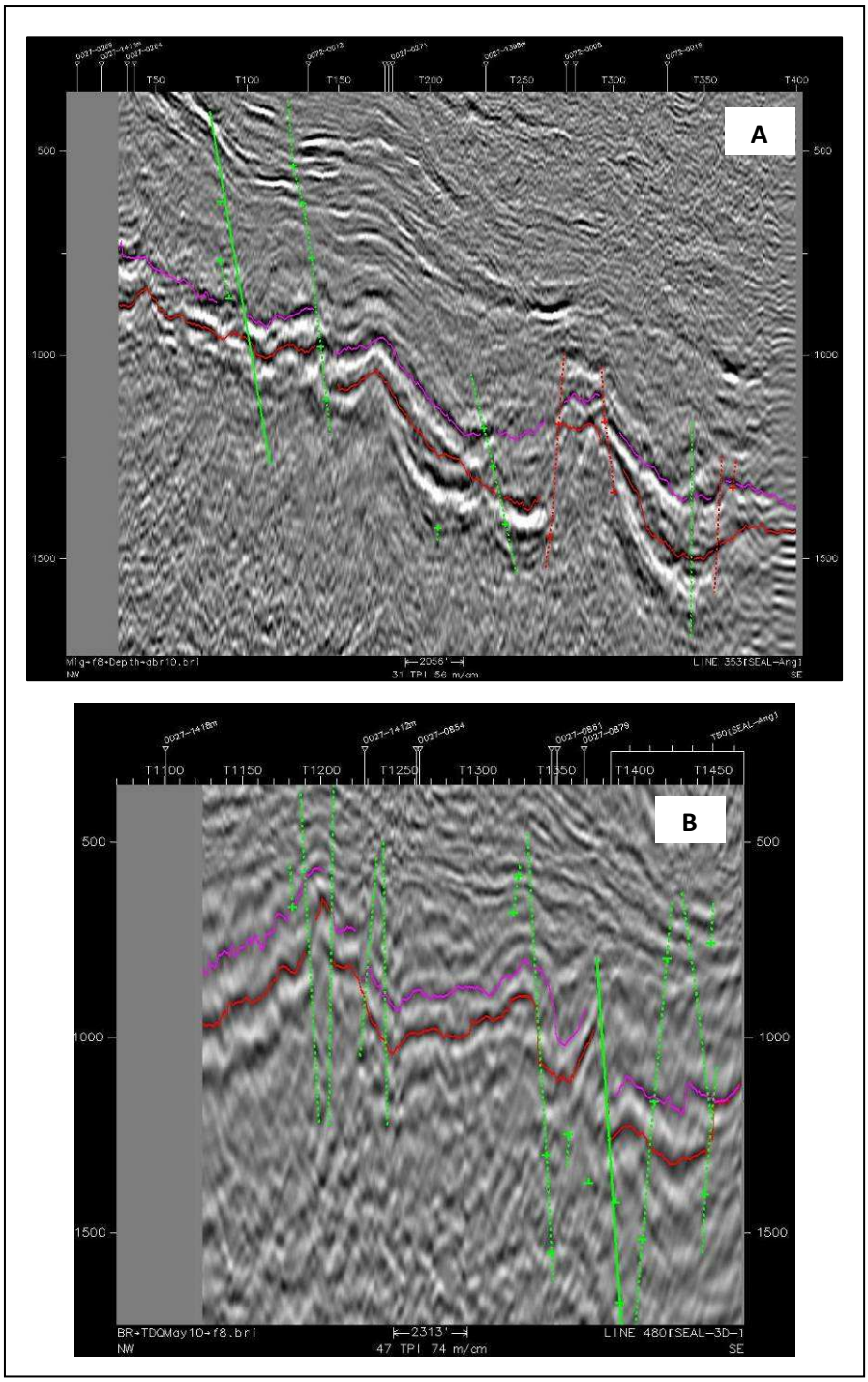

Figure 6-4: (A) Interpreted seismic line for Block-A; (B) interpreted seismic line for Block-B. Represented in purple is the Top Ibura Mb. Horizon and in red the Top Basement Horizon.

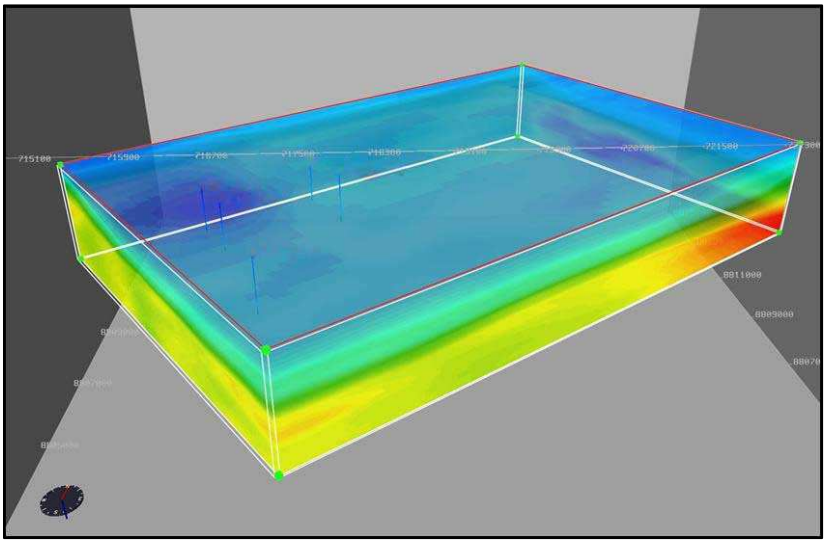

Figure 6-5: DepthTeam Express® Velocity Model for Block-A (seismic data limited to the Eastern side of the velocity model).

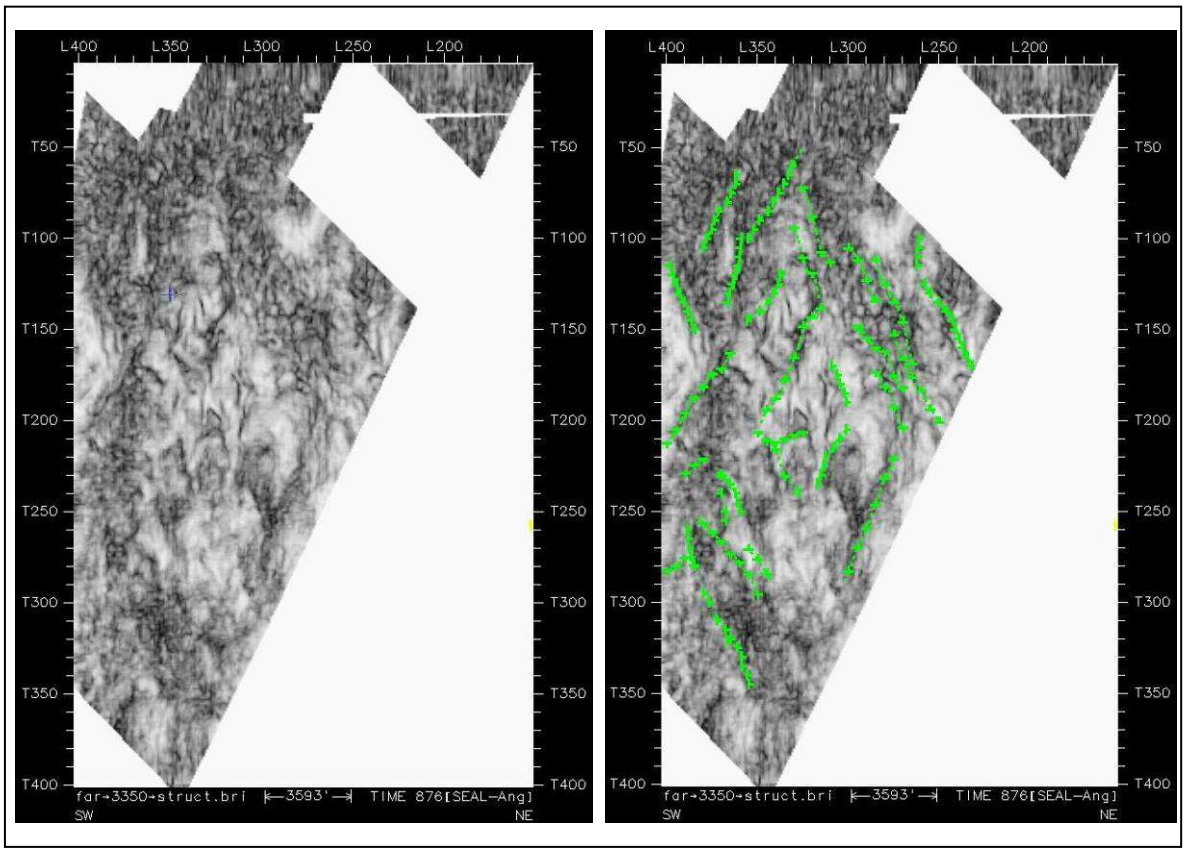

Figure 6-6: (A) Coherence cube generated from the SEAL Block-A seismic; (B) Coherence cube generated from the SEAL Block-A seismic, with interpreted faults.

2. Dip Azimuth

Figure 6-7 shows the Dip-Azimuth depth slices computed from Block-A and Block-B seismic. Notice that despite the low S/N ratio, there are still some structures that are visible when using this attribute, which is proved by the match of some of the interpreted faults with the lineaments detected in the depth slices (yellow arrows).

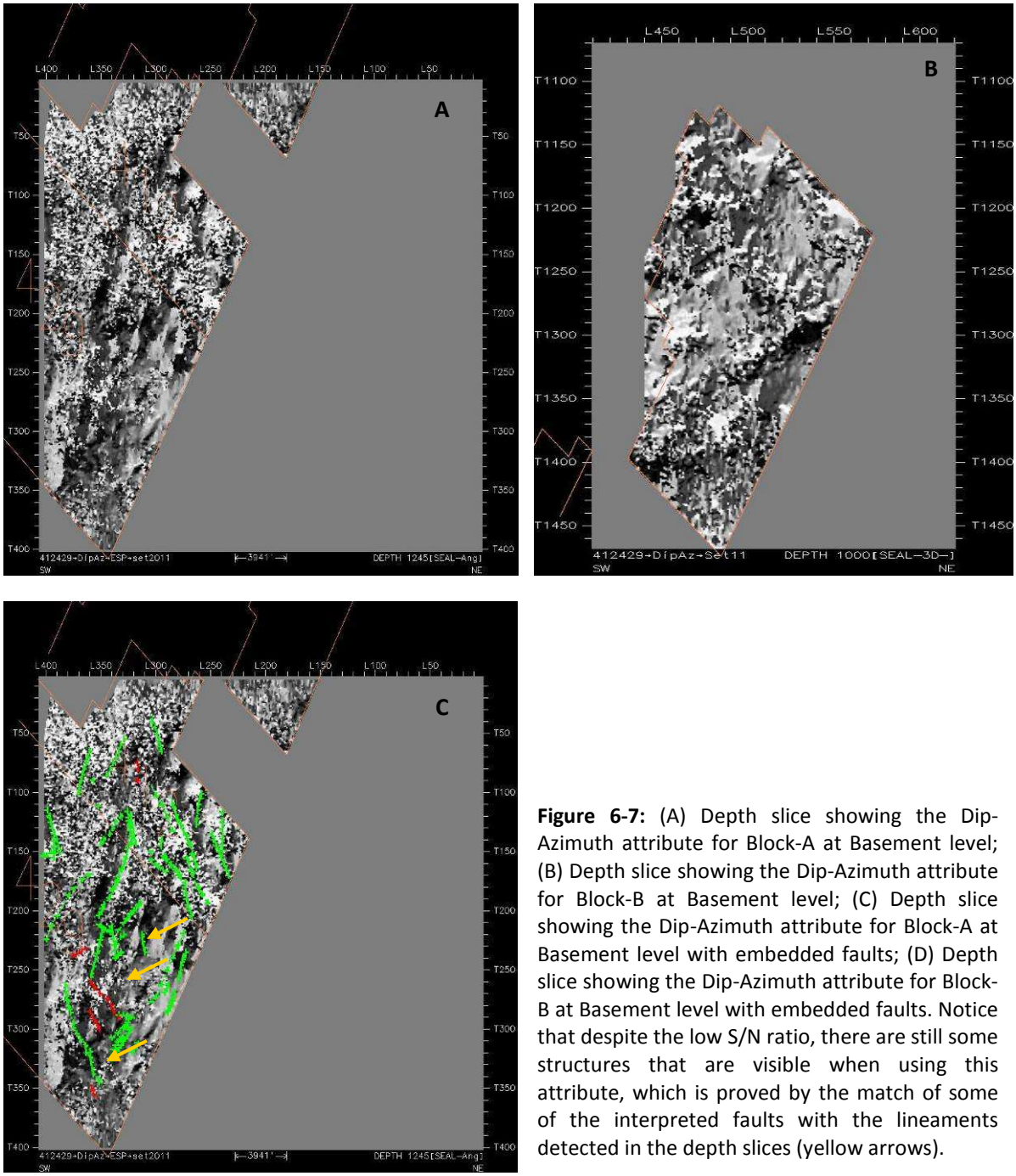

Figure 6-7: (A) Depth slice showing the Dip-Azimuth attribute for Block-A at Basement level; (B) Depth slice showing the Dip-Azimuth attribute for Block-B at Basement level; (C) Depth slice showing the Dip-Azimuth attribute for Block-A at Basement level with embedded faults; (D) Depth slice showing the Dip-Azimuth attribute for Block-B at Basement level with embedded faults. Notice that despite the low S/N ratio, there are still some structures that are visible when using this attribute, which is proved by the match of some of the interpreted faults with the lineaments detected in the depth slices (yellow arrows).

3. Dip Magnitude

Figure 6-8 shows the Dip-Magnitude depth slices computed from Block-A and Block-B seismic. Notice that the low S/N ratio, does not allow for identification of lineaments that could match faults (Figure 6-8 (C)).

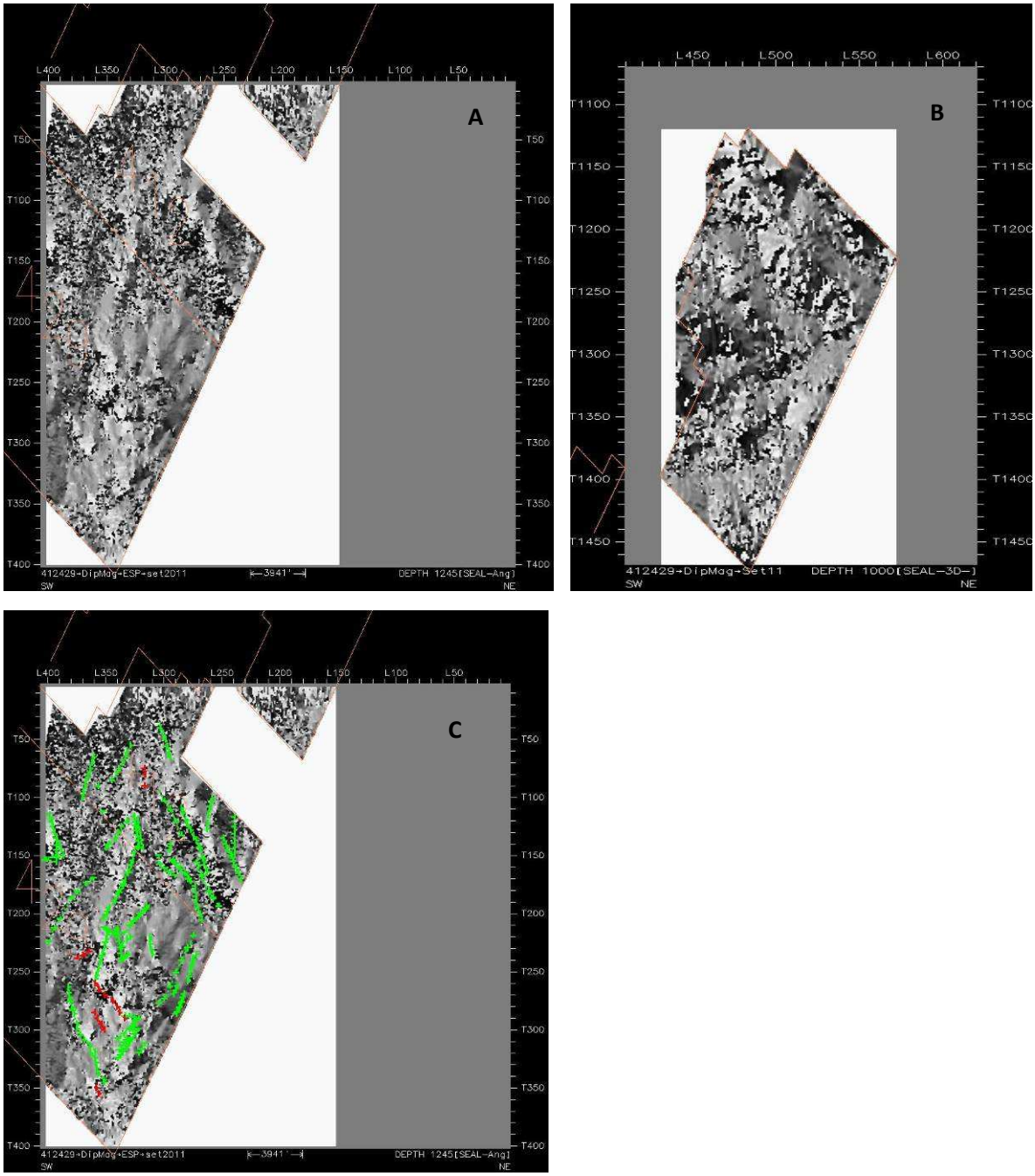

Figure 6-8: (A) Depth slice showing the Dip-Magnitude attribute for Block-A at Basement level; (B) Depth slice showing the Dip-Magnitude attribute for Block-B at Basement level; (C) Depth slice showing the Dip-Magnitude attribute for Block-A at Basement level with embedded faults; (D) Depth slice showing the Dip-Magnitude attribute for Block-B at Basement level with embedded faults. Notice that differently from the Dip-Azimuth lineaments are not as clear.

Automatic Fault Extraction Workflow – SEAL Basement Project

Automatic fault extraction algorithms are proven to reduce interpretation times by as much as three times (Silva, et al., 2005). For that reason, apart from the typical seismic interpretation, the Fractured Basement Project developed new methodology for automatic fault detection in complex geological settings with low quality seismic data. This methodology was developed by the Universidade de Aveiro, using the Ant Tracking algorithm existent in Petrel® software.

In nature, ants find the shortest path between their nest and their food source by communicating using pheromones, a chemical substance that attracts other ants. The shortest path will be marked with more pheromones than the longest path and so the next ant is more likely to choose the shortest route, and so on. Ant-Tracking uses this concept as an analogy for fault detection.
The idea is to distribute a large number of electronic "ants" in a seismic volume; and let each ant move along what appears to be a fault surface while emitting "pheromone." Ants deployed along a fault should be able to trace the fault surface for some distance before being terminated. Surfaces meeting expectations will be strongly marked by "pheromone." Surfaces unlikely to be faults will be unmarked or weakly marked. The Ant Tracking algorithm creates a new fault attribute highlighting the corresponding fault-surface features having orientations within some pre-determined settings. The algorithm automatically extracts the result as a set of fault-patches, a highly detailed mapping of discontinuities (Ant-Tracking Manual – Petrel).
The Classical Ant Tracking workflow comprises three main stages: 1) seismic conditioning; 2) edge detection; and 3) edge enhancement (the Ant Tracking cube itself). This standard workflow normally achieves good results in areas of low geological complexity and when high quality and well migrated seismic data is available, resulting in faults enhanced with a great level of detail. However, when the S/N ratio is low, such as in the present case, this workflow has some problems in detecting the discontinuities. For that reason a new methodology was created by Universidade de Aveiro (Figure 6-9) and the results were then used together with the data extracted from the FMI for the geomechanical modelling.

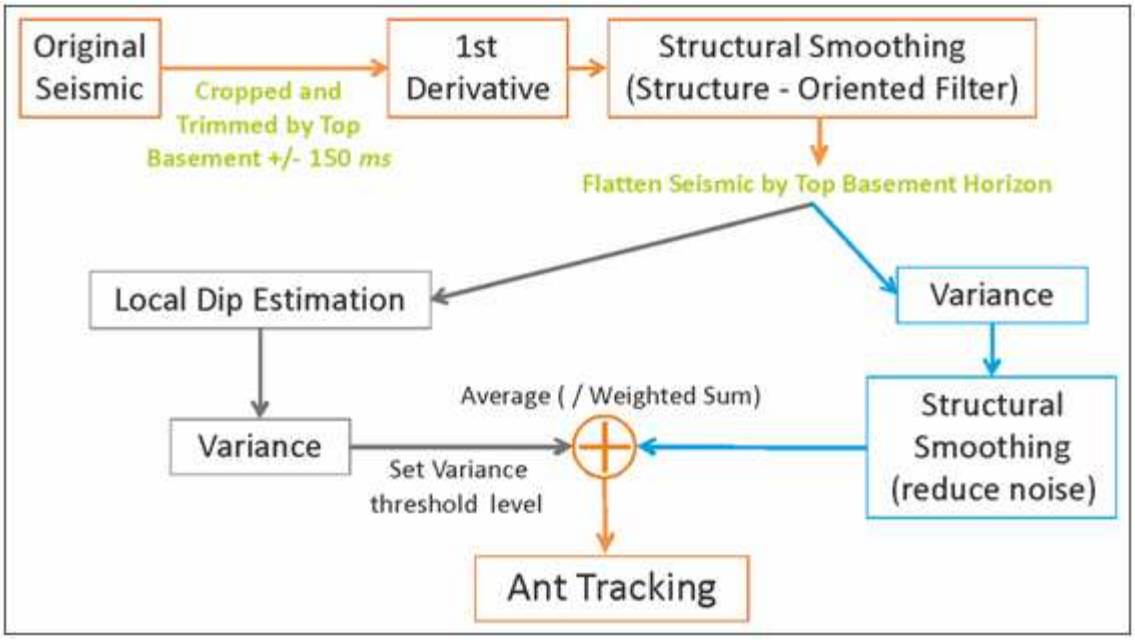

Figure 6-9: Schematic representation of the *New proposed Ant Tracking Workflow*. Proposed seismic attributes are displayed inside boxes and seismic operations are in green (UNL, UALG, UA, & IST; *Modelling and Characterization of Fractured Reservoirs -GALP E&P Internal Report;* Lisbon; 2011).

In the new methodology proposed by the Universidade de Aveiro, a first derivative attribute was first calculated over the seismic volume cropped and trimmed by Top Basement horizon. This attribute acts as a high-pass filter where low frequencies are attenuated, high frequencies are enhanced and any zero-frequency component is suppressed (Figure 6-10). Then, structural smoothing was computed over the first derivative seismic cube (Figure 6-11). This increased the signal-to-noise ratio of the input seismic data, increasing seismic reflectors' continuity, while the local orientation (dip and azimuth) of the seismic reflectors were honoured, enhancing the presence of edges. Finally a variance attribute was calculated. Its calculation results in a new cube with information only related with edges (discontinuities in the horizontal continuity of amplitudes), such as faults and fractures (Figure 6-12). In complement to the variance attribute a data volume with information corresponding to the local dip estimation of seismic reflectors was also computed as part of the edge detection step. Local Dip Estimation may be useful to enhance the presence of faults, and other discontinuities, as well as to distinguish between different seismic textures. In the presence of faults, estimated dip values change abruptly, while along the fault planes the estimated dip value remains barely constant (Figure 6-13) (UNL, UALG, UA, & IST; *Modelling and Characterization of Fractured Reservoirs -GALP E&P Internal Report;* Lisbon; 2011).

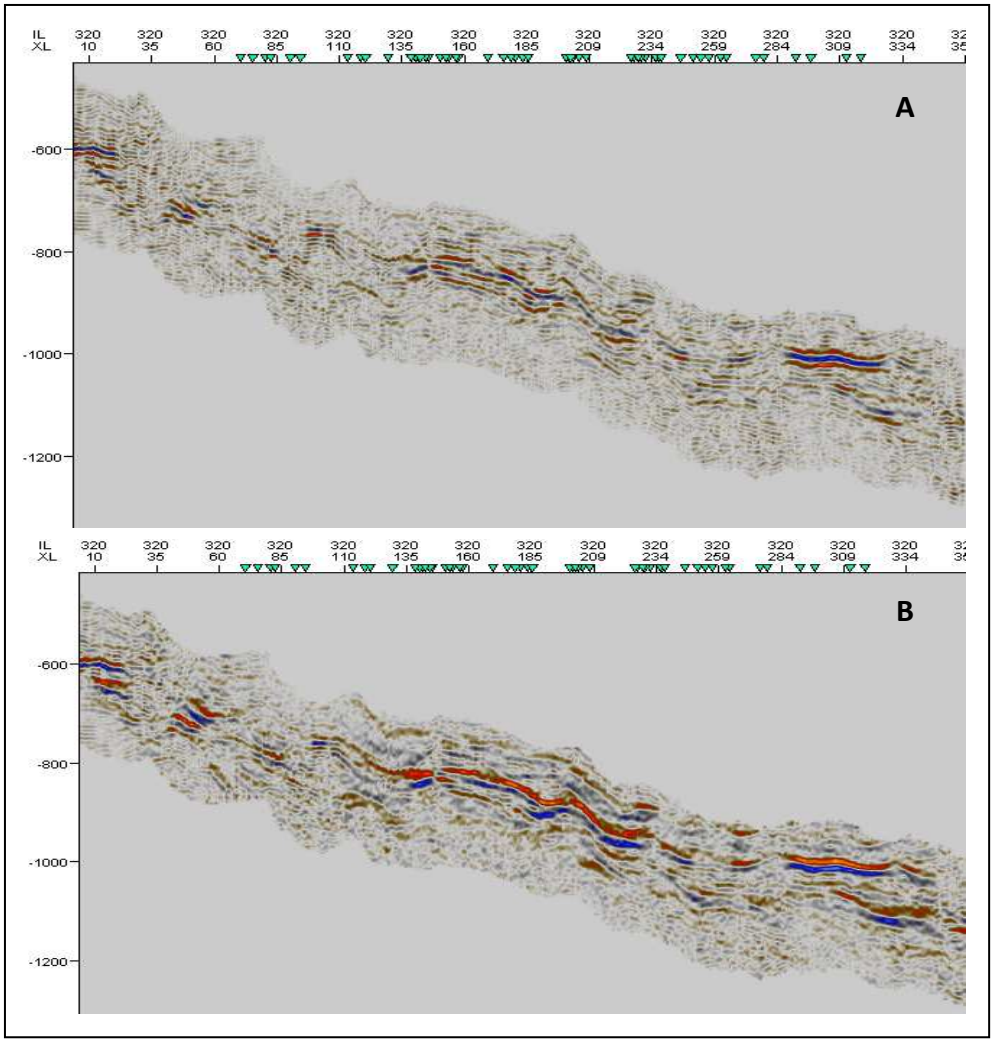

Figure 6-10: Vertical seismic sections from Block SEAL-A: (A) original seismic and (B) First Derivative attribute. The use of the First Derivative attribute enhances seismic reflectors' continuity and produces an increase in the vertical resolution of the data. A 90º-phase rotation appears with the calculation of the attribute. (UNL, UALG, UA, & IST; *Modelling and Characterization of Fractured Reservoirs -GALP E&P Internal Report;* Lisbon; 2011).

After all the seismic conditioning steps were completed, Ant-Tracking was applied (Figure 6-14). It is noticeable that the final images generated by the Ant-Tracking algorithm greatly improved fault detection, when compared to the structure cube generated from the regular seismic volume (Figure 6-6).

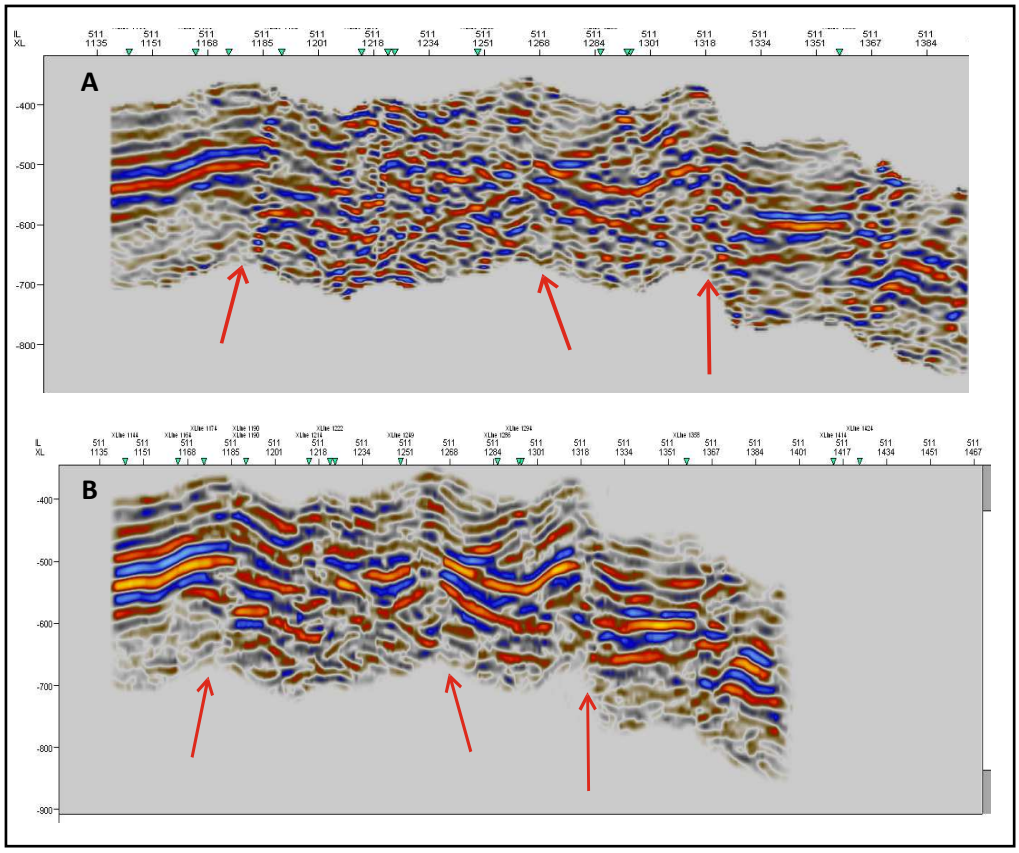

Figure 6-11: Vertical seismic sections from block SEAL-B: (A) *First Derivative* cube and (B) *Structural Smoothing* volume computed from the First Derivative cube. Notice the enhanced seismic reflectors' continuity while faults are better recognized (pointed by the red arrows). (UNL, UALG, UA, & IST; *Modelling and Characterization of Fractured Reservoirs -GALP E&P Internal Report;* Lisbon; 2011).

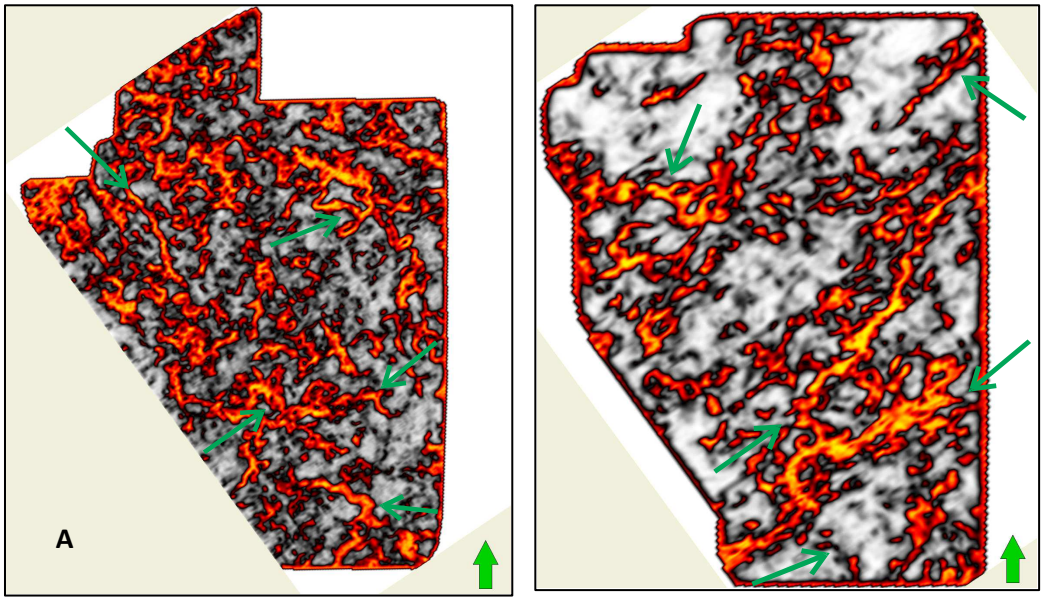

Figure 6-12: Horizontal time slices from the flatten *Variance* cubes for blocks: (A) SEAL-A and (B) SEAL-B. Green arrows represent faults detected by *Variance* which were also interpreted in the traditional seismic interpretation process. Warm colours represent high values of *Variance*, corresponding to discontinuities, and cold colours to low values of *Variance*, corresponding to continuities. Notice that the better quality of the seismic data from Block SEAL-B, allowed for a better extraction of discontinuities. (UNL, UALG, UA, & IST; *Modelling and Characterization of Fractured Reservoirs -GALP E&P Internal Report;* Lisbon; 2011).

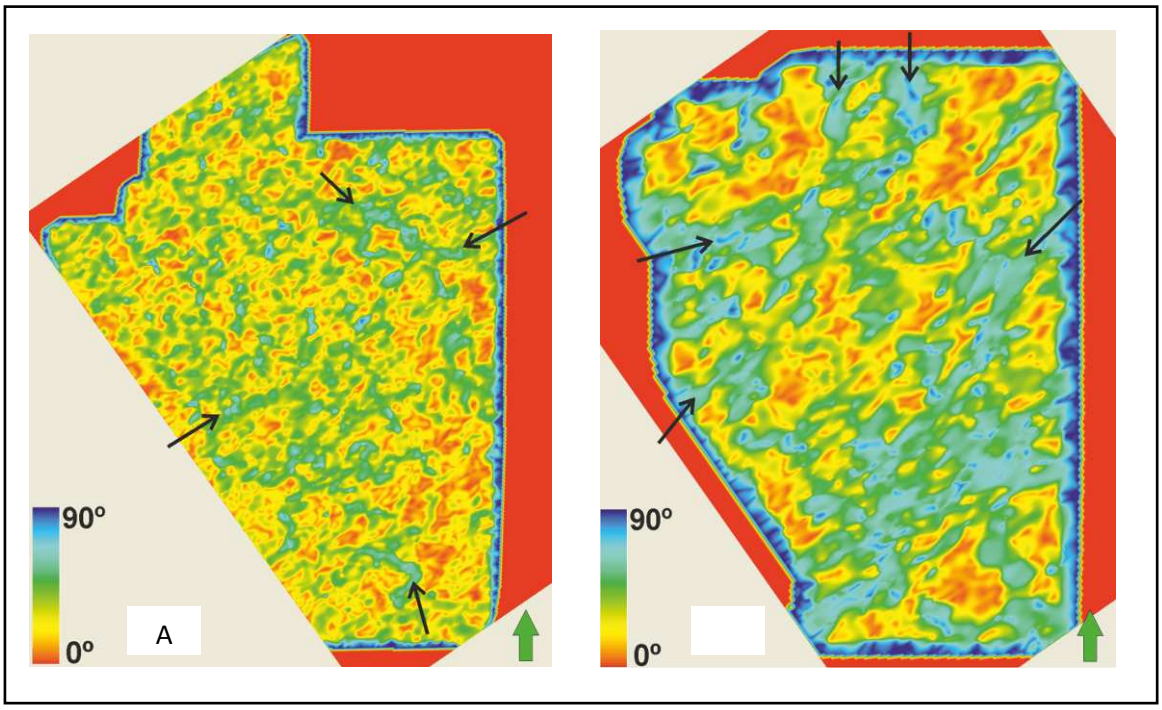

Figure 6-13: Horizontal time slices from the flatten *Local Estimation Dip* cubes from: (A) Block 412N and (B) Block T-412-429. Black arrows are example of faults, which are better delineated with higher resolution using the Dip estimated volume when compared to others (compare for example with figure 3.3). (UNL, UALG, UA, & IST; *Modelling and Characterization of Fractured Reservoirs -GALP E&P Internal Report;* Lisbon; 2011).

In order to validate the proposed methodology, verification and re-interpretation of the faults originally provided by Galp was carried out. This interpretation process was independent from the automatic fault detection workflow development and from the faults derived from the automatic fault extraction, in order not to bias it. The faults were therefore interpreted exclusively on the original seismic data, using the traditional user interpretation, and were considered as "hard data" to validate the Ant Tracking proposed methodology, without being influenced by its results (UNL, UALG, UA, & IST; *Modelling and Characterization of Fractured Reservoirs -GALP E&P Internal Report;* Lisbon; 2011). The results are presented in Figure 6-15 and 6-16. In Block-A most of the faults interpreted by U.Aveiro team had been already interpreted and received only some minor adjustments. Due to the better seismic quality and to more available working time, more faults were interpreted in Block-B, and with better positioning relative to the seismic. Figure 6-17 compares the Ant-Tracking cubes generated when the Standard or the U.Aveiro Workflow is used. It is easily noticeable that U.Aveiro workflow largely improves fault detection.

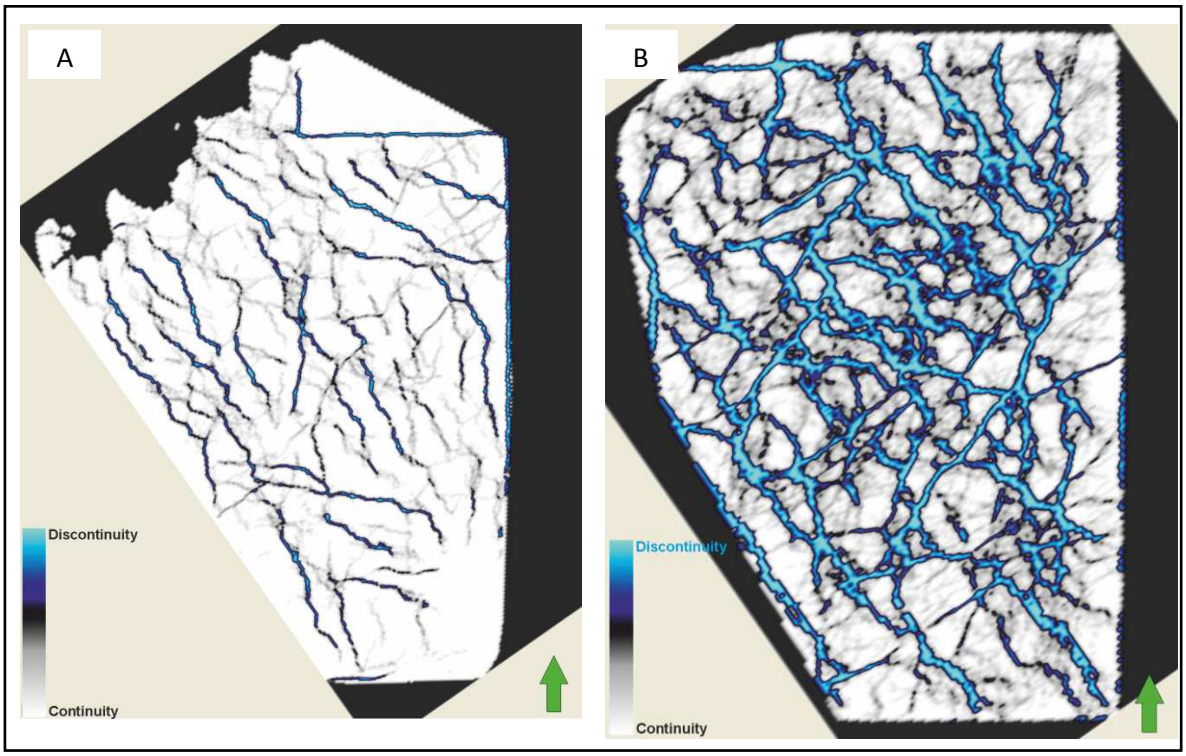

Figure 6-14: Horizontal time slices of the *Ant Tracking* cubes for: (A) Block-A and (B) Block-B. The blue lineaments represent possible faults detected by the modified Ant Tracking algorithm. Time slices extracted from the final output of the proposed methodology. (UNL, UALG, UA, & IST; *Modelling and Characterization of Fractured Reservoirs -GALP E&P Internal Report;* Lisbon; 2011).

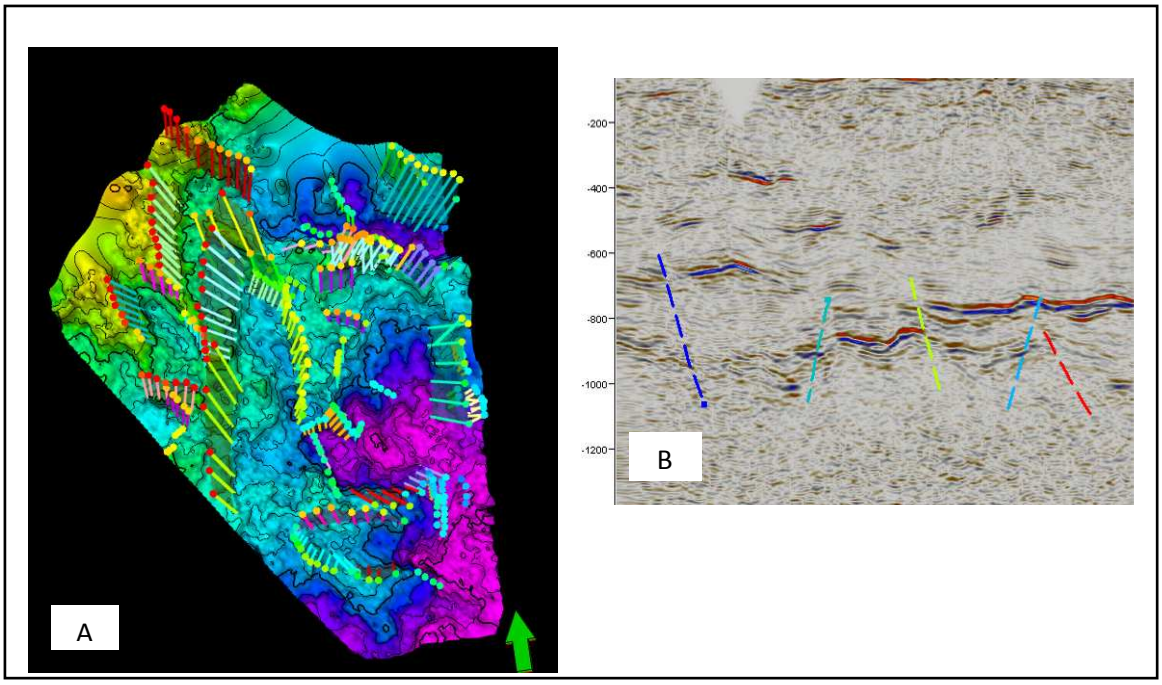

Figure 6-15: (A) Block-A Top Basement horizon surface with the main interpreted faults, in the time domain, delivered to Galp E&P. (B) Vertical seismic section with some of the interpreted faults. (UNL, UALG, UA, & IST; *Modelling and Characterization of Fractured Reservoirs -GALP E&P Internal Report;* Lisbon; 2011).

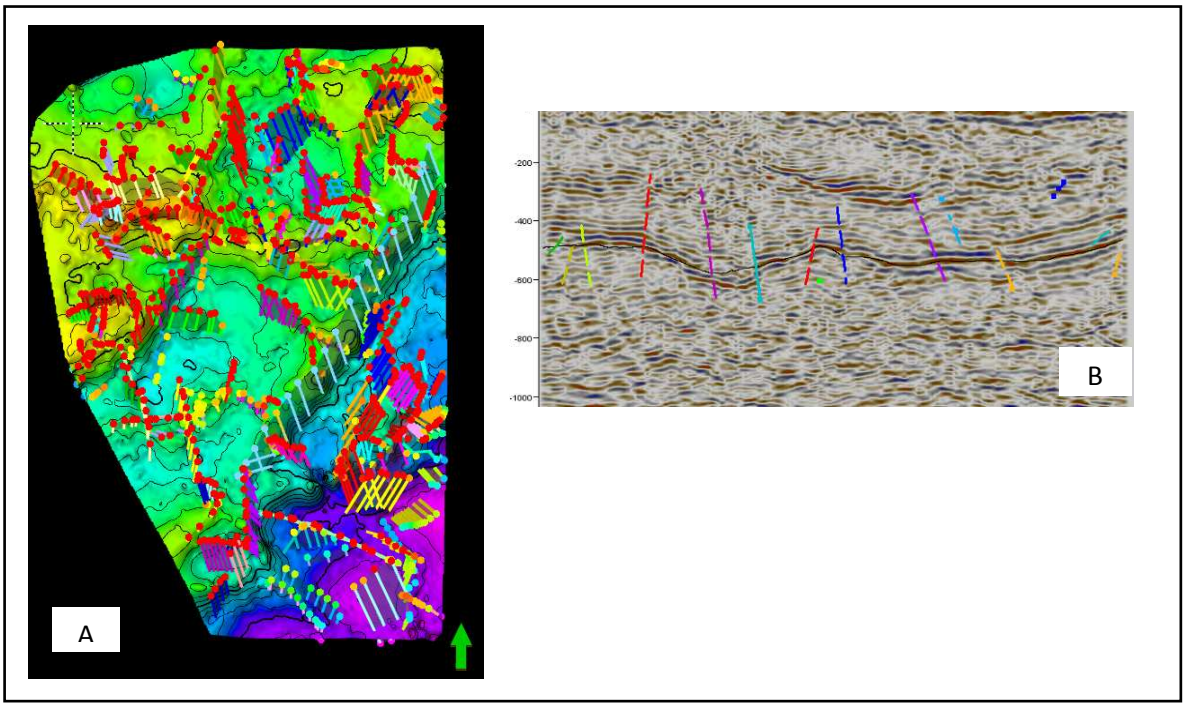

Figure 6-16: (A) Block-B Top Basement horizon surface with the main interpreted faults, in the time domain, delivered to Galp E&P. (B) Vertical seismic section with some of the interpreted faults. (UNL, UALG, UA, & IST; *Modelling and Characterization of Fractured Reservoirs -GALP E&P Internal Report;* Lisbon; 2011).

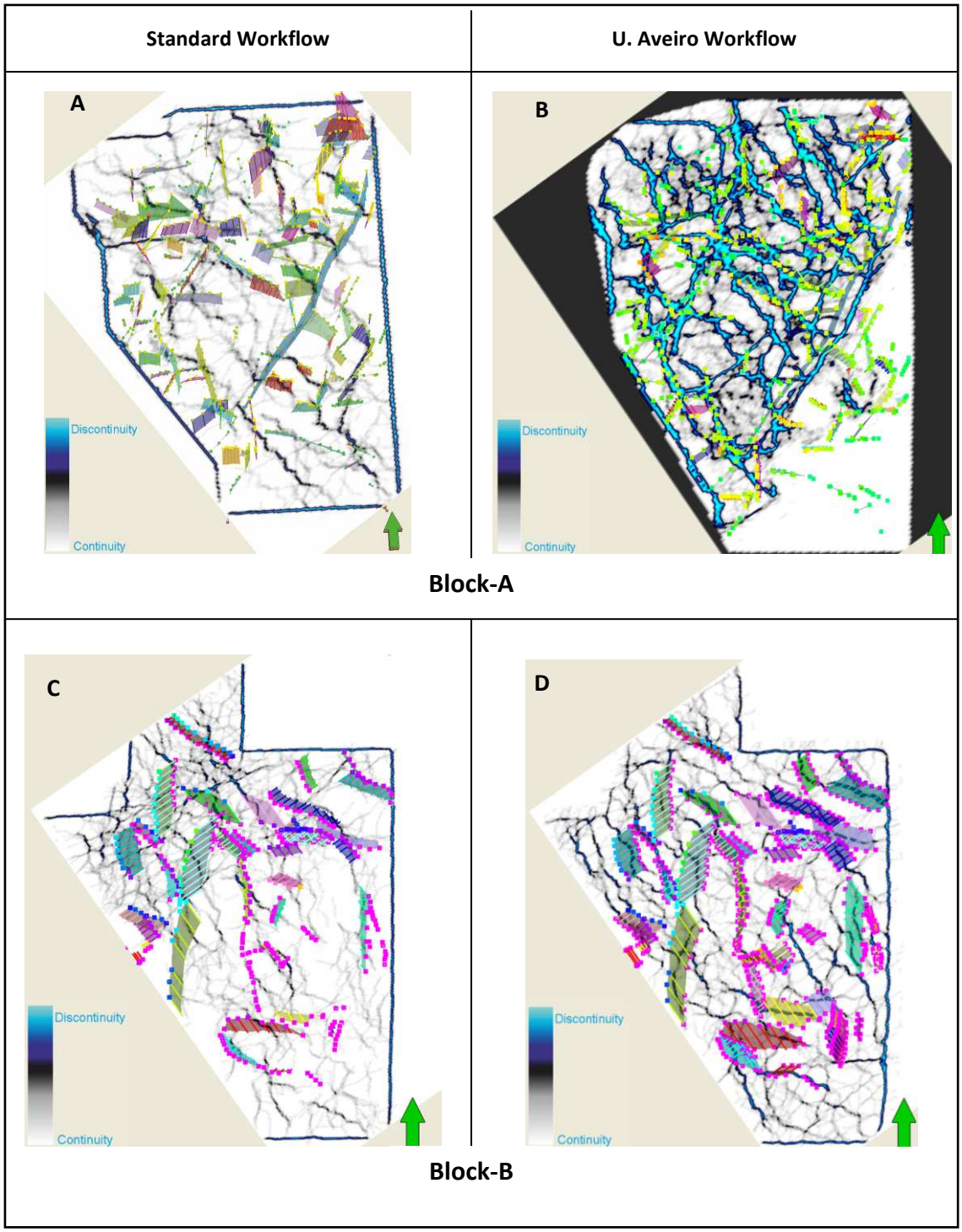

Figure 6-17: Comparison between the matching of the manually interpreted faults and the automatically detected faults in Standard Ant-Tracking workflow (A and C) and the U.Aveiro Ant-Tracking Workflow (B and D). Notice that the U. Aveiro workflow improved largely the match between the manually interpreted faults and the automatically detected faults, at the same time that improved the quality of the continuity cubes generated in the process. (UNL, UALG, UA, & IST; *Modelling and Characterization of Fractured Reservoirs - GALP E&P Internal Report;* Lisbon; 2011).

From the results presented above (Figure 6-17), the author considers that the U. Aveiro Ant-Tracking workflow is a valid methodology for improving the seismic data quality and consequent fault detection in SEAL basin. The method allows the interpreter to visualize more faults than if the Standard Workflow or just manual interpretation is used and it can also be used to have a fast overview of the structural framework or as a base to a further and more detailed structural interpretation ((UNL, UALG, UA, & IST; *Modelling and Characterization of Fractured Reservoirs -GALP E&P Internal Report;* Lisbon; 2011).

Based on his horizon interpretation and on the faults interpreted by the U. Aveiro team a Top Basement Horizon depth map, with the main interpreted faults was created. Not all faults are displayed, as they would overload the map not allowing for a good understanding. The wells displayed were not defined in this map as they were drilled previously to its elaboration. The final product can be found in Figure 7-1.

The interpreted and validated faults were then used for the construction of the Geomechanical Model that will be presented ahead.

6.1.4 Well Data

In well data the geologist can use several sources of information for detecting the fracture system and to derive information on its properties. In this section the drilling and testing procedures as well as the test results and the Formation Micro Imager (FMI) data for the seven wells performed will be analysed. Cores were not taken. Notice that the interpreted seismic sections and depth maps shown were made prior to the Fractured Basement Project.

6.1.4.1 Well Results Analysis

Alpha Well

- **Primary Objective**: testing the presence of HC in the Ibura Fm.
  Reservoir: fractured carbonates intercalated with evaporites (anhydrite).
- **Secondary Objective:** testing the presence of HC in the Calumbi Fm.
  Reservoir: sand bodies inside the turbidite levels of the Calumbi Fm.
- **Type of Well:** Vertical
- **Mud:** Conventional mud (8.7- 9 lb/gal) – Phase I
  Perflex fluid (9.2-9.8 lb/gal) – Phase II
  Perflex fluid (9.8-10 lb/gal) – Phase III (Mud weight when drilling through Basement)

The Alpha well was a vertical well positioned over a structural high at the Basement level. Figure 6-18 shows the pre-drill seismic interpretation on which the well location was based. The main horizons for the prospect identification (Top Ibura Mb. and Top Basement) are very poorly defined due to poor seismic imaging. Table 6-1 shows the comparison between the predicted and the actual drilled formation tops.

Table 6-1 - Comparison table of the predicted versus actual formation tops. Above (+). Below (-). The actual formation tops diverge from the predicted specially in Calumbi, Riachuelo and Muribeca Formations in a relatively high range of values, mainly due to interpretation errors related to poor seismic data quality and the velocity model used to create a seismic depth cube.

Formations		Depths				
		Preview		Drilled		Δ
		Measured	TVD	Measured	TVD	m
Barreiras Fm.		-	-	surface	1,17	-
Marituba Fm.		Sup	1,17	12	-6	-6
Calumbi Fm.		116	-110	140	134	-24
Cotinguiba Fm.	**Sapucari Mb.**	758	-752	767	-761	-9
	Aracaju Mb.					
Riachuelo Fm.	**Taquari Mb.**	814	-808	842	-836	-28
Muribeca Fm.	**Oiteirinhos Mb.**	841	-835	892	-886	-51
	Ibura M.	896	-890	932	-926	-36
Basement		964	-958	969	-963	-5
Final Depth		1076	-1050	1060	-1054	-4

Mudlog Analysis

For practical purposes, the mudlog shown in Figure 6-20 only displays the lower section of the well, from the Muribeca Fm. to Total Depth (TD). The oil shows found in Calumbi Fm. were not considered to be of importance due to the high content of shale in the sections where they were found. All the Retrievable Formation Test (RFT) samples made in Calumbi Fm. failed. Shows were recorded in the Cotinguiba Fm., but the sampling tests failed to recover any fluid.

The main observations from the mudlog analysis are:

- Oil shows were found from the top of the Muribeca Fm. (-878m) to TD.
- Gas peaks were registered in Muribeca Fm. at 883/890m, 918m/920m and the most important at 957m/970m (Lower Ibura Fm., Top of Basement).
- The Ibura Fm. did not contain as much anhydrite as expected, but the presence of carbonates levels were confirmed.
- The best oil shows were recorded at the base of the Ibura Fm. and Top Basement.
- Oil shows were recorded in the Basement down to a depth of approximately 1040m.

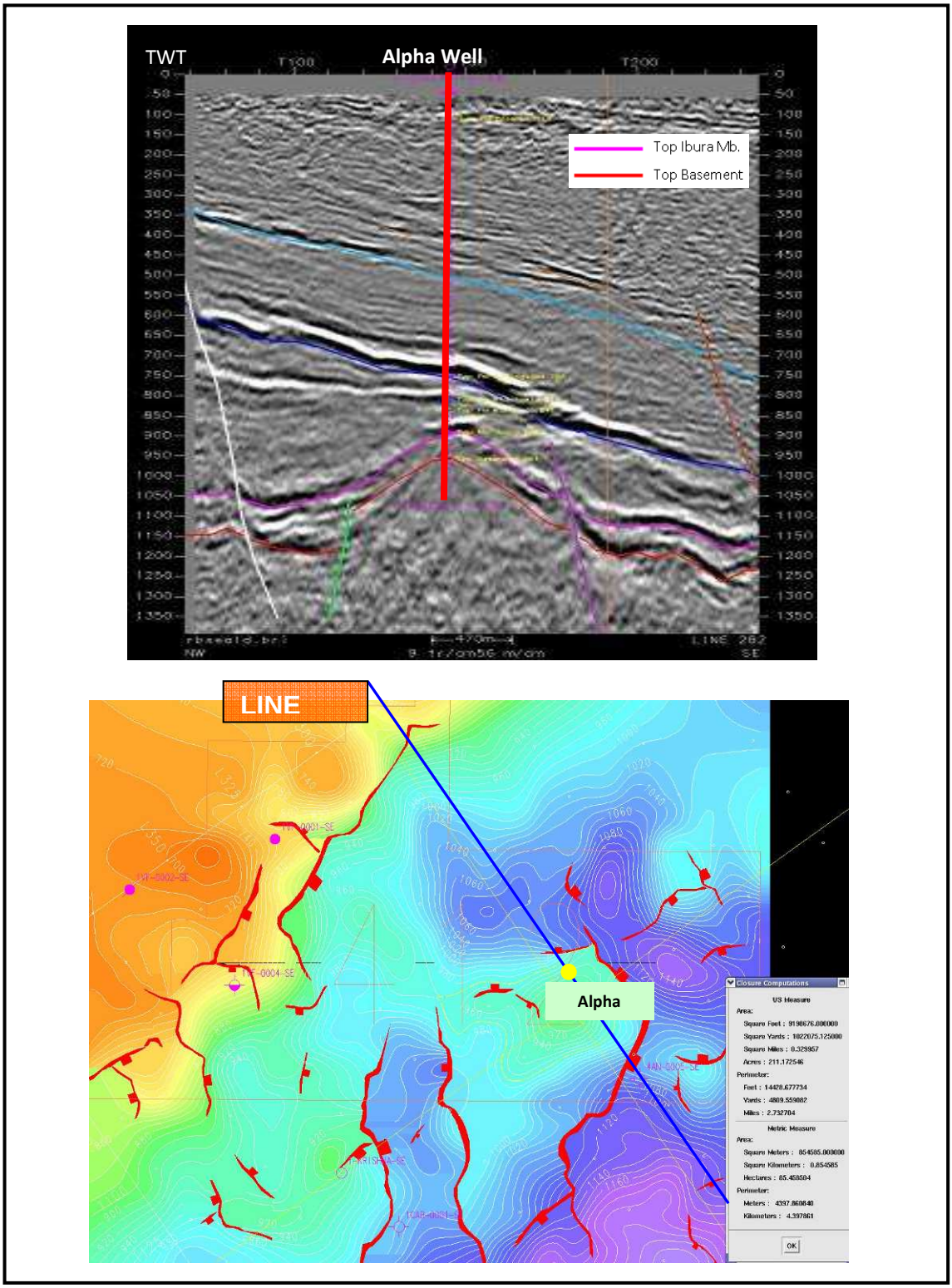

Figure 6-18: Seismic In-line in Depth and Top Ibura map section on which the positioning of the Alpha well was based. On the seismic line, notice the imprecise positioning of the faults and horizons relative to the seismic reflectors.

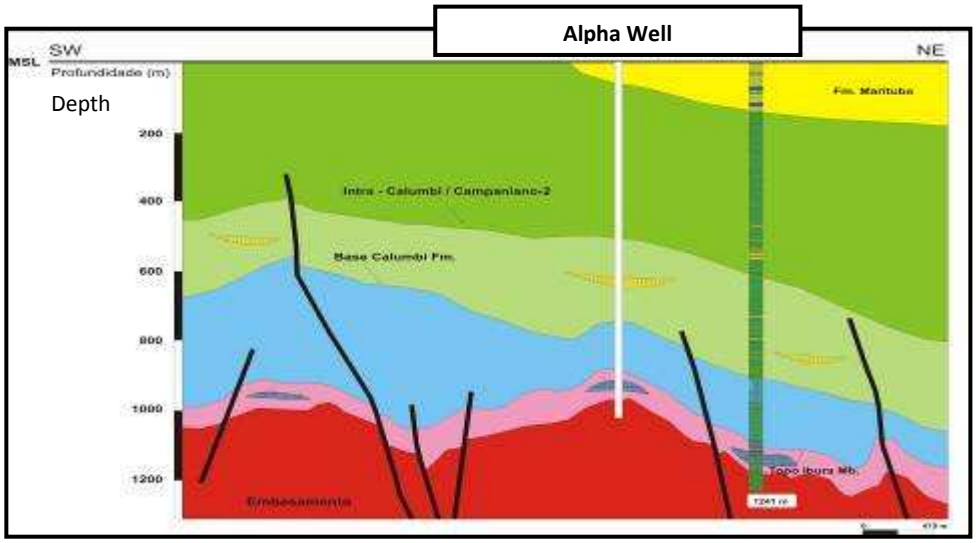

Figure 6-19: Schematic geological section of the Alpha well area. Notice that this section was made in XL direction (perpendicular to IL282 displayed in Figure 6-18)

Wireline Logging

Alpha Well was drilled in two phases. It was first drilled to 1000m and logging tools were run (including FMI). However, observations from the wireline logs indicate that zones of interest are not identified in when utilising conventional attributes (Figure 6-21). The FMI identified fractures along Oiteirinhos and Ibura Members and at the Basement and to test this interval, DST-01 was conducted. Due to the good results of the DST (See Appendix) it was decided to drill ahead (to actual TD) and test again (DST-02). Unfortunately, wireline tools were not run again not allowing for correlation between DST-02 and petrophysical properties or, even more important, with the images that the FMI could have recorded.

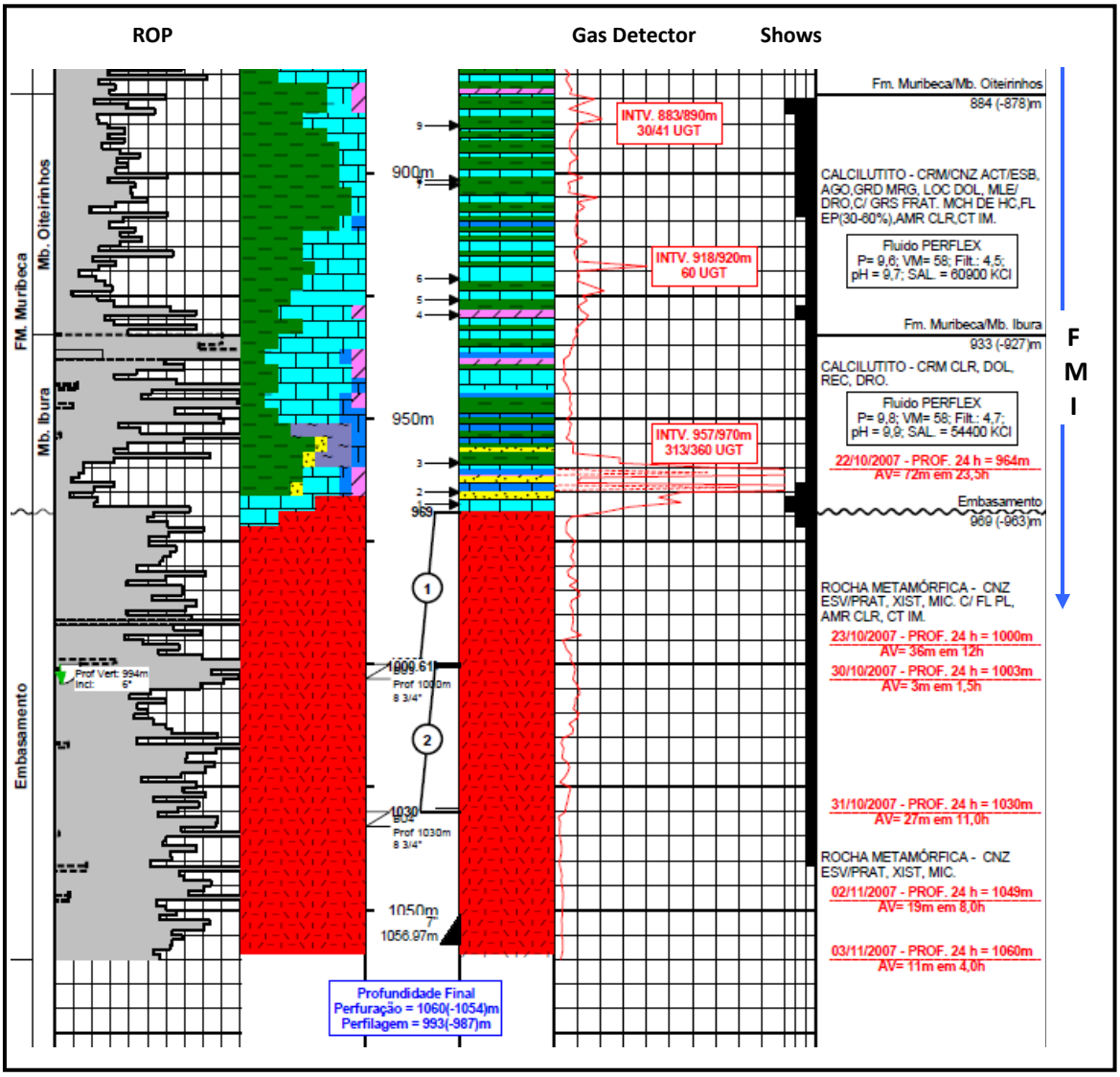

Figure 6-20: Mudlog of the lower section of the Alpha well. The blue arrow indicates the depth to which the FMI was run. The Drill Stem Test (DST) intervals are indicated by (1) and (2); the lower interval of Ibura Mb. was not tested despite the good HC shows. ROP = Rate of Penetration.

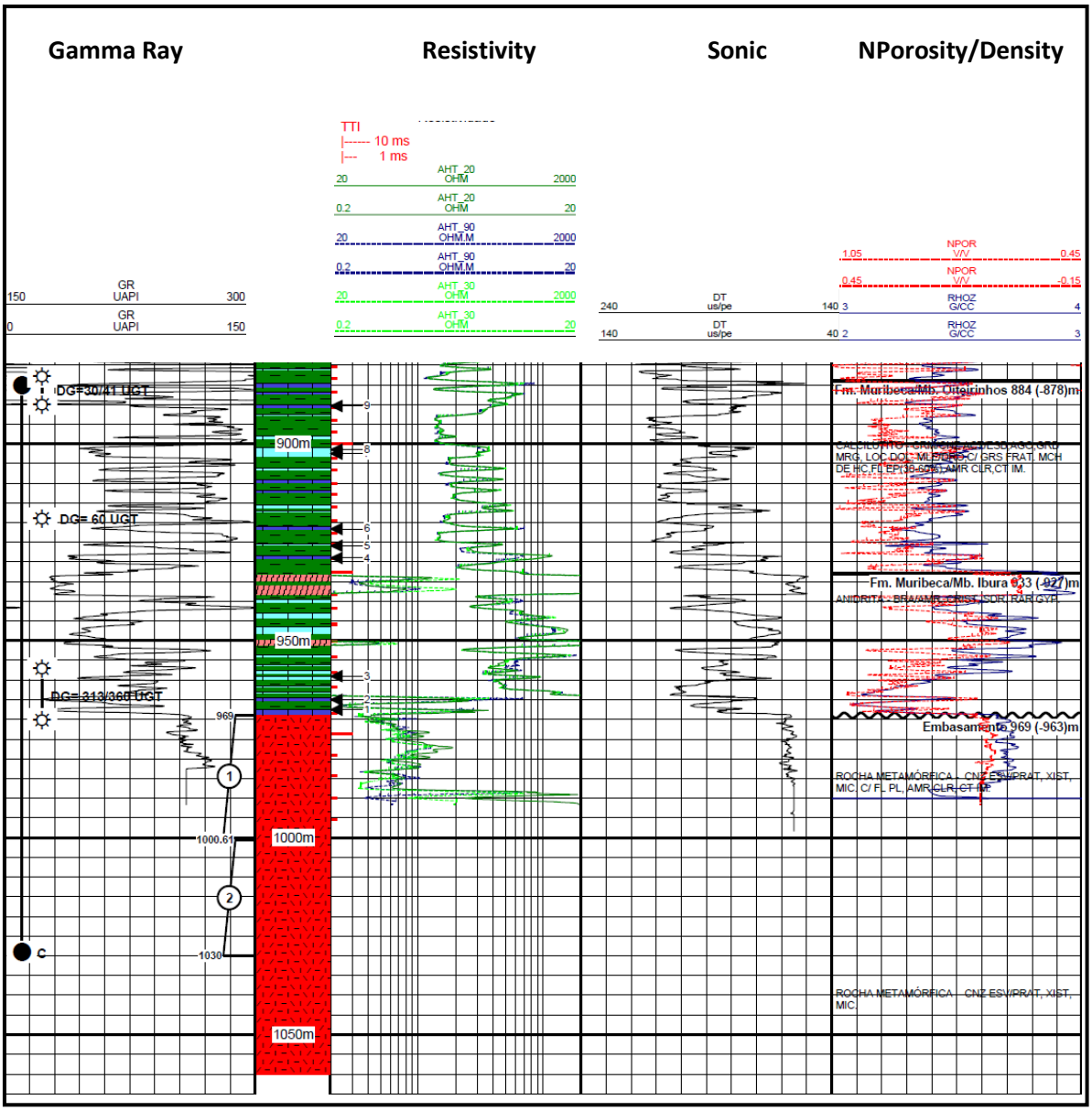

Figure 6-21: Composite well log for the Alpha prospect at the Muribeca and Basement levels. The wireline logs were not run to TD and as a result most of the basement section is not covered by the log analysis. Conventional log measurements do not appear to identify zones of interest.

DST Results: Alpha Well

DST-01 (969m - 1000m) – Figure 6-22

1st flow period - Moderate to strong blow during the entire flow period. Flow to surface. .

Due to gas flow, the burner was lit and produced a 1,5m yellow flame.

2nd flow period – non-existent

Reverse Circulation: 17 bbl of mud cut with oil and gas.

Sampling Chamber: 22l of oil cut with gas.

DST-02 (1000m-1030m) - Figure 6-23

1st flow period - Weak blow changing to moderate. No flow to surface

2nd flow period – non-existent

Reverse Circulation: 8 bbl of mud cut with oil and gas.

Sampling Chamber: 22l of oil cut with gas.

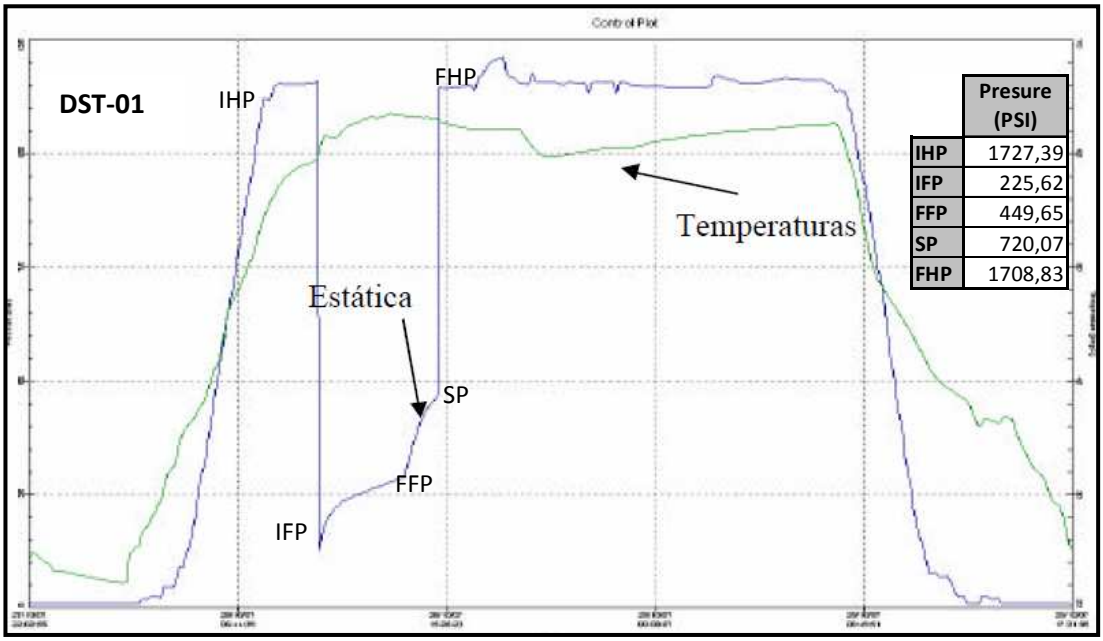

Figure 6-22: DST-01 pressure graphic. **IHP - Initial Hydrostatic Pressure, IFP – Initial Flow Pressure, FFP – Final Flow Pressure, SP – Static Pressure, FHP – Final Hydrostatic Pressure.** Notice that only one cycle of Flow-Period + Build-Up Period was performed, and that during the Build-Up Period, pressure wasn't allowed to stabilize – the curve should have flattened. Precise conclusions about the formation pressure can not be made as a result.

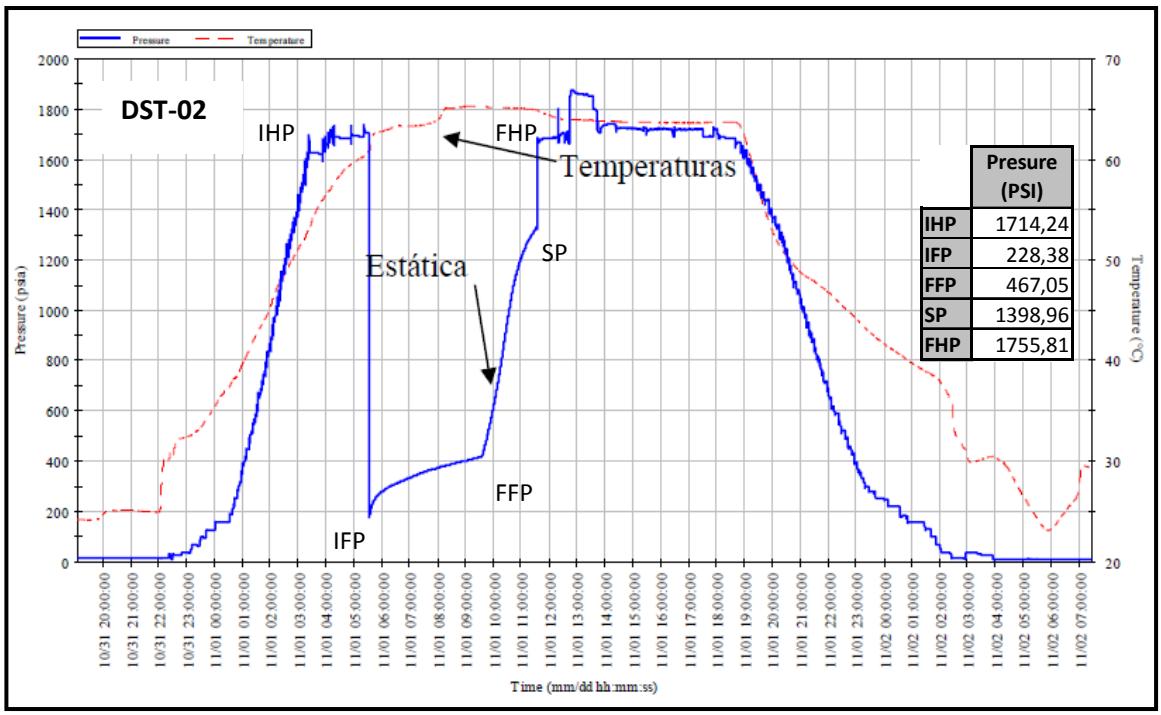

Figure 6-23: DST-02 pressure graphic. **IHP - Initial Hydrostatic Pressure, IFP – Initial Flow Pressure, FFP – Final Flow Pressure, SP – Static Pressure, FHP – Final Hydrostatic Pressure.** Notice that only one cycle of Flow-Period + Build-Up Period was performed, and that during the Build-Up Period, pressure wasn't allowed to stabilize – the curve should have flattened. Precise conclusions about the formation pressure can not be made as a result.

DST Results Analysis: Alpha Well

The DST procedures for this well were not performed according to the conventional procedures outlined in the Appendix of this thesis, as only one cycle was undertaken (Figures 6-22 and 6-23). As a result, it is difficult to make valid conclusions on the reservoir properties of the interval which was tested. The first cycle should have been performed as a clean up of the well, so that the actual pressure behaviour of the formations being tested could be registered on the second cycle. However, based on graphic analysis of the test result, it can be seen that reverse circulation started prior to Static Pressure Stabilization (SP). The pressure build-up period only lasted for two hours, time during which the formation pressure did not stabilize. Two observations can be made about this:

- The build-up time was very short, therefore making it difficult to make conclusive observations on the reservoir permabilities.
- It would appear that the interval's porosity is very tight and the pressure would have taken a extremely long time to recover based on the graphic rate of recovery.

- A third DST should have been performed on lower Ibura Mb. (check Figure 6-20) in order to test the presence of fluids in this interval and to record the pressure properties of the formation.

Bravo Well

- **Primary Objective**: testing the presence of HC in the Ibura Fm.

  Reservoir: fractured carbonates intercalated with evaporites (anhydrite).

- **Secondary Objective I:** testing the presence of HC in the Calumbi Fm.

  Reservoir: sand bodies inside the turbidite levels of the Calumbi Fm.

  Secondary Objective II: testing the presence of HC in the Basement.

  Reservoir: open fractures.

- **Type of Well:** Vertical.
- **Mud:** Conventional mud (8.7- 9 lb/gal) – Phase I

  Perflex fluid (9.2-9.8 lb/gal) – Phase II

  Perflex fluid (9.8-10 lb/gal) – Phase III (Mud weight when drilling through Basement)

Bravo well was a slightly deviated vertical well positioned over a Basement level structural high. Figure 6-24 shows the seismic interpretation made for the well positioning. The main horizons for the prospect identification (Top Ibura Mb. and Top Basement) are very poorly defined due to poor seismic imaging. Table 6-2 shows the comparison between the predicted and the actual drilled formation tops.

Table 6-2: Comparison table of the predicted versus actual formation tops. Above (+). Below (-). The actual formation tops diverge from the predicted in a relatively high range of values, mainly due to interpretation errors related to poor seismic data quality and the velocity model used to create a seismic depth cube.

Stratigraphic Tops						
Formations		Depths				
		Preview		Drilled		Δ
		Measured	TVD	Measured	TVD	m
Barreiras Fm.		-	-	surface	8	-
Marituba Fm.		surface	8	25	-12	-25
Calumbi Fm.		137	-124	144	-131	-7
Cotinguiba Fm.	Sapucari Mb.					
	Aracaju Mb.	616	-603	670	-657	-54
Riachuelo Fm.	Taquari Mb.	716	-703	691	-678	-25
Muribeca Fm.	Oiteirinhos Mb.	837	-824	884	-871	-47
	Ibura M.	939	-926	936	-923	3
Basement		999	-986	1005,5	-992	-7
Final Depth		1029	-1016	1101	-1088	-72

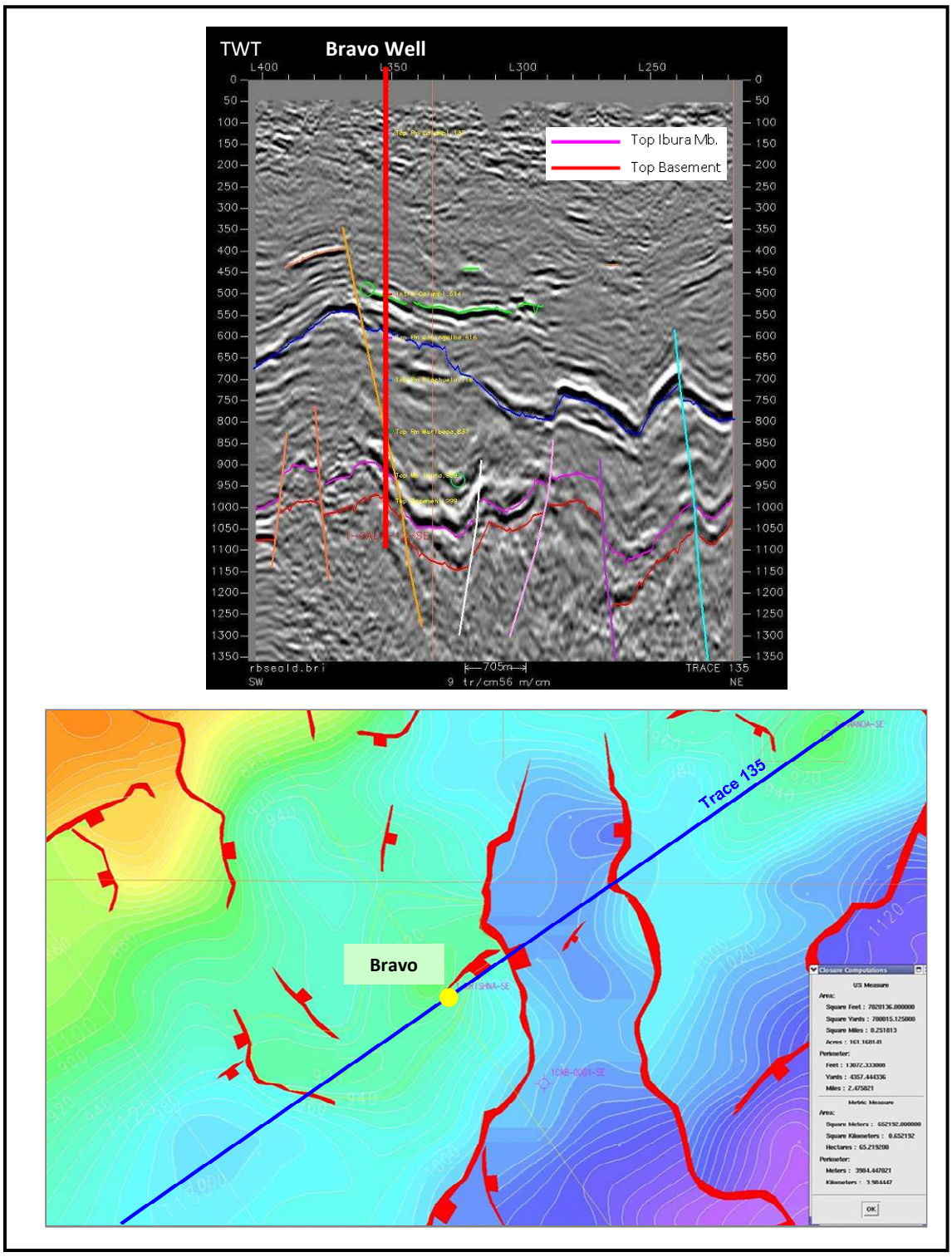

Figure 6-24: Seismic cross-line in Depth and Top Ibura Map on which the positioning of the Bravo well was based. On the seismic line, notice the imprecise positioning of the faults and horizons relative to the seismic reflectors.

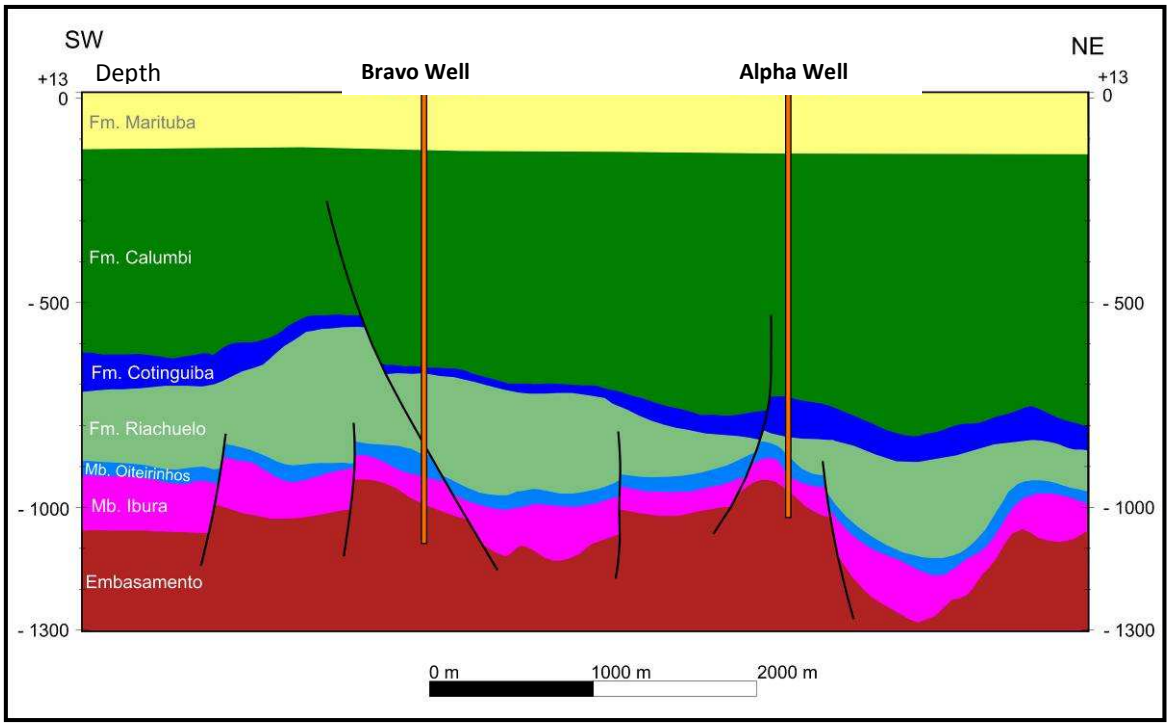

Figure 6-25: Schematic geological section of the Bravo and Alpha wells area. Notice that this section was made in cross-line direction.

Mudlog Analysis

For practical purposes the mudlog shown below displays only one section at Calumbi Fm. (Figure 6-26) and another from the Muribeca Fm. to TD (Figure 6-27).

Main observations from the log analysis:

- In the Calumbi Fm. oil shows occurred from 535m to 570m and from 600m to 610m within sand prone sections (Figure 6-26(A)). MDT tests were performed in these zones (Table 6-3). Wireline logs demonstrated that the intervals had good reservoir characteristics (Figure 6-26(B)), but were too thin to be considered for future production.
- Some minor oil shows were found in the Riachuelo Fm. but these were considered irrelevant due to the high content of shale in the Formation.
- Shows were also recorded from 884m to 1070m, in Muribeca Fm. and the Basement. The best were at the top of Ibura Mb. (Muribeca Fm.) and in the transition between this and the Basement (Figure 6-27).

Table 6-3: Results of the Sampling and Pressure tests over the sand sections of Calumbi Fm. Notice that in TCA1 oil was sampled but most of the fluid was filtrate.

Fluid Sampling Tests					
Test	**Interval**		**Fluid**	**Hydrostatic Pressure**	**Pressure (kgf/cm^2)**
	Top	**Base**			
TCA1			**Upper chamber - 4,0 L of fluid recovered** - 3,5 L of filtrate. Parameters: salinity = 42.900 mg/l NaCl; pH=8.26; Ca++ = 2160 mg/l ; Mg++ = 56 mg/l; pH = 8.26 - 0,5 l of oil. **Lower chamber - 10 L of fluid recovered** - 9.9 L of filtrate. Parameters: salinity = 42.900 mg/l NaCl; pH = 8.46; Ca++ = 2160 mg/l ; Mg++ = 141 mg/L, - 100ml of oil.	72.2	64,01
TCA2	539	-	Pressure Test	64.61	53,19
TCA3	542,5	-	Pressure Test	68.92	53,56
TCA4	548	-	Pressure Test	70.28	54,06
TCA5	619	-	Pressure Test	74.25	64,11

Wireline Logging

The analysis of the wireline logs for Calumbi Fm. (Figure 6-26), together with the results from the RFT, showed that the oil shows detected in the cuttings did not correspond to a section of interest because the sand prone interval was too thin to be considered for production.

Like Apha Well, Bravo Well was drilled in two phases. It was first drilled to 1042m and logging tools were run (including FMI). However, observations from the wireline logs indicate that zones of interest are not identified when utilising conventional attributes (Figure 6-28). Despite this FMI indentified fractures in Oiteirinhos Mb., Ibura Mb. and at the Basement. DST-01 was then performed and due to the good results it was decided to drill ahead (to actual TD) and test again in DST-02, which had very poor results. Unfortunately wireline tools were not run again. This way we cannot correlate the results of DST-02 with any specific petrophysical property of the rock, or to take conclusions on if the Oil Water Contact was reached.

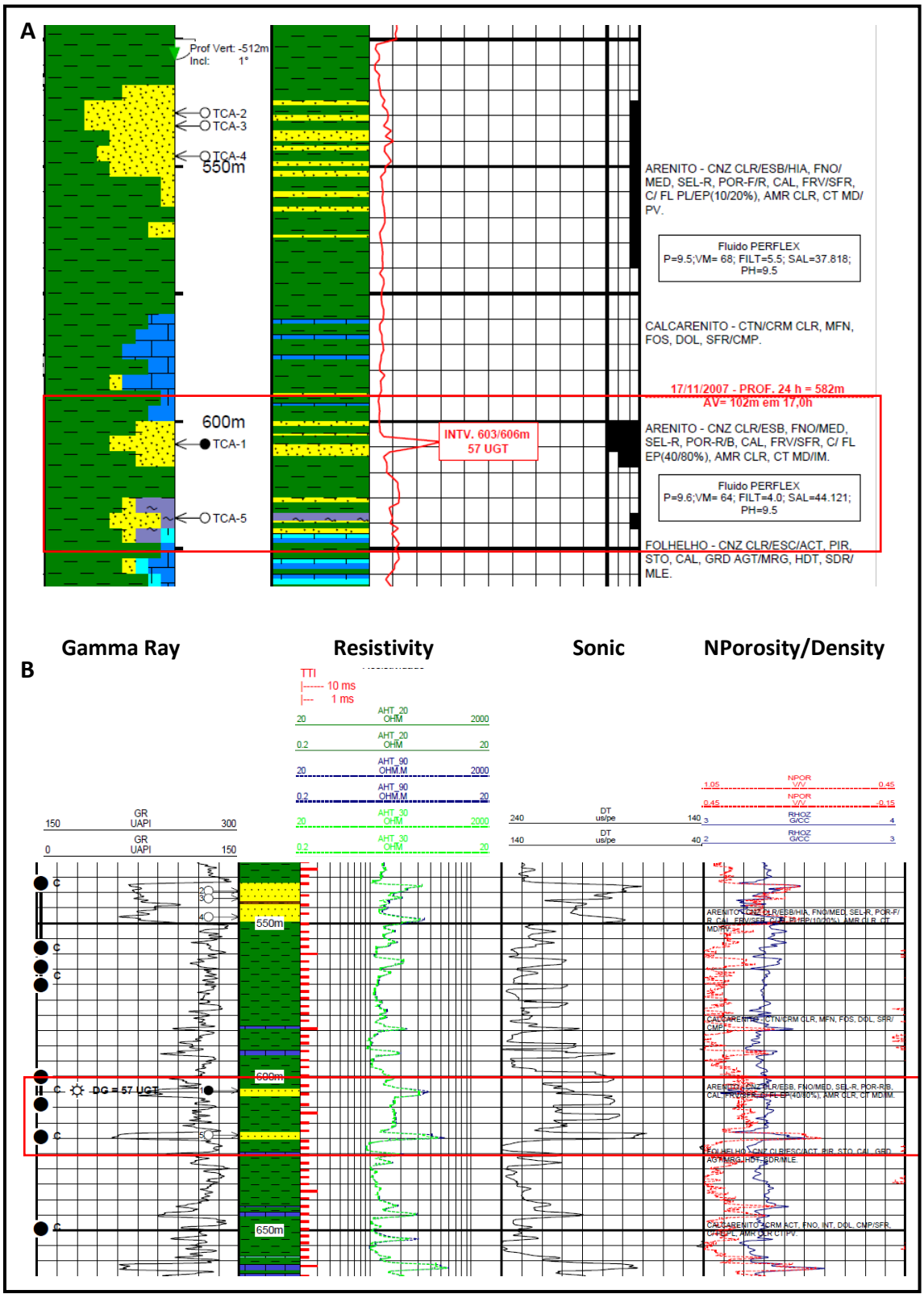

Figure 6-26: Mudlog (A) and composite log (B) showing the Calumbi Fm. section that was sampled. It may be observed that despite the good HC shows at 600m-608m the NTG ratio of clay in the interval is around 50% which reduces its reservoir quality. The wireline also identified these intervals (marked in red) and confirmed that they have a lower content of clay (relative to the over and under burden) but are very thin.

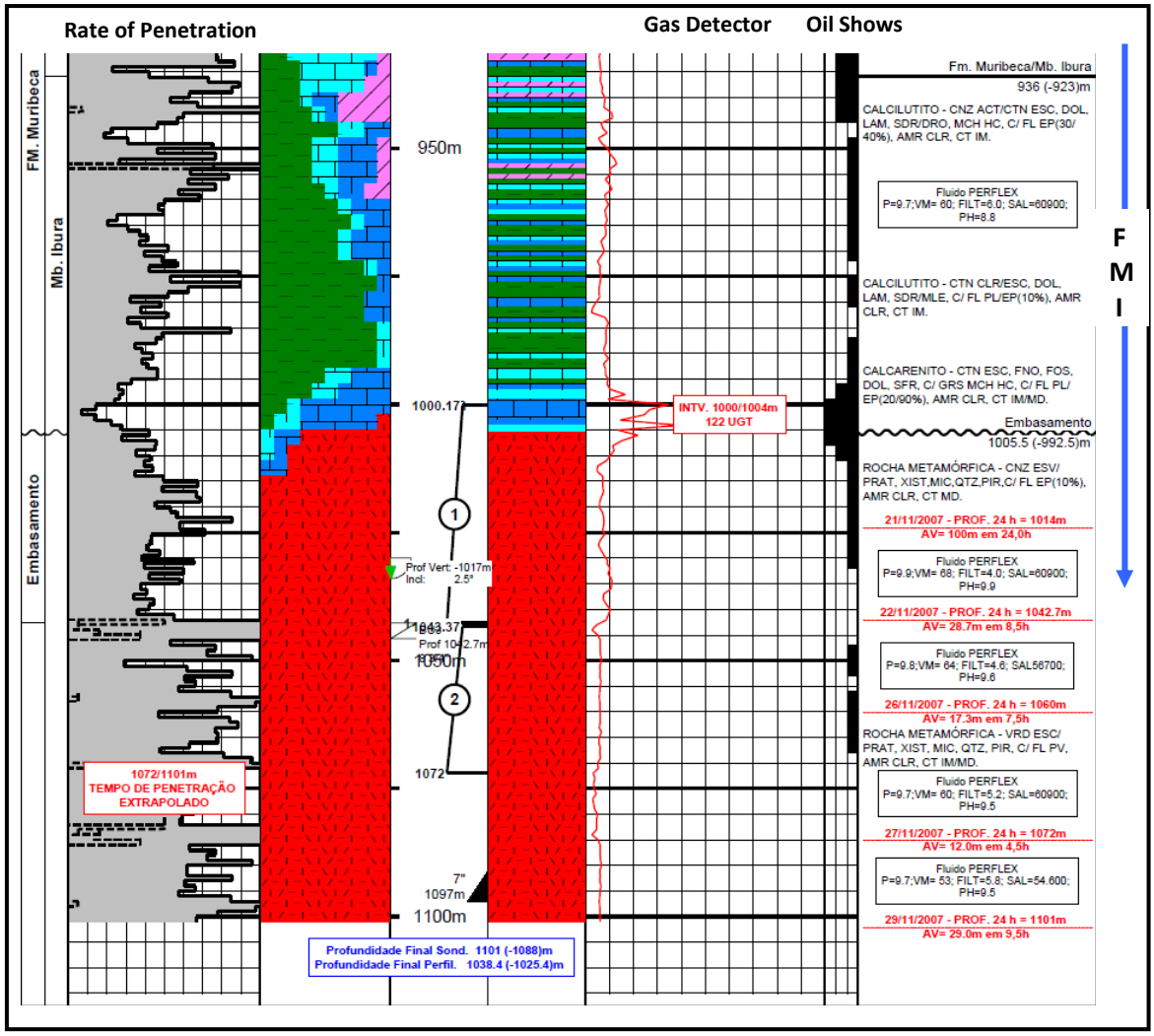

Figure 6-27: Mudlog of the lower section of the Bravo well. The blue arrow indicates the depth to which the FMI was run. The DST's intervals are indicated by (1) and (2); notice that DST-1 tested together lower Ibura Mb. and around 40m of Basement. It is therefore impossible to derive conclusive evidence about either the provenance of the sampled fluids or the pressure characteristics of each individual formation. The correct procedure would have been to test each formation independently.

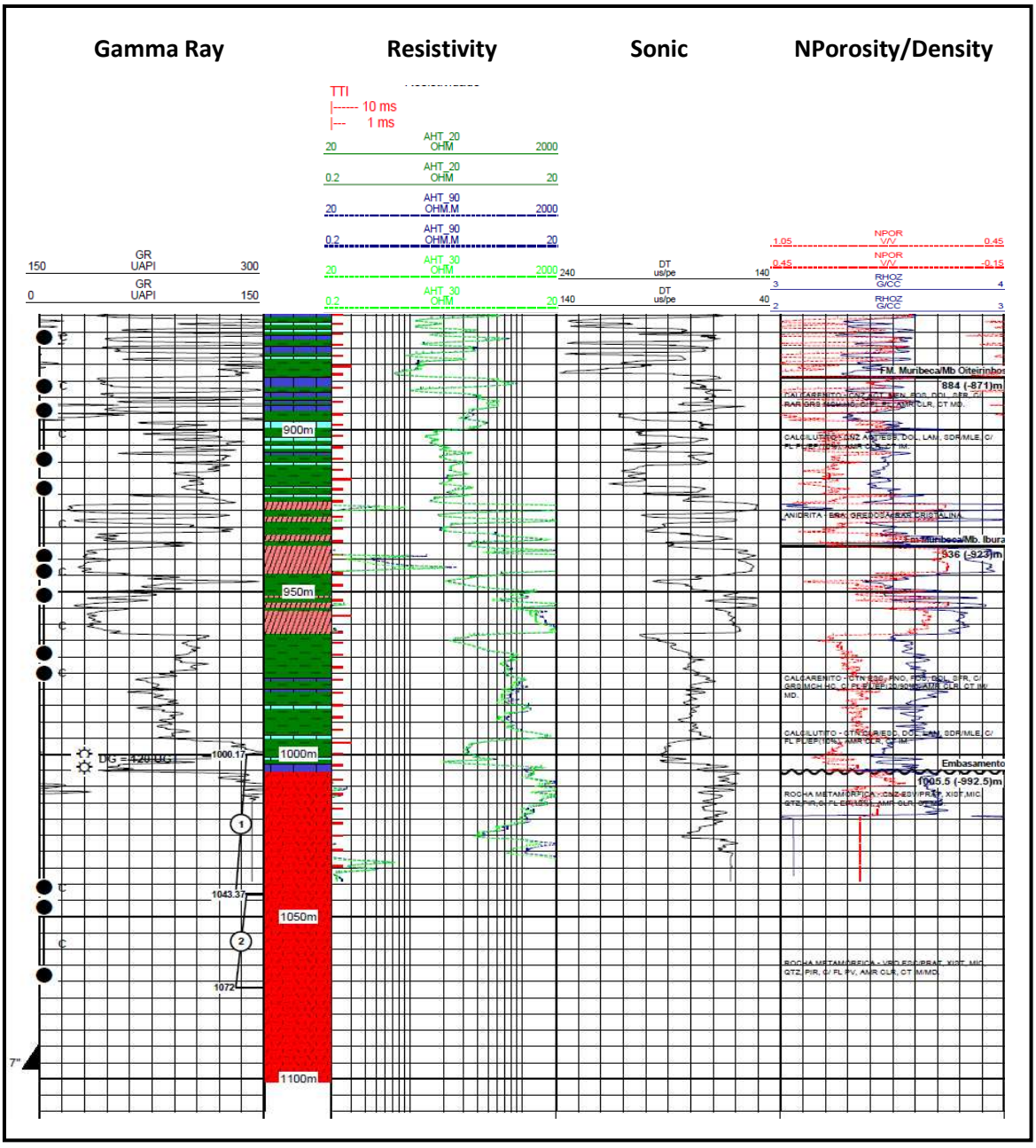

Figure 6-28: Composite well log for the Bravo well at Muribeca and Basement level. Notice that the wireline logging did not continue to TD, leaving most of the basement section uncovered by the log analysis. Conventional log measurements do not appear to identify zones of interest.

DST Results: Bravo Well

DST-01 (1000m - 1042m) - Figure 6-29.

1st flow - Moderate/strong blow during the flow period. Flow to surface. Due to gas flow, the burner lit and produced a 2m yellow flame.

2nd flow – inexistent.

Reverse Circulation: 52 bbl of mud cut with oil and gas.

Sampling Chamber: 37l of oil (29º API @ 60ºF) cut with gas.

Pressure information (PSI): IHP= 1699.83; IFP=480.89; FFP= 1202; SP= 1405.97; FHP = 1696.

DST-02 (1043m-1072m) Figure 6-30

1st flow - Weak blow. No flow to surface.

2nd flow – inexistent.

Reverse Circulation: 8 bbl of water.

Sampling Chamber: 8l of formation water (salinity = 127.050 NaCl; pH = 7,56; Cl^- = 77.000; Ca++ = 8.000 mg/l).

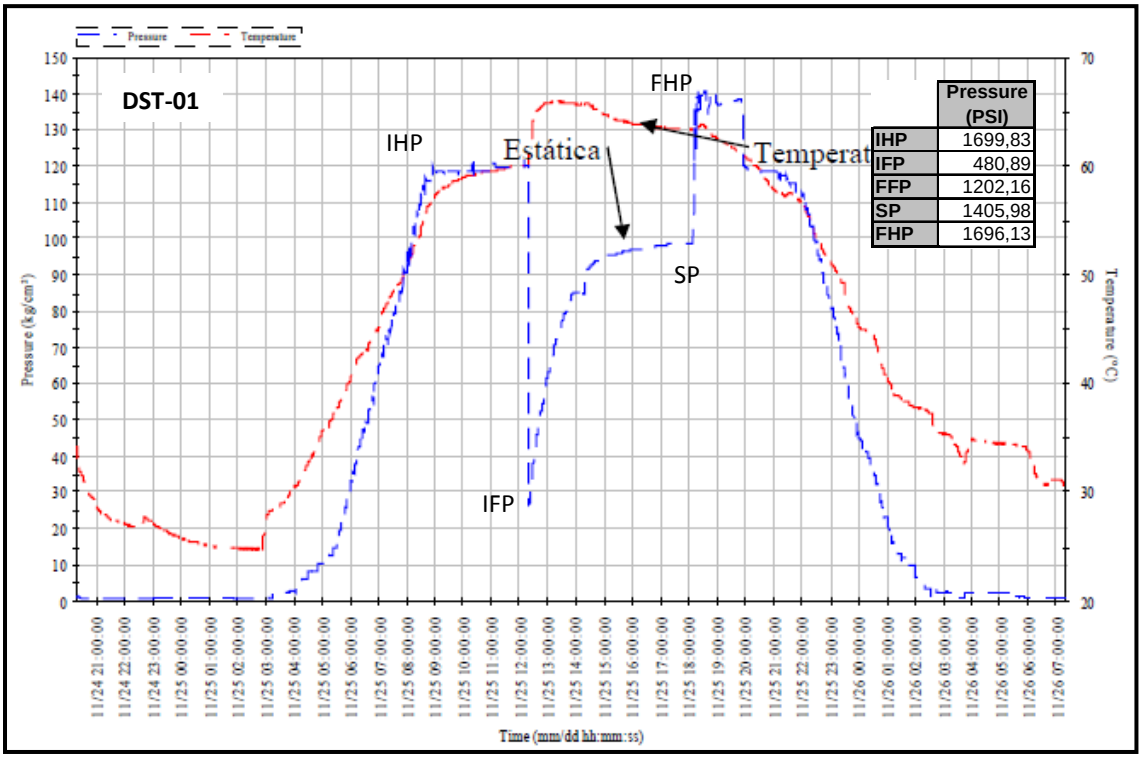

Figure 6-29: DST-01 pressure graphic. **IHP - Initial Hydrostatic Pressure, IFP – Initial Flow Pressure, FFP – Final Flow Pressure, SP – Static Pressure, FHP – Final Hydrostatic Pressure.** The graphic doesn't show an Initial Flow Period but it possible to observe that pressure rose steeply after the Build-Up, beginning to stabilize after 5 hours.

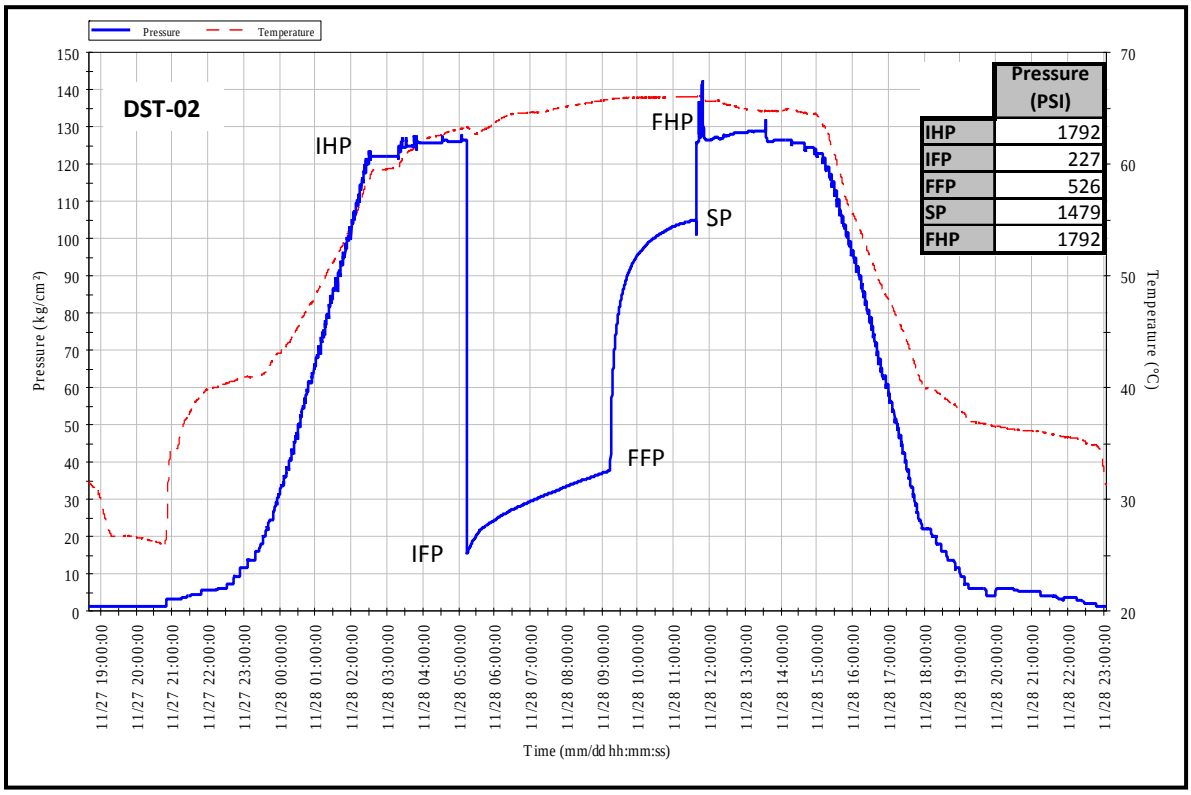

Figure 6-30: DST-02 pressure graphic. **IHP - Initial Hydrostatic Pressure, IFP – Initial Flow Pressure, FFP – Final Flow Pressure, SP – Static Pressure, FHP – Final Hydrostatic Pressure.** It is possible to observe that after the FFP the pressure rose steeply and it started to stabilize after 3 hours. It would have been necessary to open the valves for a second cycle to take conclusions on the real pressure behaviour of the well.

DST Results Analysis: Bravo Well

The DST procedures for this well were not performed according to the conventional procedures (outlined in the Appendix of this thesis), as only one cycle was undertaken (Figures 6-29 and 6-30). As a result it is difficult to make valid conclusions on the reservoir properties on the interval which was tested. The first cycle should have been done as a clean up of the well, so that the actual pressure behaviour of the formations being tested could be registered on the second cycle.

The analysis of DST-01 graphic and the reported strong blow lead us to think that this is either an interval with a relatively good permeability, or at high pressure, as a rapid increase in pressure during the build-up period is observed. Taking into account that the Basement rock that was tested was identified in mudlogging as being a micaschist, we consider it to have very low or inexistent primary porosity. This lead us to think that it is not likely that the formation is at high pressure but that the strong blow is a result of the good permeability given by the open fractures registered by the FMI. The final recorded formation pressure remains 290 PSI below the FHP

which most likely indicates that the well was drilled overbalanced. Even tough the well pressure did not actually stabilize which contradicts the difference in the formation pressure. The pressure plot however does not show a flow period despite the fact that there was blow reported at the surface and a gas flow was also registered.

Based on the DST-02 pressure plot, and the weak blow registered at the surface, it may be concluded that the lower section of the basement has low permeability.

The DST's should have been made planned and performed as in the Alpha Well, that is, the Ibura Mb. and the Basement should have been tested independently, as this is the only way to understand from which specific interval(s) the fluids are flowing from.

Charlie Well

- **Primary Objective**: testing the presence of HC in the Ibura Fm.

  Reservoir: fractured carbonates intercalated with evaporites (anhydrite).

- **Secondary Objective I:** testing the presence of HC in the Basement.

  Reservoir: fractured metamorphic rock.

- **Type of Well:** Vertical.
- **Mud:** Conventional mud (8.7- 9 lb/gal) – Phase I

  Perflex fluid (9.2-9.8 lb/gal) – Phase II

  Perflex fluid (9.8-10 lb/gal) – Phase III (Mud weight when drilling through Basement)

Charlie well was a deviated vertical well positioned over a Basement level structural high. It was deviated to try to intersect Carmopolis Mb. Figure 6-31 shows the seismic interpretation made for the well positioning. Table 6-4 shows the comparison between the predicted and the actual drilled formation tops.

Table 6-4: Comparison of the predicted versus actual formation tops**.** Above (+). Below (-). The actual formation tops diverge from the predicted in a relatively high range of values, mainly due to interpretation errors related to the poor seismic data quality and the velocity model used to create a seismic depth cube.

Stratigraphic Tops						
Formations		Depths				
		Preview		Drilled		Δ
		Measured	TVD	Measured	TVD	m
Barreiras Fm.		-	-	surface	16	-
Marituba Fm.		-	-	-	-	-
Calumbi Fm.		-	-	-	-	-
Cotinguiba Fm.	Sapucari Mb.	surface	16	8	-13	-8
	Aracaju Mb.					
Riachuelo Fm.	Maruim Mb.	117	-96	96	-75	21
	Taquari Mb.	289	-268	307	-286	-18
Muribeca Fm.	Oiteirinhos Mb.	486	-465	530	-509	-44
	Ibura Mb.	531	-510	596	-575	-65
	Carmopolis Mb.	-	-	-	-	-
Basement		603	-582	636	-615	-33
Final Depth		633	-612	757	-736	-124

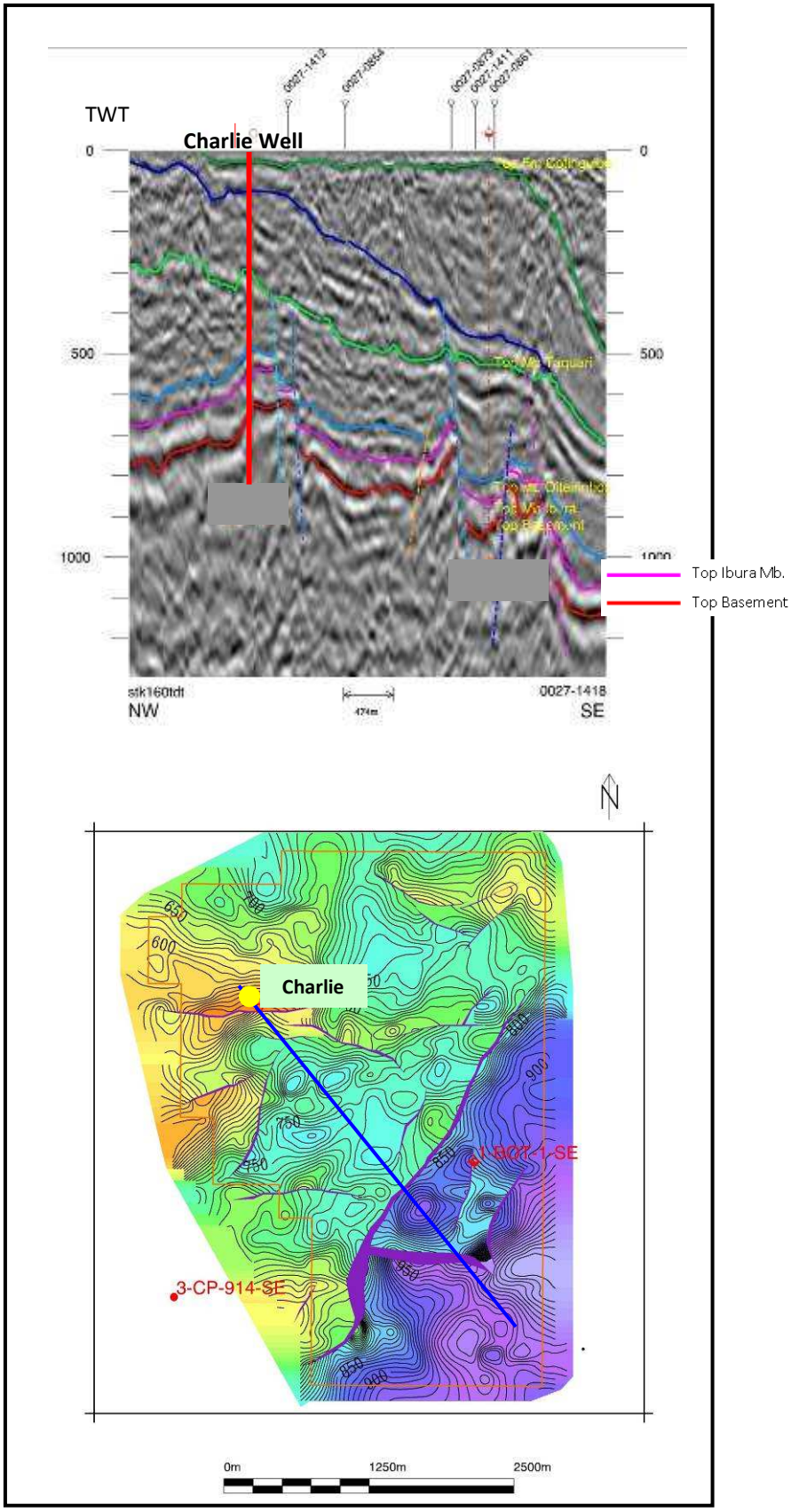

Figure 6-31: Seismic In-Line in depth and Top Ibura depth map on which was based the positioning of the Charlie well.

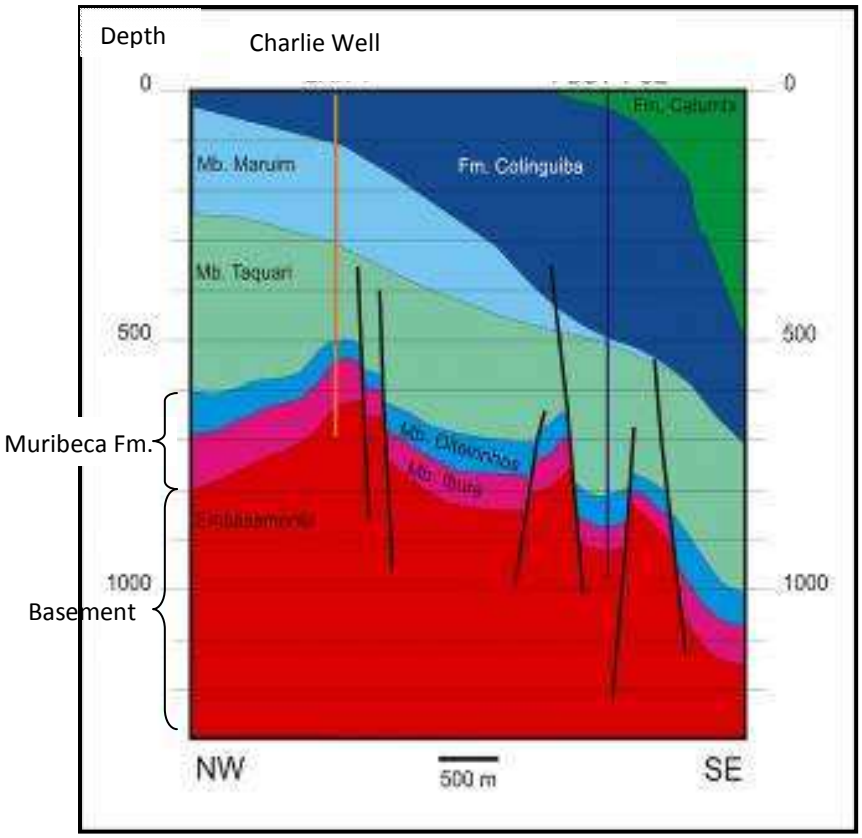

Figure 6-32: Schematic geological section of the Charlie well area.

Mudlog Analysis

Main observations from the mudlog analysis are (Figure 6-33):

1. Oil shows were relatively constant from the top of Muribeca Fm. to 700m.
2. The best oil shows were found in the Ibura Mb. and at the top Basement.
3. The Ibura Mb. presented a section of around 40m of carbonates below a 10m thick section of anhydrite. This section had good oil shows.

Wireline Logging Analysis

Given that:

a) good oil shows were present over the Basement and Ibura Mb. intervals,

b) the established potential of fractured Basement in the region, and

c) from our previous experience with Alpha and Bravo Well;

the decision was taken to perform open hole Drill Stem Testing (test – drill ahead – test procedure) and run the wireline logging tools with the FMI.

Apart from the Ibura Mb. where it is possible to identify two intervals of good porosity, the analysis of the wireline logs indicate that no zones of interest are identified in either the Oiteirinhos Member or Basement when utilising conventional attributes (Figure 6-34). It may also be observed that two different sections can be identified in the Basement on the sonic log (Figure 6-35): the average transit time in the upper section of the Basement (635m-650m) is higher than the lower section. This may indicate that the upper section has lower cohesion – therefore potentially more fractured – than the lower Basement. This hypothesis is consistent with the fact that the Basement was exposed prior to the sedimentation of Muribeca Fm. and this zone may be a weathered/soil profile. This change in the sonic transit time also coincides with a shift in the neutron and density logs over the same interval.

For practical purposes, the mudlog and wireline log shown here display only the section from the Muribeca Fm. to TD (Figure 6-33).

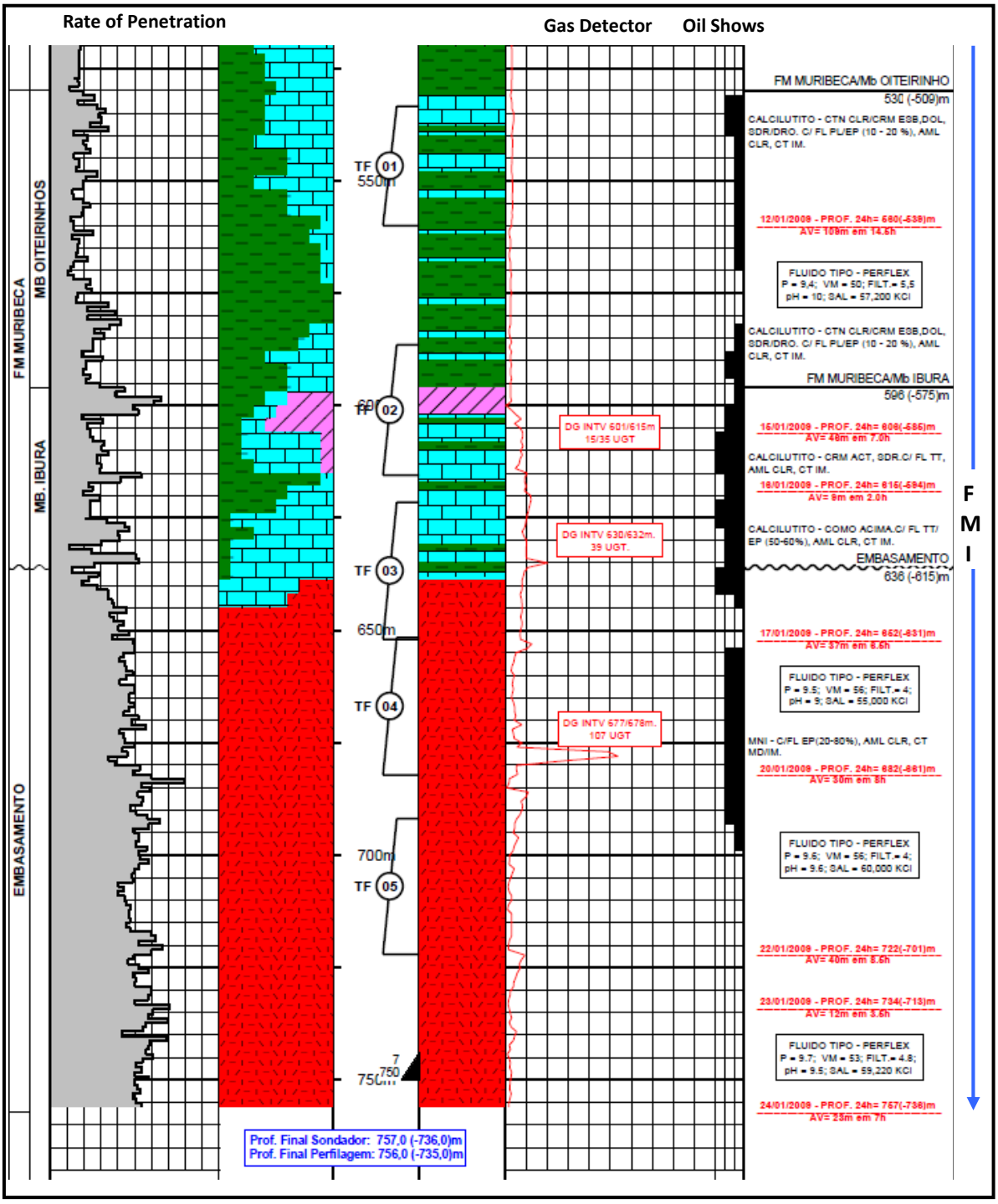

Figure 6-33: Mudlog of the lower section of the Charlie well. The blue arrow indicates the depth to which the FMI was run. The DST intervals are indicated by numbers (1) to (5); notice that DST-3 tested the lower Ibura Mb. and the upper 10m Basement together. It is therefore impossible to derive conclusive evidence about either the provenance of the sampled fluids or the pressure characteristics of each individual formation. The correct procedure would have been to test each formation independently.

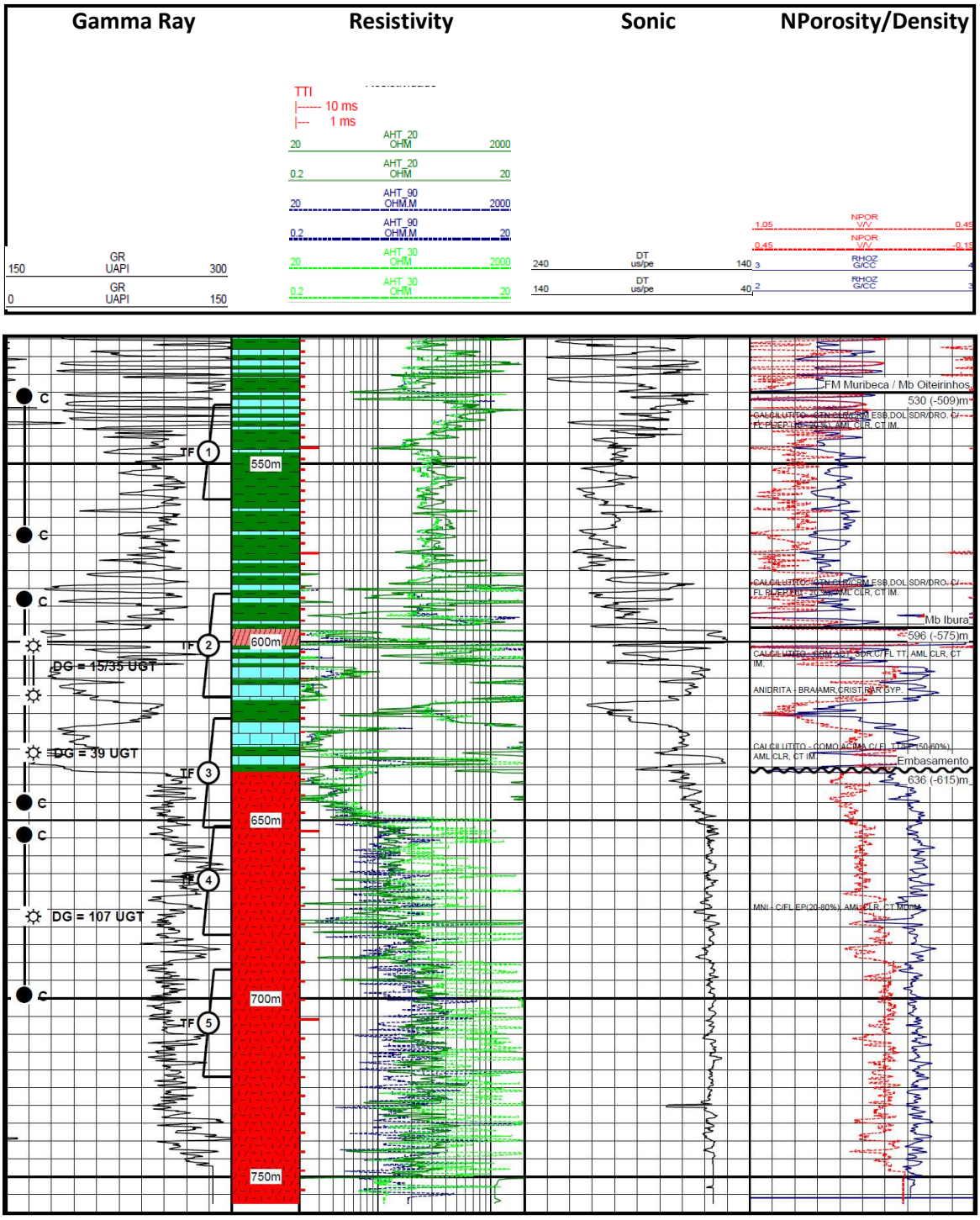

Figure 6-34: Composite well log for the Charlie prospect at Muribeca and Basement level. In order to make the observations clearer, zoomed sections are shown in Figure 6-35.

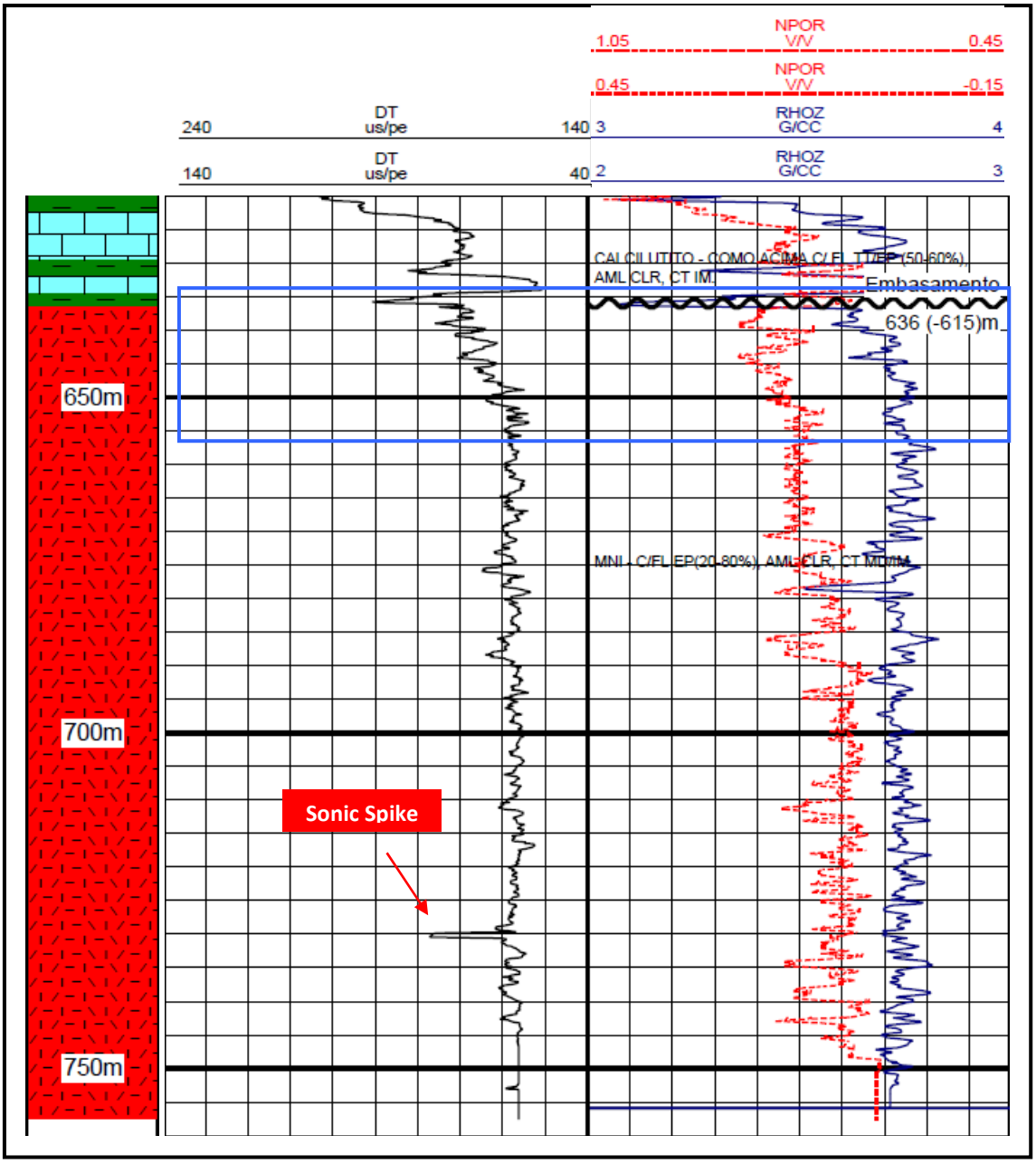

Figure 6-35: Two different sections can be identified using the sonic log in the basement; the section within the blue square, and below it. A distinct change in the neutron/density log also coincides with the change in sonic transit time over this interval. There is also a sonic spike at 730m which apparently doesn't correlate to any specific feature in the well, but that can mean a different rheological state of the rock, or represent an isolated fracture.

DST Results: Charlie Well

DST-01 (533m – 560m) – Figure 6-36

1st flow period - Weak to null blow.

2nd flow period -

Reverse Circulation: 62 bbl of drilling fluid.

Sampling chamber: 30l of drilling fluid.

Observations of the DST-01 results and pressure plot:

- The weak to null blow registered at surface can indicate two possibilities: a low permeability interval or wellbore damage.
- During the two flow periods there is a very small increase in back-pressure, which could mean low permeability.
- The first build-up curve is well developed and seems to begin stabilizing after the five hours of build –up. The second curve does not stabilize, but it appears that if it did, it would never be as high as the first; this may indicate the presence of a low pressure interval that was depleted after the first cycle.

DST-02 (586m – 615m) – Figure 6-37

1st flow period: Weak to null blow.

2nd flow period -

Reverse Circulation: 77 bbl of drilling fluid.

Sampling chamber: 30l of drilling fluid cut with oil

The DST-02 pressure plot shows that there is almost no permeability in this interval.

DST-03 (621m / 652 m) – Figure 6-38

1St Flow: immediate very strong air blow. Gas flowed to surface after 2 min and the burner was lit with a 6m high yellow flame that lasted during the whole flow period.

2nd Flow: immediate gas blow. Burner was lit with a 4m high yellow flame.

Reverse Circulation: 77 bbl of drilling fluid.

Sampling chamber: 30l of drilling fluid cut with oil

It can be seen in the graphic of Figure 6-38 that the pressure stabilized at around 69 Psi, i.e. 6 Psi below the FHP, which shows overbalance in the mud system.

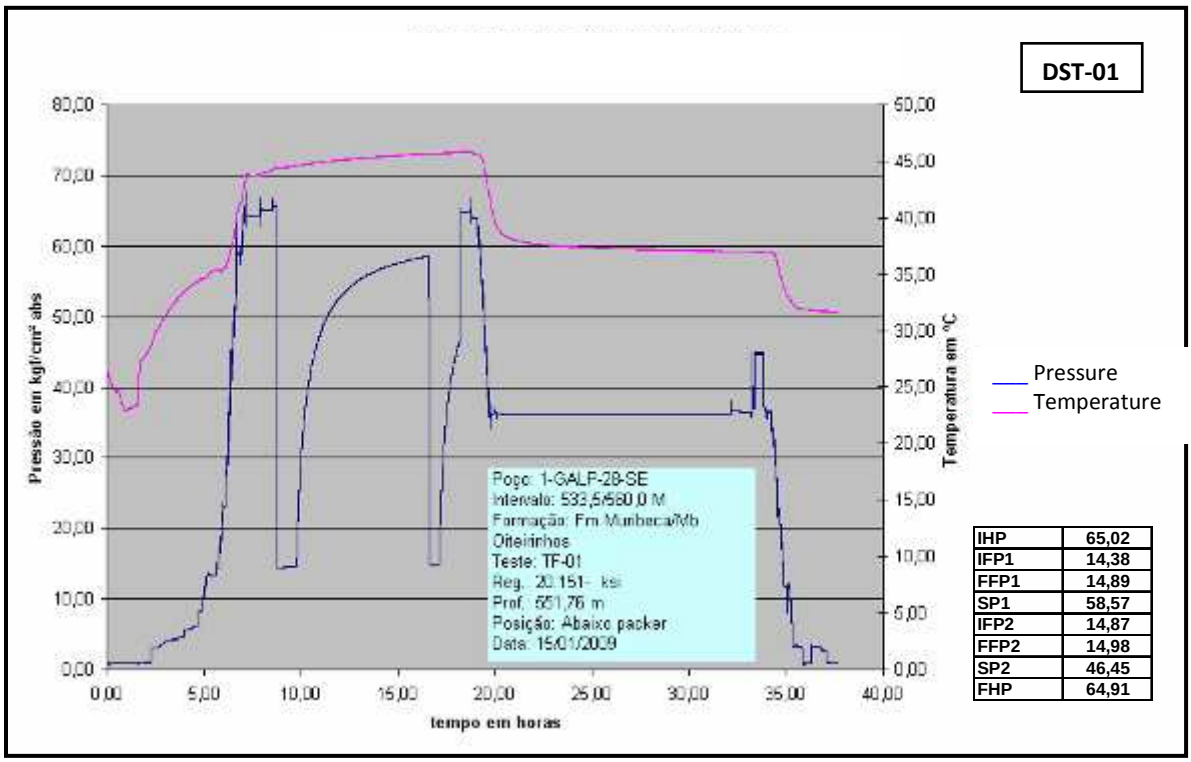

Figure 6-36: DST-01 pressure plot. Notice the rapid increase in pressure in both Build-up periods.

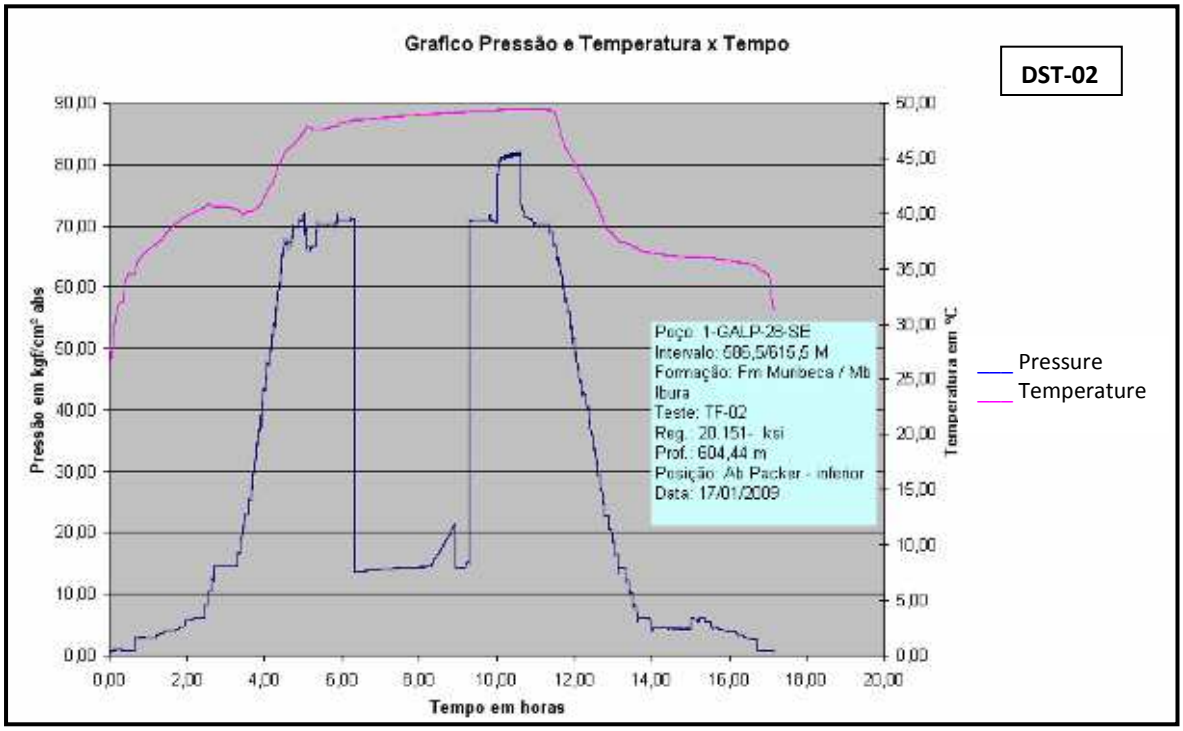

Figure 6-37: DST-02 pressure plot. The build-up curves show that there is no permeability in the formation.

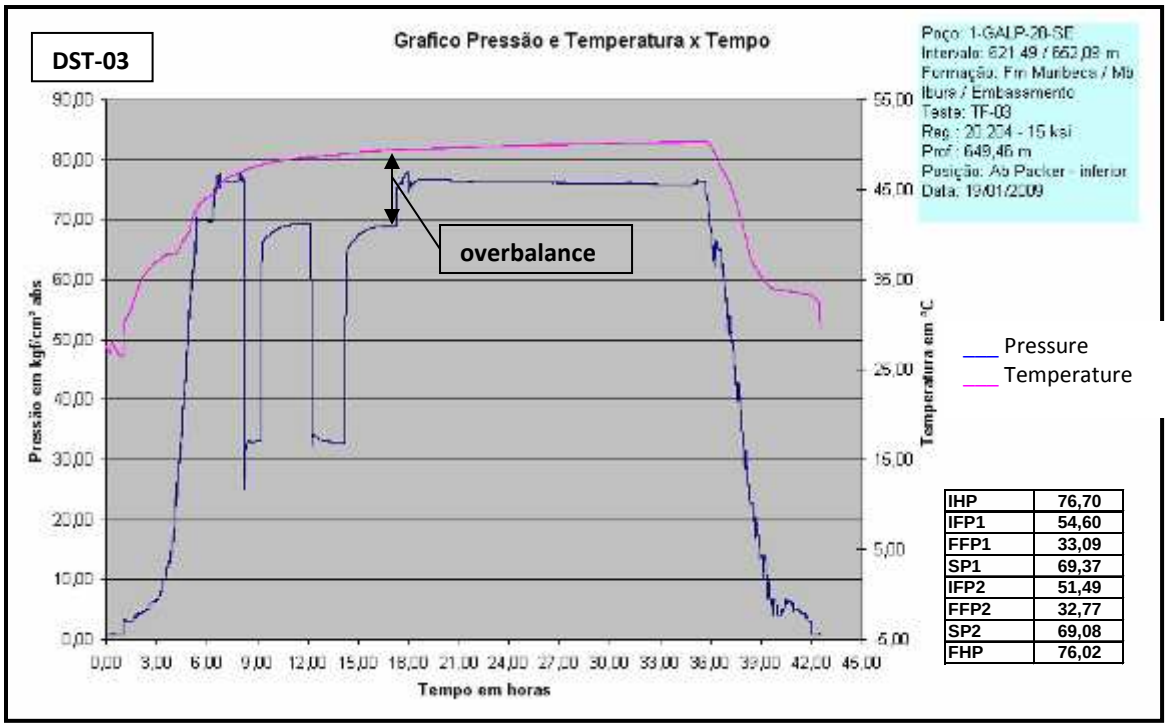

Figure 6-38: DST-03 pressure plot.

DST-04 (651m / 682m) - Figure 6-39

1st Flow: immediate very strong air blow. Gas flowed to surface after 2 min and burner was lit with a 6m high yellow flame that lasted during the whole flow period, diminishing to 2m after 45min.

2nd Flow: immediate gas blow. Burner was lit with a 3m yellow flame that was shut at the end of the flow period.

Sampling Chamber: mud with oil traces cut with gas.

Observations of DST-04 results and pressure plot:

- Low increase of pressure during the flow periods, maybe due to the fact that this is a gas reservoir.
- The build-up curves show a very slow re-adjustment that tends to stabilize at very low pressures. This means that the interval has very low permeability.
- The second build-up curve tended to stabilize at a lower pressure than the first, which indicates depletion of the reservoir.

Comparing this with the previous interval tested, it is fair to conclude that DST-03 tested a much better interval in terms of permeability. It may be observed that DST-03 and DST-04 had better results when compared to DST-02 which only tested the Ibura Mb. This leads to the conclusion that hydrocarbons are flowing from the Basement.

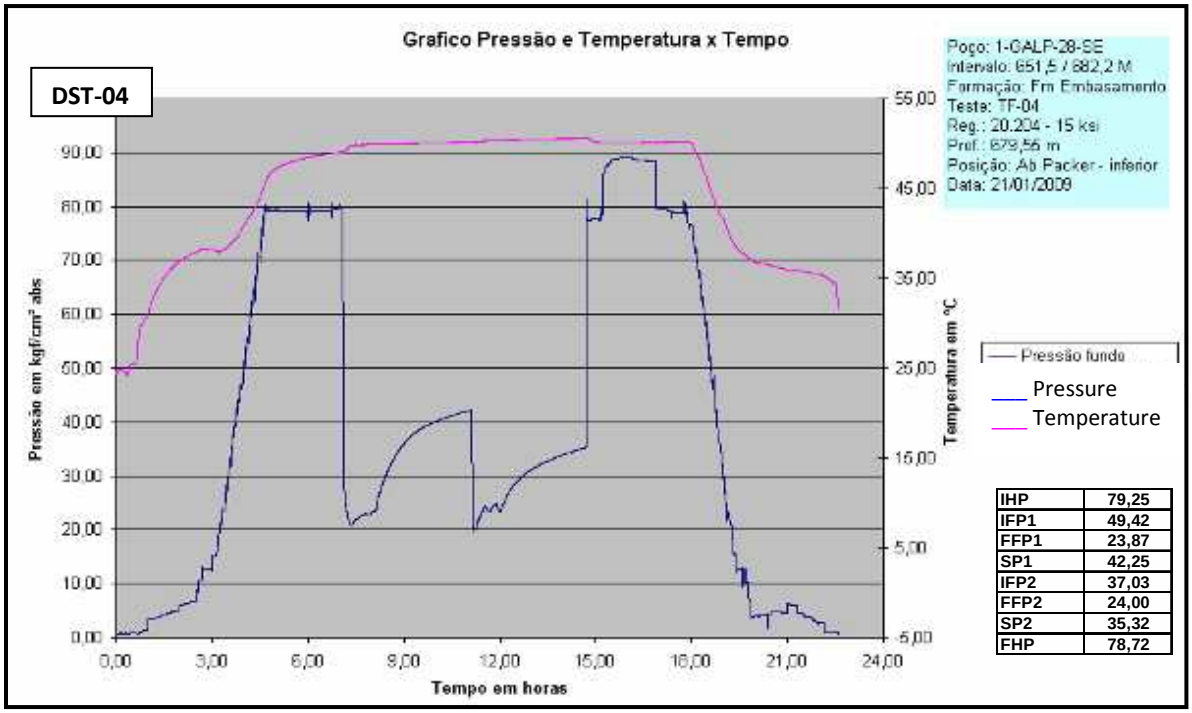

Figure 6-39: DST-04 pressure plot.

DST-05 (692m / 722 m): Failed due to tool problems.

DST Results Analysis: Charlie Well

As it can be seen from the well log in Figure 6-33, five DST's were undertaken over the Muribeca and Basement formations. Considering the procedures described in the Appendix for DST's, these were performed correctly as two cycles were run. DST-03 tested both the lower Ibura Mb. and the top 10m of Basement together. This procedure does not allow valid conclusions on the provenance of the sampled fluids and on the pressure characteristics of each particular formation. The correct procedure would have been testing each formation independently.

Delta Well

Well Planning

- **Primary Objective I:** testing the presence of HC in the Basement.

  Reservoir: fractured metamorphic rock.

- **Secondary Objective**: testing the presence of HC in the Ibura Fm.

  Reservoir: fractured carbonates intercalated with evaporites (anhydrite).

- **Type of Well:** Vertical.

- **Mud:** Conventional mud (8.7- 9 lb/gal) –Phase I

  Perflex fluid (9.2-9.8 lb/gal) – Phase II

  Perflex fluid (9.8-10 lb/gal) – Phase III (Mud weight when drilling through Basement)

Well Results

Delta well was a vertical well positioned over a structural high, at Basement level. Figure 6-40 shows the seismic interpretation on which the well positioning was based. The interpretation of Carmopolis Mb. is highly questionable. Table 6-5 shows the comparison between the predicted and the actual drilled formation tops. For practical purposes the mudlog shown here only displays one section of the well, from Muribeca Fm. to TD. The complete log can be found in the last chapter of this essay.

Table 6-5: Comparison table of the predicted versus actual formation tops. Above (+). Below (-). The actual formation tops diverge from the predicted in a relatively high range of values, mainly due to interpretation errors related to the poor seismic quality and the velocity model used to create a seismic depth cube.

Stratigraphic Tops						
Formations		Depths				
		Preview		Drilled		Δ
		Measured	TVD	Measured	TVD	m
Barreiras Fm.		surface	16	surface	16	0
Marituba Fm.		7	9	10	6	-3
Calumbi Fm.		-	-	-	-	-
Cotinguiba Fm.	Sapucari Mb.	77	-55	54	-32	23
	Aracaju Mb.					
Riachuelo Fm.	Maruim Mb.	437	-415	448	-426	-11
	Taquari Mb.	472	-450	487	-465	-15
Muribeca Fm.	Oiteirinhos Mb.	665	-643	715	-693	-50
	Ibura Mb.	739	-717	763,5	-741,5	-24,5
	Carmopolis Mb.	807	-785	852	-830	-45
Basement		808	-786	861	-839	-53
Final Depth		838	-816	936	-914	-98

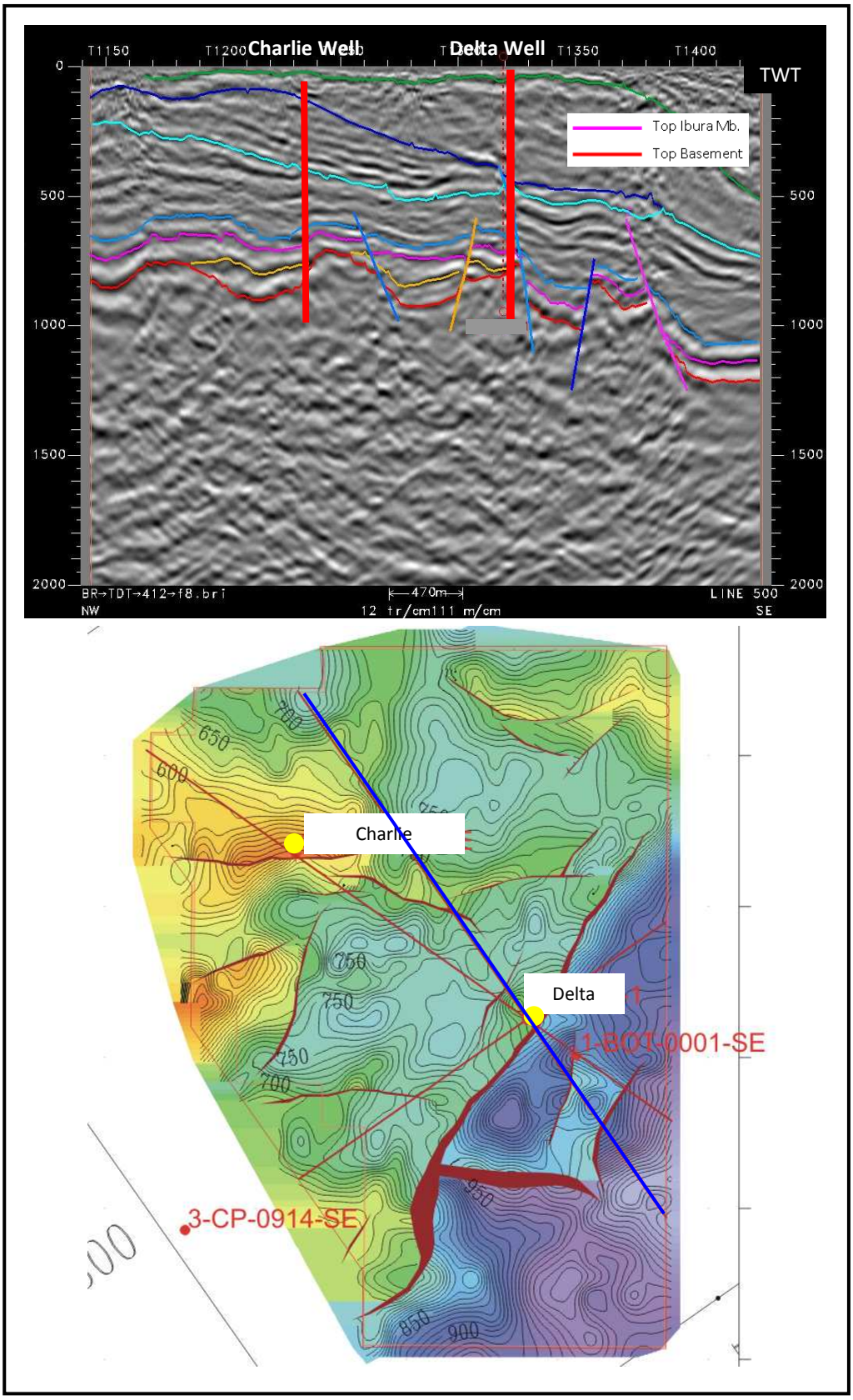

Figure 6-40: Seismic In-line in depth and Top Ibura Map on which was based the positioning of the Delta well. Notice that the interpretation of the Carmopolis Mb. (in yellow) in the seismic line here presented can be questioned.

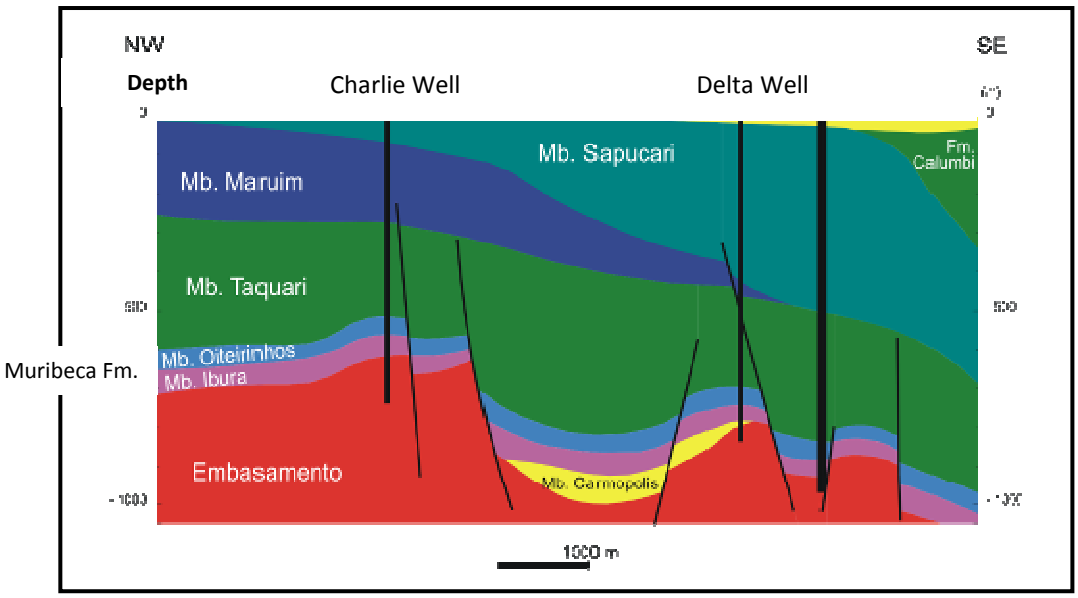

Figure 6-41: Schematic geological section of the Delta well area.

Mudlog Analysis

The following observations from the mudlog may be made (Figure 6-42):

- Oil shows were found from 800m (Muribeca Fm., Ibura Mb.) almost to TD.
- The best shows were found in Lower Ibura Mb. and Top Basement.
- The Lower Ibura Mb. is dominated by carbonates.

Wireline Logging

Observations from the wireline logs (Figure 6-43) indicate that zones of interest are not identified in the Ibura Fm. when utilising conventional attributes. In the Basement no conclusions can be made as the logs were not acquired to TD, covering only the top 20m of the formation. Given the presence of good oil shows over these intervals, and knowing the potential of fractured Basement from other locations in the region, and from our previous experience with Alpha, Bravo and Charlie Wells the decision was taken to run an FMI log and perform Drill Stem Testing (open hole). After wireline logging it was considered that what had been interpreted by the mudlogger as the Top Basement during drilling, was in fact the Carmopolis Mb. When comparing the logs from the Charlie to the logs from the Delta well however, it can be observed that the curves have the same shape (Figure 6-44). At the same time no siliciclastics were interpreted by the mudlogger at this interval (Figure 6-42). Therefore, this author believes that no Carmopolis Mb. was intersected in the Delta well, and what is being interpreted is actually a disaggregated section of basement rock caused by exposure to erosion in the past (Figure 6-44).

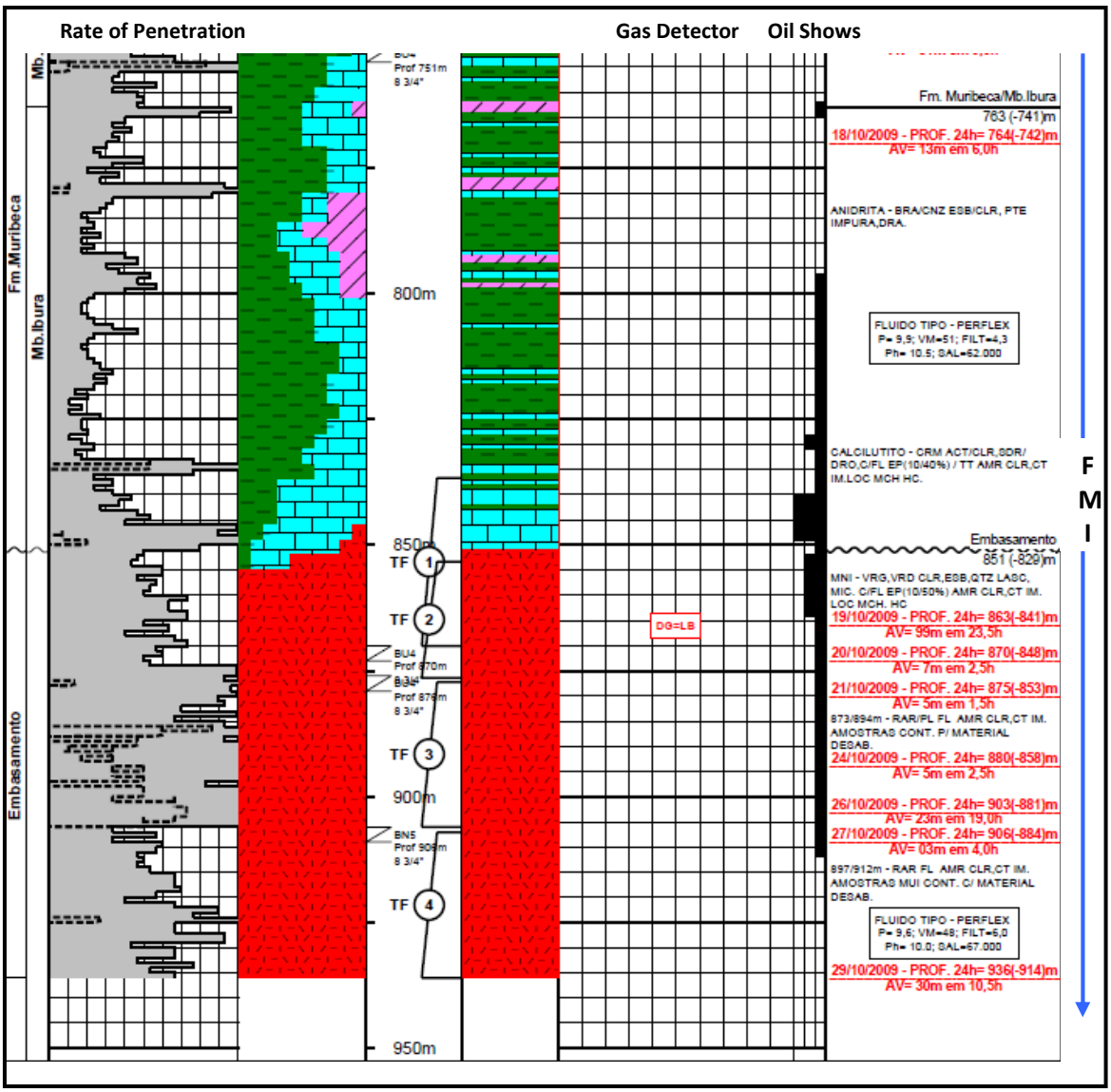

Figure 6-42: Mudlog of the lower section of the Delta well. The blue arrow indicates the depth to which the FMI was run. The DST intervals are indicated by numbers (1) to (4) notice that no DST testing was performed on the Lower Ibura Mb. (DST-01 failed).

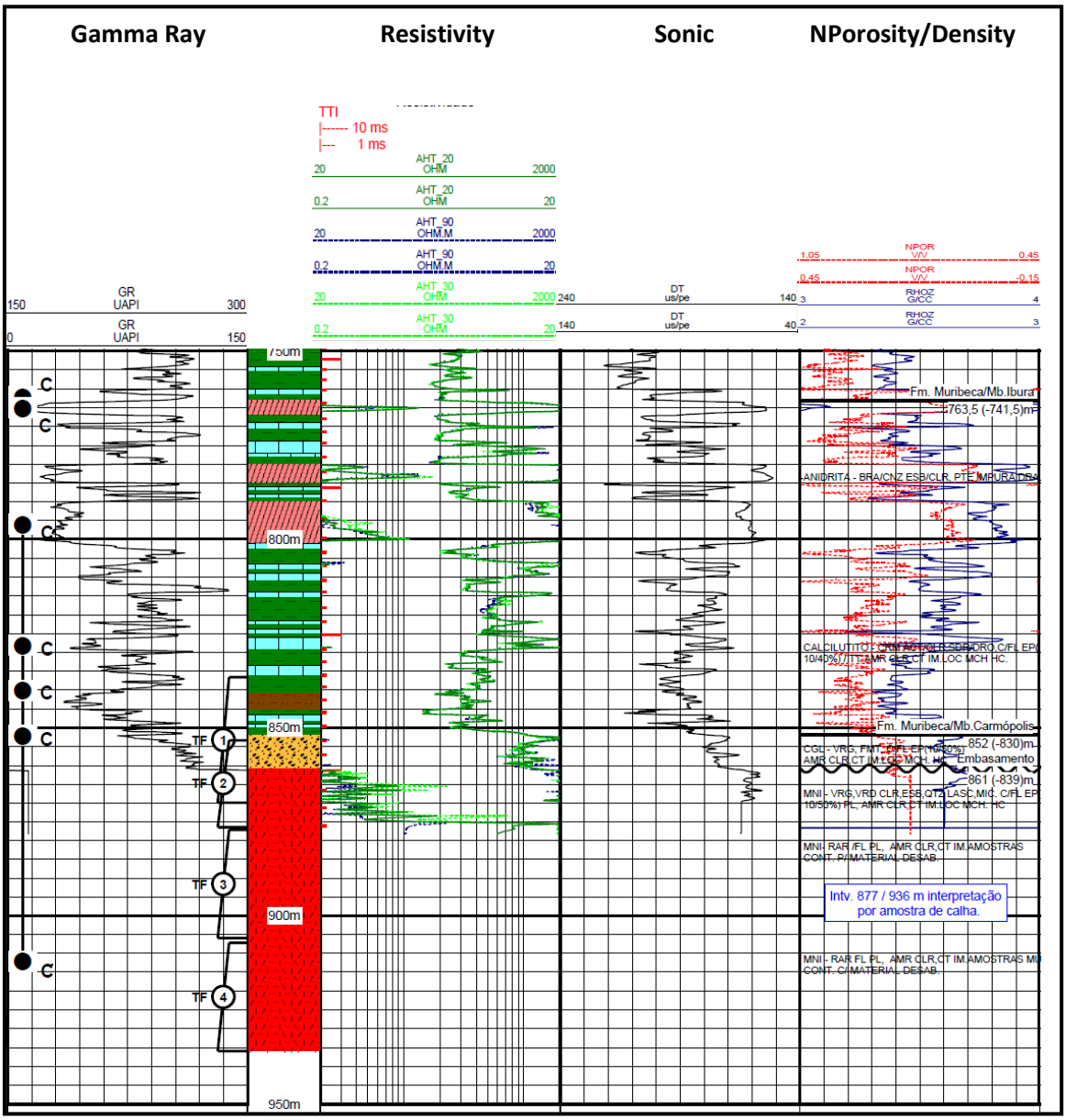

Figure 6-43 – Composite well log for the Delta prospect at Muribeca and Basement level.

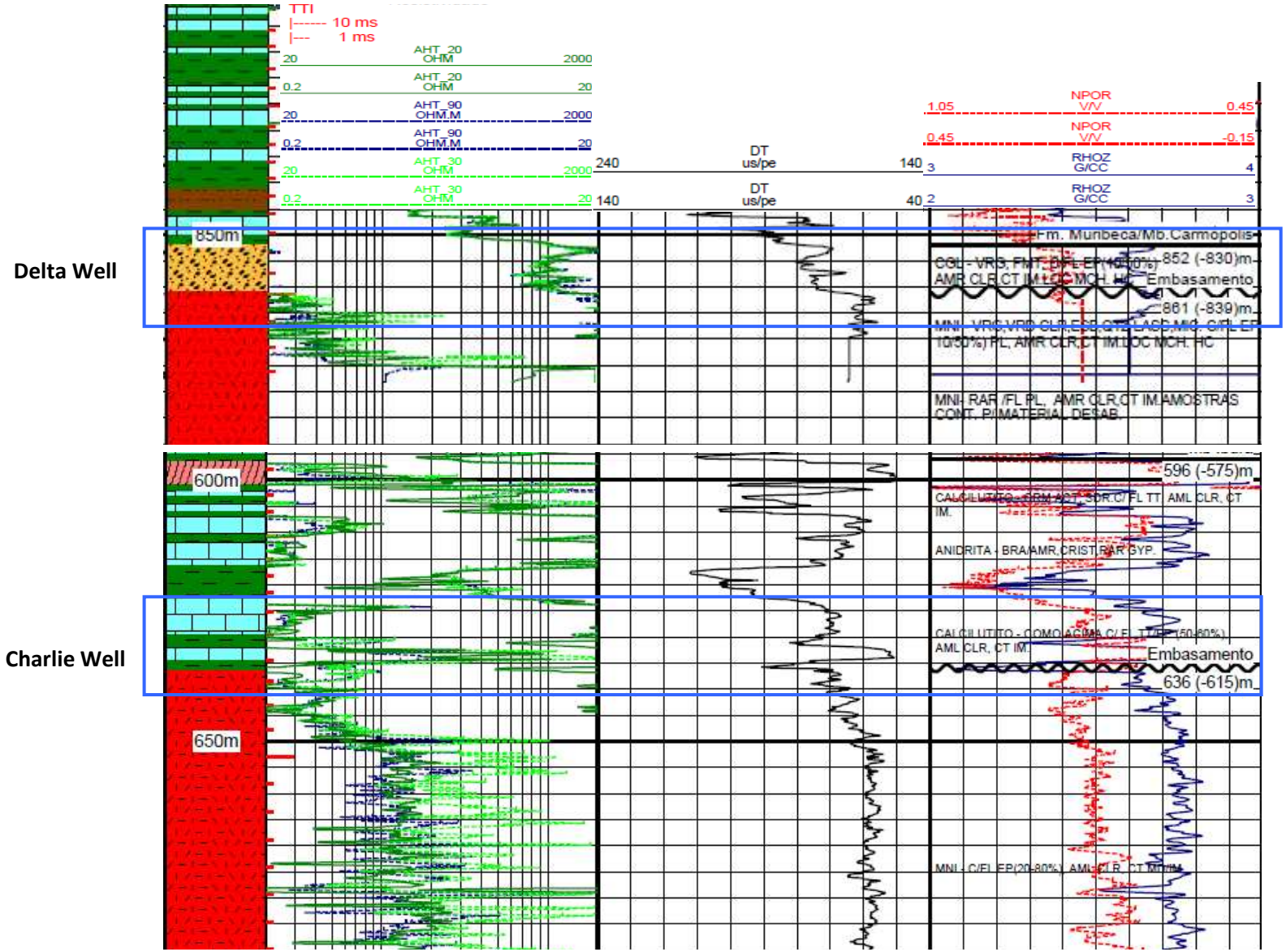

Figure 6-44: Delta and Charlie Well logs, positioned to compare the log response at the base of Ibura Mb. / top Basement – signed with the blue square. Notice that despite being interpreted as Carmópolis Mb. in Delta Well, this section has a similar response to its equivalent in Charlie well where it was not interpreted.

DST Results: Delta well

DST-01 (836m/870m): failed test.

DST-02 (853m/876m) - Figure 6-45

1st flow: immediate strong blow changing to moderate at 18 minutes.

2nd flow: immediate weak blow changing to null at 12 minutes.

Sampling Chamber: 18 litres of mud cut with oil.

If we compare the DST-02 pressure plot (Figure 6-45) with typical plots for good and low permeability formations displayed in Figure 6-46, we can see that DST-02 plot is similar to A). The low increase of back-pressure during the flow-periods might suggest low permeability, but the strong blow at surface suggests the opposite. The fact that during build-Up, the formation pressure came close to stabilizing at around 285PSI below the FHP (Final Hydrostatic Pressure), and knowing that the mud density was 9,8 lb/gal, leads to the conclusion that this well may have been drilled highly overbalanced and that the registered blow is caused by the expulsion of the mud from the fractures.

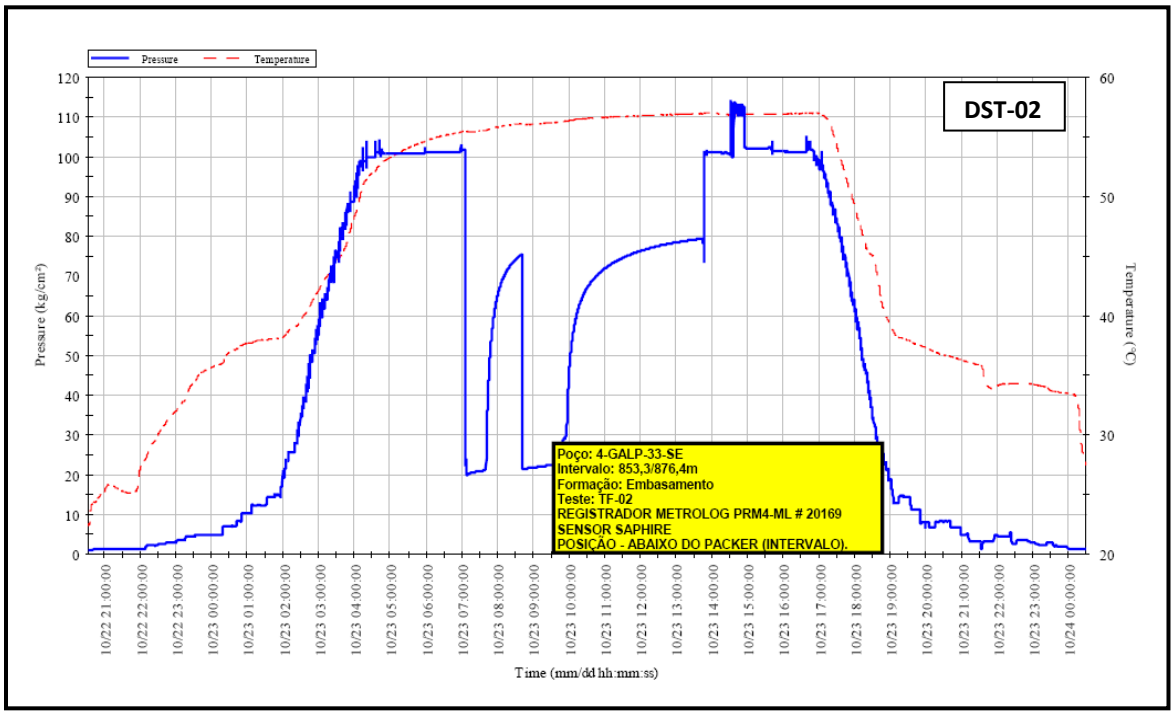

Figure 6-45: DST-02 pressure plot. A slow increase in back-pressure during the Flow-Periods and the low radius of the second Build-Up period curve may be observed, indicating average permeability in the tested interval.

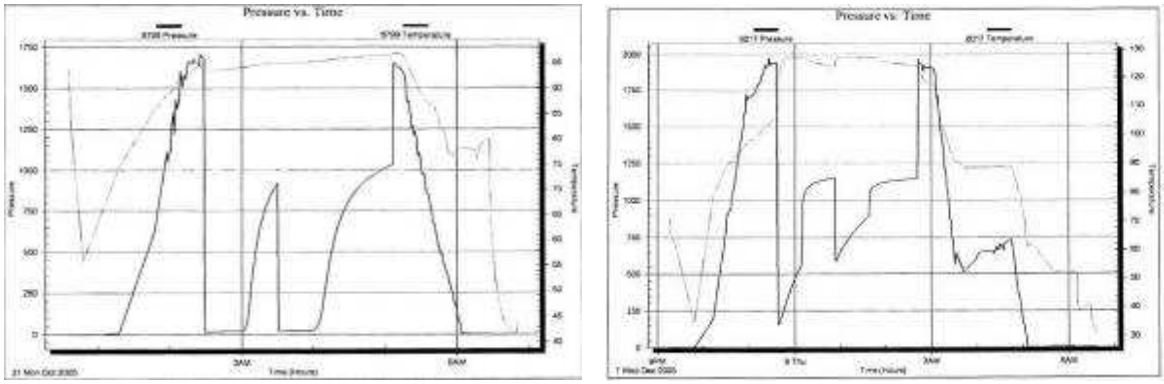

Figure 6-46: (A) Low permeability pressure plot. (B) Good permeability pressure plot. These images have the objective of showing only the ideal shape of DST curves when low permeability (A) and good permeability (B) formations are tested, therefore it is not important to read the values displayed.

DST-03 (877m/906m) Figure 6-47

1st flow: very weak blow changing to null at 5 minutes.

2nd flow: null blow.

Sampling Chamber: 5 litres of mud.

Taking into account the data from the flows (weak and null blows) and the pressure behaviour observed during the build-up periods, it is fair to conclude that this is a very low permeability interval.

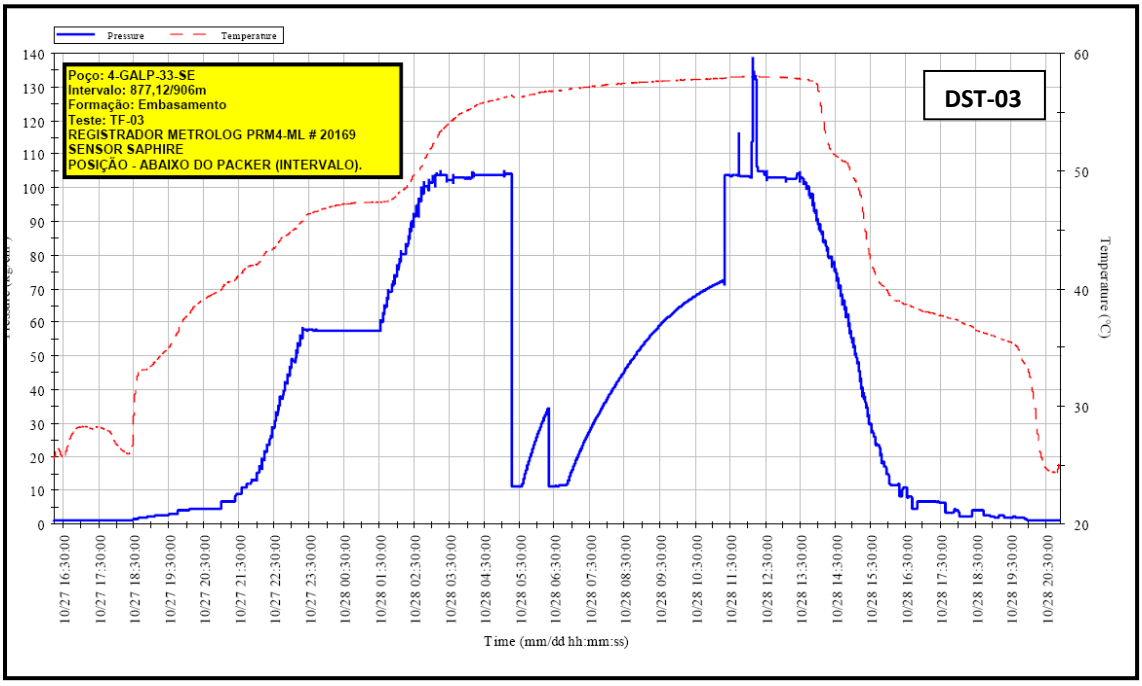

Figure 6-47: DST-03 pressure plot. The back-pressure did not increase during flow periods, and the second build-up curves rose very fast giving the idea that it would not stabilize.

DST-04 (907m/936m) – Figure 6-48

1st flow: very weak blow, changing to null at 5 minutes.

2nd flow: non-existent

Sampling Chamber: 6 litres of mud.

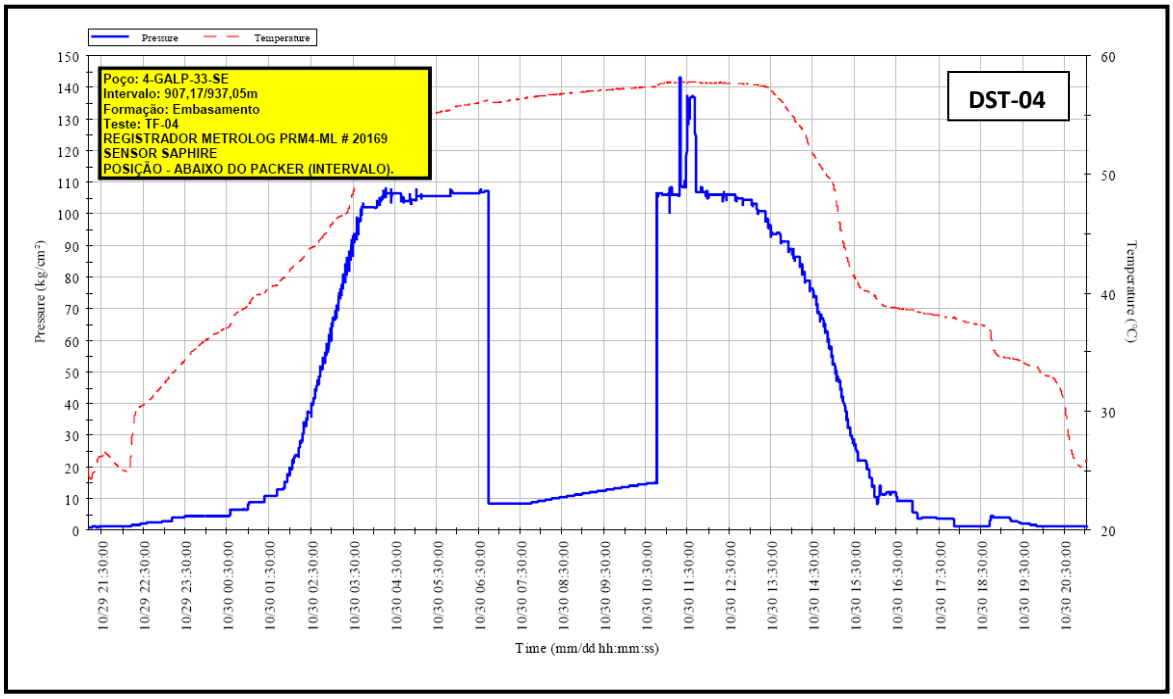

Figure 6-48: DST-04 pressure plot. Notice that there is almost no pressure registered on the valves. This is an interval with no permeability.

DST Results Analysis: Delta Well

As it can be seen from the well log in Figure 6-42, four DST's were undertaken over the Basement – as stated above this author does not consider that Carmopolis Mb. was intersected by this well. Considering the procedures described in the Appendix for DST's, these were performed correctly as two cycles were run. DST-02 tested around 30m of Basement, and presented good results, but DST-03 and DST-04 had very poor results. This may be indicative that only the upper section of the Basement is permeable. FMI log analysis could help answering this question as it was done over the entire Basement interval.

Echo Well

Well Planning

- **Primary Objective I:** testing the presence of HC in the Basement.

  Reservoir: fractured metamorphic rock

- **Secondary Objective**: testing the presence of HC in the Ibura Fm.

  Reservoir: fractured carbonates intercalated with evaporites (anhydrite).

  Secondary Objective II: testing the occurrence of HC in the turbiditic sandstones of Calumbi Fm.

- **Type of Well:** Vertical
- **Mud:** Conventional mud (8.7- 9 lb/gal) – Phase I

  Perflex fluid (9.2-9.8 lb/gal) – Phase II

  Perflex fluid (9.8-10 lb/gal) – Phase III (Mud weight when drilling through Basement)

Well Results

Echo well was a vertical well positioned over a Basement level structural high, testing an adjacent structure to the one that was tested by Alpha Well. Figure 6-49 shows the interpretation that was performed for the well positioning. Table 6-6 shows the comparison between the predicted and the actually drilled formation tops.

Table 6-6: Comparison table of the predicted versus actual formation tops. Above (+).Below(-). The actual formation tops diverge from the predicted, mainly due to interpretation errors related to the bad seismic quality and the velocity model used to create a seismic depth cube. However, relative to the previous wells, the predictions are more accurate, indicating that the seismic re-interpretation improved the geological model.

Stratigraphic Tops						
Formations		Depths				
		Preview		Drilled		Δ
		Measured	TVD	Measured	TVD	m
Barreiras Fm.		Sup.	37	Sup.	37	0
Marituba Fm.		8	34	8	34	0
Calumbi Fm.		130	-88	109	-67	21
Cotinguiba Fm.	Sapucari Mb.	532	-490	519	-477	13
	Aracaju Mb.	-	-	-	-	-
Riachuelo Fm.	Taquari Mb.	667	-625	671	-629	-4
Muribeca Fm.	Oiteirinhos Mb.	882	-840	870	-828	12
	Ibura M.	932	-880	912	-870	10
Basement		997	-955	971	-929	26
Final Depth		1078	-1036	1079,5	-1035	-2

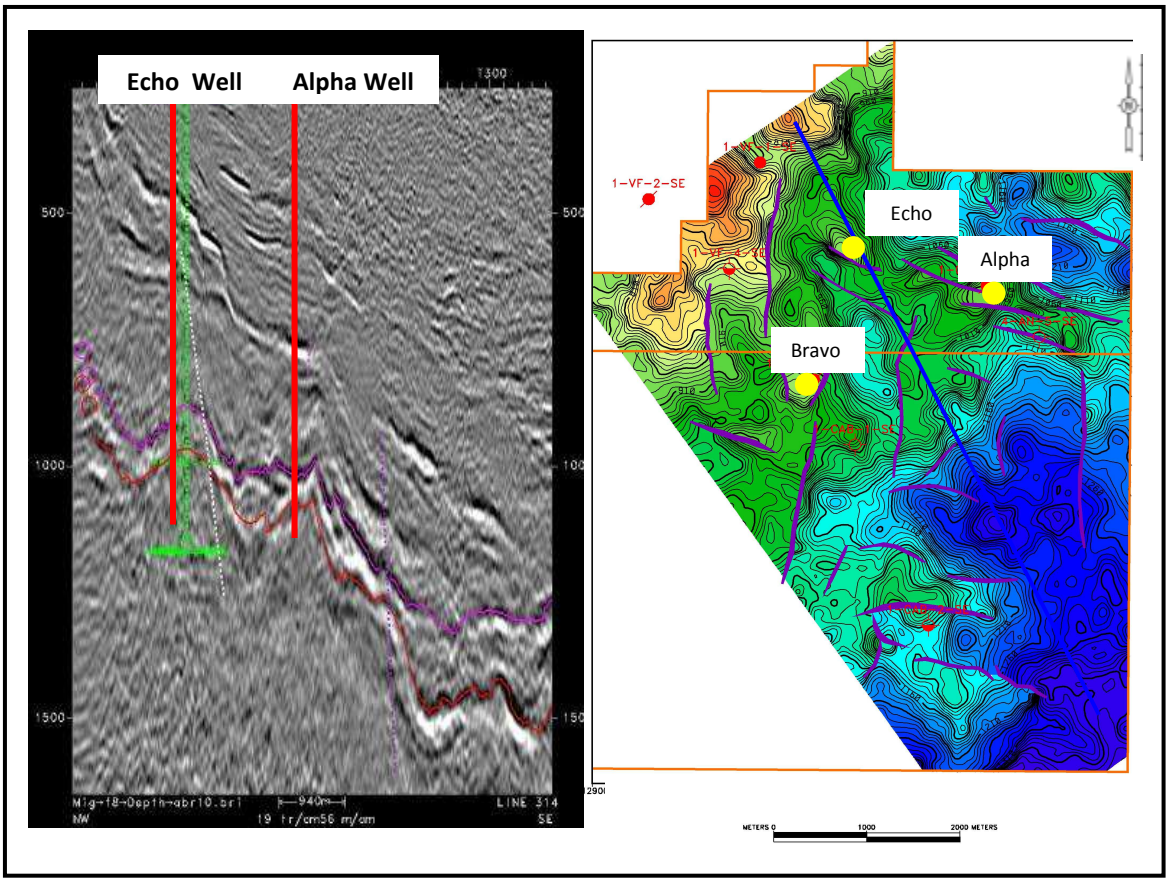

Figure 6-49: Seismic In-line in depth and Top Ibura depth map on which the position of the Echo well was based. Notice that the Top Basement and Top Ibura Mb. as well as the faults had been re-interpreted (relative to the date of Alpha Well positioning) and are more accurate.

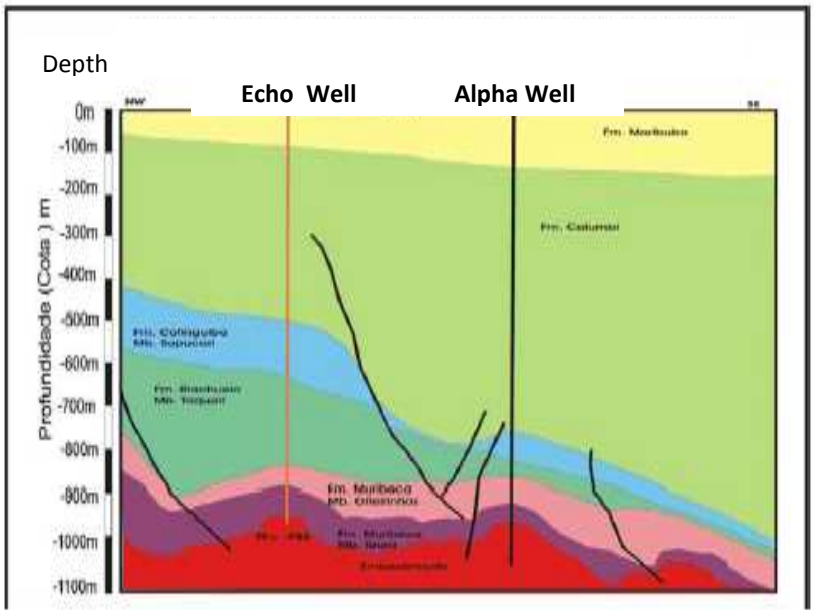

Figure 6-50: Schematic geological section of the Echo well area.

Mudlog Analysis

The main Observations from the mudlog are (Figure 6-51):

- HC shows are observed from the base of Oiteirinhos Mb. to TD.
- The basal section of Ibura Mb. contains a 5m thick section of carbonates that has good oil shows.

Wireline logging

Observations from the wireline logs indicate that zones of interest are not identified either in the Ibura Fm. or Basement when utilising conventional attributes (Figure 6-52). Given the presence of good oil shows over these intervals, and knowing the potential of fractured Basement from other locations in the region, and from our previous experience with Alpha, Bravo, Charlie and Delta Wells the decision was taken to run an FMI log and perform Drill Stem Testing (open hole).

Two different sections that can be identified in the sonic log within the Basement (Figure 6-53): the average transit time in the upper section of the Basement (971m-1030m) is higher than the rest, and these two sections are divided by a very visible spike in transit time at around 1030m. The spike is also noticeable in the NPorosity and Density logs, and Resistivity also responds differently in the upper and lower section of the basement. This may indicate that the upper section has a lower cohesion – more fractured – than the lower Basement. This hypothesis is consistent with the fact that the Basement was exposed prior to the deposition of the Muribeca Fm. It could also mean that two different basement lithologies exist.

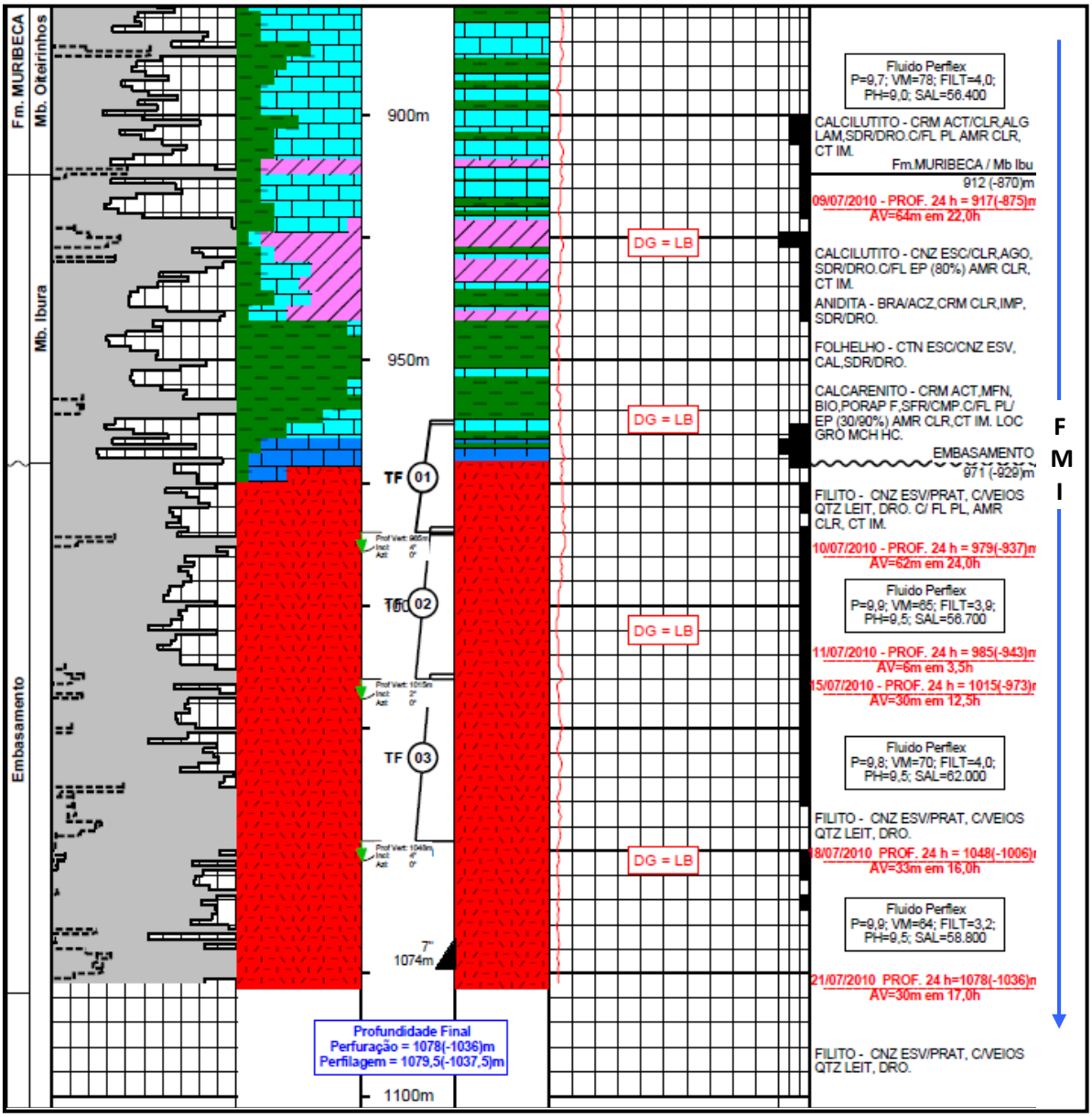

Figure 6-51: Mudlog of the lower section of the Echo well. The blue arrow indicates the depth to which the FMI was run. The DST intervals are indicated by numbers (1) to (3) notice that DST-3 tested together the lower Ibura Mb. and the upper Basement. It is therefore impossible to derive conclusive evidence about either the provenance of the sampled fluids or the pressure characteristics of each individual formation. The correct procedure would have been to test each formation independently.

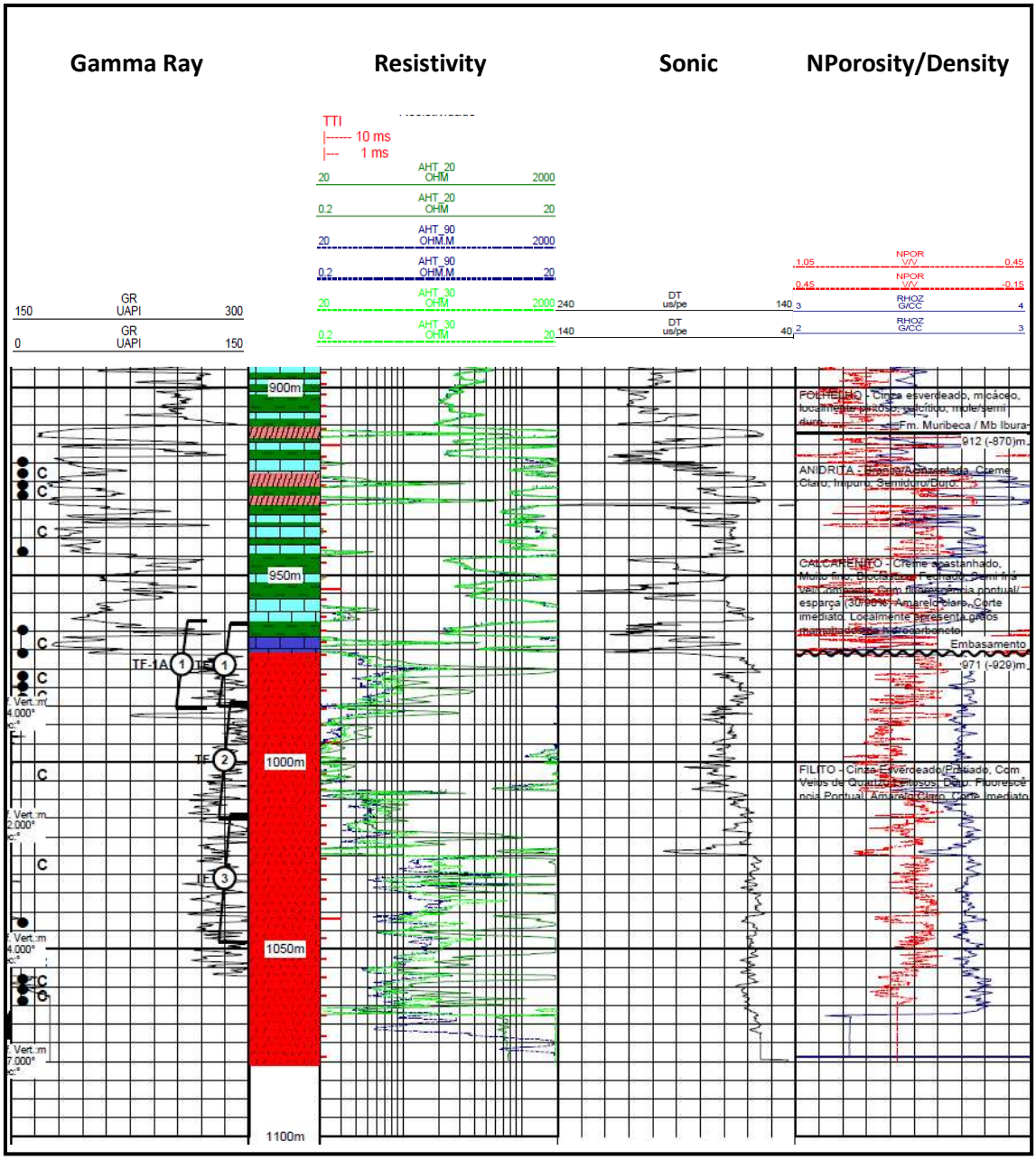

Figure 6-52: Composite well log for the Echo well at the Muribeca Fm. and Basement levels.

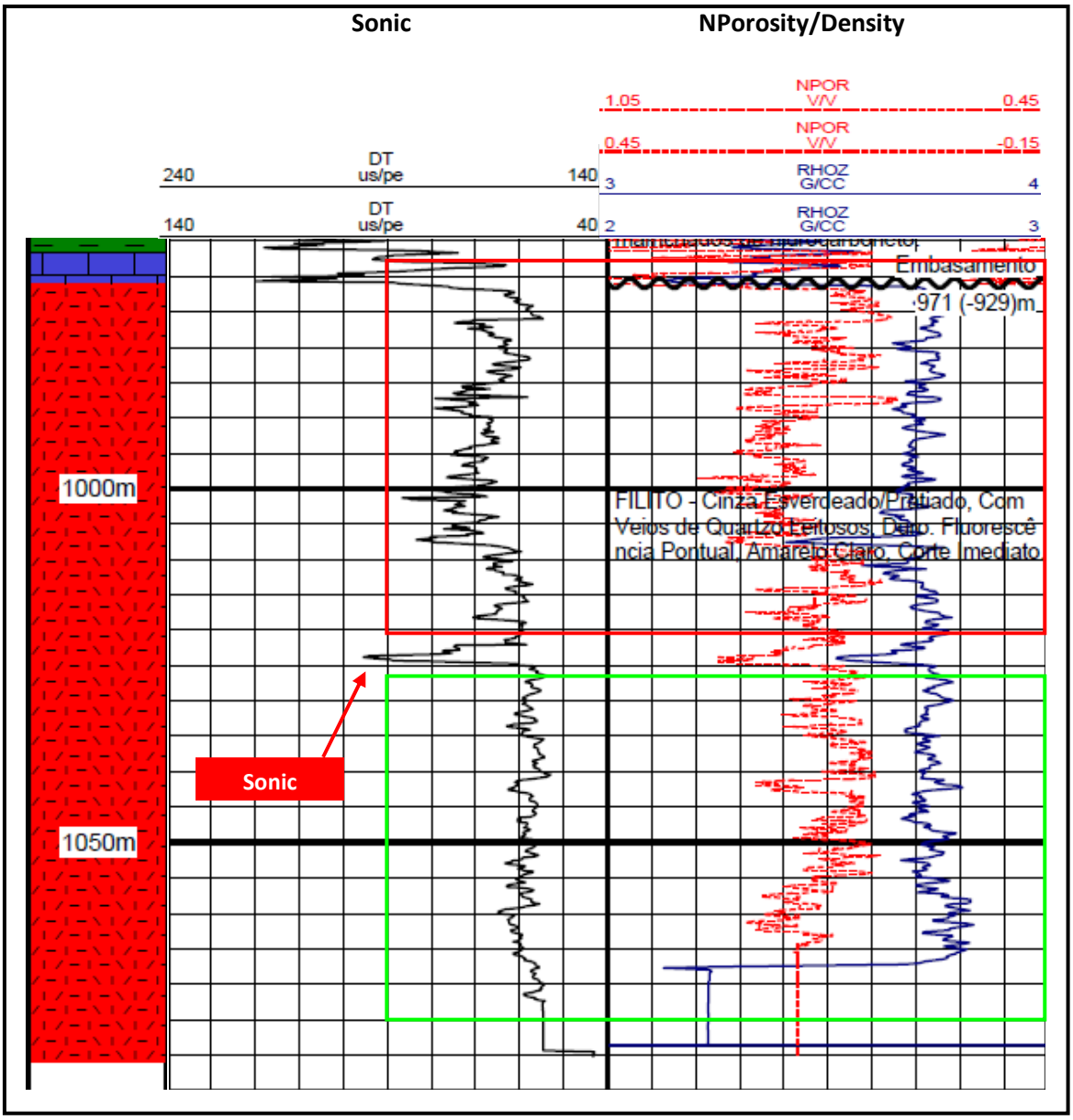

Figure 6-53: Each of the two individualized areas (red and green) has different average transit times and corresponding responses of the sonic and density logs. There is also a sonic spike at 1025m similar to what was registered in Charlie well. Because Charlie well is relatively distant from Echo well, this spike is more likely to represent a transition zone between the altered upper Basement and the non-altered lower Basement, than an isolated fracture, i.e. it is not probable that an isolated fracture extends for such a large area.

DST Results: Echo Welll

DST-01A (963m/958m) –Figure 6-54

1st flow: weak blow changing to strong after 2 minutes.

Sampling Chamber: drilling fluid cut with oil

DST-02 (984m/1015m) – Figure 6-54

1st flow: weak blow changing to strong after 15 minutes.

2nd flow: strong constant blow.

Sampling Chamber: drilling mud cut with oil

DST-03 (1014m/1048m) – Figure 6-54

1st flow: weak blow changing to strong after 2 minutes.

2nd flow: strong blow changing to weak during the flow.

Sampling Chamber: drilling mud cut with oil

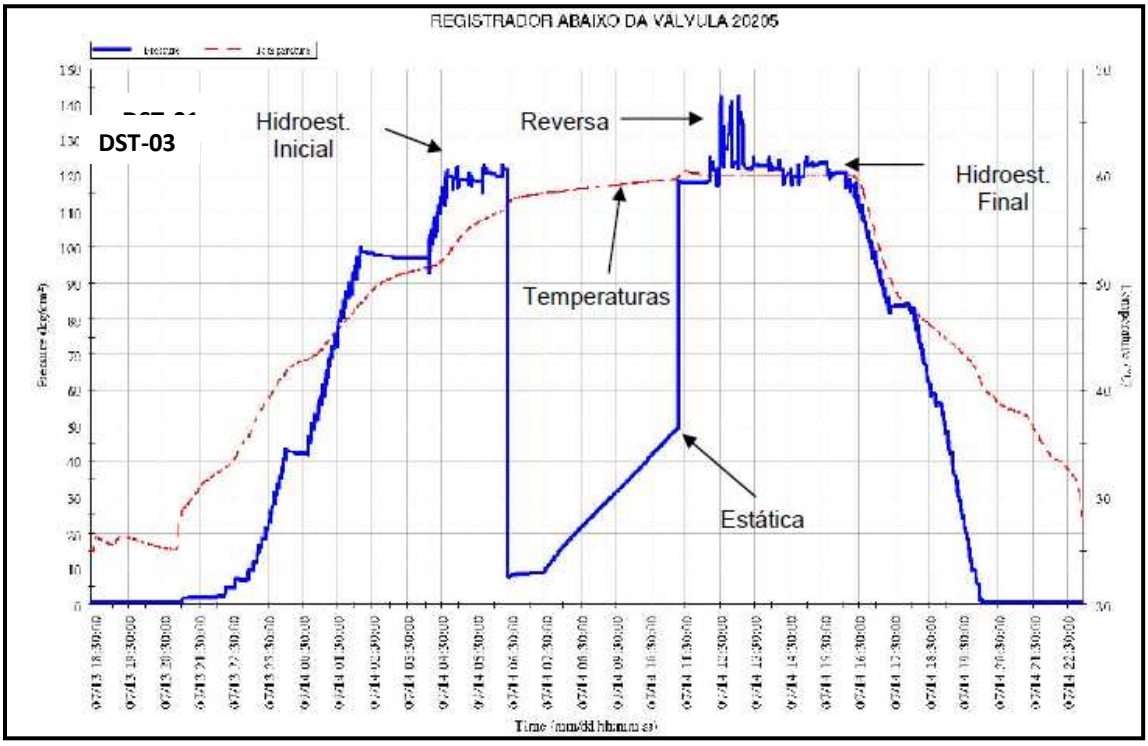

Figure 6-54: DST pressure plots for the three DST's performed on the Echo well. Notice that the entire interval tested has very low permeability, this is compatible with the blows registered at surface (continues on next page).

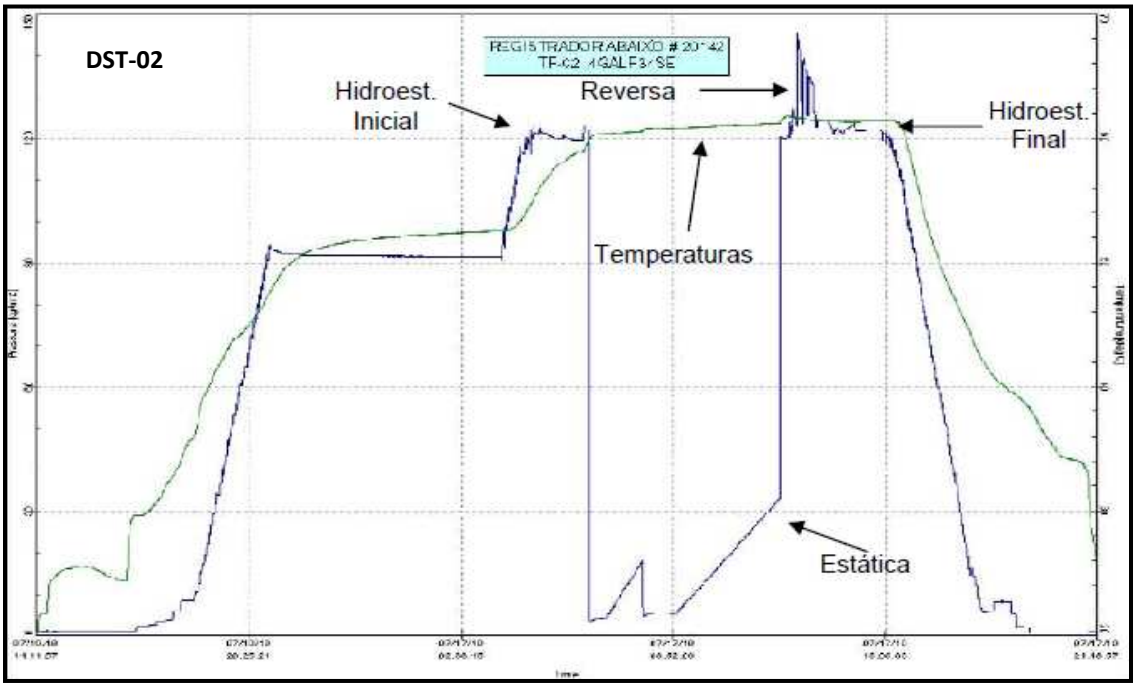

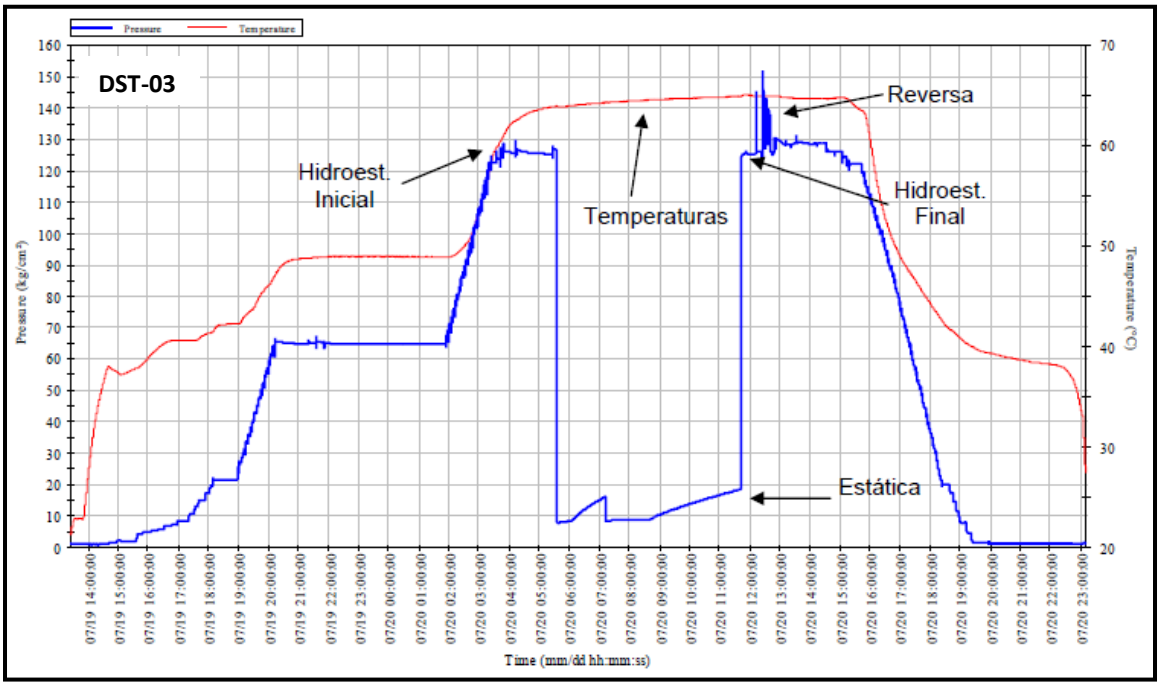

Figure 6-54 (continued): DST pressure plots for the three DST's performed on the Echo well. Notice that the entire interval tested has very low permeability, this is compatible with the blows registered at surface.

DST's Results Analysis:

Considering the results of these DST's we are lead to conclude that this is an interval of low permeability.

It would have been useful if the DST's had planned and performed similarly to the Alpha well (test Ibura Mb. and Basement independently). This would have allowed a direct comparison between both wells and made it possible to observe any trends in the reservoir behaviour.

Fox Well

- **Primary Objective I:** testing the presence of HC in the Basement.

  Reservoir: fractured metamorphic rock.

- **Secondary Objective**: testing the presence of HC in the Ibura Fm.

  Reservoir: fractured carbonates intercalated with evaporites (anhydrite).

  Secondary Objective II: testing the occurrence of HC in the turbiditic sandstones of Calumbi Fm.

- **Type of Well:** Vertical
- **Mud:** Conventional mud (8.7- 9 lb/gal) – Phase I

  Perflex fluid (9.2-9.8 lb/gal) – Phase II

  Perflex fluid (9.8-10 lb/gal) – Phase III (Mud weight when drilling through Basement)

The Fox well was a vertical well positioned over a Basement level structural high and was designed as an appraisal well of the Bravo well discovery. Figure 6-55 shows the pre-drill seismic interpretation made for the well positioning; notice the difference to the interpretation for Bravo well. Table 6-7 shows the comparison between the predicted and the actually drilled formation tops, and Table 6-8 the comparison between the measured formation tops at Fox and Bravo wells.

Table 6-7: Comparison table of the predicted versus actual formation tops. Above (+). Below (-). The actual formation tops diverge from the predicted, mainly due to interpretation errors related to the poor seismic quality and the velocity model used to create a seismic depth cube even after the seismic had been re-interpreted, and the velocity model updated.

Stratigraphic Tops						
Formations		Depths				
		Preview		Drilled		Δ
		Measured	TVD	Measured	TVD	m
Barreiras Fm.		-	-	surface	16	-
Marituba Fm.		surface	16	16	5	-11
Calumbi Fm.		121	-100	146	-125	-25
Cotinguiba Fm.	Sapucari Mb.	661	-640	-	-	-
	Aracaju Mb.	not prev.	not prev.	590	-569	-
Riachuelo Fm.	Taquari Mb.	681	-660	627	-606	54
Muribeca Fm.	Oiteirinhos Mb.	901	-880	872	-851	29
	Ibura M.	952	-931	911	-890	41
Basement		1022	-1001	979	-958	43
Final Depth		1052	-1031	1064	-1043	-12

Table 6-8: Comparison between the measured formation tops at Fox and Bravo wells. From Figure 30, it is possible to confirm that Fox is located up-dip from Bravo, this is confirmed by the formation tops intersected while drilling, except for Calumbi Fm. This may mean that Calumbi Fm. position should probably be reviewed.

		Fox Well	Bravo Well	Δ
Barreiras Fm.		surface	surface	-
Marituba Fm.		16	25	-9
Calumbi Fm.		146	144	2
Cotinguiba Fm.	**Sapucari Mb.**	-	670	-
	Aracaju Mb.	590		
Riachuelo Fm.	**Taquari Mb.**	627	691	-64
Muribeca Fm.	**Oiteirinhos Mb.**	872	884	-12
	Ibura M.	911	936	-25
Basement		979	1005,5	-26,5
	Final Depth	1064	1101	-37

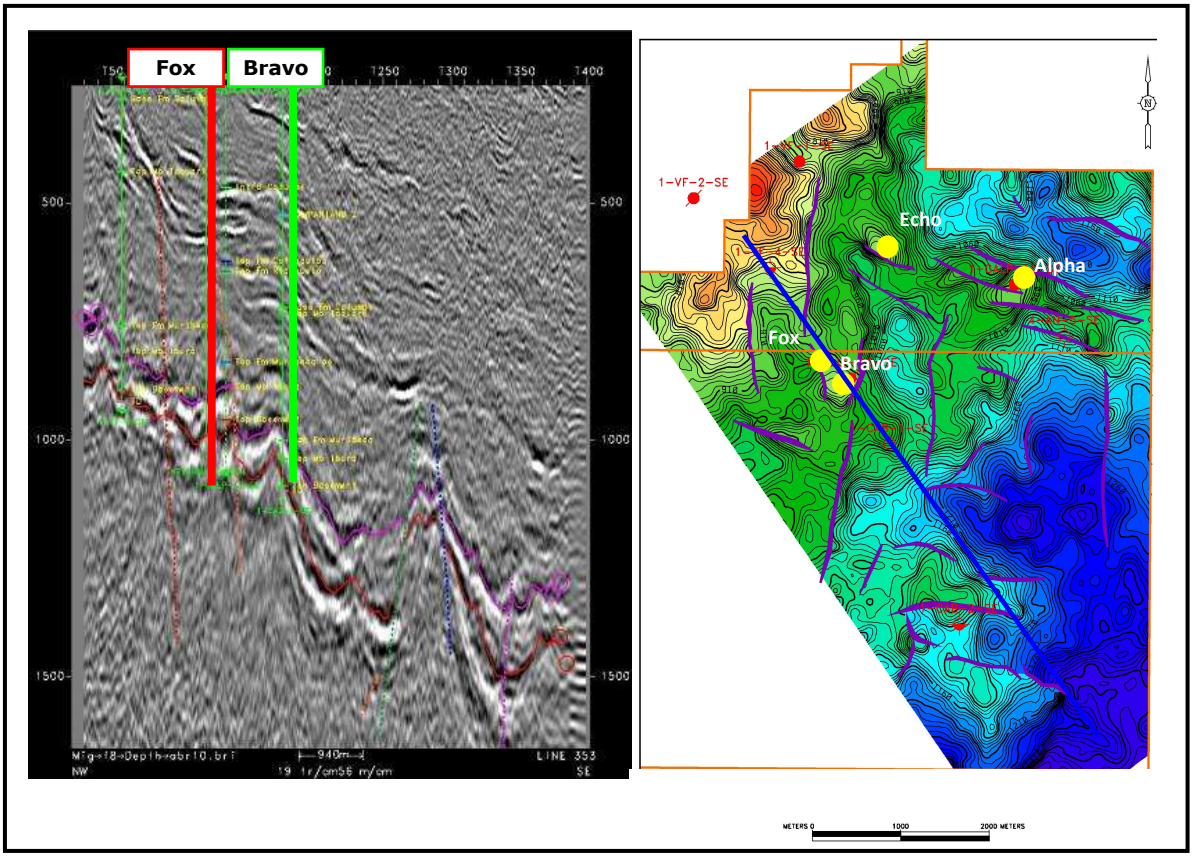

Figure 6-55: Seismic In-line in depth and Top Ibura depth map on which the position of the Fox well was based.

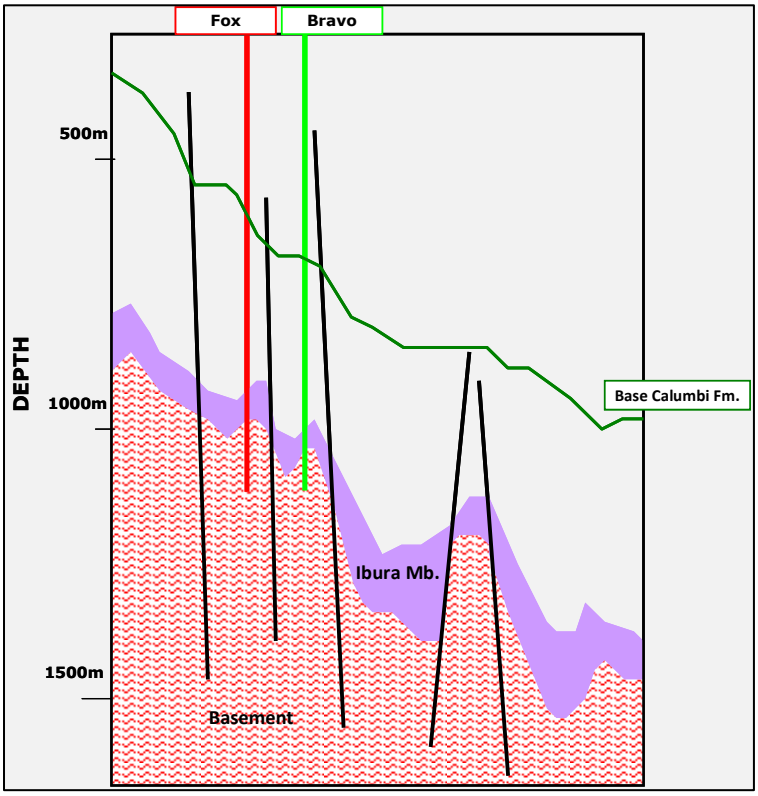

Figure 6-56: Schematic geological section of the Fox well area. Only Basement and Ibura are represented because they were the only horizons interpreted for Fox well location.

Mudlog Analysis

The main Observations from the mudlog are (Figures 6-57 and 6-60):

- HC shows were found in sandstone levels within the Calumbi Fm.
- HC shows were found from the top of Muribeca Fm. to TD.
- The Ibura Mb. is very rich in anhydrite.
- The basal section of Ibura Mb. contains a 15m thick section of carbonates that has good oil shows.

Calumbi Fm Evaluation

The Calumbi Fm. sandstone section was considered poor in terms of reservoir properties by the wireline logging (Figure 6-58). The sandstone levels with oil shows in the Fox Well at 520m-540m, can be correlated with the sandstones with oil shows in the Bravo Well at around 600m (Figure 6-26). The depth difference between these sandstones can be explained by a 14ºSE dip of the the Calumbi Fm. (see calculations below in Figure 6-58), similar to the dips registered at Riachuelo Fm. (15ºSE) by the FMI. At this point in the sedimentary column, the Fox Well is on the hanging wall of a fault, and the Bravo on the footwall of that same fault.

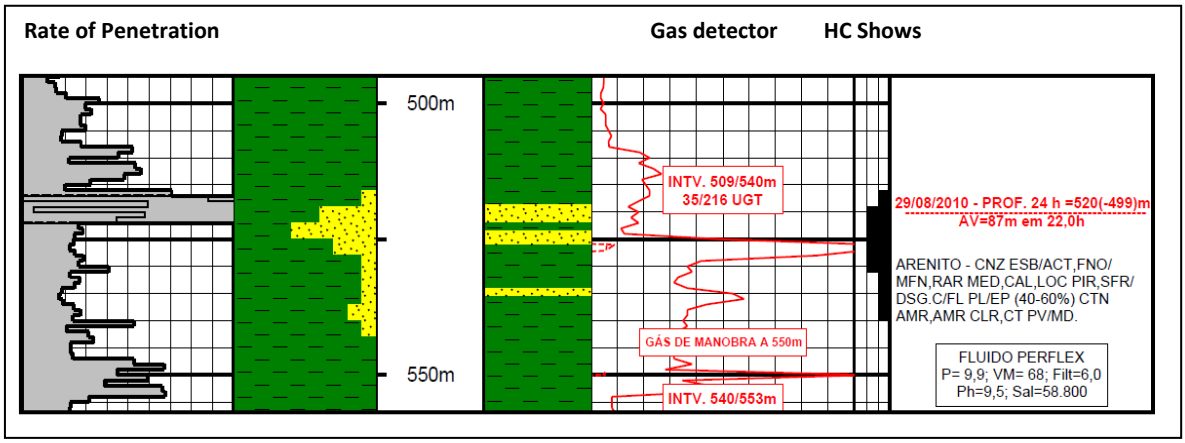

Figure 6-57: Section of the well log from Fox well at the sandstones of Calumbi Fm. which had good oil shows.

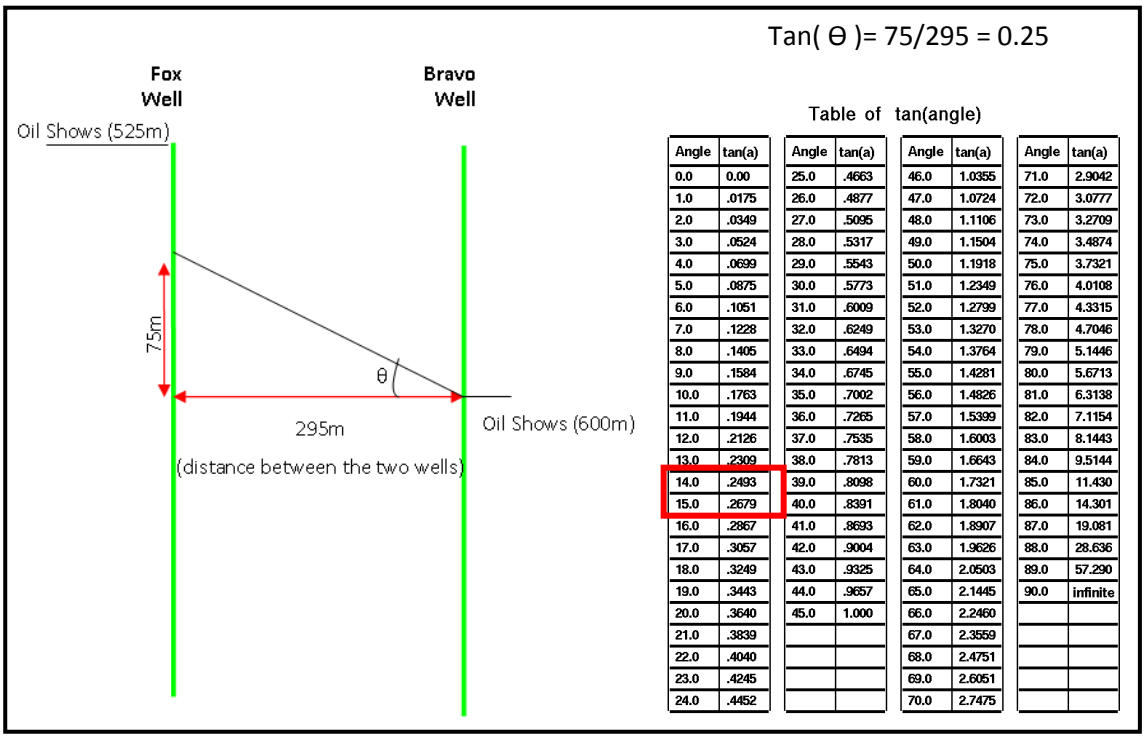

Table of tan(angle)

Angle	tan(a)	Angle	tan(a)	Angle	tan(a)	Angle	tan(a)
0.0	0.00	25.0	.4663	46.0	1.0355	71.0	2.9042
1.0	.0175	26.0	.4877	47.0	1.0724	72.0	3.0777
2.0	.0349	27.0	.5095	48.0	1.1106	73.0	3.2709
3.0	.0524	28.0	.5317	49.0	1.1504	74.0	3.4874
4.0	.0699	29.0	.5543	50.0	1.1918	75.0	3.7321
5.0	.0875	30.0	.5773	51.0	1.2349	76.0	4.0108
6.0	.1051	31.0	.6009	52.0	1.2799	77.0	4.3315
7.0	.1228	32.0	.6249	53.0	1.3270	78.0	4.7046
8.0	.1405	33.0	.6494	54.0	1.3764	79.0	5.1446
9.0	.1584	34.0	.6745	55.0	1.4281	80.0	5.6713
10.0	.1763	35.0	.7002	56.0	1.4826	81.0	6.3138
11.0	.1944	36.0	.7265	57.0	1.5399	82.0	7.1154
12.0	.2126	37.0	.7535	58.0	1.6003	83.0	8.1443
13.0	.2309	38.0	.7813	59.0	1.6643	84.0	9.5144
14.0	.2493	39.0	.8098	60.0	1.7321	85.0	11.430
15.0	.2679	40.0	.8391	61.0	1.8040	86.0	14.301
16.0	.2867	41.0	.8693	62.0	1.8907	87.0	19.081
17.0	.3057	42.0	.9004	63.0	1.9626	88.0	28.636
18.0	.3249	43.0	.9325	64.0	2.0503	89.0	57.290
19.0	.3443	44.0	.9657	65.0	2.1445	90.0	infinite
20.0	.3640	45.0	1.000	66.0	2.2460		
21.0	.3839			67.0	2.3559		
22.0	.4040			68.0	2.4751		
23.0	.4245			69.0	2.6051		
24.0	.4452			70.0	2.7475		

Figure 6-58: Simple calculations to check if it was reasonable to correlate the sandstone section of Bravo and Fox well. Dip of sedimentary levels assuming that there is no fault displacement = 14° which is close to the Riachuelo Fm. dip. (≈15°) measured by the FMI.

Reservoir Geophysics for the Calumbi Fm.

GALP's geophysics team has attempted to make a body check the sandstones in the Calumbi Fm. using the following procedure (Figure 6-59):

Data: through velocity analysis it was observed that the sands are acoustically harder than the shale. The seismic polarity convention for the SEAL dataset is such that a white loop corresponds to a soft kick (negative number). Therefore, a sand-body should be a black loop (positive number).

Workflow: A quick inversion using Alpha and Bravo wells to derive the low frequency model was attempted. Bravo well was also used to derive a wavelet from the PSTM volume, which was subsequently inverted. After this, an attempt was made to isolate the P-impedance bodies between 1940-2400 g/cm^3.m/s.

Results: "A small body was found that could be the sand package that gave the good gas shows.`` However the overall quality of the seismic is only fair and the seismic inversion result requires further analysis and should only be used as a qualitative guide. The extent of the body appears to be limited (400 x 450 m) and the thickness of the body needs to be verified. "

Calumbi Fm. Oil volumes: Two scenarios were run for the volumetrics:

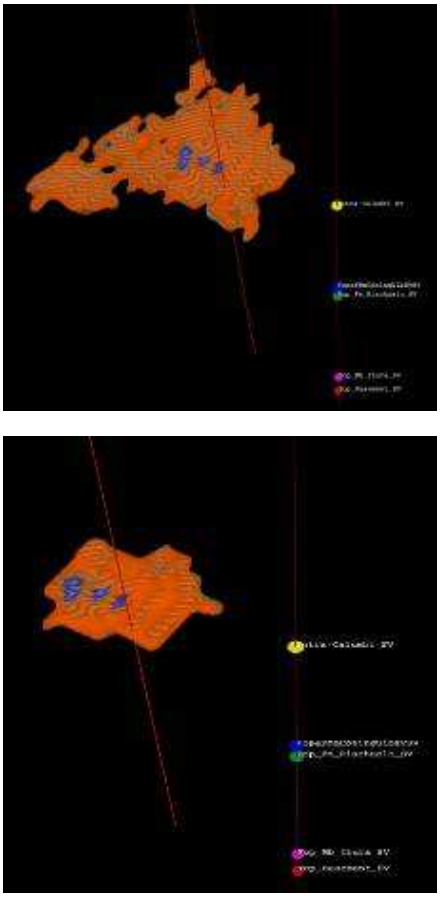

High Case Scenario – connected sand body

Assuming an average velocity of around 2600 m/s and 1m^3 ≡ 6.29 bbl:

- thickness: 15 ms TWT corresponds to ~ 19.5m;
- body volume: 2.4 x 106 m^3;
- **HIIP: 93850 m^3 ~ 590'000 bbl.**

Low Case Scenario – connected sand body

Assuming an average velocity of around 2600 m/s and 1m^3 ≡ 6.29 bbl:

- thickness: 15 ms TWT corresponds to ~ 19.5m;
- body volume: 7.2 x 105 m^3;
- **HIIP: 28225 m^3 ~ 178'000 bbl.**

Figure 6-59: Volumetrics scenarios for the sand body found at Bravo and Fox wells. HIIP – Hydrocarbons Initially in Place.

It may be seen from the volumetric scenarios that the oil in place the Calumbi Fm. is limited even in the high case (Figure 6-59). A range of recovery factors from 15% to 35% will further reduce this volume to a point whereby it may not be a viable exploration target; it may however be a useful incremental addition in the event of any futher field development in this area.

Wireline Logging Analysis

Observations from the wireline logs indicate that zones of interest are not identified either in the Ibura Fm. or Basement when utilising conventional attributes (Figure 6-61). Given the presence of good oil shows over these intervals, and knowing the potential of fractured Basement from other locations in the region, and from experience with the previous wells in the area, the decision was taken to run an FMI log and perform Drill Stem Testing (open hole).

DST Results: Fox well

DST-01 (964m – 974m) – Figure 6-63

1st Flow: initial weak blow changing to strong after 30 minutes and remaining until the end of flow period.

2nd Flow: initial strong blow changing to very strong and continuing to the end of flow period.

Reverse Circulation: mud cut with gas.

Sampling Chamber: 50l of mud cut with gas and oil**.**

DST-02 (977m – 1010m) – Figure 6-64

1st Flow: initial null blow changing immediately to very strong and remaining to the end of the flow period.

2nd Flow: initial very strong blow continuing to the end of flow period.

Reverse Circulation: mud cut with gas and oil.

Sampling Chamber: 43l of oil cut with gas**.** Oil: 37.5^{o} API, BSW= 0,5%.

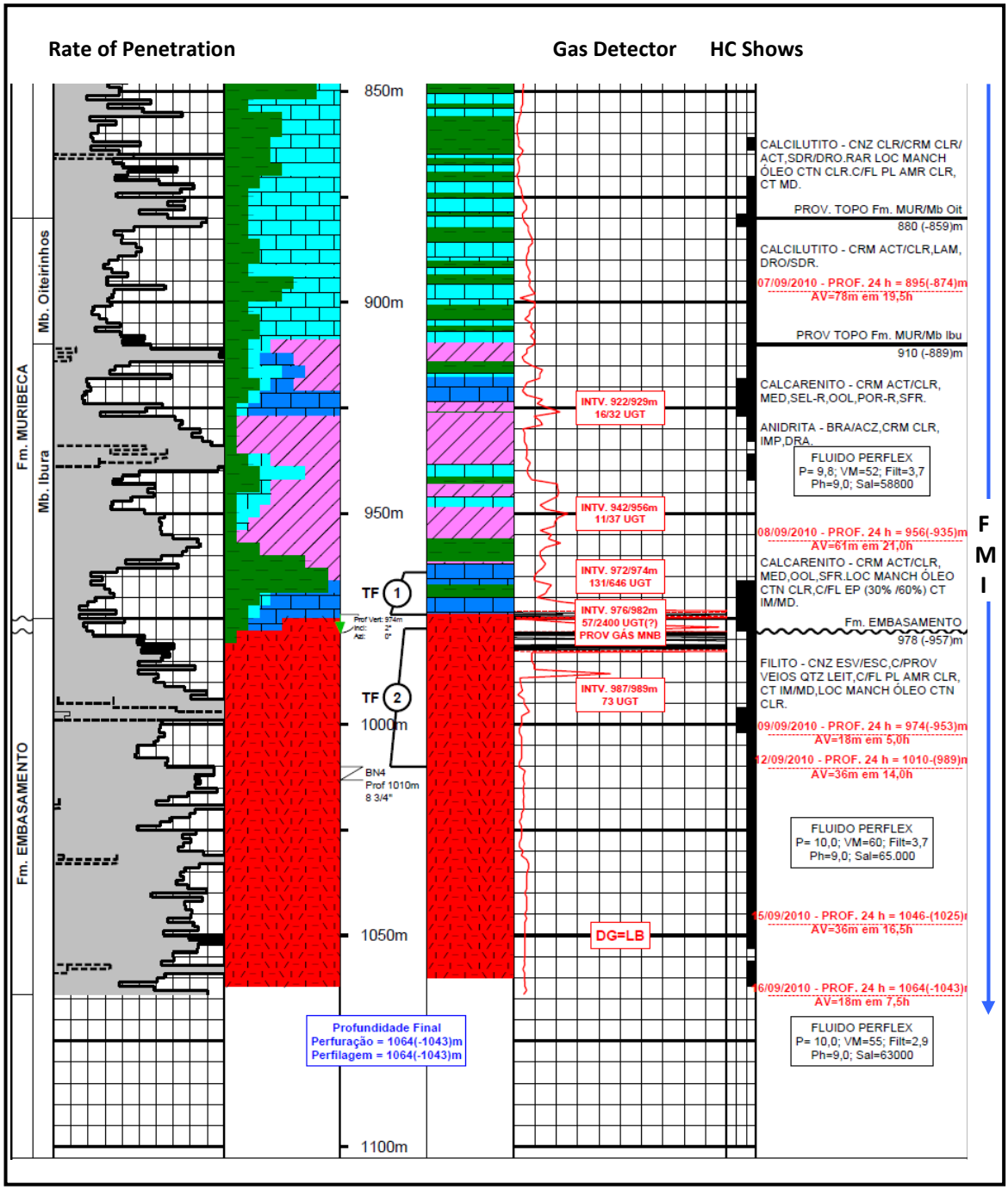

Figure 6-60: Mudlog of the lower section of the Fox well. The blue arrow indicates the depth to which the FMI was run. The DST intervals are indicated by numbers (1) to (2).

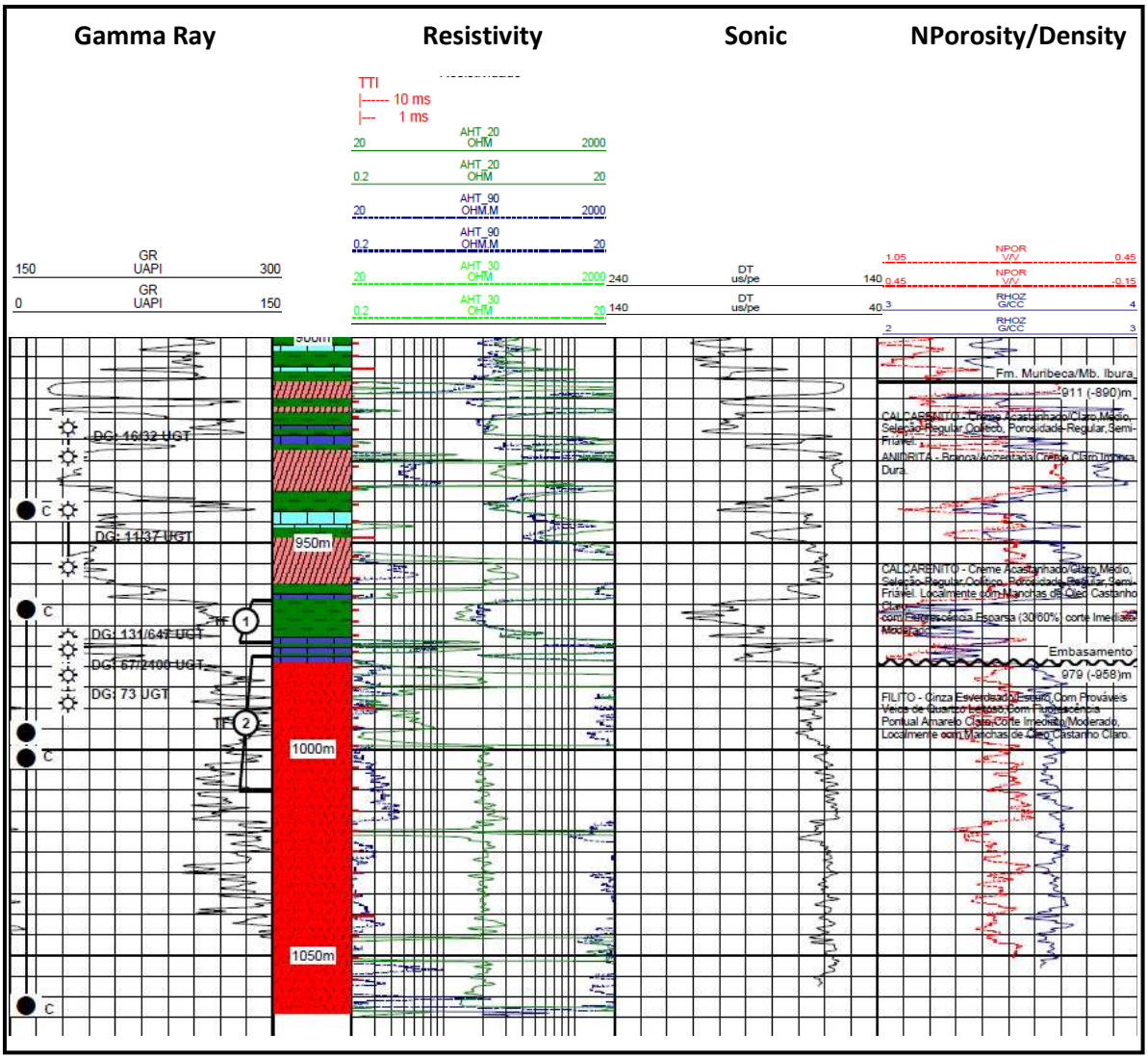

Figure 6-61: Composite well log for the Fox well at the Muribeca Fm. and Basement levels. Two different sections divided by a very visible spike in transit time at around 1025m, can be identified in the sonic log within the Basement (Figure 6-62) like in Echo well. The spike is also noticeable in the NPorosity and Density logs, and Resistivity also responds differently in the upper and lower section of the basement. The continuous registration of this spike reinforces the hypothesis of it being a transition zone between the altered upper Basement and the non-altered lower Basement, rather than an isolated fracture, i.e. it is no probable that an isolated fracture extends for such a large area.

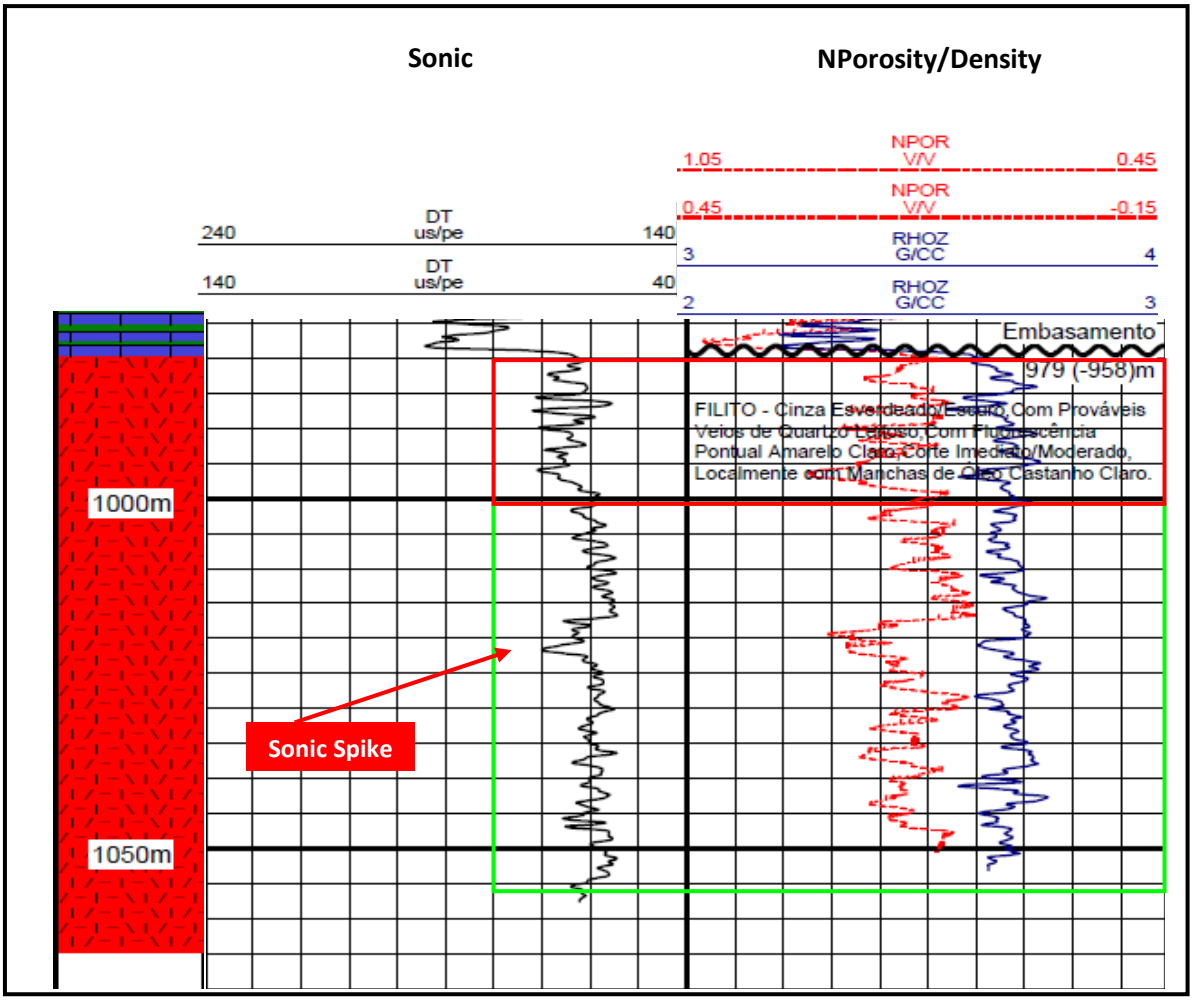

Figure 6-62: As in Echo Well, each of the two individualized areas in Fox well (red and green) have different average transit times and corresponding responses of the sonic and density logs. There is also a sonic spike at around 1025m similar to what was registered in Charlie and Echo wells. The continuous registration of this spike reinforces the hypothesis of it being a transition zone between the altered upper Basement and the non-altered lower Basement, rather than an isolated fracture, i.e. it is not probable that an isolated fracture extends for such a large area.

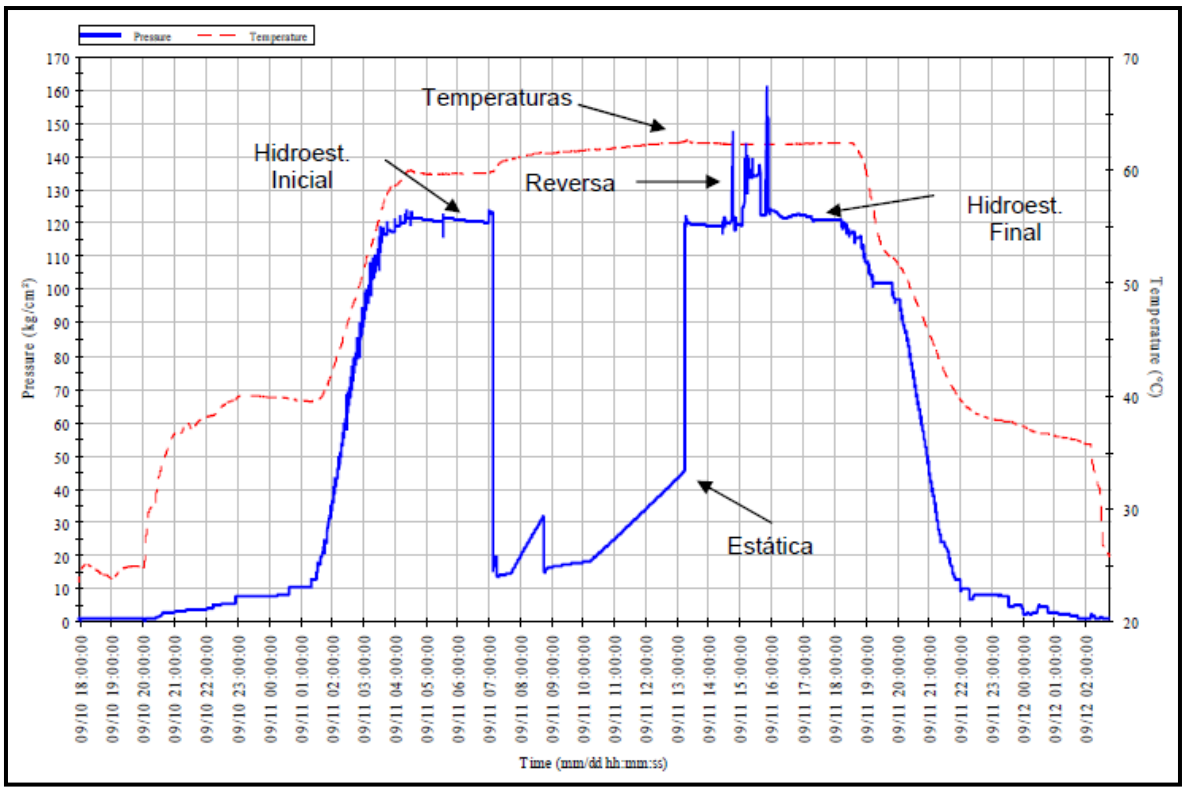

Figure 6-63: DST-01 pressure plot. The back-pressure almost did not increase during flow periods, and the build-up curves rise sharply but do not stabilize. This indicates very low permeability in the tested interval.

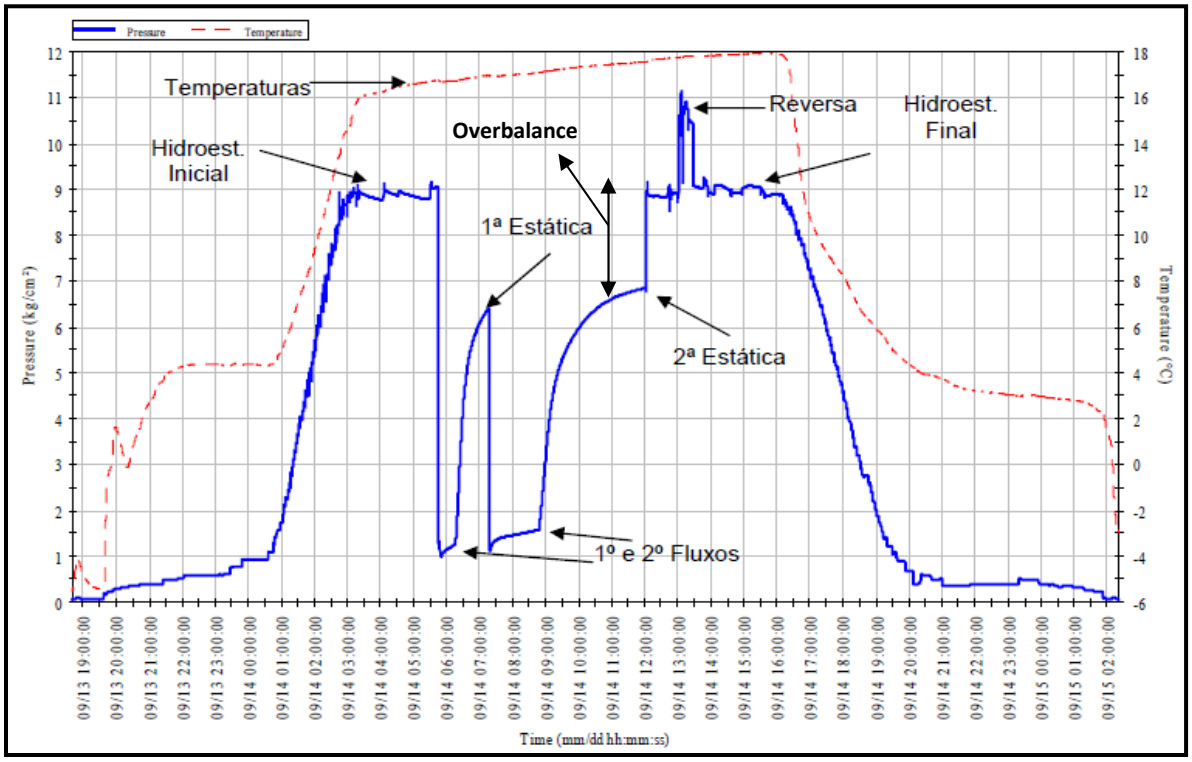

Figure 6-64: DST-02 pressure plot. This plot shows an interval with a reasonable permeability, as evidenced by the increase in back-pressure during the flow periods and by the rapid increase in pressure. The pressure was tending to stabilize in the second build-Up period. The very strong blows and the sampled oil cut with gas are consistent with this analysis. Also shows the well was highly overbalanced.

Comments on the DST's procedures and results:

- Only one DST was made at the Top Basement level, despite the fact that oil shows were observed in cuttings below that interval. A DST below DST-02 should have been made in order to understand if the pattern of results observed in the Bravo well (water production below the ≈30m interval) were consistent with those seen in here, and to try to define a possible OWC.
- DST-02 was performed over a 30m of basement section; this does not allow us to understand exactly from where in the Basement the oil is being produced.

Golf Well

- **Primary Objective I:** testing the presence of HC in the Basement.

  Reservoir: fractured metamorphic rock.

- **Secondary Objective**: testing the presence of HC in the Ibura Fm.

  Reservoir: fractured carbonates intercalated with evaporites (anhydrite).

  Secondary Objective II: testing the occurrence of HC in the turbiditic sandstones of Calumbi Fm.

- **Type of Well:** Vertical.
- **Mud:** Conventional mud (8.7- 9 lb/gal) – Phase I

  Perflex fluid (9.2-9.8 lb/gal) – Phase II

  Perflex fluid (9.8-10 lb/gal) – Phase III (Mud weight when drilling through Basement)

Golf well was a vertical well positioned over a basement level structural high. Figure 6-65 shows the interpretation that was performed for the well positioning. This was conditioned by the inexistence of seismic in cross-line direction but still the interpretation is quite precise Table 6-9 shows the comparison between the predicted and the actual drilled formation tops.

Table 6-9: Comparison table of the predicted versus actual formation tops. Above (+). Below (-). The actual formation tops diverge from the predicted, mainly due to interpretation errors related to the poor seismic data quality and the velocity model used to create a seismic depth cube. The well was positioned only using In-lines. The interpretation of Top Basement and Top Ibura Mb. is very precise comparing to the previous interpretations (Alpha, Bravo…).

Stratigraphic Tops						
Formations		Depths				
		Preview		Drilled		Δ
		Measured	TVD	Measured	TVD	m
Barreiras Fm.		surface	9	surface	9	-
Marituba Fm.		20	-6	18	-4	2
Calumbi Fm.		154	-140	160	-146	-6
Cotinguiba Fm.	Sapucari Mb.	704	-690	-	-	-
	Aracaju Mb.	-	-	690	-676	-
Riachuelo Fm.	Maruim Mb.	-	-		-	-
	Taquari Mb.	709	-695	718	-704	-9
Muribeca Fm.	Oiteirinhos Mb.	924	-910	905	-891	19
	Ibura Mb.	964	-950	948	-934	16
	Carmopolis Mb.	-	-	-	-	
Basement		1029	-1015	996	-982	33
Final Depth		1065	-1051	1062	-1048	3

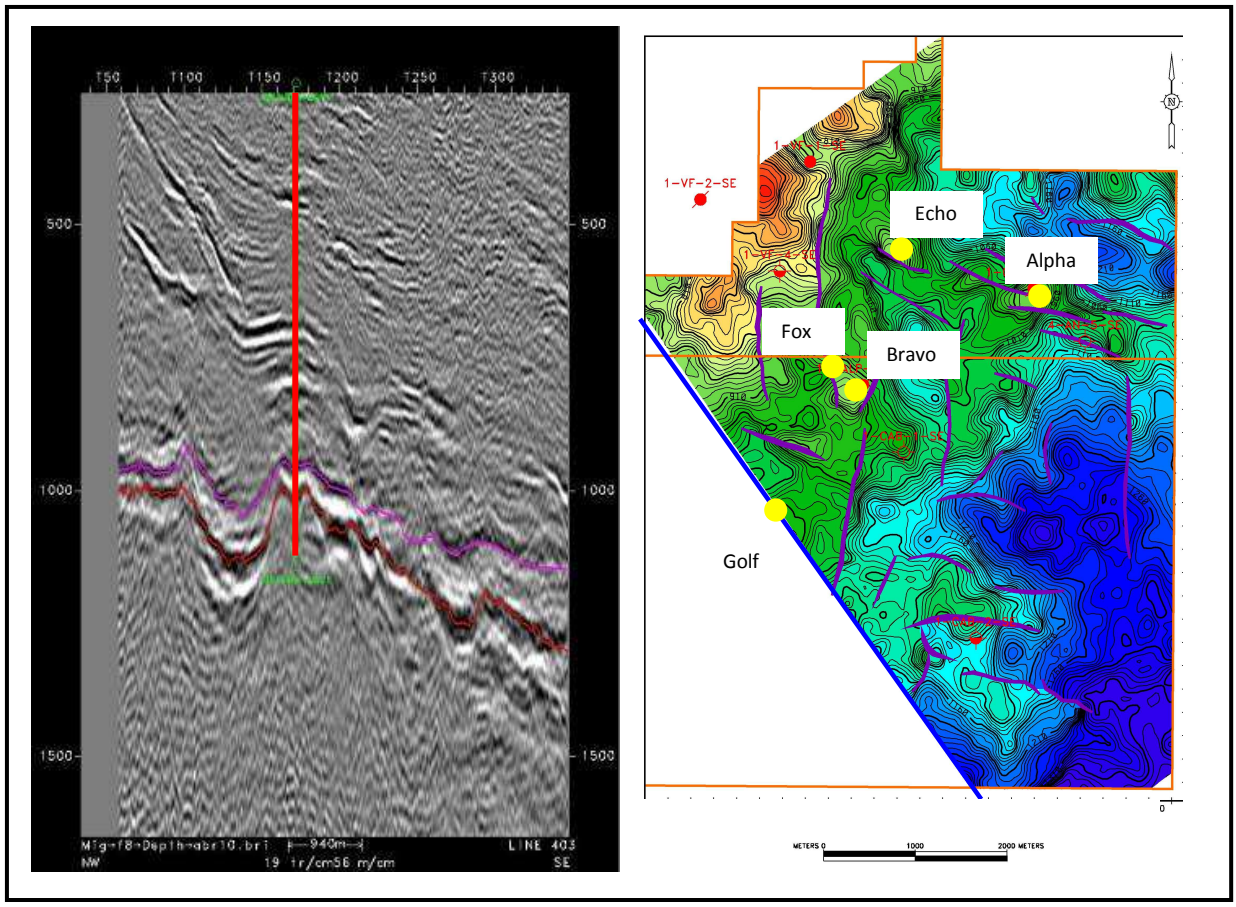

Figure 6-65: Seismic In-line in depth and Top Ibura depth map on which was based the positioning of Golf well.

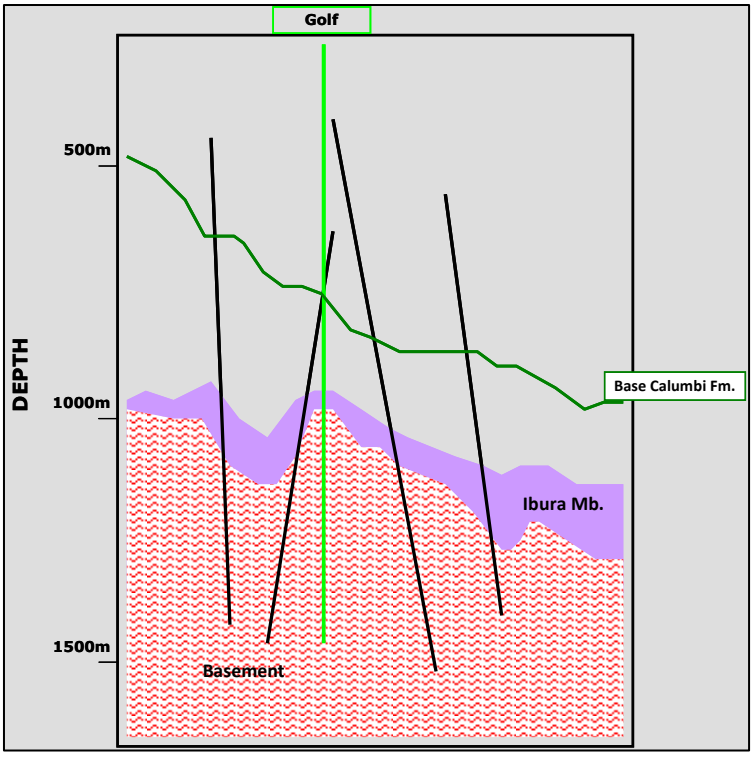

Figure 6-66: Schematic geological section of the Golf well area.

Mudlog Analysis

The main Observations from the mudlog are (Figure 6-67 and 6-68):

- A sand-body that had fair oil shows was intersected in the Calumbi Fm at 580m-600m (MD)
- Oil shows were found from the top of Muribeca Fm. to TD.
- The Ibura Fm. was poor in anhydrite but rich in carbonates, especially in its lower section where very good oil shows were found.

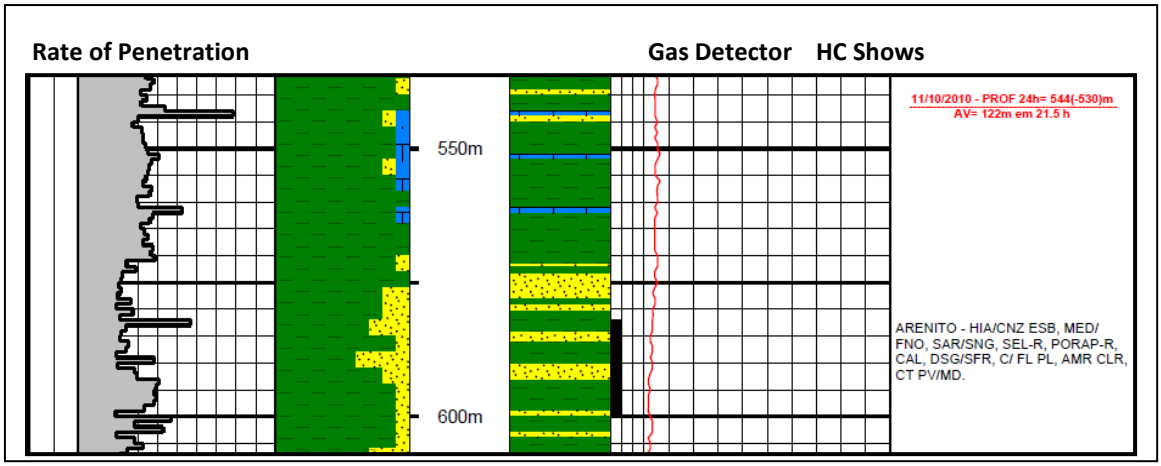

Figure 6-67: Section of the well log at the sandstones of Calumbi Fm. which had good oil shows.

Wireline Logging Analysis

Observations from the wireline logs (Figure 6-69) indicate that zones of interest are not identified in either the Ibura Fm. or the Basement when utilising conventional attributes. Given the presence of good oil shows over these intervals, and knowing the potential of fractured Basement from other locations in the region, and from previous experience with the wells in the area the decision was taken to run an FMI log and perform Drill Stem Testing (open hole).

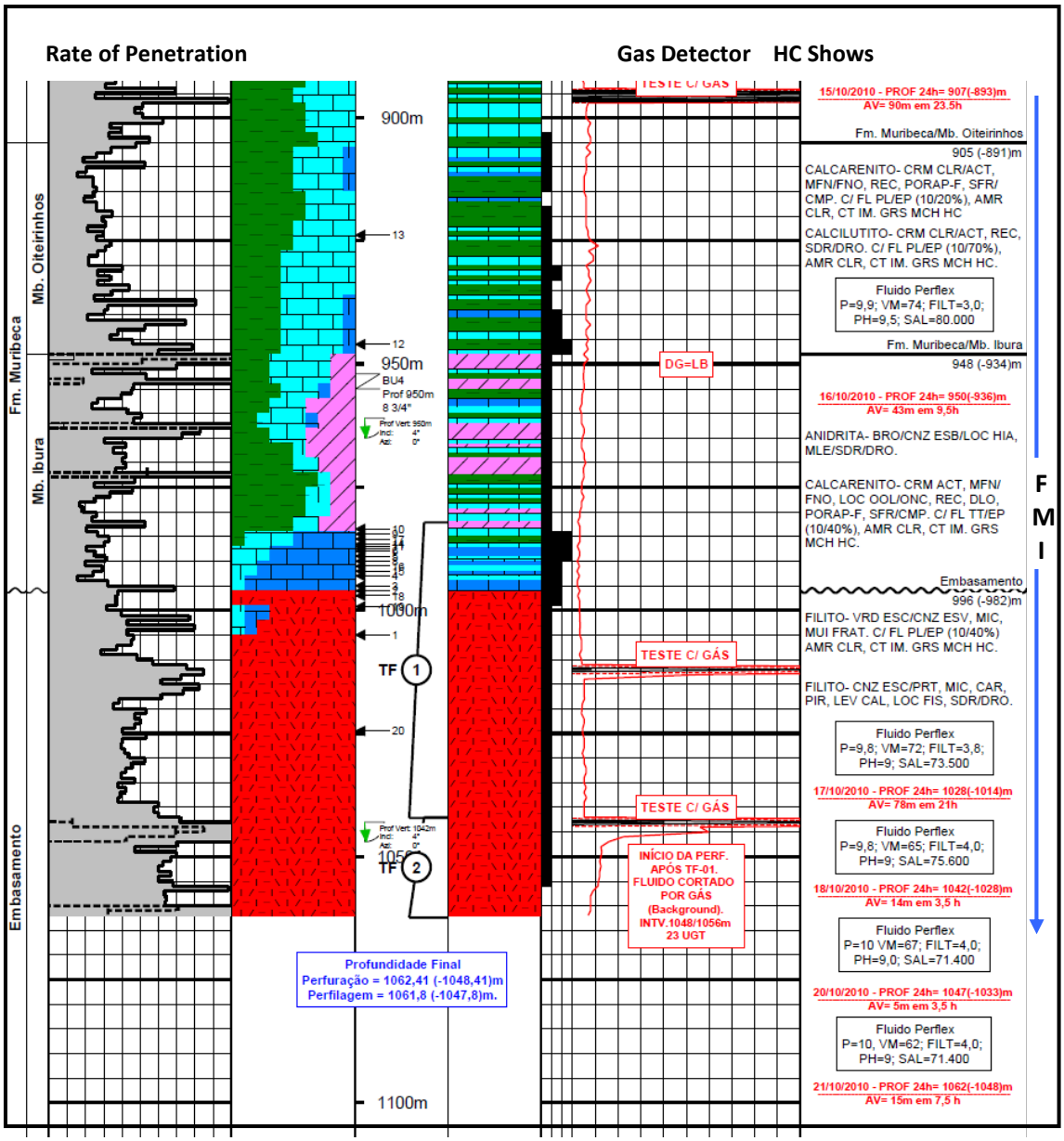

Figure 6-68: Well log of the lower section of the Golf well. The blue arrow indicates the depth to which the FMI was performed. Notice the extension of DST-01, and the fact that it has been done over the Ibura and Basement once again.

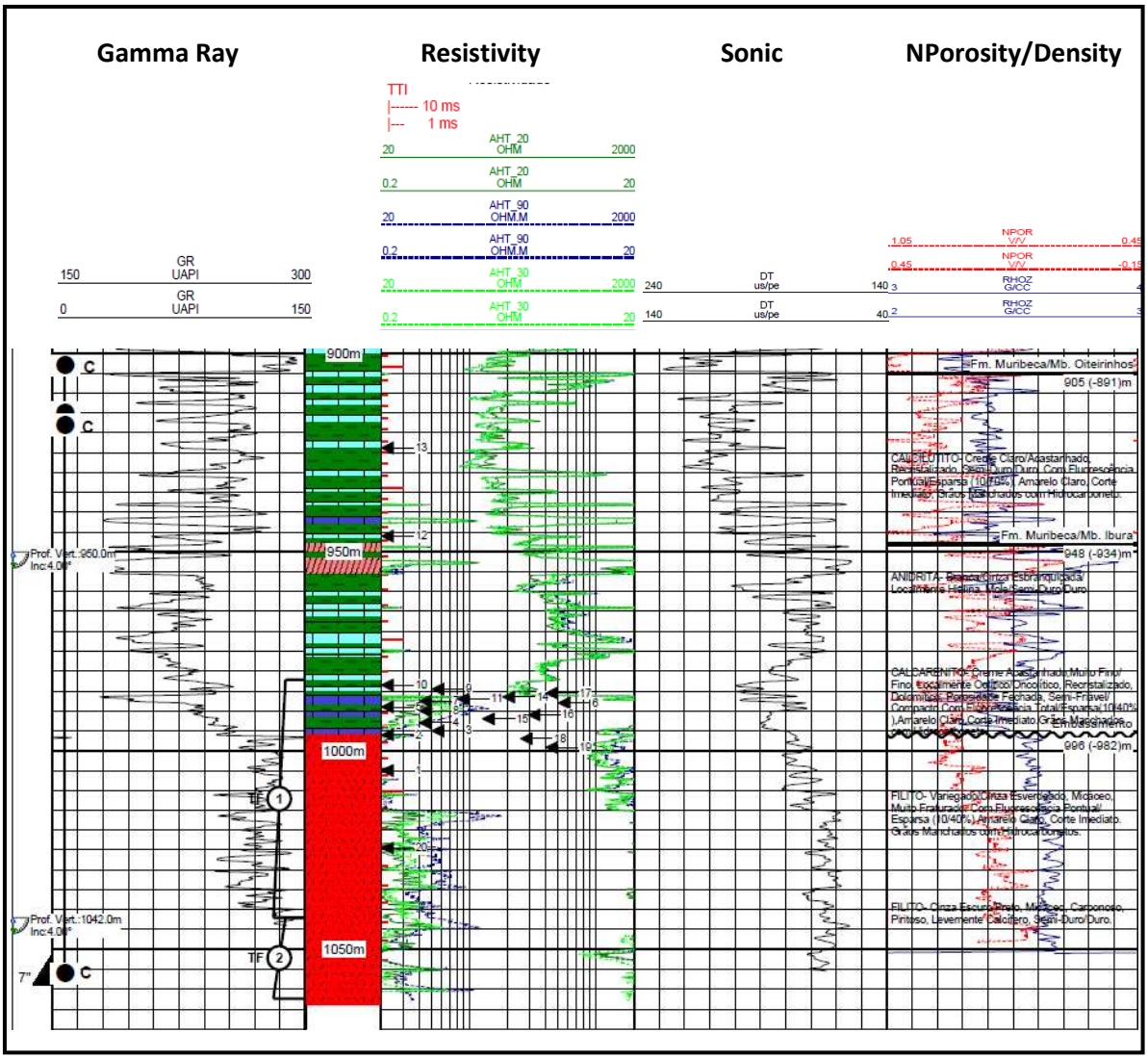

Figure 6-69: Composite well log for the Golf prospect at Muribeca and Basement level.

The same differences in the sonic log that were registered in Echo and Fox Wells, were also registered in Golf well – Figure 6-70.

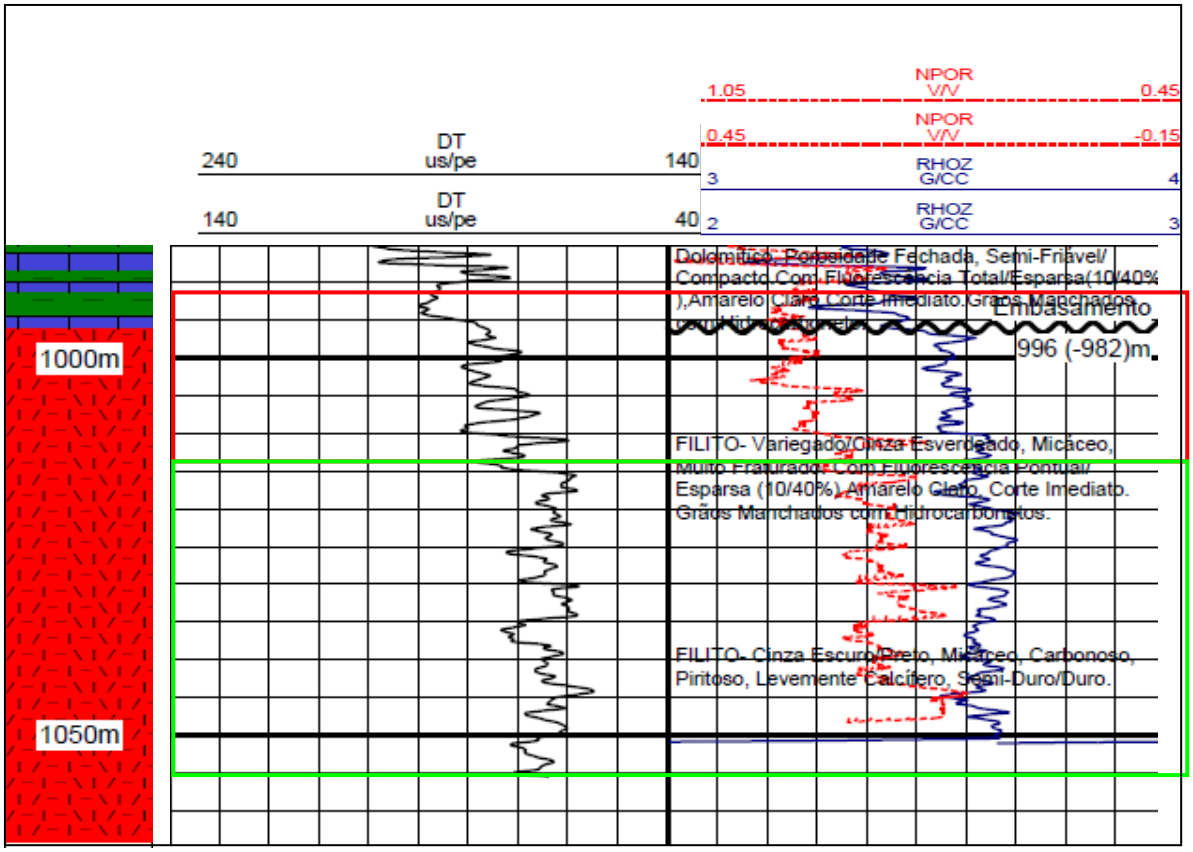

Figure 6-70: Again in Golf Well, each of the individualized areas (red, and green) have different average transit times and corresponding responses of the sonic and density logs. There is also a sonic spike at around 1035m (not as clear as in other wells) similar to what was registered in Charlie, Echo and Fox wells. The continuous registration of this spike reinforces the hypothesis of it being a transition zone between the altered upper Basement and the non-altered lower Basement, rather than an isolated fracture, i.e. it is no probable that an isolated fracture extends for such a large area.

DST Results Analysis: Golf Well

DST-01 (984m – 1042m) – Figure 6-71

1st Flow: initial strong blow, changing to very strong until the end. Flow to surface. . Due to gas flow, the burner lit and produced a 5 m yellow flame.

2nd Flow: non-existent.

Reverse Circulation: - no information.

Sampling Chamber: - no information.

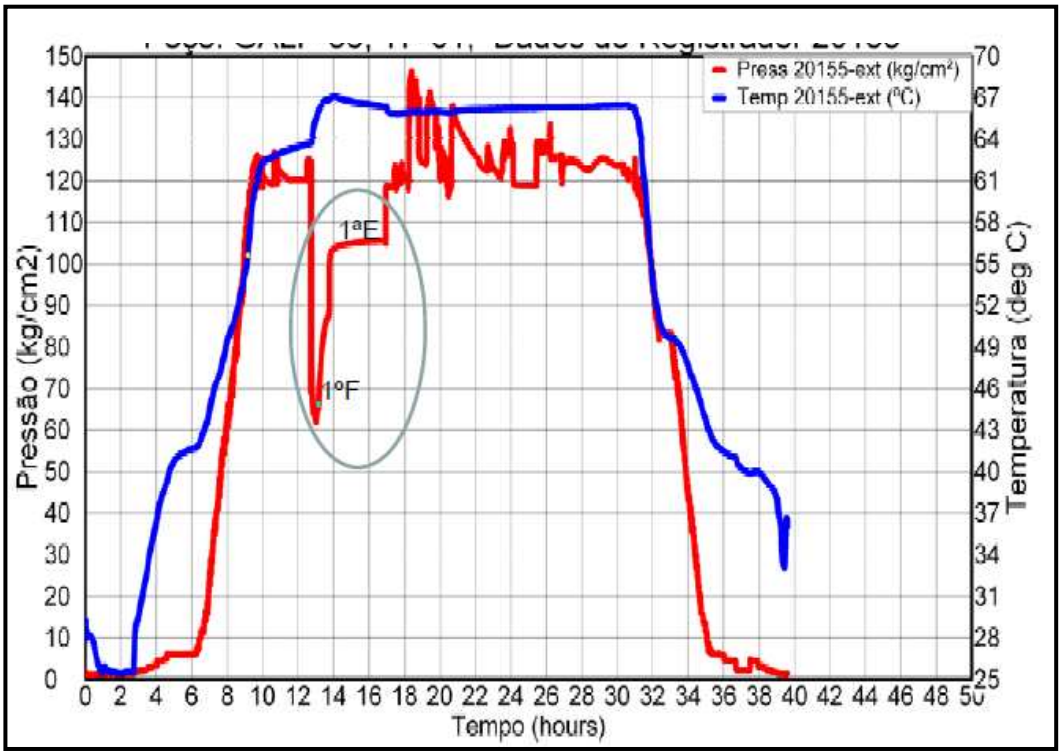

Figure 6-71: Golf well DST-01 pressure plot. With only one cycle and a very little volume of oil produced (which is not stated in the reports) it is not possible to make any conclusions on the reservoir pressures or permeability, even tough the pressure stabilized very quicly. Having tested a very large extension of well, including two different formations, with very different lithological properties, did not help to evaluation. Only the fact that a very strong gas blow, with a 5m flame, was registered at surface allows the interpretation that this is a good reservoir. Nevertheless no conclusions can be taken on the specific interval that should be considered for future production.

DST-02 (1042m-1062m)

1st Flow: null blow.

2nd Flow: null blow.

Reverse Circulation: 12 l of mud.

Sampling Chamber: -

From the above data, it is fair to conclude that this is a very poor interval with respect to permeability. Unfortunately the pressure plot for this DST was not available.

Considerations on Drilling and Testing Procedures

To date all the wells have been drilled vertically and in overbalance, with mud weights ranging from 8.7 lb/gal to 10 lb/gal. Considering that the main targets are Naturally Fractured Reservoirs, this may not be the most efficient approach to drilling and evaluating these fractured reservoirs:

- Vertical wells are not able to intersect most of the open fractures as these are not horizontally distributed.
- Overbalanced drilling in a fractured reservoir will cause damage to the reservoir due to the amount of mud invasion that can occur. This will have an influence on the way the reservoir behaves when, for example a DST is operated.

Well testing procedures were also erroneous, both in terms of the well sections tested and in the way the tests themselves were conducted:

- The same sections should have been tested in different wells and independently; i.e. in each well Ibura Mb. and Basement should have been tested independently.
- Every well should have been tested to TD with short to medium range DST's.
- The DST's should have followed the standard procedure of two Flow-periods and two Shut-in periods, so that conclusions on the reservoirs pressure behaviour could have been taken.

Due to these procedures, and to the fact that we do not have reliable pressure values for the tested intervals, it was not possible to take conclusions on the permeability of the Fractured Basement.

6.1.4.2 Image Logs Analysis

To make the visualization easier and because this is one of the most important sections of the well analysis, the FMI logs that were run, will be analysed together for all wells. As all the wells were made in the same geographic area it's not surprising that the features that were found are similar for all of them. These are:

- **Bed Boundary -** these events are very common along the wells. They mark lithological changes in the sedimentary record.
- **Foliations:** the events that were interpreted as foliations are very common particularly in the Basement. Figure 6-72 and 6-73 show them in detail for Alpha Well, but they appear in all of the drilled wells. These can be misinterpreted as natural open fractures, which very often occur parallel to the foliation due to decompression effect while drilling.

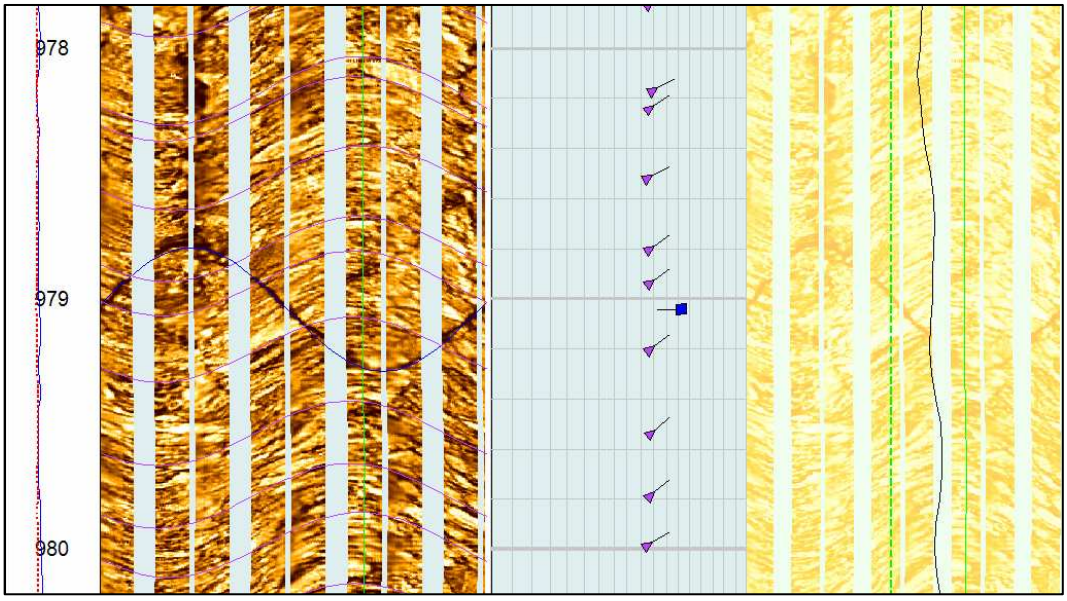

Figure 6-72: dynamic and static images from the Basement, showing foliation – purple tadpoles – dipping around 50º towards NE. Vertical scale 1/20. The rock shows high resistivity.

Natural Fractures: natural fractures, conductive (dark colour) or resistive (light colour) appearance (Figure 6-74) were observed along the several logged intervals, being more common than the induced. As these are the object of the present study, they will be given more importance than the other features observed and previously described. Fracture aperture and porosity can be calculated using the FMI data. The values presented below correspond to the calculations done using the interpretation software from Schlumberger.

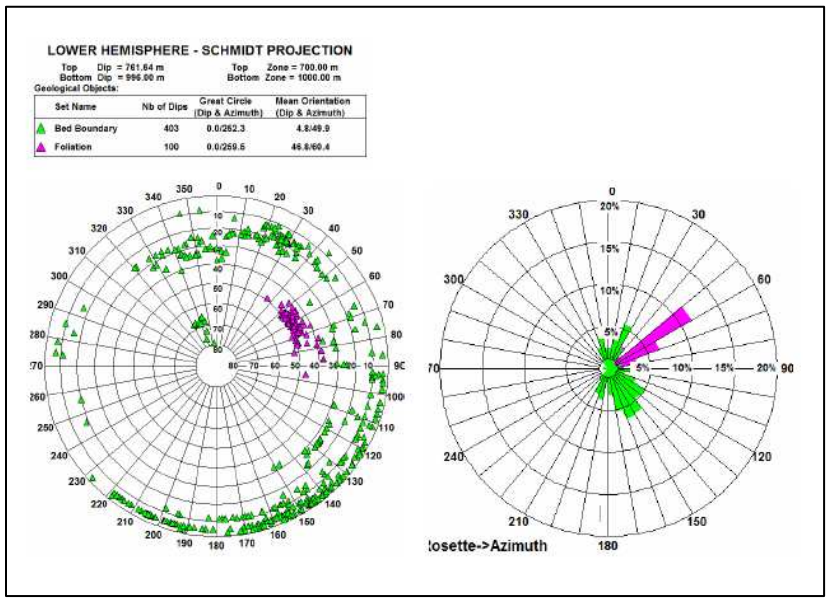

Figure 6-73: Schmidt diagram (Lower Hemisphere) and Rose Diagram for the bed boundary events (green tadpoles) and foliation (purple tadpoles) for Alpha well.

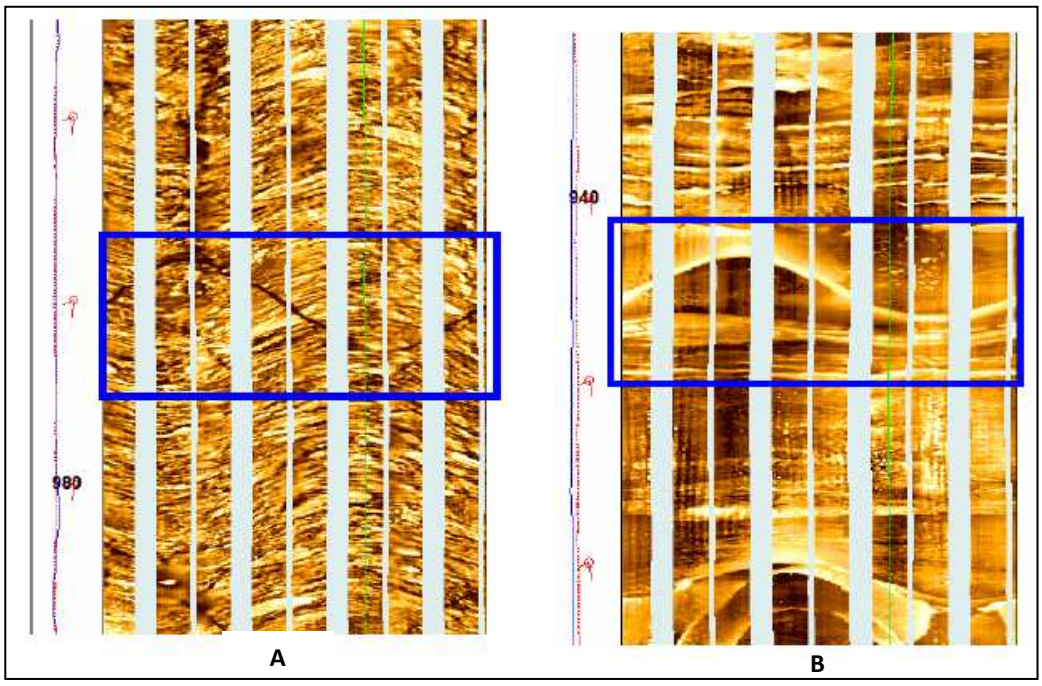

Figure 6-74: example of the appearance of conductive - dark (A) and resistive -light natural fractures (B) in Basement of Alpha well.

Fracture Aperture (fracture width): fracture aperture is calculated taking into account the mud resistivity, the rock resistivity and specific tool parameters. Fracture dip angle and extension are also an input, as well as the degree of aperture (partially or totally open). Luthi and Souhaité (1990) describe the calculation algorithm:

$$W = c \cdot A \cdot Rm^{b} \cdot Rxo^{1-b}$$

W: fracture aperture
b and c: specific tool parameters
A: excess of current divided by the voltage integrated along a line perpendicular to the fracture strike.
Rm: mud resistivity
Rxo: rock resistivity

Considering that Rm and Rxo have influence on the calculation of the aperture, they should be as precise as possible. In general, if Rm is too high, it tends to increase the calculated aperture, and vice-versa. An high Rxo will diminish the aperture and vice-versa. Two types of fractures can be calculated: *mean aperture* and *hydraulic*. For porosity calculation it is the hydraulic aperture that is used.

Fracture porosity: fracture porosity for this purpose is defined by the percentage of wellbore wall that is covered by the fracture. The calculation of this property uses the parameters fracture density and the area of wellbore that is covered by the image log. It is important to highlight that only the fracture porosity is being calculated here as there is no contribution of primary porosity. Literature shows that fracture porosity doesn't normally go beyond 1.5% - 2% (Nelson, 1985).

Fracture aperture and fracture porosity values are presented in Table 6-10

Induced Fractures: these are generated during drilling operations, and are related to the subsurface stresses. Their strike is in general parallel to the largest stress, and when associated with breakouts (well deformation in a preferential direction) they help characterizing the principal tensors in the region (Figure 6-75).

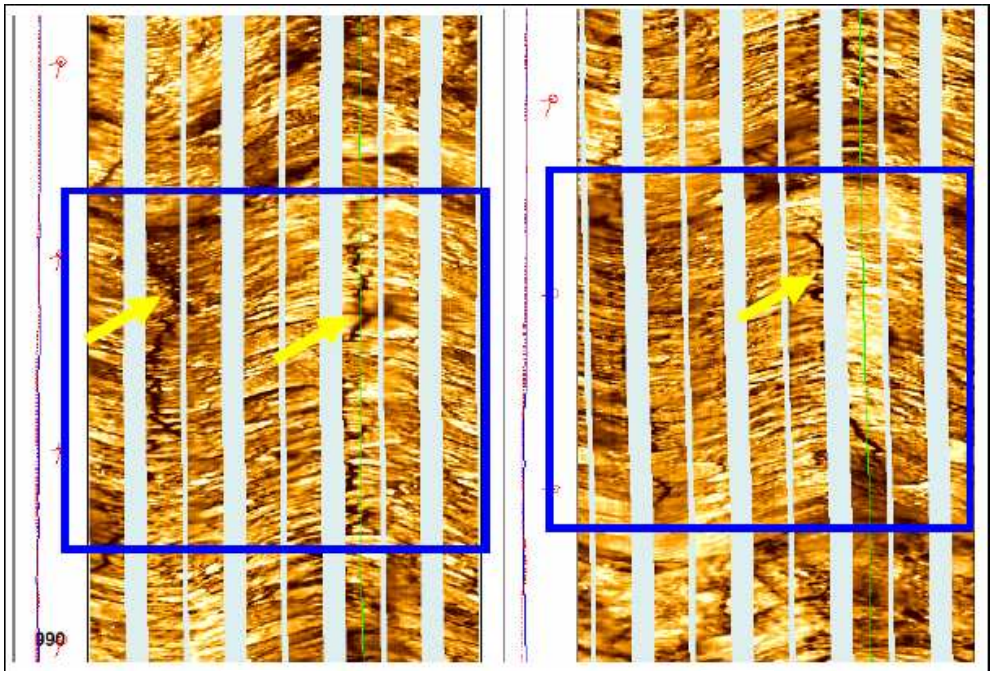

A B

Figure 6-75: dynamic (A) and static image (B) (scale 1/20) showing induced fractures in Alpha Well. Observe the non-planar, sub-vertical features marked with the yellow arrows.

FMI Results

The next pages will be dedicated to the analysis of the FMI data over the Basement with the objective of understanding the characteristics of the fractures that cut through it. Below, Table 6-10 summarises some important qualitative results after the FMI analysis for the different wells, as previously described:

Table 6-10: results from the FMI analysis for the different wells. Values of aperture corresponding to porosities below 0.01% were not considered. Notice that the porosities and apertures here presented are indirectly measured by the FMI tool, i.e. the values are extrapolated using the calculations presented above. As porosity is determined by the percentage of wellbore wall that is covered by the fracture, and the well is vertical, it is likely that porosity is highly underestimated.

Well	Total Well Depth (m)	Logged Interval (m)	Top Basement	% of Basement Imagged	Average Fracture density (fracs/m)	Fracture Porosity (%)	Fracture Aperture (mm)
Alpha	1060	740 -1000	969	34	2	0,01-0,05	0,01-0,1
Bravo	1101	800-1035	1005,5	31	5	0,01-0,1	0,02-0,61
Charlie	757	620-755	636	100	3	0,01-0,02	0,02-0,05
Delta	937	750-937	851	100	3.5	0,01-0,06	0,017 -0,17
Echo	1080	840-1080	971	100	4	0,01-0,05	0,01-0,2
Fox	1064	848-1062	978	100	processing of CMI data was not possible to make		
Golf	1062	896-1059	996	100			

In order to evaluate what were the main fracture trends in the wells, and consequently in the study area (Distribution of Fracture Patterns in the NFR Worlflow – Figure 6-1) Universidade Nova de Lisboa (UNL) team (part of the Fractured Basement Project) made an analysis of the dip and strike measurements taken from the FMI. These measurements were plotted in a Schmidt Equal Area Projection - southern hemisphere - grid and statistically analysed. The conclusions are presented below in the form of pictures (Figure 6-76 to 6-80). Notice that measurements for Charlie and Echo well were not available. This caused that for Block-B, models and predictions were based only in one well, causing them to be less accurate.

Alpha Well

Family	Nº Fracs	Strike/Dip	Dip, Dip-Az.
Alpha-1	92	N40ºE/78ºNW	78,310
Alpha-2	16	N29ºW/ 61ºNE	61,61

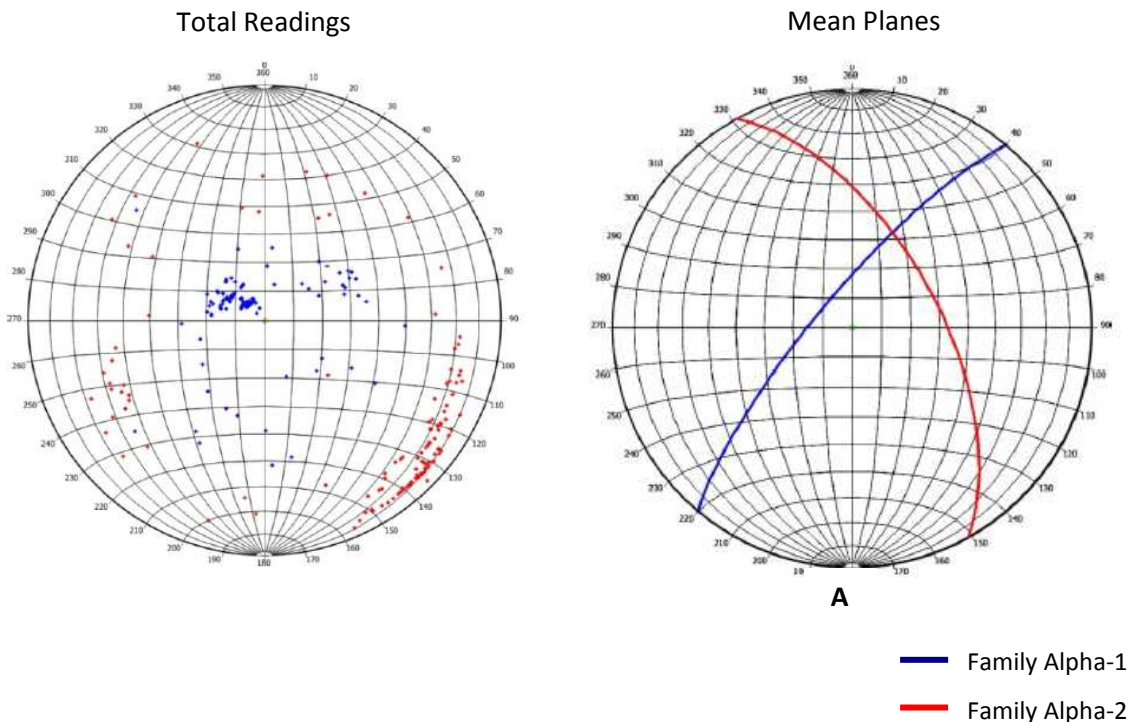

Figure 6-76: (A) Schmidt Equal Area projection for Alpha well with poles in red and dip-azimuths in blue. (B) Schmidt Equal Area projection of the mean planes of the fracture families found in Alpha well. (Adapted from UNL, UALG, UA, & IST; *Modelling and Characterization of Fractured Reservoirs -GALP E&P Internal Report;* Lisbon; 2011).

Beta Well

Family	Nº Fracs	Strike/Dip	Dip, Dip-Az.
Beta-1	55	N29ºW/55ºNE	55,61
Beta-2A	16	N30ºE/35ºSE	35,300
Beta-2B	20	N35ºE/47ºNW	47,305

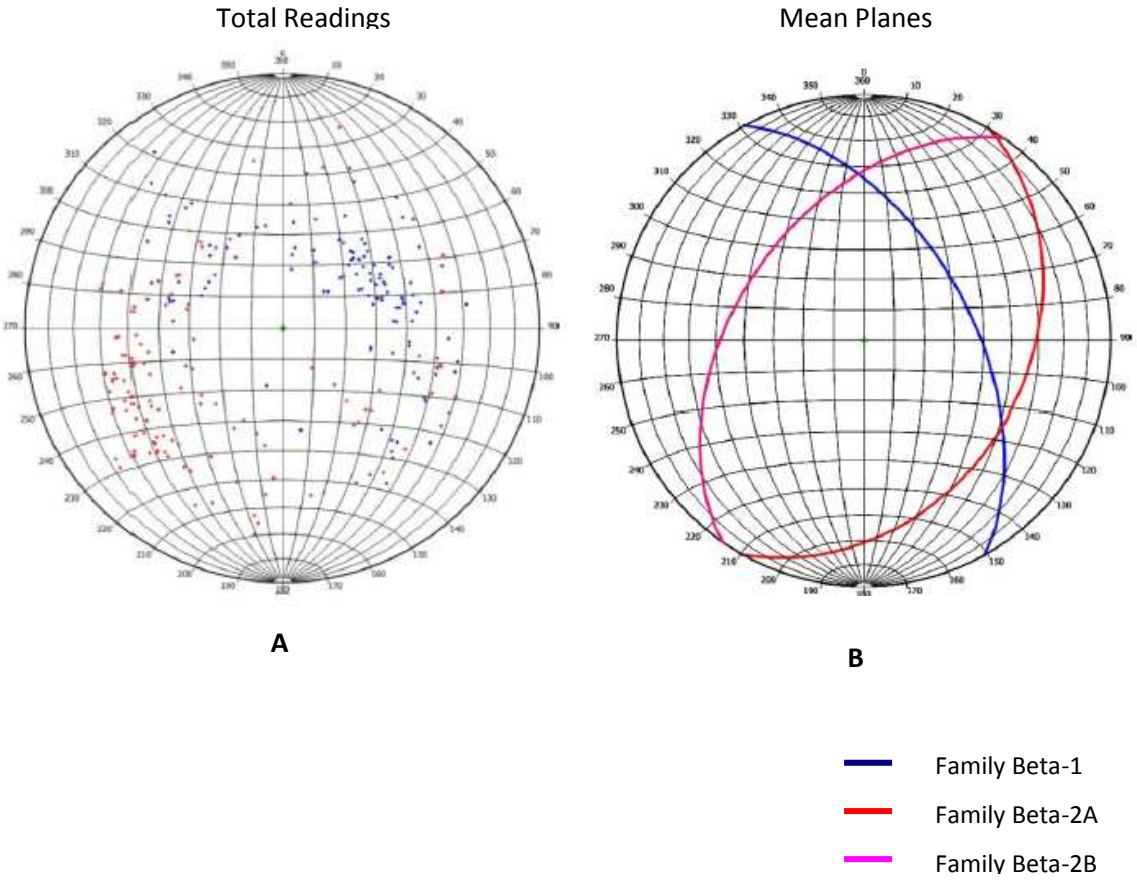

Figure 6-77: (A) Schmidt Equal Area projection for Beta well with poles in red and dip-azimuths in blue. (B) Schmidt Equal Area projection of the mean planes of the fracture families found in Beta well. (Adapted from UNL, UALG, UA, & IST; *Modelling and Characterization of Fractured Reservoirs -GALP E&P Internal Report;* Lisbon; 2011).

Delta Well

Family	Nº Fracs	Strike/Dip	Dip, Dip-Az.
Delta-1	48	N65ºE/55ºNW	55,335
Delta-2A	11	N20ºW/60ºE	60,70
Delta-2B	20	N9ºE/49ºW	49,279
Delta-3	19	N88ºE/40ºS	40,358

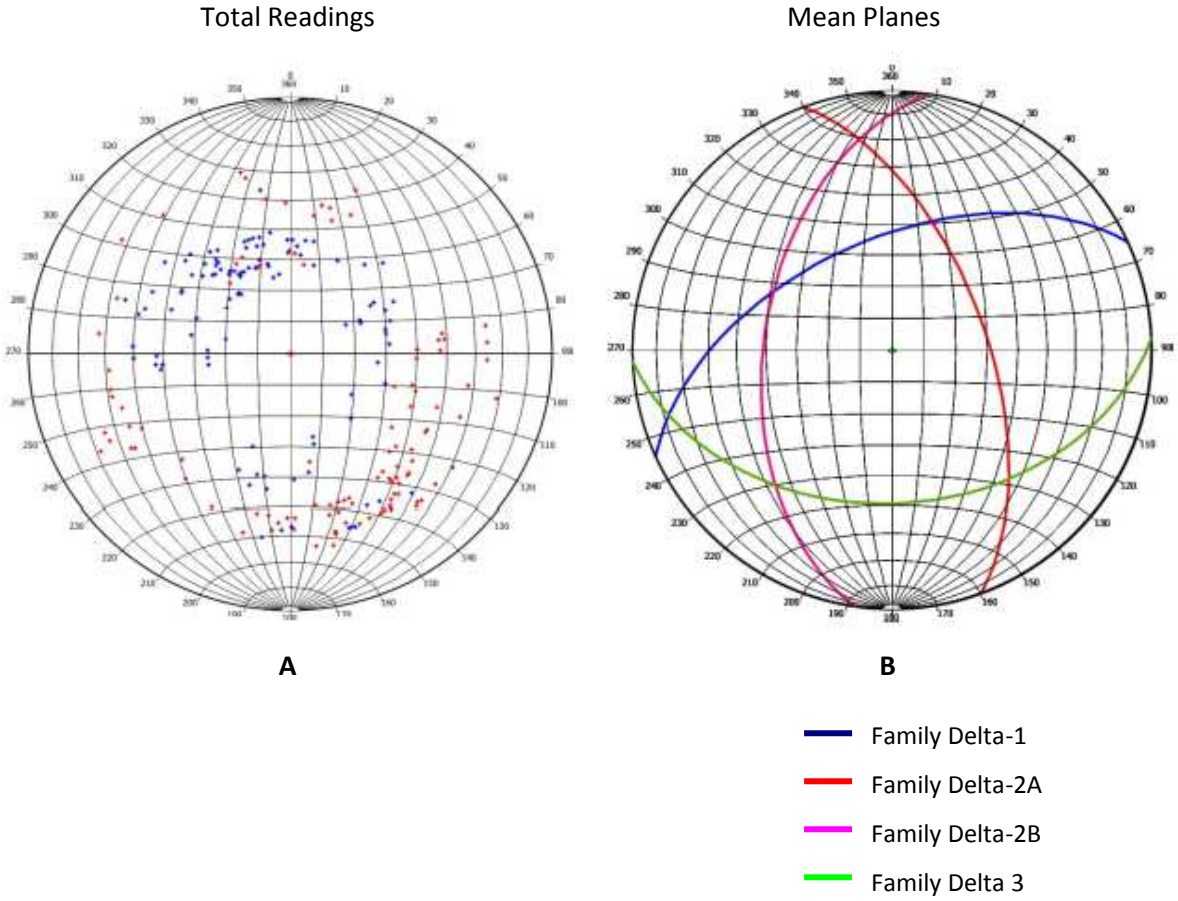

Figure 6-78: (A) Schmidt Equal Area projection for Delta well with poles in red and dip-azimuths in blue. (B) Schmidt Equal Area projection of the mean planes of the fracture families found in Delta well. (Adapted from UNL, UALG, UA, & IST; *Modelling and Characterization of Fractured Reservoirs -GALP E&P Internal Report;* Lisbon; 2011).

Fox Well

Family	Nº Fracs	Strike/Dip	Dip, Dip-Az.
Fox-1A	14	N12ºW/65ºNE	65,78
Fox-1B	8	N6ºE/64ºNW	64,276
Fox-2	8	N31ºE/50ºSE	50,121

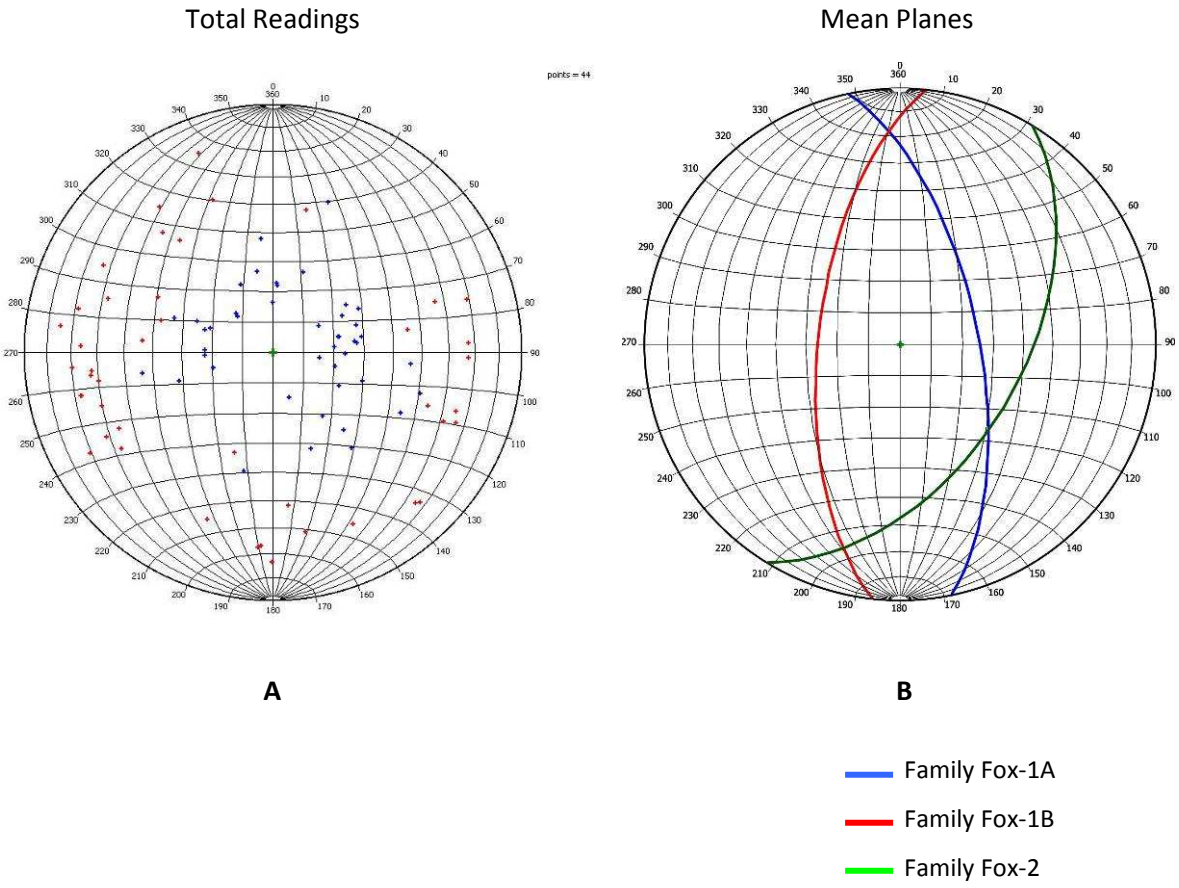

Figure 6-79: (A) Schmidt Equal Area projection for Fox well with poles in red and dip-azimuths in blue. (B) Schmidt Equal Area projection of the mean planes of the fracture families found in Fox well. (Adapted from UNL, UALG, UA, & IST; *Modelling and Characterization of Fractured Reservoirs -GALP E&P Internal Report;* Lisbon; 2011).

Golf Well

Family	Nº Fracs	Strike/Dip	Dip, Dip-Az.
Golf-1A	21	N18ºW/51ºNE	51,72
Golf-1B	11	N20ºW/39ºSW	39,250
Golf-2	6	Nº86E/31ºSE	31,176

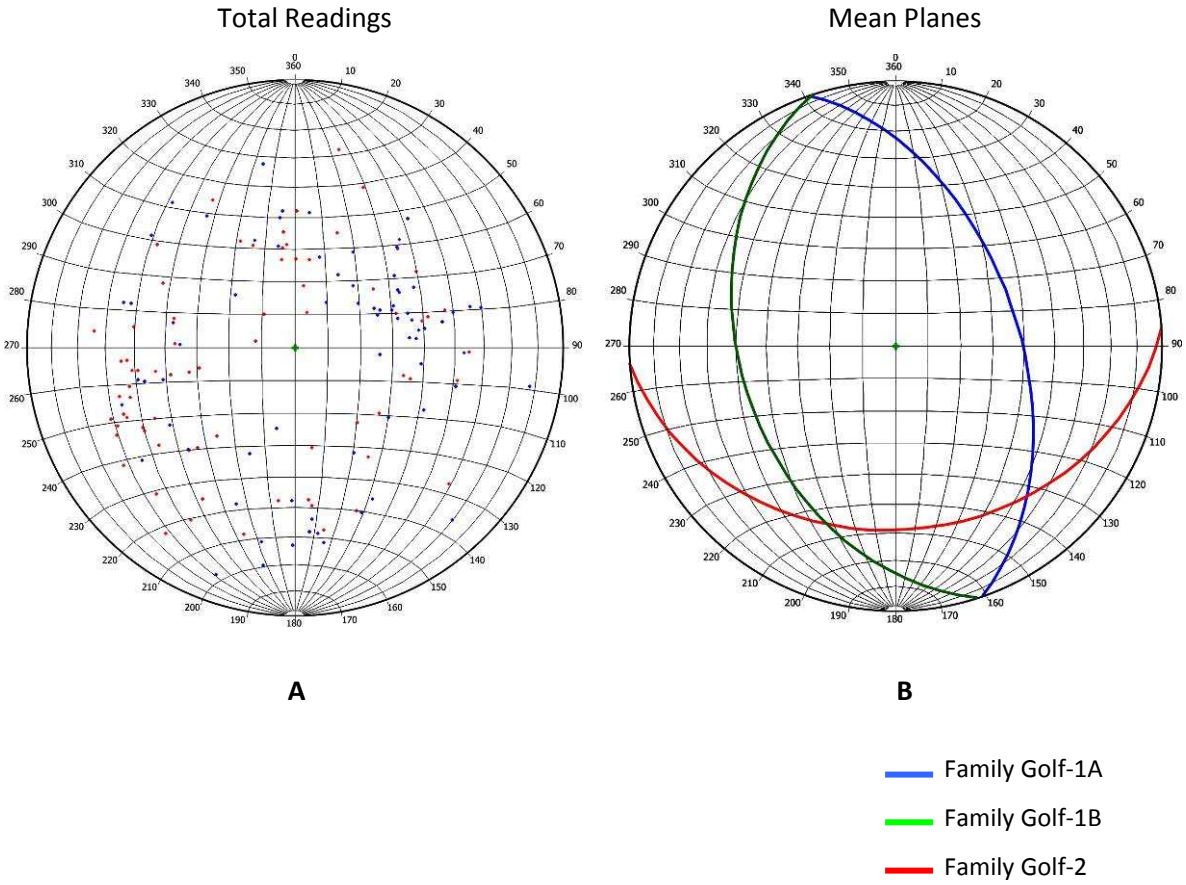

Figure 6-80: (A) Schmidt Equal Area projection for Golf well with poles in red and dip-azimuths in blue. (B) Schmidt Equal Area projection of the mean planes of the fracture families found in Golf well. (Adapted from UNL, UALG, UA, & IST; *Modelling and Characterization of Fractured Reservoirs -GALP E&P Internal Report;* Lisbon; 2011).

Because only the fractures located in the Basement section are of interest to this work it is important to locate them relative to the stratigraphic column. Figure 6-81 shows the distribution of the families relative to depth.

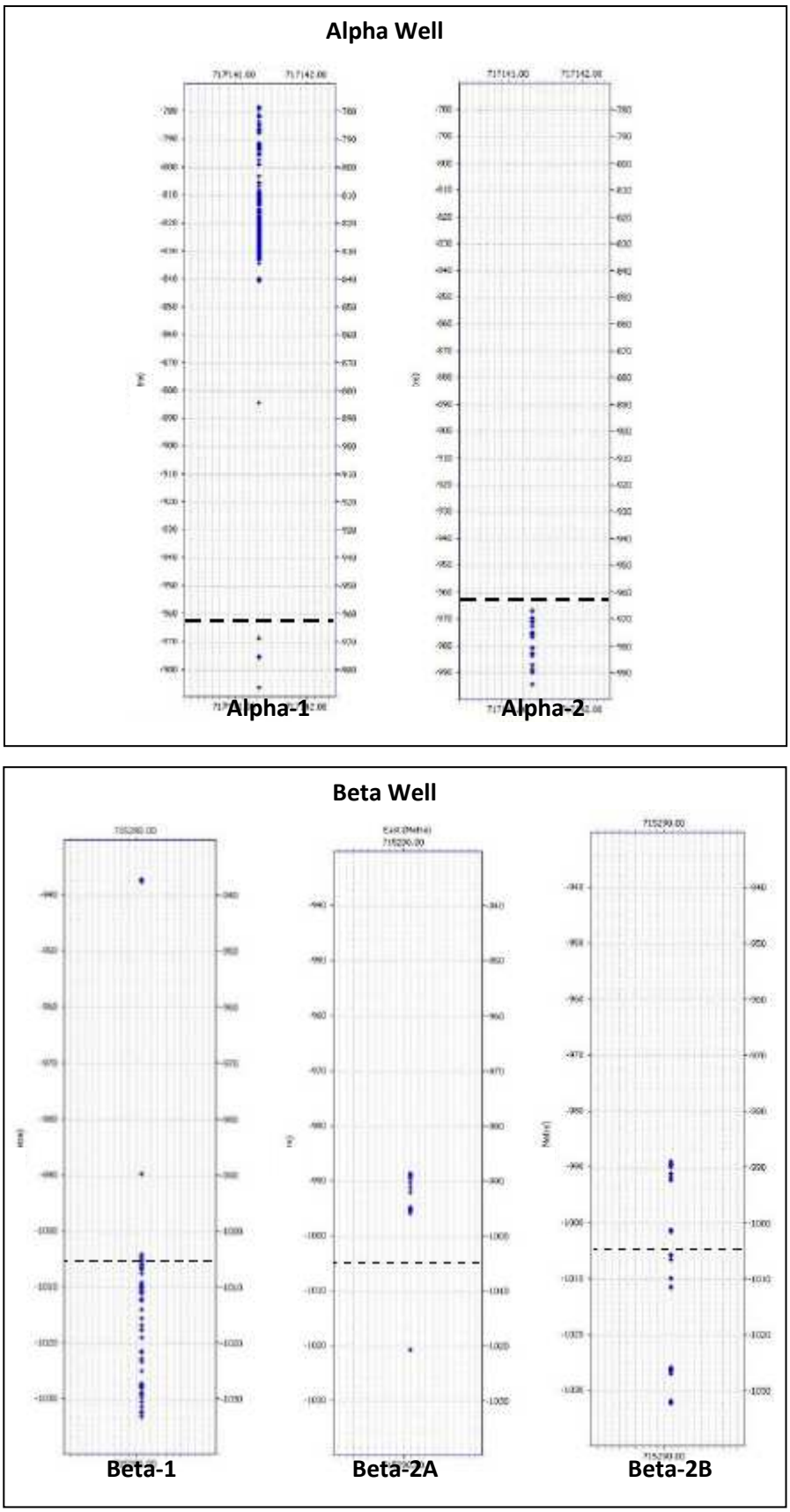

Figure 6-81: Distribution of open fractures measurements in depth by family for Alpha, Beta, Delta, Fox and Golf wells. Black dashed line represents Top of Basement. (Adapted from UNL, UALG, UA, & IST; *Modelling and Characterization of Fractured Reservoirs -GALP E&P Internal Report;* Lisbon; 2011).

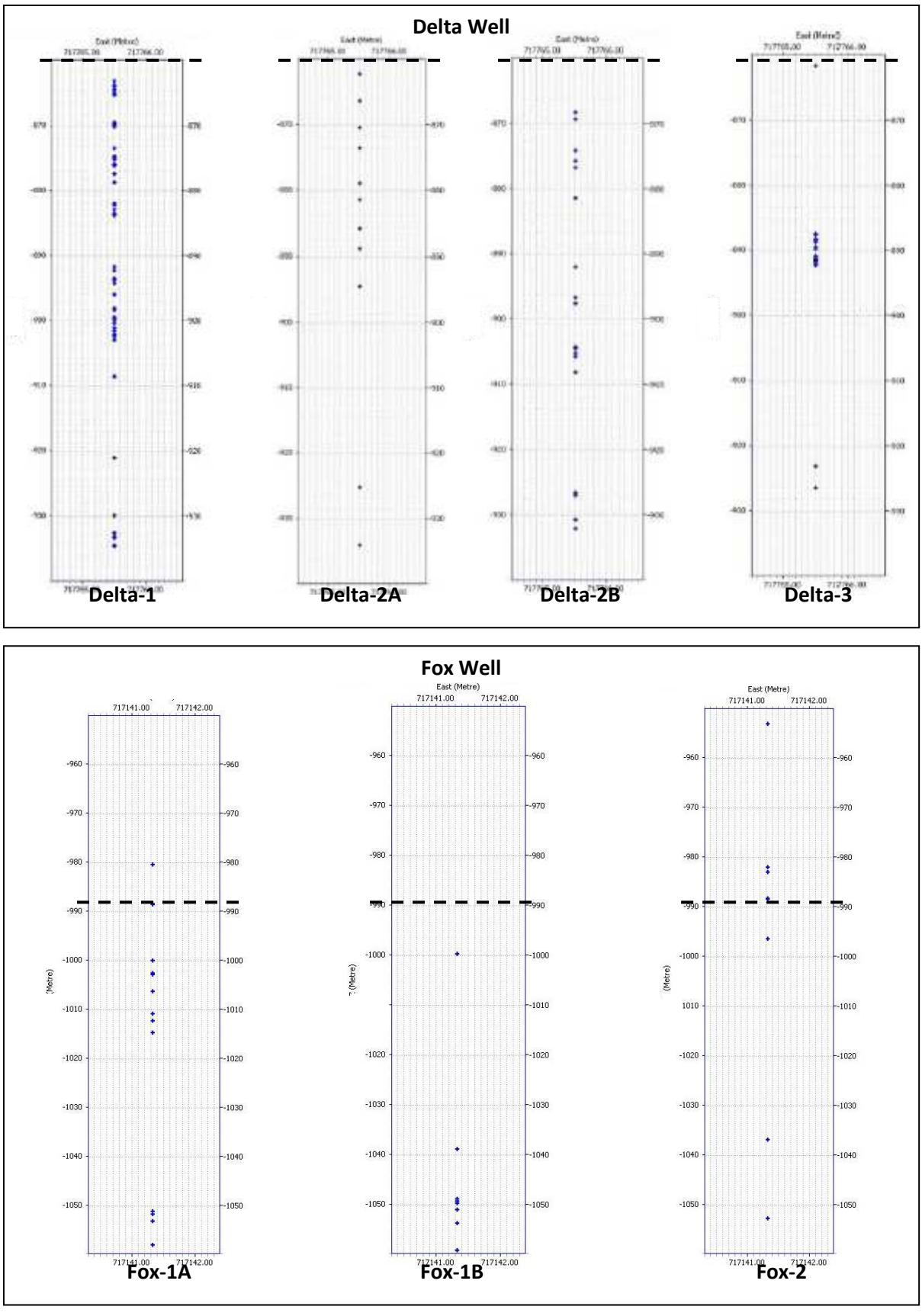

Figure 6-81 (contd): Distribution of open fractures measurements in depth by family for Alpha, Beta, Delta, Fox and Golf wells. Black dashed line represents Top of Basement. (Adapted from UNL, UALG, UA, & IST; *Modelling and Characterization of Fractured Reservoirs -GALP E&P Internal Report;* Lisbon; 2011).

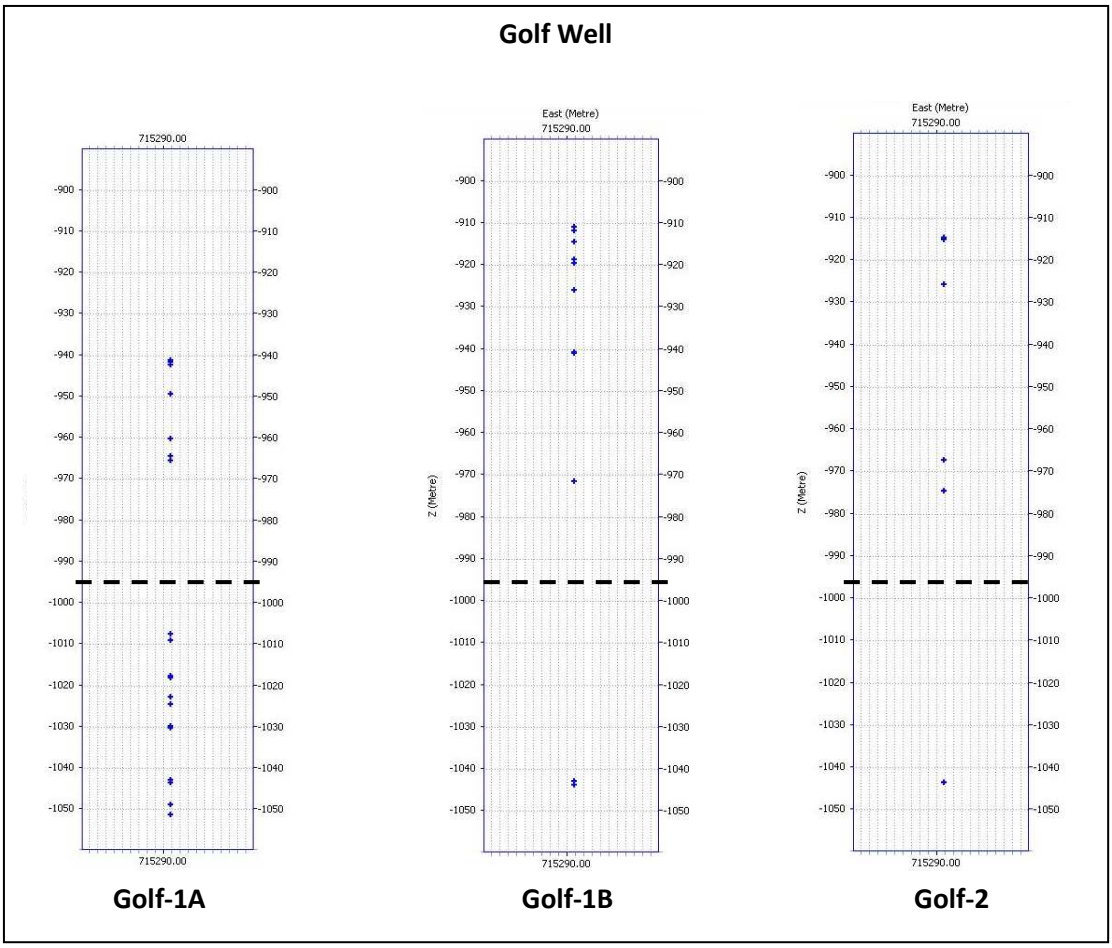

Figure 6-81 (contd): Distribution of open fractures measurements in depth by family for Alpha, Beta, Delta, Fox and Golf wells. Black dashed line represents Top of Basement. (Adapted from UNL, UALG, UA, & IST; *Modelling and Characterization of Fractured Reservoirs -GALP E&P Internal Report;* Lisbon; 2011).

From the analysis of Figure 6-81, it is possible to take the following conclusions:

Alpha: family Alpha-2 is located only in the Basement.

Beta: family Beta-1 is the most expressive in the Basement, but Beta-2B has some measurements in the Basement.

Delta: all measurements were made inside the Basement, but families Delta-1 and Delta-2B are more expressive.

Fox: most measurements were made inside the Basement, but the most expressive family is Fox-1A.

Golf: Golf-1A is the most expressive, being the other two insignificant at Basement depths.

The next step was to harmonise all the measurements so that a general set of fracture families could be considered for the area. This can be done based on the assumption that deformation occurred over the entire area and thus fractures should be present in both blocks even if they are not identified in wells. Table 6-11 shows the final families after the comparison. Figure 6-82 helps comparing the families present in each well.

Table 6-11: Correspondence of fracture families per well. Notice that the final family A is the most predominant fracture family with 104 measurements inside the Basement and present in every well. The general trends were obtained by averaging the strike and dip of the correspondent fracture families. It differs from the general trend calculated by UNL team because this team only used measurements from Alpha, Beta and Delta wells. (Adapted from UNL, UALG, UA, & IST; *Modelling and Characterization of Fractured Reservoirs -GALP E&P Internal Report;* Lisbon; 2011).

Correspondence of Fracture Families Per well					Final	Measurements in Basement	General Trend (GALP)	General Trend (U.N.L)
Alpha	Beta	Delta	Fox	Golf				
Alpha-2	Beta-1	Delta-2A	Fox-1A	Golf-1A	A	104	N22ºW/60ºNE	N30ºW/57ºNE
Alpha-1	Beta-2B	-	-	-	B2	16	N38ºE/63ºNW	N43ºE/79ºNW
-	Beta-2A	-	Fox-2	-	B1	7	N30ºE/42ºSE	N30ºE/35ºSE
-	-	Delta-1	-	-	-	-	-	-
		Delta-2B	Fox-1B	-	D	28	N8ºE/56ºNW	-
-	-	Delta-3	-	Golf-2	E	25	N87ºE/35ºSE	-
-	-	-	-	Golf-1B	-	-	N20ºW/39ºSW	-

(unfold next page)

Figure 6-82: Shmidt Diagrams of the fracture families present in the six wells with the objective of a better comparison between them.

Final Considerations for FMI analysis

From the analysis of Table 5-11 it is obvious that Family A, which strikes at N22^{o}W and dips 60^{o} towards NE (GALP general trends differ from UNL trends because more wells were used for the calculation as Fox and Golf wells haven't been drilled by the Fractured Basement Project was developed), is the most common, being present in every well (see Figure 6-82), with a total of 104 measurements inside the Basement.

Because all the wells were drilled vertically and the fracture planes are not horizontal, all measurements are underestimated. This means that the most accurate measurements are those of fractures which inclination is closer to horizontal (See Section 4), case of family B1 and E. From this comes that, if family A is dipping at 60^{o} and still is the most common, it is probably the predominant fracture direction in the area, and the one that future drilling campaigns should be aiming to intersect.

6.2 FRACTURE SYSTEM ORIGIN

The literature for SEAL Basin structural evolution describes the Basement as part of a complex fold belt, created by the collision of two cratonic masses – Section 1. For this reason, and because there was no data suggesting another origin, this was the premise used for the fracture system origin of the Basement.

In tectonic related systems, fractures are formed by the application of surface forces and form in networks with specific spatial relationships to folds and faults, and generally are widespread across the Basin. In this case, and due to the mapped structures it was decided to study the SEAL Basement fracture system in light of these principles. This means that the location of the study area is not important as wherever it is, the fracture system will be generically be equal. By making this assumption it was possible to use geomechanical modelling to derive fracture density and orientation, as it will be demonstrated in the following section (Universidade do Algarve – UALG work).

6.3 FRACTURE PROPERTIES AFFECTING RESERVOIR PERFORMANCE

The four petrophysical determinations most useful in this evaluation are: fracture permeability; fracture porosity; fluid saturations within the fractures and the recovery factor expected from the fracture system. These properties are directly dependant on three fracture properties:

- fracture morphology,
- fracture spacing,
- fracture width and permeability.

For determining these, core analysis, well tests and image logs are the best methods. As previously stated, cores were not available at the time this study was carried, leaving us with well tests and image logs to try to obtain the properties that affect reservoir performance.

6.3.1 Fracture Morphology

Defining the fracture morphology only from FMI data is a very imprecise task. It is only possible to detect if fractures are open, partially open or healed (amongst other physical characteristics), but not their physical shape. In order learn on the fractures morphology (which can influence the permeability of the reservoir – See Section 4.2.3.1), extracting full diameter cores would have been essential.

6.3.2 Fracture Spacing and Permeability

As evaluation of outcrops and cores (the most reliable source to determine fracture density) was not available, FMI data and faults mapped by seismic interpretation was used in the context of the Fractured Basement Project, (for further reading please refer to: Modelling and characterization of fractured reservoirs, blocks SEAL-T-A and SEAL-T-B Project Report – May 2011).

6.3.2.1 Geomechanical Modelling

Despite being observed in borehole data (FMI Logs), fractures could not be detected in seismic – due to small their small size (which causes them to be sub-seismic), and to the poor seismic quality. For this reason these discontinuities could not be detected in the rock volume between the wells. The aim of the geomechanical modelling was to simulate the density and orientation of the fractures on that space. The following description is based on the final report of the Fractured Basement Project (Modelling and characterization of fractured reservoirs, blocks SEAL-T-A and SEAL-T-B Project Report – May 2011), more specifically on the UALG's team work. Describing and explaining in detail the geomechanical modelling done for the SEAL area is outside the scope of this thesis, for that reason, only the input data and the results will be presented. For more detail please refer to the mentioned work.

Initial Assumptions

In any tectonic setting, the regional stress field is perturbed by local factors, of which mechanical discontinuities such as faults are the most important. The modelling used on this project assumed that the distribution of the small-scale discontinuities (the fractures) was determined by:

a) the superposition the regional tectonic stress

(b) the local perturbation of that stress state resulting from the nearby larger faults

The larger mapped faults (faults interpreted by the U.Aveiro Ant-Tracking Workflow presented in section 6.1.3) were considered pre-existing structures and input for the model, and the predicted fractures were assumed to form later as the result of the interaction between those faults and the regional tectonic field. Coulomb failure criterion (Jaeger and Cook, 1979) was used to estimate the fault strike:

$$\tan 2\theta = \mp\frac{1}{\mu}$$

Where θ is the angle of the failure planes to the maximum principal compressive stress (σ_1), and μ is the coefficient of internal friction. The theory predicts that two conjugate failure planes intersect along the principal intermediate stress σ_2 (Figure 6-83), and the fault orientation is influenced only by μ and the orientation of the principal stresses.

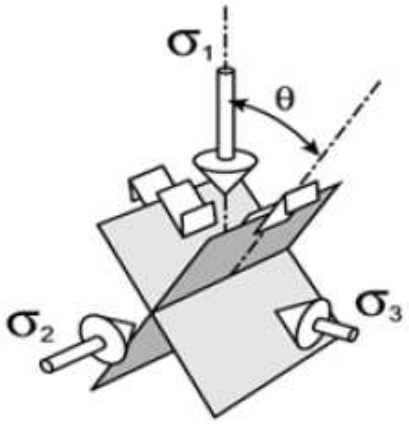

Figure 6-83: According to Anderson's theory of faulting, the principal stresses are vertical and horizontal. The most favourable fault planes intersect along the intermediate principal direction and make an angle with the maximum principal compressive stress and are equally probable (UNL, UALG, UA, & IST; *Modelling and Characterization of Fractured Reservoirs -GALP E&P Internal Report;* Lisbon; 2011).

Assuming that the faulting regime is determined by Anderson's theory of faulting, the optimally oriented conjugate shear fractures are the most likely planes to be formed on the vicinity of faults, and maximum Coulomb shear stress (MCSS) can be used to infer their densit (UALG, 2011):

$$MCSS = \left(\left(\frac{\sigma_1 - \sigma_3}{2}\right)\sqrt{1+\mu^2}\right) - \mu\frac{\sigma_1 + \sigma_3}{2}$$

Where,$\sigma_1 > \sigma_2 > \sigma_3$.

The development of the modelling carried out by UALG involved the following steps:

- Build the 3D model geometry after recognition of the basic structural scenario;
- Specify material properties;
- Impose remote loading and local boundary conditions;

- Run the models to compute the stress and strain fields;
- Apply a failure criteria to compute small-scale fracture density and orientation;
- Perform sensitivity tests to boundary conditions and material parameters.

The grid for the model was formed by quadrilateral elements in the horizontal and 30 elements in vertical direction, 5m thick. Faults interpreted previously (See Section 5.3) were embedded in this grid (Figure 6-84).

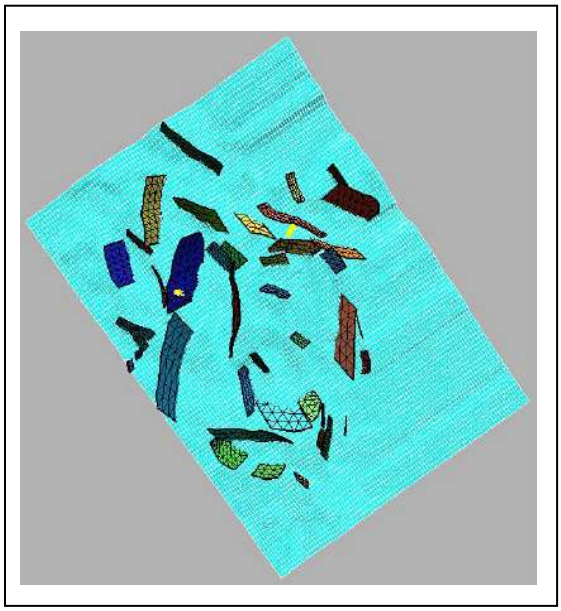

Figure 6-84: (A) Top view of the Block-A block reservoir grid with the faults embedded. At each fault, local boundary conditions are applied. In the absence of known displacements along the faults, the interpreter either considered faults locked or completely free to slip, depending on the tectonic stage considered. (UNL, UALG, UA, & IST; *Modelling and Characterization of Fractured Reservoirs -GALP E&P Internal Report;* Lisbon; 2011).

The linear-elastic behaviour that simulates the reservoir rock is characterized by two constants, the Poisson's ratio,υ, and the Young's modulus, E. The values of these constants are essentially determined by the reservoir lithology at the time of deformation. For the present study it was decided to use E= 28 Gpa and υ = 0.14, values for shale (UALG, 2011)

Because the pore pressure influences the normal components of the stress tensor, the value of the pore pressure (*Pp*) in the reservoir must also be given.

- **Beta Well**: 98.85 kgf/cm^2 at 1000-1052 m depth and 104.0 kgf/cm^2 at 1043-1072 m depth.

- **Alpha Well**: 49.66 kgf/cm^2 at 969-1000 m depth and 96.48 kgf/cm2 at 1000-1030 m depth.

It was decided to use a pore pressure value at 1000 m depth, corresponding approximately to the top of the basement in the SEAL-T-A Block, equal to 100 kgf/cm^2. Hence, Pp for the Basement =10 MPa, which is equivalent to consider hydrostatic pore pressure conditions; that is, a pore pressure gradient of 10 MPa/km.

As the remote loading (the regional stress regimes) responsible for some large-scale faults seen in the seismic, was not enough to predict the small-scale discontinuities that were registered by the FMI logs, it was decided to adapt it. The result is listed in Table 6-12.

Table 6-12: Remote stress loading in the final set of models. (UNL, UALG, UA, & IST; *Modelling and Characterization of Fractured Reservoirs -GALP E&P Internal Report;* Lisbon; 2011).

Model	Fractures in the FMI logs	Stress regime	Maximum extension
I	N30W - normal discontinuities	Normal ($\sigma_1 = \sigma_V - P_p$)	N60E
II	N40E - normal discontinuities	Normal ($\sigma_1 = \sigma_V - P_p$)	N50W
III	E-W and N30W - transfer	Strike-slip ($\sigma_1 = \sigma_H - P_p$)	N30E

Combining the Mohr-Coulomb Theory, with the Anderson's principles and the frictional fault theory, the computed stresses were as listed in Table 6-13:

Table 6-13: values of the input stress tensors for the SEAL geomechanical model. Where: σv = vertical stress; σh= minimum horizontal stress; σH= maximum horizontal stress. These were calculated using Pp= 10 MPa, and an average density of overburden= 2300 kg/m^3. (Adapted from UNL, UALG, UA, & IST; *Modelling and Characterization of Fractured Reservoirs -GALP E&P Internal Report;* Lisbon; 2011).

Normal Regime	
Stress Tensor	Value (Mpa)
σv	23
σh	14,2
σH	18,6
σH-σh	4,4

Strike-Slip Regime	
Stress Tensor	Value (Mpa)
σv	23
σh	15,2
σH	26
σH-σh	10,8

The effect of modelling two cycles of extension (1) E-W with N-S faults active; 2) NW-SE with N-S faults locked and remaining active) was tested, and it was concluded that modelling the second stage only with all faults simultaneously active would essentially produce the superposition of the predicted fault planes in the two stages. For this reason this last option was used.

Results:

As the Mohr-Coulomb criterion predicts that the two conjugate shear discontinuities are in theory equally probable (Figure 6-83), for each tectonic scenario and at each grid observation point two conjugate predicted fractures were outputted. Hence, the outputs were the MCSS (Mohr-Coulomb Shear Stress) values and the predicted conjugated fractures shear strikes and dips at each point of the reservoir grid, for each tectonic loading listed in Table 6-13. This information was used in the UNL Discrete Fracture Network (DFN) model. Table 6-14 shows the composite geomechanical scenarios (GMS1 and GMS2) from the combination of the three geomechanical models / stress regimes (I, II and III see table 6-13).

Table 6-14: Proposal for two composite geomechanical scenarios (GMS1 and GMS2) from combination of the three geomechanical models / stress regimes (I, II and III see table 6-13). (Adapted from UNL, UALG, UA, & IST; *Modelling and Characterization of Fractured Reservoirs -GALP E&P Internal Report;* Lisbon; 2011).

Blocks	Scenarios	Stress regime (Table 6.12)	Generated fracture families (conjugated pair)	FMI / Faults Predicted	Figure
A	GMS1	Normal (I)	A1 and A2	N30W discontinuities	6-87 (A)
		Normal (II)	B1 and B2	N40E discontinuities	6-87 (B)
	GMS2	Strike-slip (III)	A1 and A2	E-W and N30W discontinuities	6-87 (C)
		Normal (II)	B1 and B2	N40E discontinuities	6-88 (A)
B	GMS1	Normal (I)	A1 and A2	N30W discontinuities	6-88(A)
		Normal (II)	B1 and B2	N40E discontinuities	6-88(B)
	GMS2	Strike-slip (III)	A1 and A2	E-W and N30W discontinuities	6-88 (C)
		Normal (II)	B1 and B2	N40E discontinuities	6-88 (C)

The analysis of the MCSS distribution in Figures 6-85 and 6-86 shows that the largest predicted fracture densities occur near the faults. The UALG team explains this by theoretical models of faulting but these theoretical predictions can also be proven by real examples. One example is the Natih Field, Oman where the chalky limestones are heavily fractured. The use of high-quality 3D data sets, allowed the detection of flexures and faults with throws as small as 3m. Overlaying the fracture orientation data from core and FMI on a seismic dip map (Figure 6-87a) allowed establishing a relation between fractures and faults. By doing this the operator was able to revise the well-targeting strategy and placed wells near small faults and flexures. These wells had an average improvement of 30% in gross productivity, indicating that these wells are intersecting more open fractures than before (Figure 6-87 b) (Whyte, S.; unknown date).

The same association between fracturing and faulting was observed in FMI images from horizontal wells in Idd El Shargi Field, offshore Qatar. Here, combining borehole images with the relatively poor 3D seismic allowed to plan horizontal wells, resulting in immediate results with the

first and second horizontal wells producing ten times more than the earlier vertical wells (Figure 6-88) (Cosgrove, P and Jubralla, A.F.; unknown date).

The geomechanical models together with the proven field situations where higher open fracture densities occur near the fault, is a very strong argument that should be taken into account when planning a well in SEAL, i.e. a future well should be planned so that it is drilled near a fault rather than between two faults, for example.

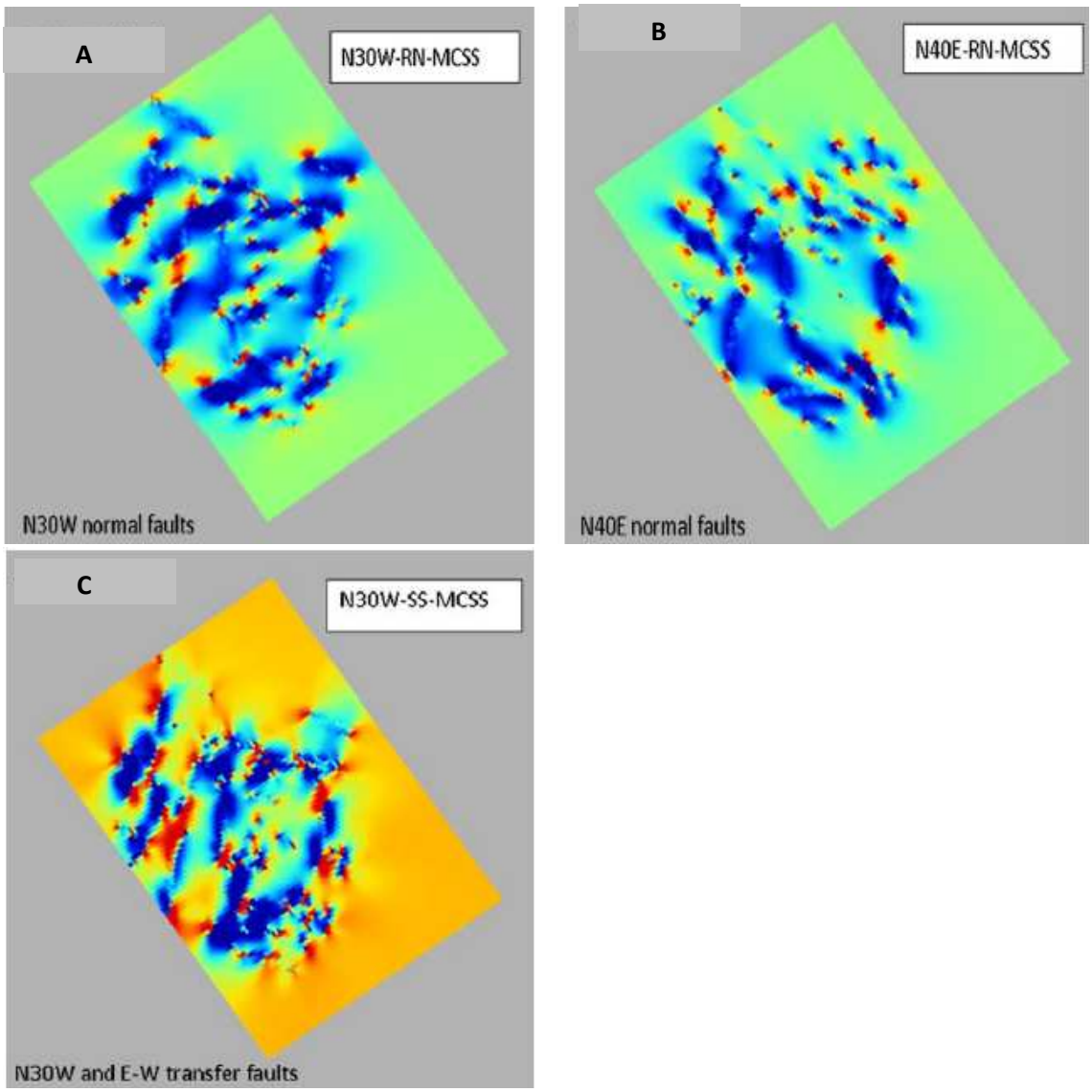

Figure 6-85: Predicted small-scale discontinuities density distribution in the Block-A for: (A) N30W and (B) N40E normal faulting regimes. Cold coloured (blue, green) zones represent regions of low discontinuities density and hot coloured (yellow to red) zones regions of enhanced discontinuities density. Low densities occur along and sideways of large faults and high densities at their tips. The linkage of large-scale faults by small scale fracturing is favoured at particular locations, which depend on the faulting regime. (C) Predicted discontinuities density distribution in the Block-A for the N30W/E-W strike-slip faulting regime. The predicted density of small-scale transfer faults is much higher than the predicted density of small-scale normal faults (in figure 5.8). The clusters of predicted transfer faults are also more widely distributed in these regimes. The dominant trends of the most intense fault clustering (red regions) follow approximately the N10° and N120° azimuths. (UNL, UALG, UA, & IST; *Modelling and Characterization of Fractured Reservoirs -GALP E&P Internal Report;* Lisbon; 2011).

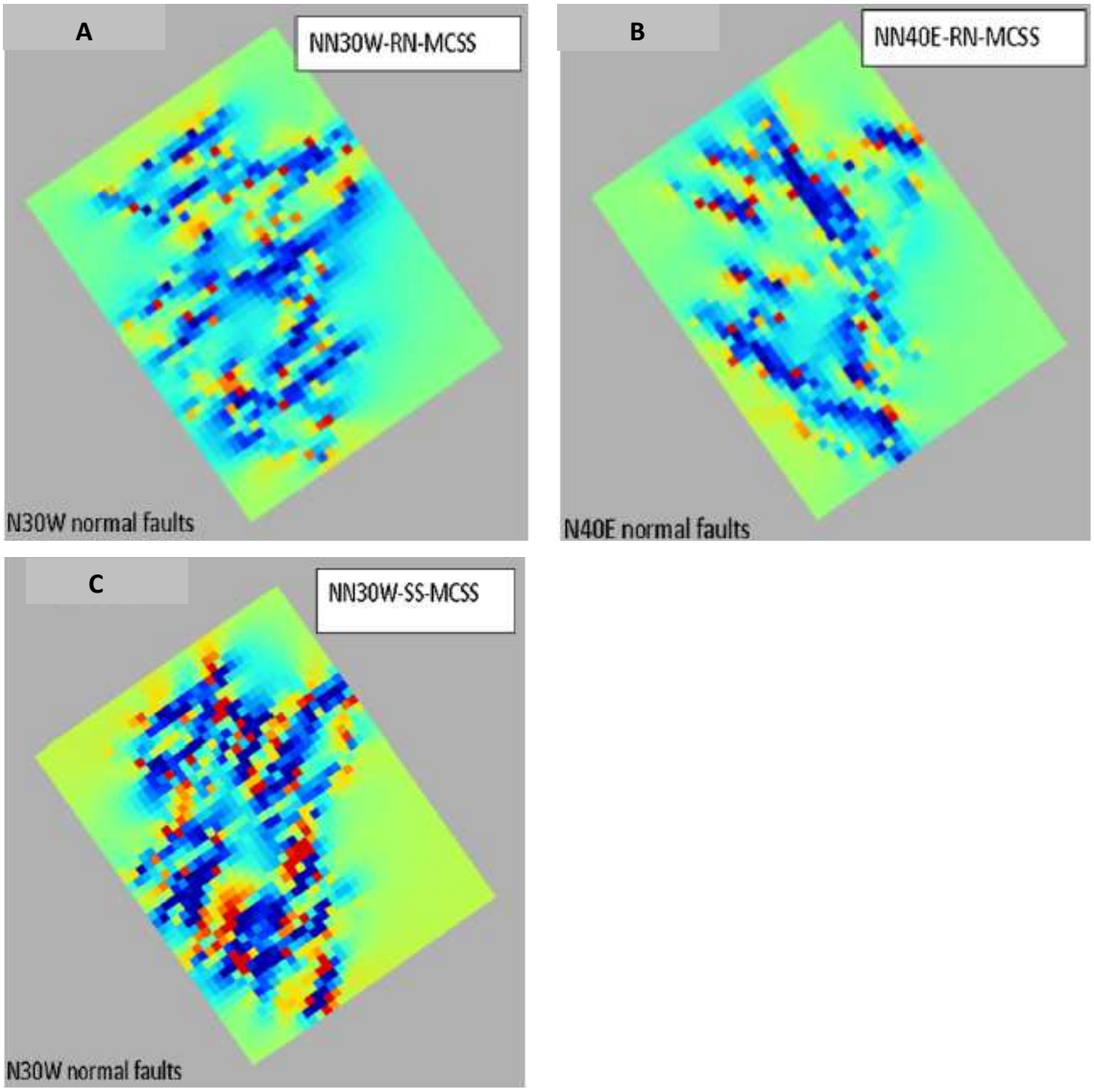

Figure 6-86: Predicted small-scale discontinuities density distribution in the Block-B for: (A) N30W and (B) N40E normal faulting regimes. Poor image resolution due to the limited number of grid elements makes the interpretation of the modelling results difficult in this case. The main trends of small-scale normal fault predictions are nonetheless similar to the ones in SEAL-T-A block. (C) Predicted discontinuities density distribution in the for the E-W/N30W strike-slip faulting regime. As in the SEAL-T-B block the predicted density of small scale transfer faults is higher than the predicted density of small scale normal faults (in figure 5.10). Again, the clusters of predicted transfer faults are also more widely distributed. (UNL, UALG, UA, & IST; *Modelling and Characterization of Fractured Reservoirs -GALP E&P Internal Report;* Lisbon; 2011).

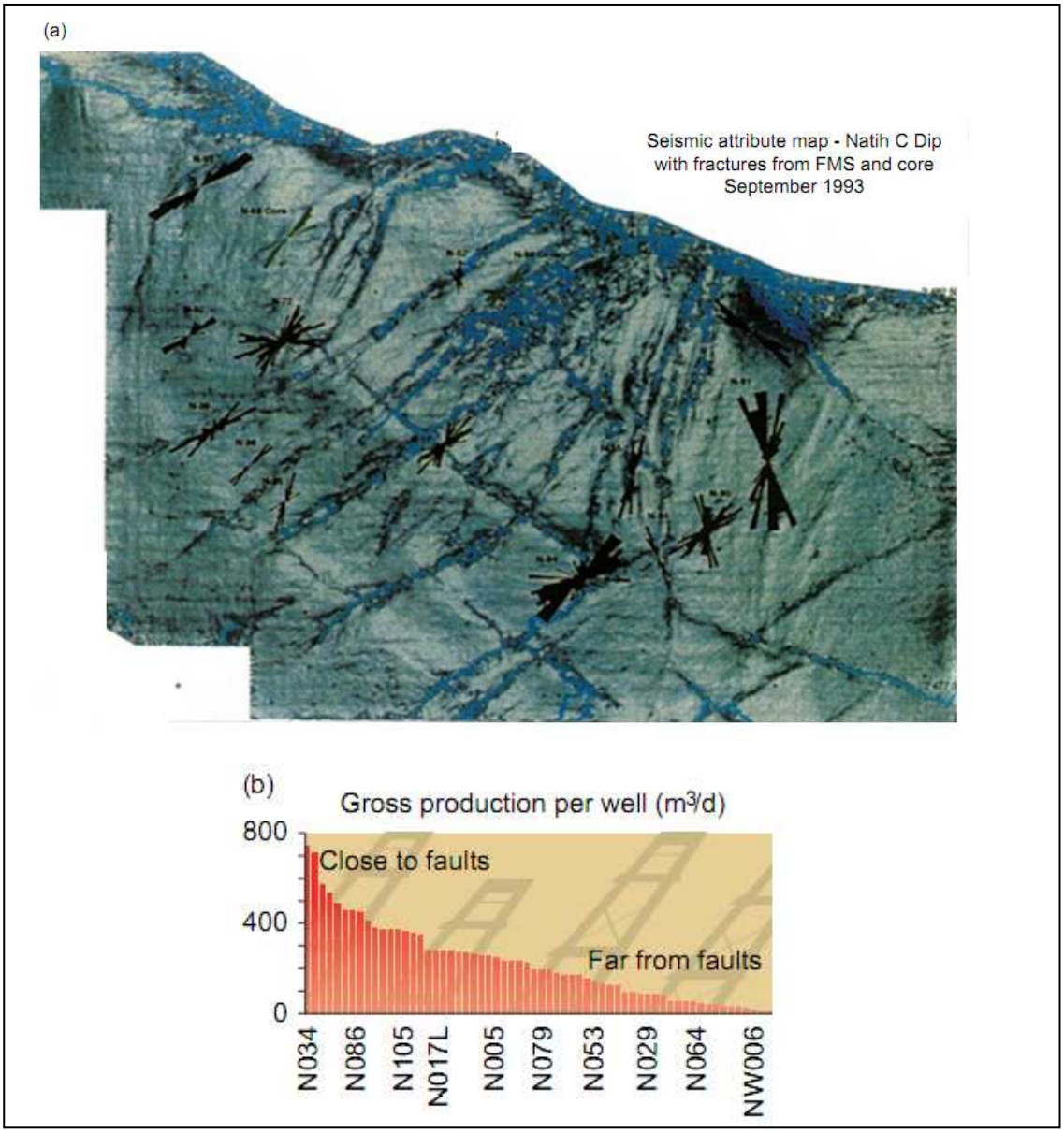

Figure 6-87: (a) Natih field 3D seismic revealing faults coupled with borehole data to reveal fracture orientation. (b) Gross production per well was found to closely correlate with proximity to faults defined by the seismic (www.slb.com – Horizontal Highlights based on an article from Whyte, S.; unknown date).

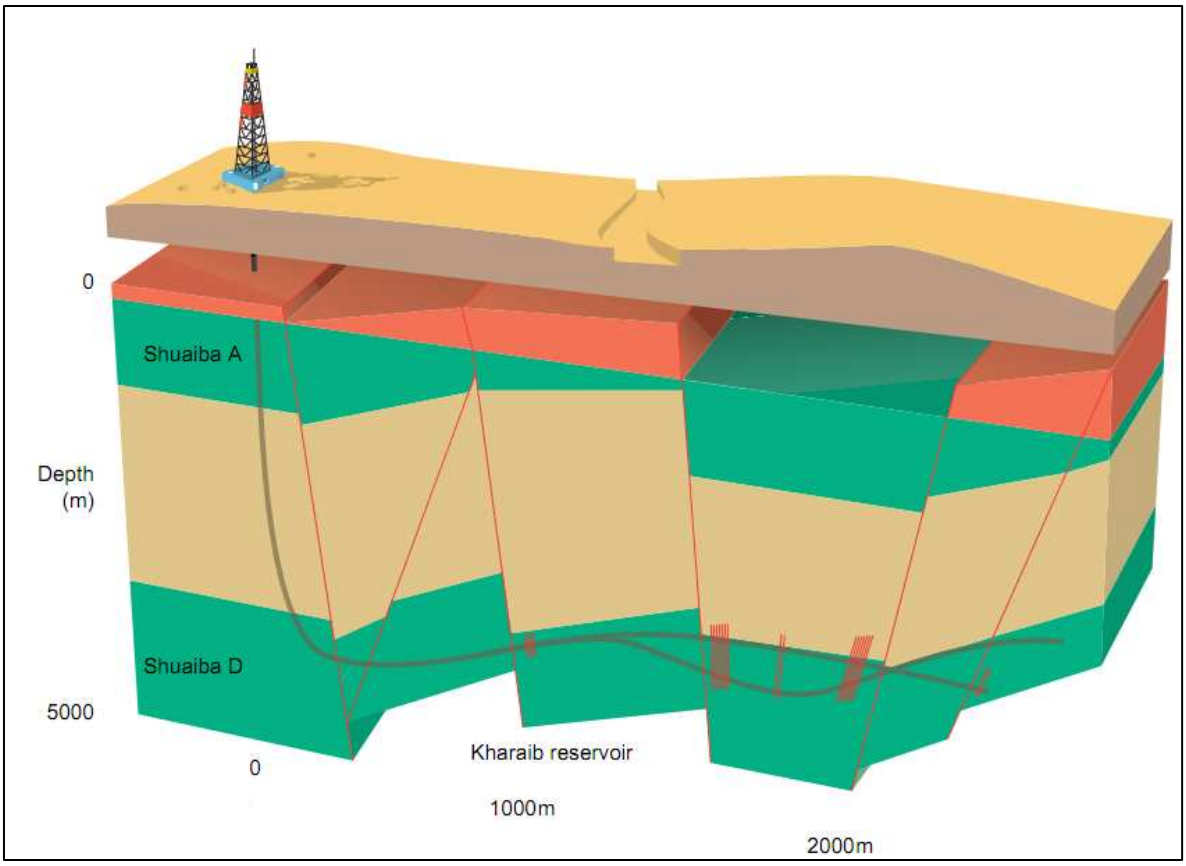

Figure 6-88: Idd El Shargi Field, offshore Qatar. The directional well allowed the operator to drill trough the reservoir layer despite the heavily faulted blocks found, and establish a relation between the faults and the fractures by using borehole images (www.slb.com – Horizontal Highlights, from an article of Cosgrove, P and Jubralla, A.F.; unknown date).

6.6.2.2 Discrete Fracture Network Modelling (DFN) and Permeability Simulation

Fracture width or aperture measurements can be taken from the FMI logs in the absence of cores. In Table 6-10 values for fracture aperture were presented, which are relative to the aperture interval found in each well. As already stated, the objective of this thesis is to provide a future drilling location (positioning and orientation), which depends on the evaluation of the properties of each of the fracture families found. Hence, values of Table 6-10 are not useful because with them it is not possible to accurately determine the aperture of Family A, for example.

To try to solve this problem DFN models and Permeability Simulation (PS) based on them can be used. Again, the Fracture Basement Project was crucial. Below this methodology – developed by Universidade Nova de Lisboa (UNL) - and results are presented. For further reading please refer

to: Modelling and characterization of fractured reservoirs, blocks SEAL-T-A and SEAL-T-B Project Report – May 2011.

In this phase of the project, equivalent permeability histograms of each FMI fracture family were generated by UNL, using both data from the FMI statistical analysis and from the geomechanical modelling. This was done in two steps:

I) Characterize the relationship between fracture number (N), fracture area (P32) and linear fracture density (LFD index) per fracture family.

II) Generation of histograms of equivalent permeability using the Oda method, conditioned to the LFD index, fracture family and reservoir block.

"To simulate 3D fracture networks that allow the calculation of histograms of permeability it is necessary to characterize the relationship between the LFD (measured at wells with FMI data, Section 6.4.2), number of fractures (*N*) and fracture areas (*P32*) per fracture family. This means, for a specific 3D reservoir block, estimate the number of fractures by family and correspondent distribution of areas (*P32*) that match a specific LFD at vertical direction, the same direction evaluated by FMI." - Modelling and characterization of fractured reservoirs, blocks SEAL-T-A and SEAL-T-B Project Report – May 2011.

The problem that the UNL team faced to achieve this was that fracture orientation is not constant, which mean s that the relationship between LFD, fracture number (*N*) and area (*P32*) is unknown. To solve this problem, an inverse approach was used through the application of the FTRIAN software created by UNL, an algorithm of fracture simulation that allows the generation of equally probable fracture network scenarios within a volume constraint by a LFD index (Almeida, Barbosa, 2008) (Figure 6-89). Fracture networks are simulated using a polygonal approximation. In the present case squares were used, but triangles can also be used (Figure 6-90): the software first generates random locations with Monte Carlo (each random location is the geometric centre of a fracture), and then for each creates a vector allowing the positioning of the first square vertex; successive rotations of the vector (four rotations of 90º) generates a square. After each cycle, the model is then sampled with scan-lines (simulating a well). In the present study, it was considered enough generating three realizations for each evaluation and sampling the model with 1000 vertical scan-lines. After several iterations, look up tables relating N, P32 and LFD can be built.

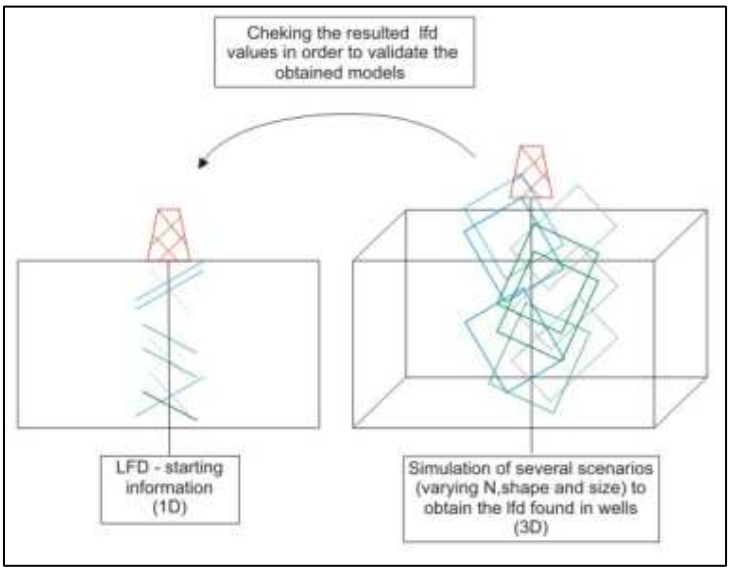

Figure 6-89: Inverse model approach to relate N, P32 and LFD. (UNL, UALG, UA, & IST; *Modelling and Characterization of Fractured Reservoirs -GALP E&P Internal Report;* Lisbon; 2011).

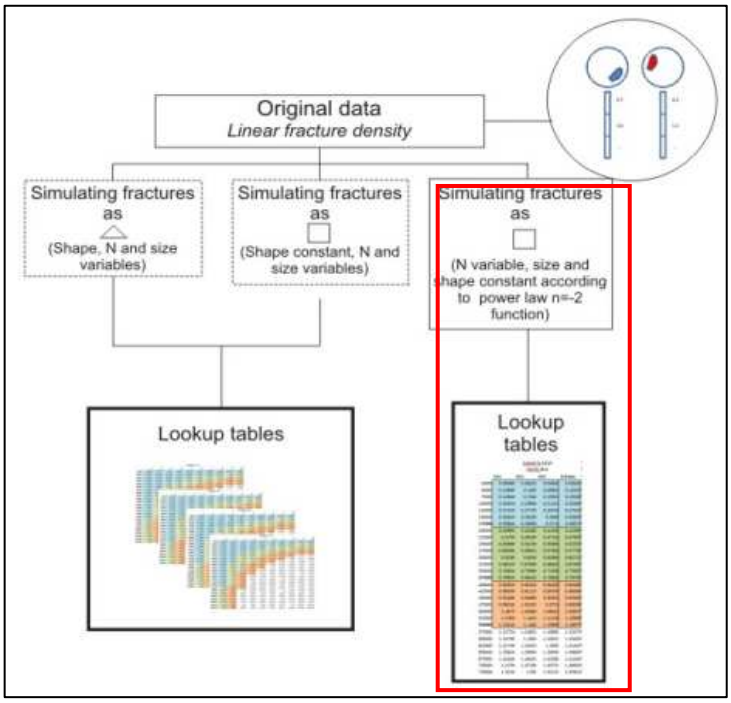

Figure 6-90: – Synthesis of compared fracture shape variants results: i) fractures are approximated as a mesh of triangles; ii) fractures are approximated as equal size squares; iii) fractures are approximated by squares whose areas follow a power model distribution function of lateral sizes. (UNL, UALG, UA, & IST; *Modelling and Characterization of Fractured Reservoirs -GALP E&P Internal Report;* Lisbon; 2011).

For the present case, it was considered that simulating fractures as squares whose areas follow a power model distribution function of lateral sizes was the most adequate methodology, as it is geologically more realistic and at the same time runs efficiently allowing equivalent permeability calculation using expedite methods, such as the proposed by Oda, 1985[(1)]. In this model (called variant iii) in Figure 6-90), square areas range from 0.09 m^2 (0.3 m side, assumed to be the minimum detection of the FMI data) to 25 m^2 (5m side, assumed to be the maximum size of the

small-scale fractures). As the fracture areas follow a predefined distribution law, lookup tables will show LFD values conditioned only to the number of fractures (N).

(1) According to Oda, if fractures areas (Ak) and transmissivities Tk are known within a specific volume, it is possible to calculate an empirical fracture tensor summing the contributions of all fractures:

$$F_{ij} = 1/v \sum_{k=1}^{N} f_k A_k T_k n_{ij} n_{jk}$$

Where:

F_{ij}	=	Fracture tensor
v	=	Block volume
N	=	Number of fractures within block
f_k	=	Percolation factor of the fracture (usually assumed as 1)
A_k	=	Fracture area
T_k	=	Fractures transmissitivity
$n_{ij}\, n_{jk}$	=	Normal components to fractures

The permeability tensor derives from the fracture tensor F_{ij} with the assumption that F_{ij} represents the flow along the fracture. In addition, fractures are impermeable at the perpendicular, thus F_{ij} must be rotated to the fracture planes:

$$k_{ij} = 1/12 \, (F_{ij}\, \delta_{ij} - F_{ij})$$

Where:

K_{ij}	=	Permeability tensor
F_{ij}	=	Fracture tensor
δ_{ij}	=	Kroenecker Delta

Results

As it was referred above, the simulation is constrained by the Linear Fracture Density observed in the wells, using the FMI data. At the same time, and because the final objective is to provide a well orientation, it only makes sense to generate permeability histograms of fractures that are found in the wells even when in geomechanical modelling, other families are predicted. Hence, three permeability curves were generated for FMI fracture families A, B1 and B2 conditioned to

the LFD calculated from FMI data and to orientation statistics from correspondent geomechanical grid models (Table 6-15).

It is important to note that in the geomechanical modelling two grids (one for Block A and other for Block B) were used to simulate fracture density but the applied stress regimes were the same (GMS1 and GMS2). This way, it is possible to use the same LFD index for both blocks and generate orientation classes (strike and dip) for each family according to the geomechanical scenarios (Tables 6-16 and 6-17). From the geomechanical modelling, it can be observed that families GB1 and GB2, are generated only through one stress regime (normal). For that reason, histograms can be generated for GMS1 and GMS2 together.

Table 6-15 lists the families of fractures from both the geomechanical modelling and FMI data with minimum and maximum observed LFD. Tables 6-16 and 6-17 present two examples of frequency of azimuth and dip angle histograms for family A (A2 in GMS1) for Block-A and Block-B calculated from the geomechanical grid values.

Table 6-15: correspondence between the geomechanical generated families and the families found in the well data, with the LFD index for each. In green are the families for which the permeability curves were generated. (Adapted from: UNL, UALG, UA, & IST; *Modelling and Characterization of Fractured Reservoirs - GALP E&P Internal Report;* Lisbon; 2011).

Geomechanical Scenarios	Stress regime	Geomechanical generated families (conjugate pairs)	Correspondence with FMI data	LFD index found in wells [min; max]
GMS1	Normal (I)	A1	No correspondence	
		A2	A	[0; 2.6]
	Normal (II)	B1	B1	[0; 1.6]
		B2	B2	[0; 1.0]
GMS2	Strike-slip (III)	C1	No correspondence	
		C2	No correspondence	
	Normal (II)	B1	B1	[0; 1.6]
		B2	B2	[0; 1.0]

Table 6-16: table of frequencies of strike and dip for fracture family A (A2 in GMS1) in Block-A. (Adapted from: UNL, UALG, UA, & IST; *Modelling and Characterization of Fractured Reservoirs -GALP E&P Internal Report;* Lisbon; 2011).

Strike				Dip			
Azimuth Classes	Frequency			Dip Angle Classes	Frequency		
	Absolute	Relative	Cumulative		Absolute	Relative	Cumulative
[0.01;32.73[	1269	0.005	0.005	**[2.04;46.01[**	2059	0.008	0.008
[32.73;65.46[	230221	0.860	0.865	**[46.01;60.67[**	215817	0.806	0.814
[65.46;98.19[	32944	0.123	0.988	**[60.67;75.33[**	47878	0.179	0.993
[98.19;360]	3286	0.012	1.000	**[75.33;89.99]**	1966	0.007	1.000
Sum	267720	1.000		**Sum**	267720	1.000	

Table 6-17: table of frequencies of strike and dip for fracture family A (A2 in GMS1) in Block-B. (Adapted from: UNL, UALG, UA, & IST; Modelling and Characterization of Fractured Reservoirs -GALP E&P Internal Report; Lisbon; 2011).

Strike				Dip			
Azimuth Classes	Frequency			Dip Angle Classes	Frequency		
	Absolute	Relative	Cumulative		Absolute	Relative	Cumulative
[-90.1;30[	723	0.016	0.016	**[2.59;53.41[**	638	0.015	0.015
[30;49.98[	2869	0.065	0.082	**[53.41;60.67[**	34660	0.790	0.805
[49.98;69.97[	38358	0.875	0.956	**[60.67;67.93]**	8051	0.184	0.988
[69.97;90]	1910	0.044	1.000	**[67.96;90]**	511	0.012	1.000
Sum	43860	1.000		**Sum**	43860	1.000	

Notice that the frequency of strike and dip values is different between the two blocks, meaning that when using the same stress regimes, the biggest influence on the way fractures are distributed is the grid over which the simulation is made. This is the same as saying that over the same stress regime, fracture orientation is conditioned by the shape of the rock volume and the faults embedded in it - in each Block the interpreted basement horizon and faults, that were used to generate the grids is different which means that when applying the same MCSS to both grids (which are geometrically different) the final result will be different.

Tablesx 6-18 and 6-19, show the LFD results of three realisations and the resultant average value, for the model using the FTRIAN algorithm described before (fractures are approximated by squares and areas follow a power model distribution function of lateral sizes), within a 100 x 100 x 5m reference grid, for the three fracture families and for both blocks. As an example, Table 6-18 can be read in the following way:

- It is necessary to generate approximately 175000 fractures of family A (A2 in GMS1) to reach a LFD index of 2.6 (maximum observed).
- It is necessary to generate approximately 97500 fractures of family B1 to reach a LFD index of 1.6 (maximum observed)
- It is necessary to generate approximately 62500 fractures of family B2 to reach a LFD index of 1.0 (maximum observed)

Table 6-18: LFD results from FTRIAN algorithm, for the several fracture families found in the FMI's in Block-A, simulated on a 100 x100x5 m grid. (Adapted from: UNL, UALG, UA, & IST; *Modelling and Characterization of Fractured Reservoirs -GALP E&P Internal Report;* Lisbon; 2011).

(unfold next page)

Table 6-19: LFD results from FTRIAN algorithm, for the several fracture families found in the FMI's in Block-B, simulated on a 100 x100x5 m grid. (Adapted from: UNL, UALG, UA, & IST; *Modelling and Characterization of Fractured Reservoirs -GALP E&P Internal Report;* Lisbon; 2011).

(unfold next page)

From here the relationship between LFD index and number of fractures by reference block of 100m x 100m x 5m and by cubic meter could be found. Table 6-20 presents the results. Notice that A, is the fracture family which presents a higher density value, which had already been observed when using the FMI counting only (Table 6-11).

The similarity in density values for both Blocks is due to the fact that LFD max used is the same. Again the small difference in the values is due to the differences in the grid shape and consequent simulated fractures strike and dip.

Table 6-20: LFD values for Block-A and Block-B, per fracture family. In yellow are highlighted the LFD classes that contain the maximum LFD value observed in the wells. Notice that A, is the fracture family which presents a higher density value, which had already been observed when using the FMI counting only (Table 6-11). (Adapted from: UNL, UALG, UA, & IST; *Modelling and Characterization of Fractured Reservoirs -GALP E&P Internal Report;* Lisbon; 2011).

Block-A				
Fracture Family	**LFD classes**		**Number of fractures for a grid block (100x100x5m) at maximum of the class**	**Number of fractures by m^3**
A	Low	[0.0; 0.867[	59456	1.189
	Intermediate	[0.867; 1.734[	118022	2.360
	High	[1.734; 2.60]	176685	3.534
B1	Low	[0.0; 0.53[	31876	0.638
	Intermediate	[0.53; 1.06 [	64016	1.280
	High	[1.06; 1.60]	97932	1.959
B2	Low	[0.0; 0.335[	21239	0.425
	Intermediate	[0.335; 0.67[	42698	0.854
	High	[0.67; 1.00]	62547	1.251

Block-B				
Fracture Family	**LFD classes**		**Number of fractures for a grid block (100x100x5m) at maximum of the class**	**Number of fractures by m^3**
A	Low	[0.0; 0.867[	60427	1.208
	Intermediate	[0.867; 1.734[	122775	2.455
	High	[1.734; 2.60]	182885	3.657
B1	Low	[0.0; 0.53[	31433	0.629
	Intermediate	[0.53; 1.06 [	62972	1.259
	High	[1.06; 1.60]	95485	1.910
B2	Low	[0.0; 0.335[	19403	0.388
	Intermediate	[0.335; 0.67[	38678	0.774
	High	[0.67; 1.00]	58327	1.167

Using the values from Table 6-20 it was possible to estimate permeability for each of the fracture families using the Oda method (see page 194). Here, fractures are simulated considering the average strike azimuth at 0^o and average dip at 90^o, which causes the calculated permeability tensor to have two major components of permeability which are close to equality (Kx and Kz), and a component close to zero (Ky) – See Section 4.2.3.1. At the same, time fracture aperture, which largely influences fracture permeability, was set to 1mm. This way, it was possible to compare all the fracture families, which would not be possible if the orientation and aperture effects were taken into account. Figure 6-91 shows the Maximum equivalent permeability graphics for each of the fracture families for Block-A and Block-B. The graphics were obtained by plotting the values of permeability obtained for a 5x5x5m dimension cell.

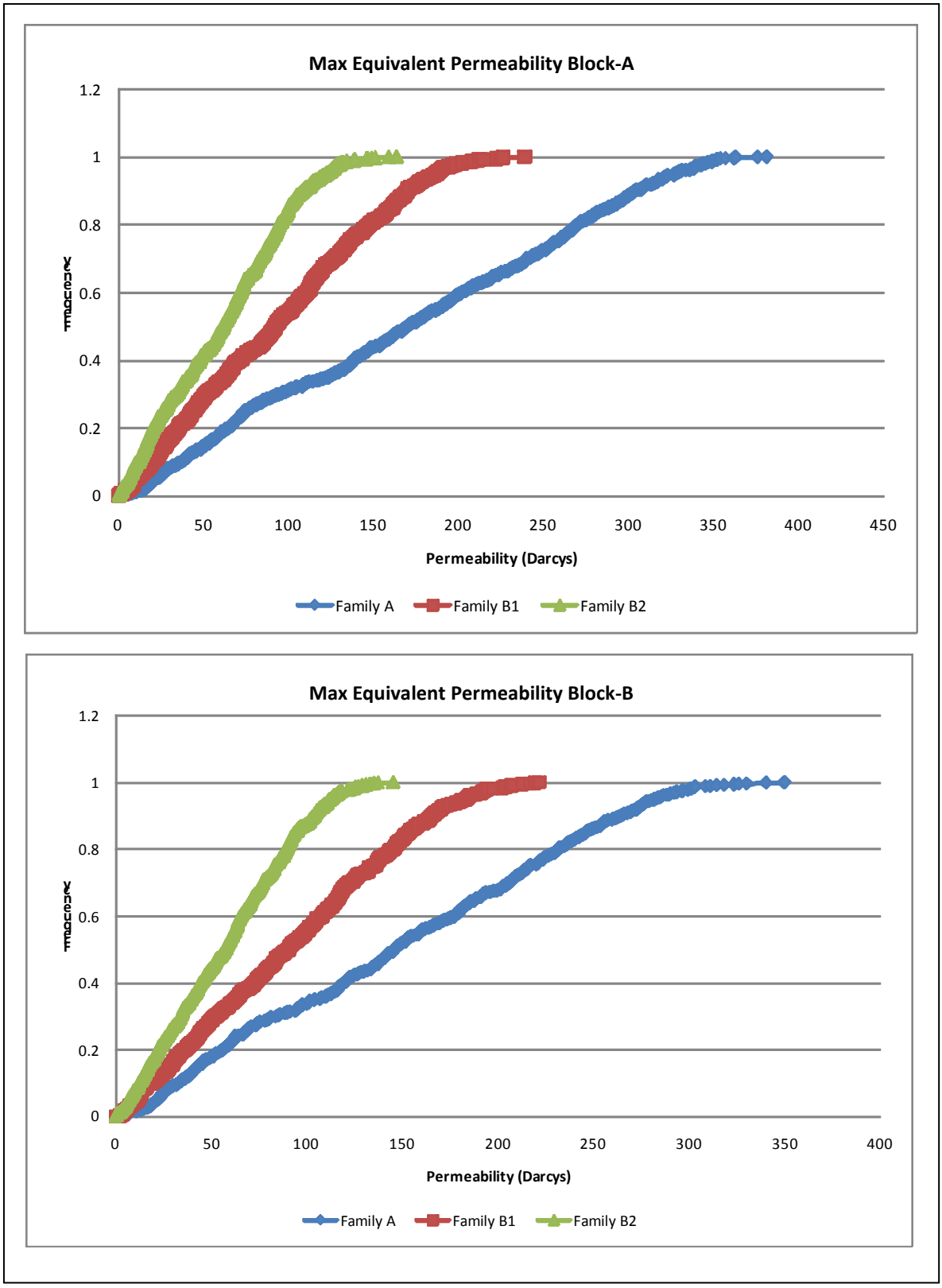

Figure 6-91: Cumulative curves for equivalent permeability (principal permeability component and parallel to fractures) for each of the fracture families A, B1 and B2. Notice that Family A is in both blocks the one which presents the best permeability values. (UNL, UALG, UA, & IST; *Modelling and Characterization of Fractured Reservoirs -GALP E&P Internal Report;* Lisbon; 2011).

Porosity is calculated by the ratio between the volume of fractures and the volume of each cell (which is 5x5x5m). The volume of fractures is calculated through fracture area x aperture. Graphics of Figure 6-92 are obtained by plotting the porosity values obtained per cell.

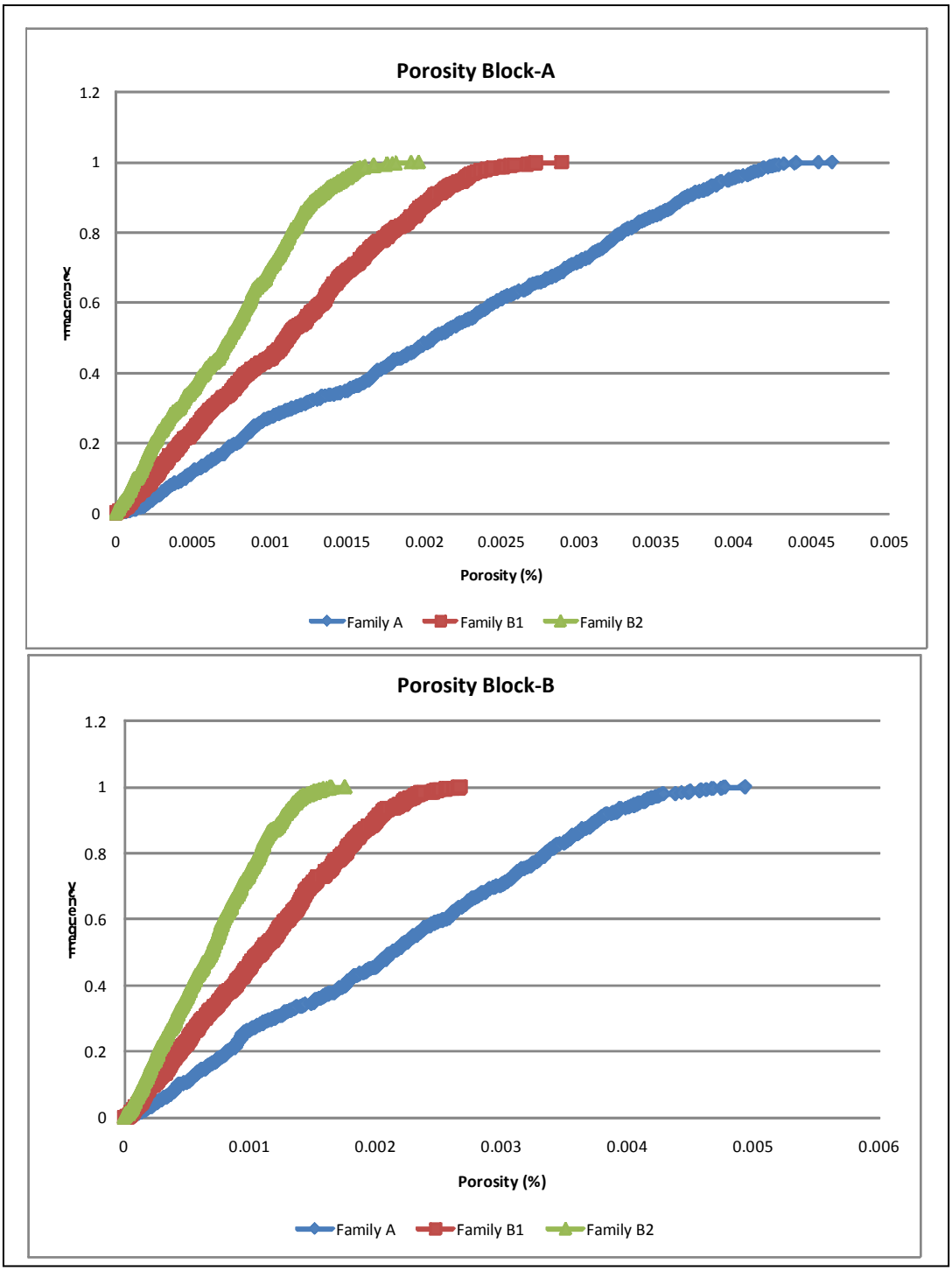

Figure 6-92: Cumulative curves for porosity for each of the fracture families A, B1 and B2. Notice that Family A is in both blocks the one which presents the best porosity values (UNL, UALG, UA, & IST; *Modelling and Characterization of Fractured Reservoirs -GALP E&P Internal Report;* Lisbon; 2011).

Table 6-21 sums the results of the modelling by showing the maximum and minimum permeability and porosity values, as well as the average for each fracture family and exploration block. Again it is easy to conclude that Family A is the one which presents the highest values of both permeability and porosity. This result is not surprising as this family is the most expressive in terms of density. As the models assumed aperture values of 1mm for every family, then it is mainly density which is conditioning the final results.

Table 6-21: Average permeability and porosity values by LFD class, fracture family and exploration Block. (Adapted from: UNL, UALG, UA, & IST; *Modelling and Characterization of Fractured Reservoirs -GALP E&P Internal Report;* Lisbon; 2011).

Block	Fracture family	Permeability (Darcys)		Porosity (%)	
		Interval	Average	Interval	Average
A	A	[0; 381.524]	171.526	[0; 0.0046]	0.0021
	B1	[0; 238.733]	93.131	[0; 0.0029]	0.0011
	B2	[0; 163.818]	60.454	[0; 0.0019]	0.00072
B	A	[0; 350.346]	147.504	[0; 0.0049]	0.0021
	B1	[0; 221.449]	91.235	[0; 0.0026]	0.0011
	B2	[0; 145.246]	57.182	[0; 0.0017]	0.00068

Final Considerations on DFN Model

Not having core or outcrop data and relying exclusively on seismic and FMI data to constrain the reservoir model creates a certain degree of uncertainty. Nevertheless, the same methodology was used for treating the data from the five wells, meaning that any possible error will affect that data the same way, hence allowing for a fair comparison between them.

In terms of the presented results it can be seen that the permeability values are very high (they are actually overestimated as Wf used equals 1mm, when it is usually around 0.1-0.01mm) and porosity is very low, which is a typical characteristic of a fractured reservoir. At the same time, when testing the validity of these results by using the following empirical formula,

$$\mathbf{Kfrac = 83300 \times Wf^3 \times LFD \times KF}$$

Where: **Kfrac**= fracture permeability; **Wf**= fracture aperture (millimetres); **LFD**= fracture frequency (fractures/meter), given by the Linear Fracture Density; **KF**= number of main fracture directions.

, it can be seen that Kfrac = 83300 x 1^3 x 2.6 x 1 = 216 darcys; which is a value with approximately the same magnitude of the presented maximum permeability value for family A.

Finally it is important to mention that unless long term well tests or laboratory core tests had been done to properly estimate permeability, this approach is probably the most complete and accurate that can be done by using only FMI data.

Considerations on the Fracture System

As it was already mentioned, the absence of core or outcrop data makes that any consideration about the fracture system will have the same level of uncertainty. At the same time the fact that the wells have been drilled vertically leads to an underestimation of the fracture families' density. Even though, and considering what was observed in the previous section, from the 3 fracture families present, Family A is the best candidate to be intersected with a well, as it is the family that presents the best density, permeability and porosity indexes (Figures 2 and 3; Table 7). Relative to the fracture-matrix interaction, it was also already stated that this is a Type 1 reservoir (p. 76), which means that only fractures provide the essential permeability, and the rock matrix should not be considered in the models.

The next section is dedicated to the Technical Recommendations for future work on Block-A and Block –B area, which should be seen as the main a conclusion of the present thesis.

7. TECHNICAL RECOMMENDATIONS

The final objective of this exercise is to provide GALP a well location which, relative to the seven wells drilled previously, assures better production rates. In order to establish a successful well location, i.e. a location which has higher chances of becoming a discovery well, the geologist must collect the most information he can on the area where he is placing that well location. This chapter is dedicated to provide a series of technical recommendations, based on what was presented in the previous sections, and that in the author's opinion will lead to an improvement of the exploration and production results in the Basement of the SEAL Basin.

This section is divided into two parts: the first will be dedicated to the data that should be acquired for better understanding of the fracture system; and the second to the actual definition of a well location and the associated volumes – which have not been previously calculated for this area. Figure 7-1 shows the new proposed exploration workflow for the part which is dedicated to volume calculations and drilling a well.

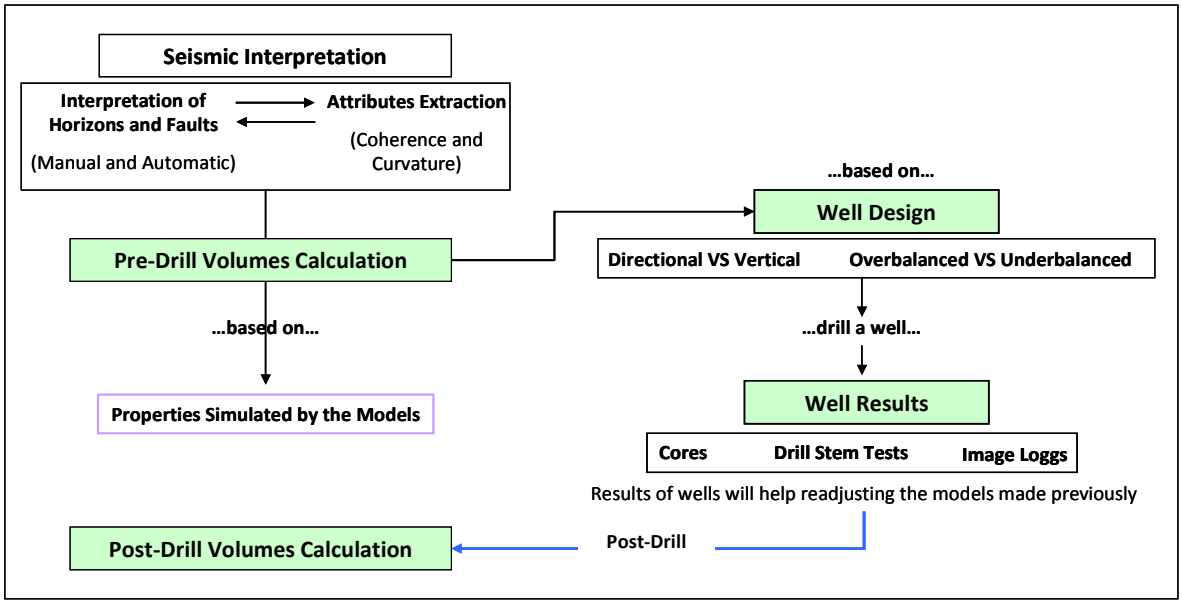

Figure 7-1: part of the New Exploration workflow dedicated to the volume calculations and well design.

7.1 TECHNICAL RECOMMENDATIONS FOR DATA PROCESSING AND ACQUISITION

7.1.2 Seismic Processing of the existing data

Even though post-stack migration is much faster than pre-stack migration (because stacking reduces the number of traces that must be processed) and it is cheaper, pre-stack migration gives a better imaging quality and is the most efficient type of migration when geological structures are complex (Section 4.2.7). This is the case of SEAL, where the Basement rocks have undergone high deformation presenting complex structures and, most importantly for HC production, fractures. Re-processing the already available seismic with pre-stack techniques, giving more attention to the picking of the initial stacking velocities particularly at Basement depth, would probably produce better imaging, hence allowing for better definition of the fracture patterns, which in its turn allow for better planning of drilling campaigns.

It is strongly recommended that this technique is applied before a new seismic acquisition campaign is considered as it represents a relatively low cost and it can largely improve the way the Basement is evaluated.

7.1.1 Seismic Acquisition of new data – Narrow VS Wide Azimuth

In the SEAL Basin, the use of Wide-Azimuth seismic, despite the fact that it would definitely improve seismic imaging and hence the way that the fracture system is understood, is determined by the volume of HC that can be proven to exist in the Basement reservoir. Calculating volumes for this reservoir is a very difficult task and has a high degree of uncertainty. As a result of this Wide-Azimuth seismic acquisition may be an operation harder to justify to the management, given its extra acquisition expense. Even though, the small area to be covered by the acquisition (Block-A and Block-B totalize an area of around 60 Km^2) may represent a small cost increase relative to the gain in seismic quality and hence in the understanding of the fractures system. As such, acquiring Wide-Azimuth seismic should be an option to consider.

If the option of Wide-Azimuth seismic acquisition is not taken, is still possible to improve the seismic image quality by applying different methods of processing than those that have been used to process the 3D seismic that was used for this work.

7.2 TECHNICAL RECOMMENDATIONS FOR FUTURE DRILLING CAMPAIGNS

The well location is supported by the following:

- Results of the seven wells drilled previously. The current wells did not produce well during testing. All seven found HC, demonstrating that the area has good potential, and that these poor results in testing might be due to erroneous drilling procedures (vertical wells, overbalance, improperly executed DST's). At the same time, it is not expected that maintaining these procedures will lead to different results. The proposed well will use different methodologies to try to overcome these problems.

- Data Acquired in the wells. The FMI data acquired, shows that there are several fracture families present in the Basement. From these, Family A (Section 6, Table 6-11) is the most promising due to its predominance. The proposed well will be projected in a way so that the contact of the well with the fractures is maximized – a directional well, intersecting fracture planes perpendicularly.

- Geomechanical + DFN Modelling: predicted the fracture density, permeability and porosity of the several fracture families, data that will be used ahead for volumetric calculations. It also helps supporting the idea that in every Basement high, HC will be found because these fractures are distributed throughout the entire Basement.

- Worldwide Analogues. Similar situations for fractured basement are found everywhere around the globe. In these analogues the exploration techniques used are substantially different from the ones used in SEAL by GALP (Section 5), namely directional and underbalanced drilling.

- Volume Calculations: In order to justify any well location, the calculation of the Oil-in-Place is essential. Without a proper and reliable assessment it is not possible to evaluate which techniques are economically sustainable or even if drilling a well is justifiable.

7.2.1 Volumes Calculations for SEAL Fractured Basement Reservoir

In order to justify any well location, the calculation of the Hydrocarbons Initially In Place is essential. Without a proper and reliable assessment it is not possible to evaluate which techniques are economically sustainable or even if drilling a well is justifiable. The following calculations are based on Figure 7-2 map. Notice that the Hydrocarbons Initially In Place are going to be assessed for the sum of the three fracture families defined previously.

(unfold next page)

Figure 7-2: Top Basement depth map, for Block-A and Block-B showing the interpreted faults and the well locations. Not all interpreted faults are displayed, as they would overload the map precluding a good understanding. The wells displayed were not defined in this map as they were drilled prior to its construction. Map created using Petrosys®.

Volumetrics can be assessed by using the Oil in Place formula, HIIP (Hydrocarbons Initially In Place):

HIIP = GRV x NTG x Phi (Φ) x Shc x FVF

Where:

GRV: gross rock volume.

NTG: Net-to-gross

Phi (Φ): porosity

Shc: Hydrocarbon saturation

FVF: formation volume factor.

For the present case study, it was decided to use this formula by changing the way each of the variables is calculated. Below is a description of the workflow used to calculate the HIIP for the SEAL Basement. Notice that for the reservoir characteristics that Naturally Fractured Reservoirs present, it is difficult to place a reasonable certainty on volumetric estimates of original HIIP, recoveries and hence reserves. As a consequence, the following volumetric calculations should be placed in the possible category.

GRV: Is the total rock volume of a potential hydrocarbon bearing trap. This can be assessed in two different ways:

1. Area/Depth graphs confined by the spill point* (which may or may not be deeper than the OWC contact).
2. Geostatistical simulation.

Both methods require the mapping of the prospect and the identification of the uncertainties which are usually large, depending on the type of opportunity under evaluation (structure, OWC type). Commonly, the GRV is assessed by the first method in the following logic:

GRV = Area of closure x Thickness

The Area of Closure is assessed by measuring the areas enclosed by successive contours until the deepest closing contour of the structure. These areas are then plotted against the thickness (depth) of the reservoir, which is confined by the spill point (Figure 7-3). Two options have been tested:

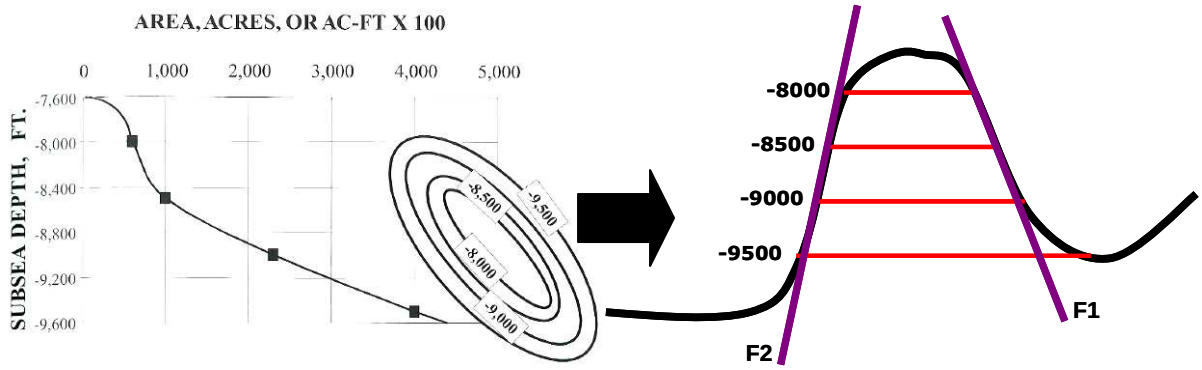

Figure 7-3: definition of the structure, and area of closure for the GRV calculation. Here the last closing contour is at -9500 ft. F1 and F2 represent faults.

*Spill Point: the structurally lowest point in a hydrocarbon trap that can retain hydrocarbons. Once a trap has been filled to its spill point, further storage or retention of hydrocarbons will not occur for lack of reservoir space within that trap. The hydrocarbons spill or leak out and they continue to migrate until they are trapped in another structure.

1. Assessing GRV per Basement High: To quickly evaluate the validity of calculating the GRV – and consequently the volumes – for each single Basement structure, it was decided to make the calculation for the Basement high where the well with best results was located. That was the Bravo and Fox structure (Section 6). For this, the 1060m contour (depth to which HC were found) was used. The map can be seen in Figure 7-4 and the GRV calculations for this structure can be found in Table 7-1. It can be seen that structure and consequently the HIIP that would have been calculated using this method would have been very small and economically not sustainable as the total area of the structure is less then $1km^2$.

2. Assessing the GRV for the total Area of Basement above a certain depth: In Figure 7-2 it is possible to observe that Basement highs are structurally narrow which causes them to have small areas. It is possible that, as they are very close to each other they could be interconnected structures. In Figure 7-5 and 7-6 the red contour shows the maximum depth to which HC was found in GALP wells (1060m). It was considered to use it for GRV calculations, but the fact that in well BR-01 (a well from the database drilled in 1981), oil shows below 1200m depth, within the Basement, were found suggests that open fractures can be found at this depth. At the same time the fact that HC were found in all the wells, makes reasonable to assume that every basement high was charged and consequently there are HC stored in the open fractures of those basement highs. These observations lead this author to consider that a common lowest closing contour can be chosen for calculation purposes, making the final GRV much higher. Table 7-2 shows the GRV values when the 1200m base contour is chosen for Block-A, and Table 7-3 for Block-B.

After identifying the structure and calculating the GRV, it is necessary to identify the reservoir rocks by log analysis, calculate porosities on those intervals and to calculate the hydrocarbon saturation of those same intervals. It is necessary to calculate the Net-To-Gross (NTG), Porosity (Φ) and Saturation (Sh).

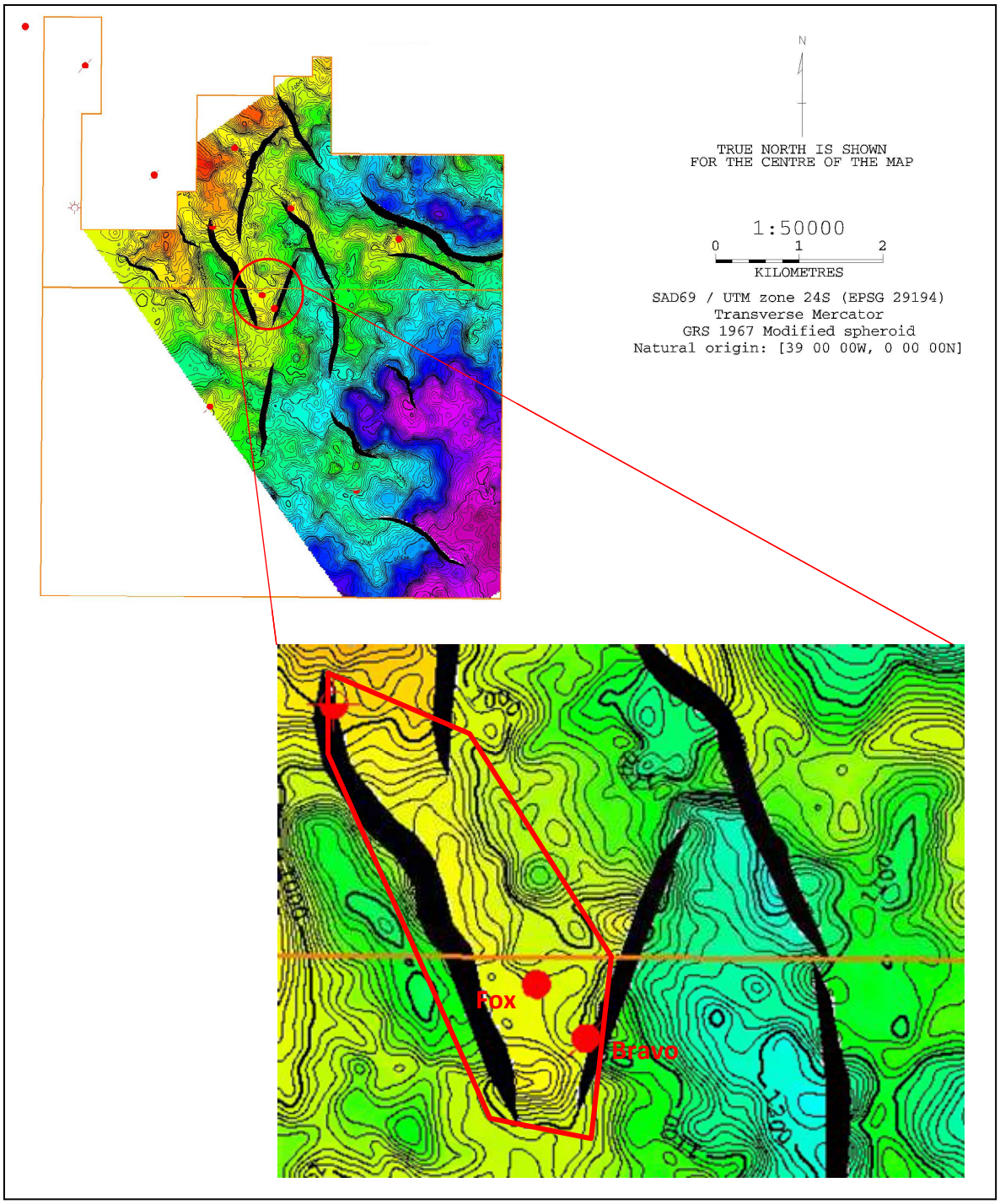

Figure 7-4: Bravo-Fox Basement structure that was used to calculate the GRV of Table 7-1. Inside the red polygon is the approximate area of the structure. Map created using Petrosys®.

Table 7-1: Area-depth pairs for the Bravo Well area. Notice that the total area (highlighted in red) corresponding to the Basement high where this well is located is less then 1 km^2, which is a substantially small area for a prospect to be considered economically valid. Calculations made using Petrosys®.

CONTACT SUMMARY
Top 900.0
OWC 1070.0

VOLUME SCALE FACTOR SUMMARY
900.0 to 1070.0 scale factor 1.00
User defined

SLICE VOLUMES FOR SLICE THICKNESS 10.0 Metres

Area_Bravo top level 900.0 to OWC 1070.0

Volume recovery scale factor 1.000

Top	Base	Area (KM^2)	Slice Volume (KM2-M)	Total vol above
900.00	910.00	0.001	0.003	0.003
910.00	920.00	0.004	0.017	0.021
920.00	930.00	0.019	0.111	0.132
930.00	940.00	0.040	0.299	0.430
940.00	950.00	0.091	0.620	1.051
950.00	960.00	0.163	1.240	2.290
960.00	970.00	0.259	2.129	4.419
970.00	980.00	0.334	2.966	7.385
980.00	990.00	0.405	3.697	11.082
990.00	1000.00	0.485	4.450	15.532
1000.00	1010.00	0.564	5.238	20.770
1010.00	1020.00	0.644	6.062	26.832
1020.00	1030.00	0.716	6.795	33.627
1030.00	1040.00	0.812	7.649	41.277
1040.00	1050.00	0.874	8.473	49.749
1050.00	1060.00	0.927	9.007	58.757
1060.00	1070.00	0.994	9.606	68.363
Total volume for range			68.363	

Total volume for polygon Area_Bravo 68.363

Total volume for all polygons 68.363

Multiple Polygon Volumetrics Summary Report

Reference level 1070.00

Polygon	Max slice area (KM^2)	Volume (KM2-M)	Total above
Area_Bravo	0.994	68.363	68.363
Totals:	0.994	68.363	68.363

Task completed : 2011-09-13T17:42:15WEST (0:00:00:00)

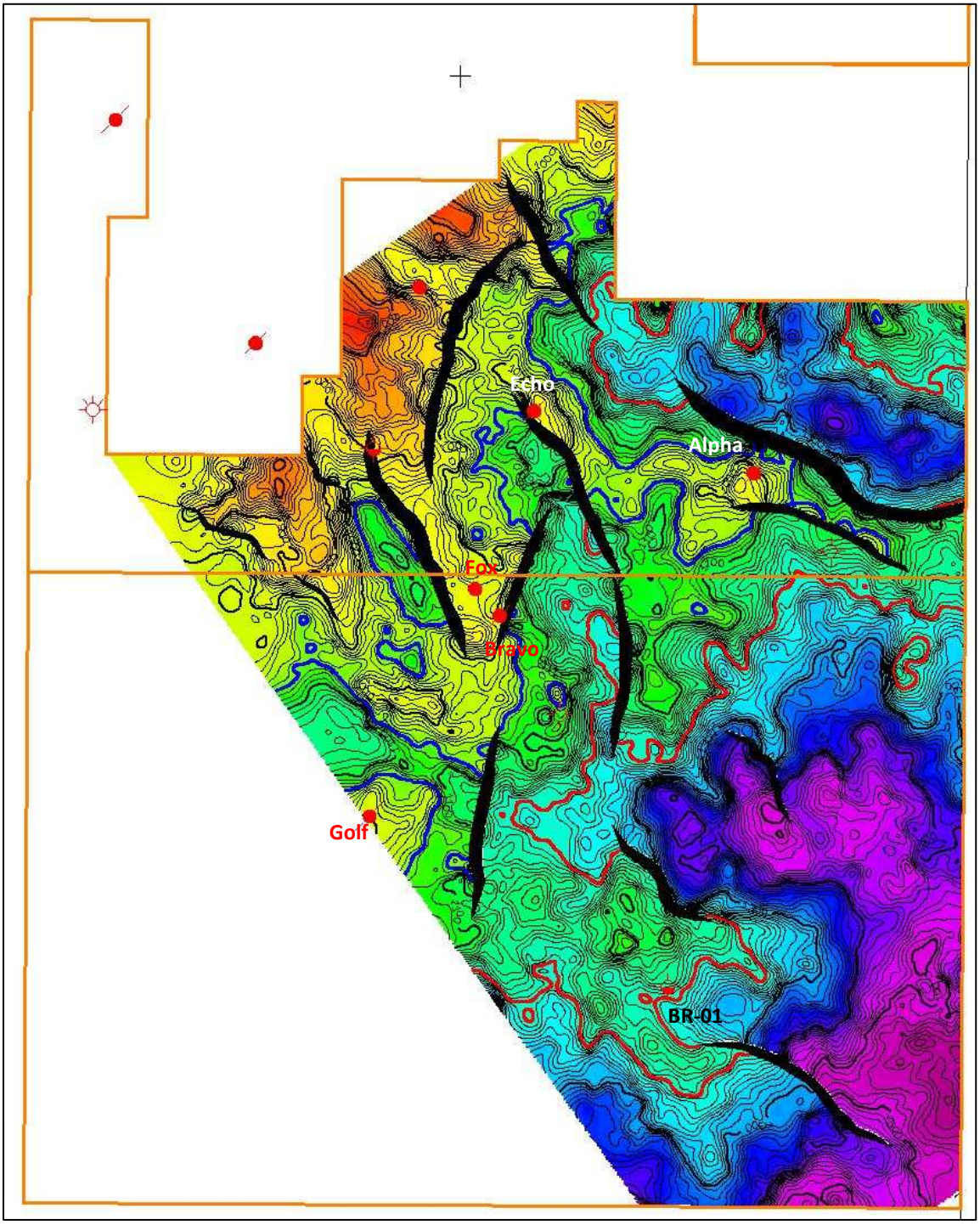

Figure 7-5: Top Basement depth map for Block-A, showing the interpreted faults and the well locations. Highlighted in blue is the 1060m contour, maximum depth to which HC shows were found in the GALP wells. Highlighted in red is the 1200m contour, the depth to wich shows in well BR-01 were found and which was considered to be the lowest closing contour. Map created using Petrosys®.

Table 7-2: Area-depth pairs for the total area above the 1200m contour in Block-A. Notice that the total area has increased relative to the calculation done for the Bravo well area (Figure 7-5).

CONTACT SUMMARY

Top	800.0
OWC	1200.0

VOLUME SCALE FACTOR SUMMARY
800.0 to 1200.0 scale factor 1.00
User defined

SLICE VOLUMES FOR SLICE THICKNESS 10.0 Metres

Block_Area top level 800.0 to OWC 1200.0

Volume recovery scale factor 1.000

Top	Base	Area (KM^2)	Slice Volume (KM2-M)	Total vol above
800.00	810.00	0.286	2.268	2.268
810.00	820.00	0.398	3.412	5.680
820.00	830.00	0.524	4.585	10.265
830.00	840.00	0.675	6.007	16.271
840.00	850.00	0.809	7.413	23.684
850.00	860.00	0.946	8.756	32.441
860.00	870.00	1.095	10.184	42.625
870.00	880.00	1.286	11.880	54.505
880.00	890.00	1.480	13.839	68.344
890.00	900.00	1.670	15.747	84.090
900.00	910.00	1.883	17.767	101.857
910.00	920.00	2.083	19.782	121.639
920.00	930.00	2.260	21.718	143.356
930.00	940.00	2.428	23.435	166.792
940.00	950.00	2.624	25.240	192.032
950.00	960.00	2.833	27.273	219.304
960.00	970.00	3.105	29.614	248.918
970.00	980.00	3.469	32.802	281.720
980.00	990.00	3.846	36.514	318.234
990.00	1000.00	4.266	40.464	358.698
1000.00	1010.00	4.830	45.488	404.186
1010.00	1020.00	5.362	50.945	455.132
1020.00	1030.00	5.920	56.341	511.472
1030.00	1040.00	6.587	62.514	573.986
1040.00	1050.00	7.202	69.016	643.003
1050.00	1060.00	7.829	75.170	718.173
1060.00	1070.00	8.409	81.174	799.347
1070.00	1080.00	9.036	87.170	886.517
1080.00	1090.00	9.689	93.567	980.084
1090.00	1100.00	10.448	100.603	1,080.688
1100.00	1110.00	11.077	107.728	1,188.416
1110.00	1120.00	11.681	113.830	1,302.246
1120.00	1130.00	12.238	119.578	1,421.823
1130.00	1140.00	12.841	125.391	1,547.214
1140.00	1150.00	13.393	131.146	1,678.360
1150.00	1160.00	14.003	136.793	1,815.153
1160.00	1170.00	14.575	142.941	1,958.095
1170.00	1180.00	15.195	148.901	2,106.996
1180.00	1190.00	15.828	155.066	2,262.061
1190.00	1200.00	16.499	161.710	2,423.772
Total volume for range			2,423.772	

Total volume for polygon Block_Area 2,423.772

Total volume for all polygons 2,423.772

Multiple Polygon Volumetrics Summary Report

Reference level 1200.00

Polygon	Max slice area (KM^2)	Volume (KM2-M)	Total above
Block_Area	16.499	2,423.772	2,423.772
Totals:	16.499	2,423.772	2,423.772

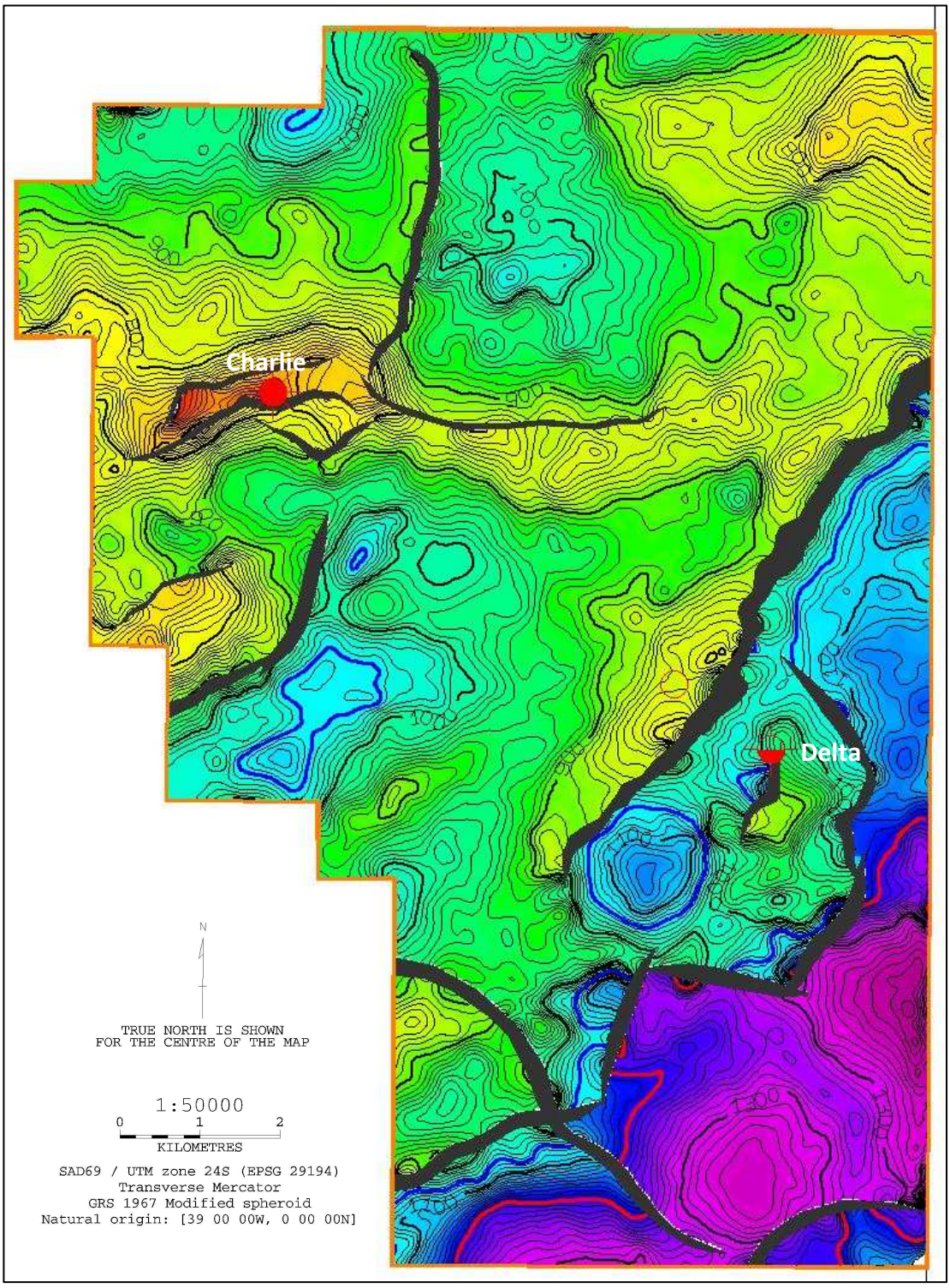

Figure 7-6: Top Basement depth map for Block-B, showing the interpreted faults and the well locations. Highlighted in blue is the 1060m contour, maximum depth to which HC shows were found in the GALP wells. Highlighted in red is the 1200m contour, depth which was considered to be the lowest closing contour (See Figure 7-6). Map created using Petrosys®.

CONTACT SUMMARY

Top 590.5
OWC 1200.0

VOLUME SCALE FACTOR SUMMARY
590.5 to 1200.0 scale factor 1.00
User defined

SLICE VOLUMES FOR SLICE THICKNESS 10.0 Metres

Block_B top level 590.5 to OWC 1200.0

Volume recovery scale factor 1.000

Top	Base	Area (KM^2)	Slice Volume (KM2-M)	Total vol above
590.47	600.00	0.001	0.009	0.009
600.00	610.00	0.003	0.019	0.028
610.00	620.00	0.004	0.033	0.061
620.00	630.00	0.009	0.061	0.122
630.00	640.00	0.011	0.098	0.220
640.00	650.00	0.016	0.134	0.354
650.00	660.00	0.025	0.194	0.548
660.00	670.00	0.033	0.284	0.832
670.00	680.00	0.039	0.351	1.183
680.00	690.00	0.046	0.414	1.597
690.00	700.00	0.058	0.511	2.107
700.00	710.00	0.067	0.627	2.734
710.00	720.00	0.085	0.730	3.464
720.00	730.00	0.116	0.987	4.451
730.00	740.00	0.147	1.302	5.753
740.00	750.00	0.212	1.752	7.505
750.00	760.00	0.273	2.440	9.945
760.00	770.00	0.347	3.138	13.083
770.00	780.00	0.426	3.819	16.902
780.00	790.00	0.526	4.741	21.643
790.00	800.00	0.628	5.752	27.396
800.00	810.00	0.752	6.917	34.313
810.00	820.00	0.898	8.225	42.538
820.00	830.00	1.089	9.964	52.502
830.00	840.00	1.294	11.930	64.432
840.00	850.00	1.530	14.058	78.490
850.00	860.00	1.845	16.859	95.349
860.00	870.00	2.192	20.147	115.495
870.00	880.00	2.706	24.450	139.945
880.00	890.00	3.240	29.752	169.698
890.00	900.00	3.688	34.631	204.329
900.00	910.00	4.202	39.486	243.815
910.00	920.00	4.673	44.375	288.190
920.00	930.00	5.068	48.700	336.890
930.00	940.00	5.498	52.862	389.752
940.00	950.00	6.019	57.492	447.244
950.00	960.00	6.468	62.434	509.678
960.00	970.00	6.886	66.749	576.427
970.00	980.00	7.306	70.807	647.234
980.00	990.00	7.620	74.683	721.917
990.00	1000.00	7.924	77.724	799.641
1000.00	1010.00	8.161	80.537	880.178
1010.00	1020.00	8.374	82.656	962.835
1020.00	1030.00	8.592	84.784	1,047.618
1030.00	1040.00	8.811	87.074	1,134.693
1040.00	1050.00	8.987	89.012	1,223.705
1050.00	1060.00	9.133	90.577	1,314.282
1060.00	1070.00	9.299	92.181	1,406.463
1070.00	1080.00	9.420	93.639	1,500.102
1080.00	1090.00	9.526	94.733	1,594.835
1090.00	1100.00	9.645	95.917	1,690.752
1100.00	1110.00	9.731	96.858	1,787.610
1110.00	1120.00	9.806	97.697	1,885.307
1120.00	1130.00	9.872	98.396	1,983.704
1130.00	1140.00	9.969	99.163	2,082.867
1140.00	1150.00	10.047	100.133	2,183.000
1150.00	1160.00	10.092	100.696	2,283.696
1160.00	1170.00	10.128	101.123	2,384.818
1170.00	1180.00	10.174	101.524	2,486.343
1180.00	1190.00	10.220	101.981	2,588.324
1190.00	1200.00	10.274	102.470	2,690.794
Total volume for range			2,690.794	

Total volume for polygon Block_B 2,690.794

Total volume for all polygons 2,690.794

Multiple Polygon Volumetrics Summary Report

Reference level 1200.00

Polygon	Max slice area (KM^2)	Volume (KM2-M)	Total above
Block_B	10.274	2,690.794	2,690.794
Totals:	10.274	2,690.794	2,690.794

Table 7-3: Area-depth pairs for the total area above the 1200m contour in Block-B. Notice that the total area has increased relative to the calculation done for the Bravo well area (Figure 7-6).

NTG and Phi (Φ)

NTG or Net-to-Gross, is the average ratio of the net-reservoir-rock volume to the gross volume. Calculating NTG corresponds to identifying the percentage of rock that is reservoir. It is derived from petrophysical evaluation of well data allied with play analysis for lithological variation that can modify the NTG (Figure 7-7).

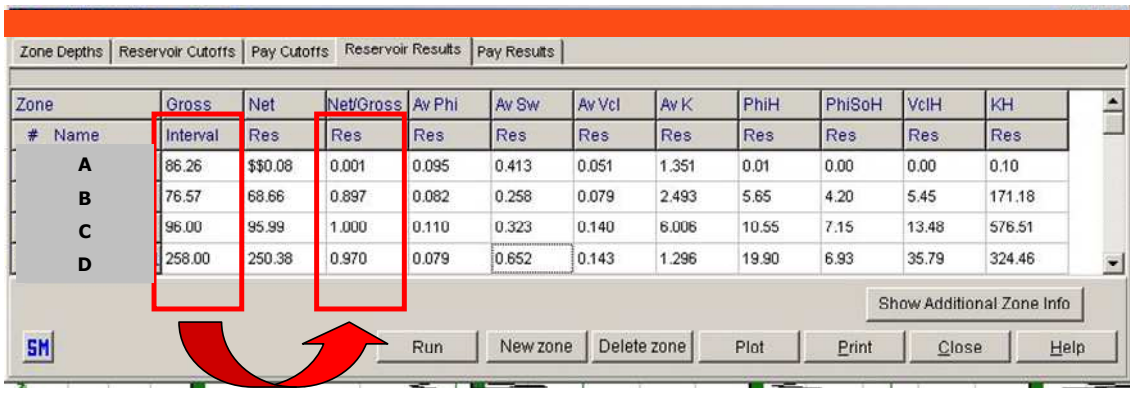

Figure 7-7: example of table generated by Schlumberger IP software that shows the results of the petrophysicist interpretation. Of the B interval, 89.7% is considered to be reservoir – which means that NTG is 0.897 - while C is 100% reservoir.

In a Basement Naturally Fractured Reservoir, where matrix porosity is close to zero, or non-existent, all the storage space is in the fractures. Consequently, the net-to-gross calculation corresponds to an assessment of the percentage of rock volume that is occupied by fractures, which is the same as calculating the fracture density.

In the case of SEAL Fractured Basement, fracture density was assessed using data from the FMI and data from the DFN modelling (Table 6-20 reproduced below). This way it is possible to obtain the theoretical fracture density per family. Here we can read the number of fractures that need to be simulated to reach the linear density found in the wells. Notice that these values have been calculated using FMI density data, which is underestimated as the wells have been drilled vertical and fractures are sub-vertical.

In order to obtain the percentage of rock volume that corresponds to fractures, these were simulated by UNL team (in squares or triangles) using FTRIAN software in a 100 x 100 x 5 reference block, until the density that was observed in the wells per family was reached (Section 6.6.2.2) As the fractures are simple polygons, the area was calculated by FTRIAN software for each polygon using a polynomial law.

Table 6-20 (from Chapter 6): LFD values for Block-A and Block-B. Notice that A, is the fracture family which presents a higher density value, which had already been observed when using the FMI counting only (Table 6-11). (Adapted from UNL, UALG, UA, & IST; *Modelling and Characterization of Fractured Reservoirs -GALP E&P Internal Report;* Lisbon; 2011).

Block-A				
Fracture Family	**LFD classes**		**Number of fractures for a grid block (100x100x5m) at maximum of the class**	**Number of fractures by m^3**
A	High	[1.734; 2.60]	176685	3.534
B1	High	[1.06; 1.60]	97932	1.959
B2	High	[0.67; 1.00]	62547	1.251

Block-B				
Fracture Family	**LFD classes**		**Number of fractures for a grid block (100x100x5m) at maximum of the class**	**Number of fractures by m^3**
A	High	[1.734; 2.60]	182885	3.657
B1	High	[1.06; 1.60]	95485	1.910
B2	High	[0.67; 1.00]	58327	1.167

Example for Family A:

In a reference block of 100m x 100m x 5m= 50000 m^3 , 176685 fractures were simulated with an average area of 1.75 m^2 so that the linear density value of 2.6 could be reached.

For an apperture of 1mm comes: 176685*1.75*0.001= 309.19 m^3. Which means that there is 309.19m^3 of fractures in a 50000m^3 volume. This is the same as having 0.00618 m^3 of fracture per cubic meter of rock volume. For obtaining net to gross: 0.00618 x 100% ≈0.618 %.

As apertures from the FMI vary within 0.01mm and 0.6mm, NTG will be calculated for these two extremes. Table 7-4 shows the range of NTG values for Block A and Block B.

Table 7-4: Range of NTG values for Block A and Block B.

Block A					
Fracture Family	Simulated LFD	Nº of Fracs	Average Area (sq. m)	Frac. Apperture (mm)	NTG (%)
A	2,6	176685	1,75	0,01	0,0062
	2,6	176685	1,75	0,6	0,3710
B1	1,6	97932	1,75	0,01	0,0034
	1,6	97932	1,75	0,6	0,2057
B2	1	62547	1,75	0,01	0,0022
	1	62547	1,75	0,6	0,1313

Block B					
Fracture Family	Simulated LFD	Nº of Fracs	Average Area (sq. m)	Frac. Apperture (mm)	NTG (%)
A	2,6	182885	1,75	0,01	0,0064
	2,6	182885	1,75	0,6	0,3841
B1	1,6	95485	1,75	0,01	0,0033
	1,6	95485	1,75	0,6	0,2005
B2	1	58327	1,75	0,01	0,0020
	1	58327	1,75	0,6	0,1225

As the NTG values for Block A and Block B are within the same magnitude, it was decided to use the same values for both blocks. As a result, the final values used in the volumes calculation will be (Table 7-5):

Table 7-5: Final range of NTG values for Block A and Block B.

Fracture Family	Interval	NTG (%)
A	Min	0,0062
	Max	0,3841
B1	Min	0,0033
	Max	0,2057
B2	Min	0,002
	Max	0,1313

Now that NTG has been assessed, how is porosity calculated?

Phi (Φ) or Porosity is a measure of the void spaces in a rock, and is a fraction of the volume of voids over the total volume of rock. In a regular clastic or carbonate rock, porosity is assessed by calculating the voids that exist in the volume of rock that was considered to be reservoir, i.e. the NTG. Using the example of Figure 7-7, in unit B, the NTG is 89.7%, and porosity is 8,2%. This means that of those 89.7% of rock that is considered reservoir, only 8.2% is pore space.

In a Basement rock, where there is no reservoir space apart from that given by the fractures, when NTG is calculated (in the present case it was calculated by DFN simulation), it is already accounting for the pore space that would be given by porosity, because what is being calculated is the total volume of rock that is occupied by open fractures, i.e. the volume of space that exists between fracture walls – or fracture porosity. Hence, for volume calculation purposes two alternatives can be used:

1. Assess NTG and use $\Phi = 1$.
2. Assess porosity (methods on how calculate fracture porosity are described ahead) and use NTG=1, using the same logic described above.

For obtaining fracture porosity, the following methods can be used:

1. Using the empirical formula:

Phi = 0.001 x Wf x Df x KF1

Where: **Wf**= fracture aperture (millimetres); **Df**= fracture frequency (fractures/meter); **KF**= number of main fracture directions (1, 2, 3…)

Using data from the FMI measurements we can calculate the porosity for the three fracture families using Wf= 0.001-0.6 mm; Df= 2.6 + 1.6 + 1 (maximum observed density in wells for each family); KF=3 because we are calculating values for the three families. Table 7-6 shows the porosity values calculated for the three fracture families observed in the wells. The same values will be used for Blocks A and B.

Table 7-6: Range of porosities using the empirical formula Phi = 0.001 x Wf xDf x KF1, and data from the FMI readings.

Fracture Family	Inputs	Block A+B	
		Minimumm	Maximum
A+B1+B2	**Aperture (mm)**	0,01	0,6
	Porosity (%)	0,0156	0,936

2. Using Permeability modelling results where porosity was calculated through the area of fractures and apertures. Notice that the area was calculated by FTRIAN software for each polygon using a polynomial law and it has an average of 1.75 m^2, which means that values of porosity are highly conditioned by this value, which in its turn is conditioned by the inputs given on the models (the FMI data). Porosity values per fracture family are presented in Table 7-7.

Table 7-7: simulated porosity for the three fracture families and both Blocks based on Figure 6-93 porosity graphics.

Fracture Family	Porosity (%)		
	Minimumm	Average	Maximum
A	0,001	0,0021	0,005
B1	0,0005	0,0011	0,003
B2	0,00025	0,0072	0,002

3. Using average porosity values found in the literature. Bulk fracture porosity values of between 0.1 and 1% are typical for fractured reservoirs including basement (Nelson 2001, Narr et al 2000; Gutmanis, GeoSciense Ltd, 2010); hence, for volume calculation, a range of fracture porosity between a minimum of 0.1% and a maximum of 1% and will be used.

Notice that assuming that there is no matrix porosity is considered to be a valid approach because we are dealing with a micashist, and even if there was porosity, it would be so low that it would be insignificant in terms of storage capacity of the reservoir.

Shc: Hydrocarbon Saturation is the average ratio of the pore volume occupied by hydrocarbons before hydrocarbon production. Water saturation is usually calculated first because of its direct derivation mainly from the petrophysical evaluation of well data.

Shc = 1- Sw Where Sw is the water saturation - the average ratio of pore volume in a rock that is occupied by formation water.

From the well logs presented in Section 6, determining water saturation is not possible, because accurate resistivity measurements to input in Archie's equation, for Sw derivation are not possible to make. This way, and because we are calculating volumes for the HC bearing zone of the basement (given by the GRV) we assume that the fractures are saturated with hydrocarbons. Hence Shc= 100%.

FVF: Formation volume factor (FVF) is the average ratio of the hydrocarbon volume (oil, gas) at standard surface conditions to the hydrocarbon volume (oil, gas) at reservoir conditions.

When oil is produced, the high reservoir temperature and pressure decreases to surface conditions and gas bubbles out of the oil. As the gas bubbles out of the oil, the volume of the oil decreases. Stabilized oil under surface conditions (either 60º F and 14.7 psi or 15º C and 101.325 kPa) is called stock tank oil.

Oil reserves are calculated in terms of stock tank oil volumes rather than reservoir oil volumes. The ratio of stock tank volume to oil volume under reservoir conditions is called the Formation Volume Factor (FVF). It usually varies from 1.0 to 1.7. A formation volume factor of 1.4 is characteristic of high-shrinkage oil and 1.2 of low-shrinkage oil, and it should be calculated. FVF values are dependant on the hydrocarbon composition and depth (initial pressure) of the reservoir.

For the SEAL Basin, FVF was calculated by using HC properties such as the API gravity, formation temperature and pressure data (taken from the DST's at Basement depth). As Gas-Oil-Ratio (GOR) was not available, a series of plausible values were used, excluding the results which returned bubble point pressure values higher than the formation pressure. The results suggest that a range of FVF between a minimum of 1.07 (m^3/Sm^3) and a maximum of 1.23 (m^3/Sm^3) with a mode value of 1.14 (m^3/Sm^3) can be used in a Stretched Beta distribution.

HC Water Contact: In the SEAL Basement, establishing the HCWC is a difficult task. As it can be seen from Section 6 the depth to where HC was found varies from well to well. The fact that DST's have not been undertaken in a consistent manner, and the presence of a well with positive results in a structurally lower position than GALP wells, does not help to determine where the OWC should be placed. Two situations were considered (Figure 7-8):

HCWC determined by field wide communication: If a fracture extends below the HCWC, it can contain both water and HC, but if the fracture system is in pressure communication, which is common, it is expected to encounter a linear HCWC that reflects that pressure communication and does not let water rise above a certain depth.

HCWC determined by fracture extension: in the case of a Basement reservoir, matrix porosity is null, and hence only fractures can contain HC or water. This causes the HCWC to be defined accordingly to the open fractures extension, which is not linear, and consequently it will be an irregular limit.

As the HCWC value had to be considered and there was no available data on a field wide fracture communication, it was decided to assume that this contact was irregular and determined by the fracture extension. HCWC was confined to the spill point, which was decided to position at the lowest contour, above which HC were found (1200m, as it can be seen in Figure 7-2, BR-01 well). As the deepest oil found (confirmed by DST testing) was at 1402m depth – Bravo and Golf wells – it was decided to use a uniform distribution between 1042 m and 1200m.

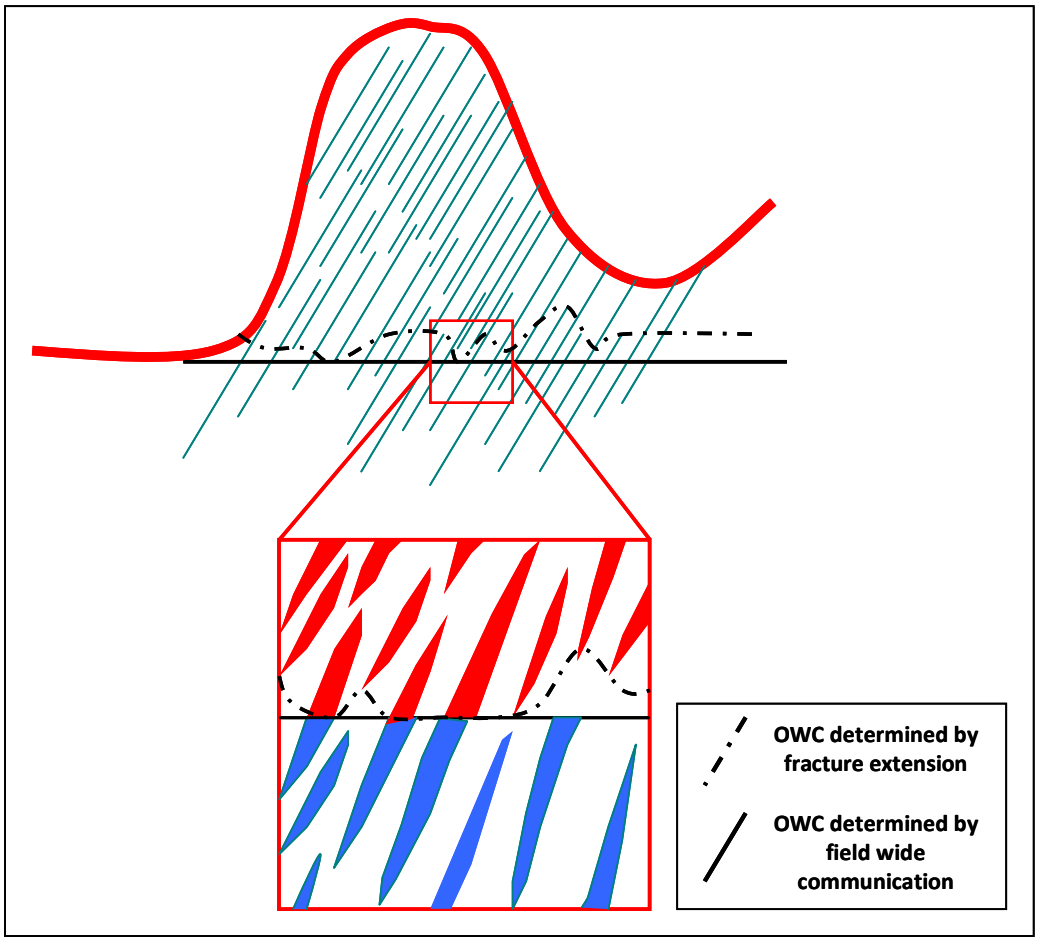

Figure 7-8: Difference between the expected OWC in a regular reservoir and the OWC in a Basement NFR. Notice that it is not linear, as some fractures may extend below the oil column and contain water. The water content will depend on the extent of the fractures below the oil column.

Spill Point: as stated the spill point was decided to position at 1200m, the lowest contour, above which HC were found.

Reservoir Thickness: 455m for Block A and 610m for Block B corresponding to the maximum thickness between the lowest depth to which HC were found and the crest of the structure.

Recovery Factor: without any long-term test data and/or historical data, establishing the Recovery Factors was based on analogues. For Haaban field in Yemen, fractured basement recovery factors are described to be around 15% (Legrand, Kok, Neff, & Clemens, 2010). It was then decided to assume a distribution of recovery factors between 10 and 20%.

Several scenarios for volume calculations will be run for each of the fracture families.

- Scenario 1: NTG is a uniform distribution between minimum and maximum values of Table 7-5 and Φ=1 for each of the fracture families.
- Scenario 2: Porosity is uniform distribution between minimum and maximum values of Table 7-6 and NTG=1 for each of the fracture families.
- Scenario 3: Porosity is a stretched beta distribution between values of Table 7-7 and NTG=1 for each of the fracture families.
- Scenario 4: uses porosity values taken from literature on Fractured Basement reservoirs in a uniform distribution and NTG=1.

Calculations were made in GeoX® using the above parameters. Total Mean STOOIP (Stock Tank Oil Originally In Place) are shown in Table 7-8.

Table 7-8: Total Mean STOOIP for each of the Scenarios for Block-A and Block-B. Calculations were made in GeoX® .

Scenario	Based On	Block A Total Mean STOOIP (MMBO)	Block B Total Mean STOOIP (MMBO)
1	NTG from FMI fracture density	30,2	40,4
2	Φ from empirical formula	38,7	52,1
3	Φ from modelling	0,38	0,51
4	Φ common range in analogues	44,7	60,2

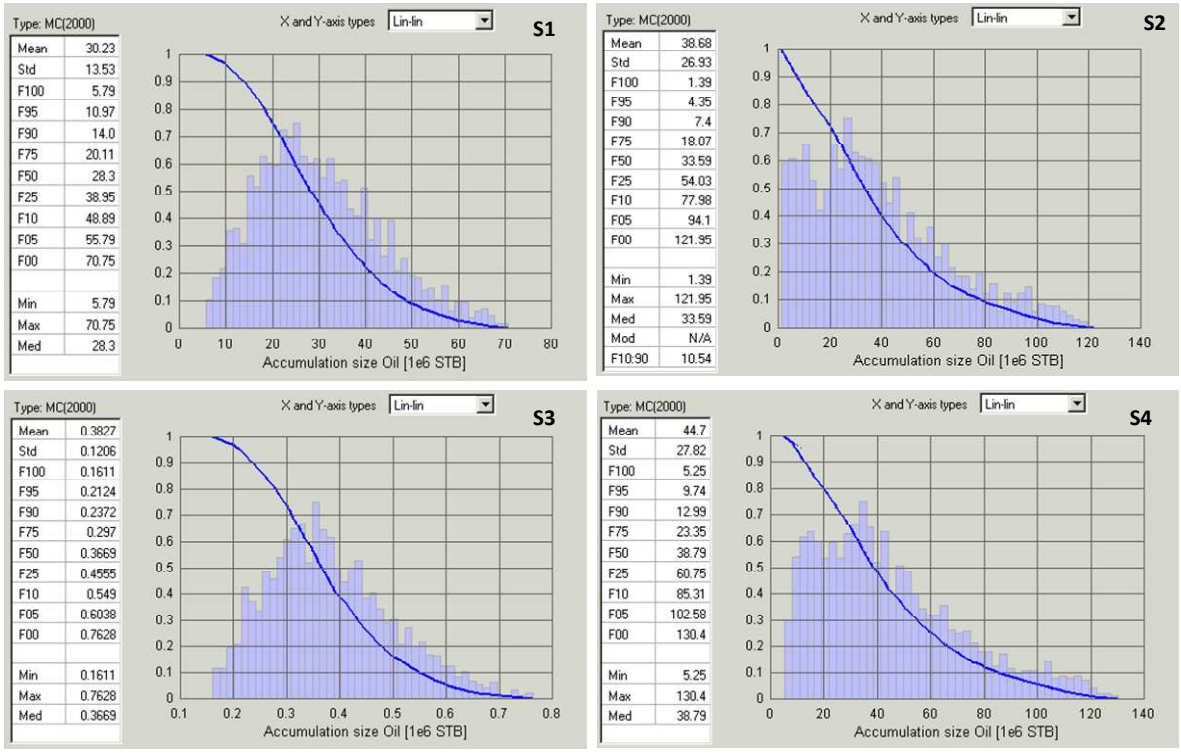

Figure 7-9: Distribution graphics for the four tested Scenarios in Block-A. S1-Scenario 1; S2- Scenario 2; S3-Scenario 3; S4- Scenario 4.

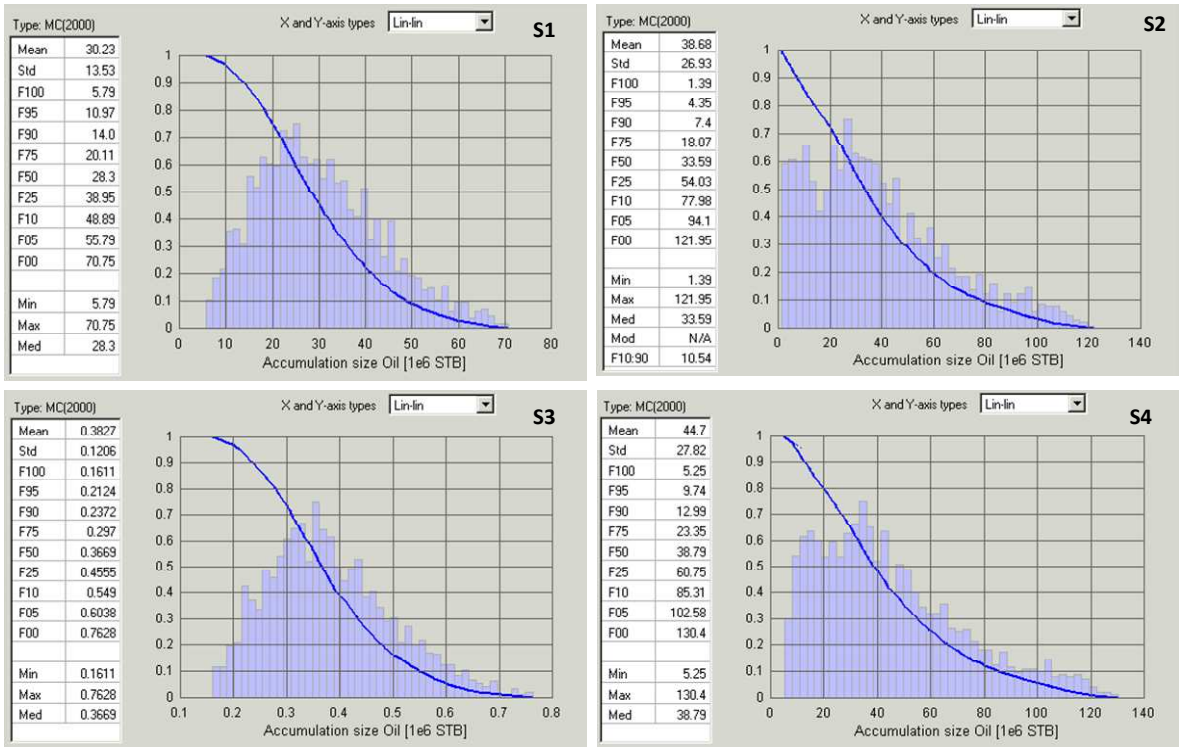

Figure 7-10: Distribution graphics for the four tested Scenarios in Block-B. A-Scenario 1; B- Scenario 2; C-Scenario 3; D- Scenario 4.

The following considerations can be made relative to the results presented in Table 7-8 and Figures 7-9 and 7-10:

- Scenario 1 and Scenario 2 output similar volumes. Notice that both scenarios use FMI data (fracture aperture and maximum observed density in wells) to calculate NTG (Scenario 1) or Porosity (Scenario 2). The difference between them is the methodology:

  In Scenario 1, an inverse approach was used and NTG was assessed by simulating fractures with a determined area so that the linear density value of 2.6 could be reached, and then it was calculated what was the correspondent fracture density – the NTG – was calculated.

  In Scenario 2, a well known and empirical formula uses values of aperture and density together with a multiplication factor that corresponds to the number of families found, to calculate porosity.

  The fact that NTG values from Scenario 1 and Porosity values from Scenario 2 are of the same order of magnitude, supports the logic used for volumes calculations described above (see page 210), and explains why STOOIIP values are similar.

- Scenario 3 shows very low values of STOOIIP. This method utilises data derived from modelling and can be seen as either highly pessimistic or realistic. Pessimistic due to the possibility of the existence of a series of compounding errors caused by the various inputs used to create the models. The low porosity, however may be a realistic estimation of fracture porosity within a non-brittle rock (such as this mica-schist) compared to the analogue data which represents more brittle fractured reservoirs – Scenario 4.

- As expected, Scenario 4 shows the largest values of STOOIIP as fracture porosity used was taken from literature on Fractured Basement Reservoirs. Most of these consist of brittle rocks such as granites, gneisses or basalts, rheological characteristic that causes the rock to be more prone to fracturing and hence fracture density and fracture apertures to be larger. This, in its turn influences the storage capacity of the rock - more volumes of HC are capable of being stored in brittle rocks. Scenario 4 can be seen as the comparison term for the other three scenarios, as all parameters except porosity are the same. Notice that Scenario 1 and Scenario 2 have STOOIP values which are close – but lower – than STOOIP outputted from this Scenario 4. This difference can be explained by lithological differences: SEAL Basement rocks are michashits which are less brittle than those rocks used as a model in Scenario 4 and consequently will have

lower fracture density and porosity which will account for lower volumes of stored hydrocarbons.

In sum, all the four simulated scenarios are relatively inaccurate, which is supported by the large variation of STOOIIP, ranging from 60 MMBo (Scenario 4 – Block-B) to 0.38 MMBo (Scenario 3 – Block A). Nevertheless, it was decided to consider Scenario 1 and 2 as the most acceptable. Notice that both are based on direct observations using the FMI tool (aperture and density), meaning that there are no errors related to modelling assumptions, and at the same time STOOIIP is probably higher than what has been calculated, as measurements from FMI tool are underestimated due to the relation between vertical well and sub-vertical fractures as stated previously.

Considering this, and the recoverable factor that was decided to use (10%-20%) it's expected around 4.5 to 7.8 MMBo to be recovered. Even though these values can be largely increased depending on the production methods used, and hence this estimation should not be considered as definitive as it can change along the field development cycle.

7.2.2 Directional and Underbalanced Drilling

As it was mentioned in Section 4.2.8.1, drilling directional wells at an angle from vertical in a direction normal to fracture planes and parallel to the minimum *in situ* stress, where most fractures can be intersected, is the recommend strategy by most authors (Nelson, 2001; Aguilera, 1995, Ehlig, 2000). Using an analogy with horizontal wells it's useful to demonstrate how this strategy is standard use in the industry.

Horizontal drilling was not a popular technique before the 1990's. Oil companies only drilled horizontal wells in difficult situations as a "last resort". Analysing a graphic of the global total for 1989 it is easy to verify that only 200 horizontal wells had been drilled. In 1990 that total increased to almost 1200 wells, with nearly 1000 of these drilled in the USA (Figure 7-11). What was then the factor that determined this dramatic change?

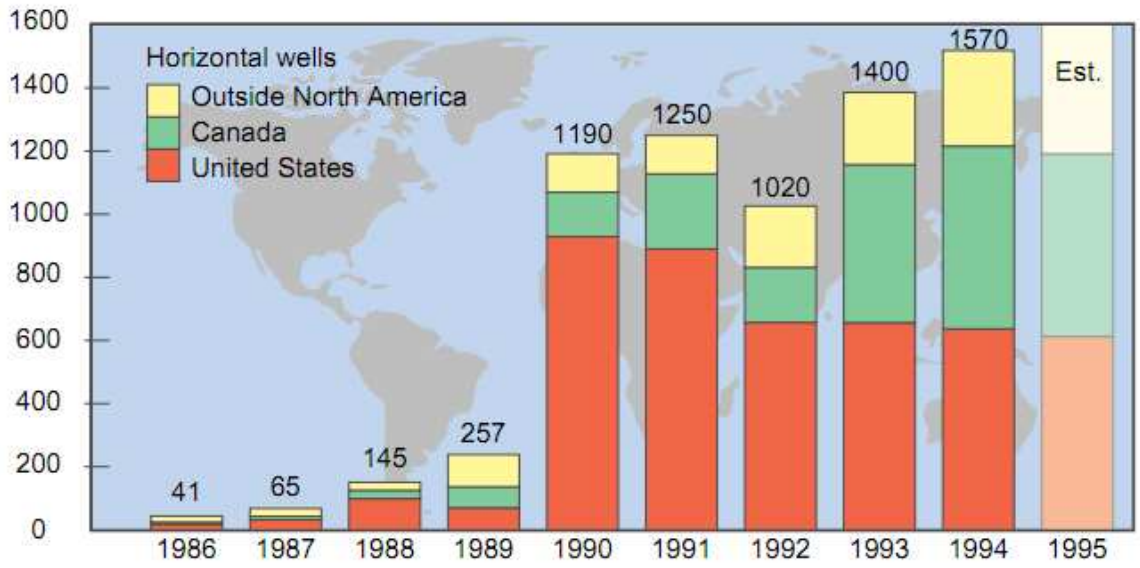

Figure 7-11: After great success in the USA in 1989, the global number of horizontal wells increased dramatically (www.slb.com – Horizontal Highlights).

It was the great success obtained in the Austin Chalk play in Texas, which transformed horizontal drilling into a mainstream technique. Activity in this formation soared from just 10 horizontal wells in 1989 to more than 200 in 1990.

The efficiency of this method relative to vertical wells is demonstrated by several examples:

1. In Canada, horizontal drilling became the solution for the oil sands where the viscous oils resulted in excessive water and/or gas production through coning effect, when vertical wells were

used. Through horizontal wells, oil can be produced at low pressures without reducing production rates and keeping gas and water away from production wells (Figure 7-12).

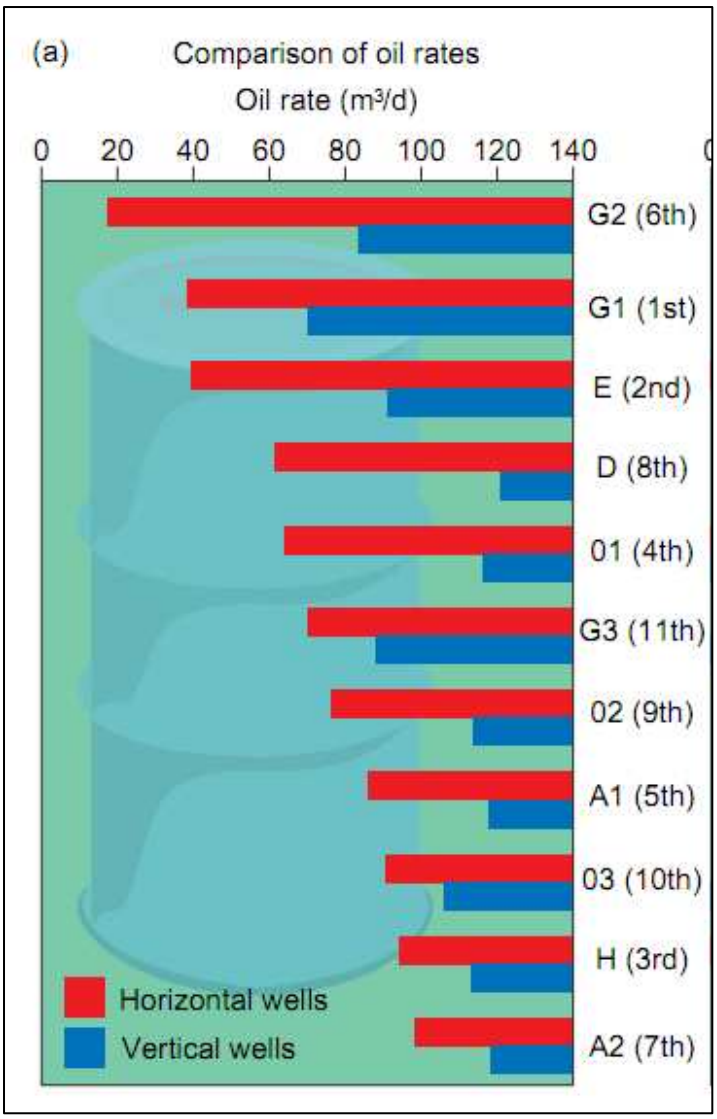

Figure 7-12: Comparison of oil production rates between vertical and horizontal wells in Canada's Devonian Rainbow Reef Reservoir, adapted from F.J. McIntyre, et. al. (1994) (www.slb.com – Horizontal Highlights).

2. As stated previously in the Natih Field, Oman, the chalky limestones are heavily fractured. The difference in production rates between a directional well and a vertical well spans from around 3700 bbl/day to 530 bbl/day, respectively.

3. In Georgia's Ninotsiminda Field, a vertical well was drilled in 2000 into the oil producing formation, with production tests stabilising at a flow of 200 bbl/day. In 2003 an appraisal horizontal well was drilled increasing the production to 2200 bbl/day.

These successful examples from different parts of the world prove that horizontal/directional drilling is a valid technique that can be used in very different geological settings. This author considers that in SEAL the execution of a directional well, instead of the traditional vertical wells, would lead to better results, i.e. higher production rates, by increasing the contact area of the well with the fractures. Adding to this, the well should be planned in a way so that it is drilled near a fault, particularly at a fault tip, as it was explained in Section 5.6.2.1.

As stated previously Family A is the fracture family which should be intersected with this well. Two reasons support this option:

- **Higher Density**: FMI well data show that Family A is the most frequent fracture family to be found with 104 measurements of open fractures inside the Basement. This is supported by DFN models.

- **Higher Permeability and Porosity:** Permeability models based on DFN and Geomechanical modelling show that Family A is by far the fracture family with higher permeability and porosity values.

According to Family A average fracture orientation taken from the FMI readings (Table 6-11), obtaining a well orientation which is perpendicular to it is straightforward (Figure 7-13) This well should have a 30^{o} inclination and should be drilled in the direction of the 240^{o} azimuth in order to perpendicularly intersect the N22^{o}W/60^{o}NE Family A fractures. With this orientation it is expected that the well (which is called Hotel following the same alphabetic logic used previously) presents better results than the seven wells drilled previously, as it is intersecting the open fractures which are predominant in the Basement rock. Figure 7-14 shows a schematic representation of Hotel Well relative to Bravo Well.

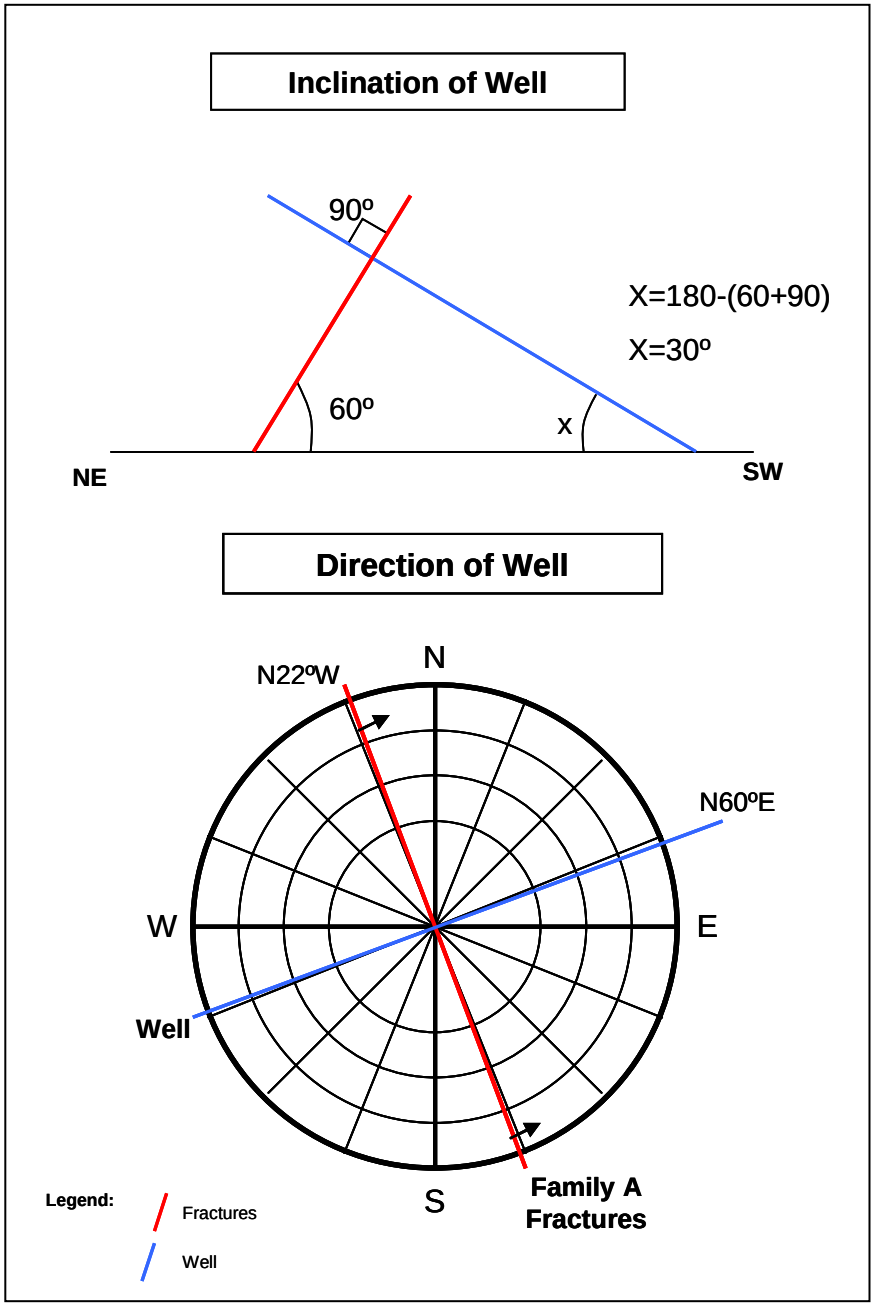

Figure 7-13: simple calculations for inclination and direction of the proposed directional well. This well should have a 30º inclination and should be drilled in the direction of the 240 º azimuth in order to perpendicularly intersect the N22ºW/60 ºNE Family A fractures.

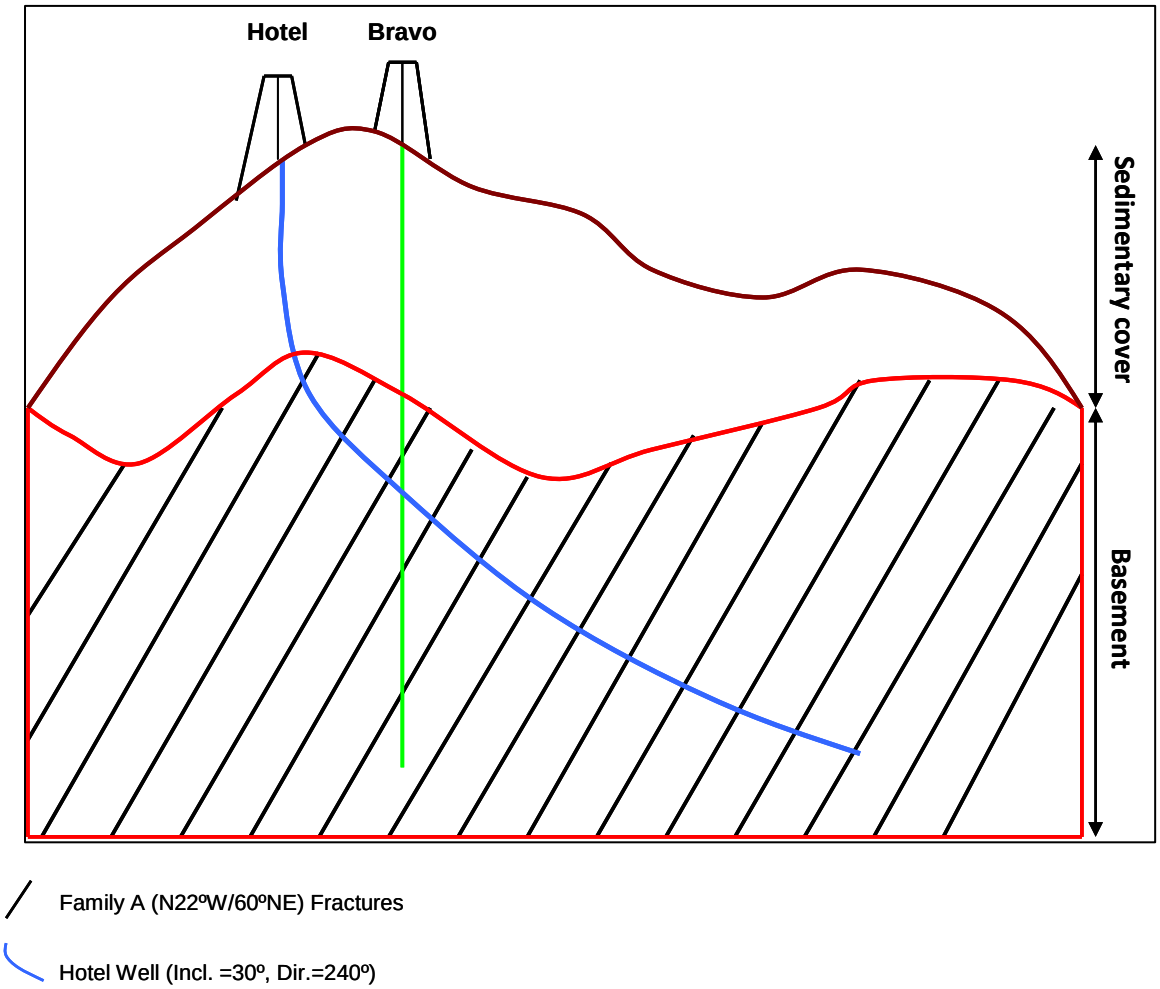

Figure 7-14: schematic representation of the Hotel Well, relative to the Bravo well. Notice that, relative to Bravo, the contact area of the Hotel Well with the fractures is greatly increased.

In any well proposal, justifying the costs is imperative. To do so, a well cost simulation was made, using as a reference Fox well, as well as other wells done in Brazil in a different basin but with similar drilling equipment, timeline and geological conditions. The simulation is presented in Table 7-9. The complete cost breakdown is presented in the Appendix of this thesis.

Table 7-9: Cost comparison between Fox Well and the Hotel Well. Hotel is simulated directional and directional+underbalanced, both for a maximum inclination of 30º and an average build-up-rate (BUR) of 3º/30m. Notice that the extra cost in order to drill in underbalanced conditions relative to a directional well is close to $70.000 and that the total cost of the well is of $2.9M, which is around $590K more than a regular vertical well.

	Fox	Hotel-D	Hotel-D+Ubd
		Directional	Directional Underbalanced
	$	$	$
PLANNING	27.027,350	38.612,164	38.612,164
LOCATION	146.149,410	104.138,482	104.138,482
RIG	957.385,730	1.302.660,155	1.302.660,155
OUTSOURCING SERVICES	338.417,550	423.082,221	423.082,221
MATERIALS	414.456,130	433.687,246	494.837,246
HUMAN SUPERVISION	90.615,750	123.903,150	123.903,150
LOGISTIC SUPPORT	81.380,950	81.380,940	81.380,940
TOTAL	**2.363.747,801**	**2.883.584,012**	**2.953.906,512**
	Δ to Fox	519.836,212	590.158,712
	Δ to Hotel-D	-	70.322,500

From this simulation, it can be observed that the extra cost in order to drill in underbalanced conditions relative to a directional well is close to $70.000 and that the total cost of the well is of $2.9M, which is around $590K more than a regular vertical well (relative to Fox). Hence, a directional well would have a 22% cost increase and a directional plus underbalanced well an increase of 25%. As such, and taking into account the advantages that were outlined in Section 4.2.8.1 and 4.2.8.2 for directional and underbalance drilling , this author considers that:

- Drilling the Hotel well directionally and according to the orientation that was presented above is imperative in order to maximize the contact are of the well with the fracture network of Family A.
- With an increase of 3% in cost relative to a directional well, drilling Hotel underbalanced is an option to be taken into account, as examples show that the reduction in well count (the number of wells drilled to achieve a certain productivity) could be as high as 25% as a result of the increased productivity – answering to this question immediately as there is early production of HC while drilling due to the non-invasion of the fractures by heavy drilling fluid.

8. FINAL CONSIDERATIONS

The final considerations to sum the analysis of the SEAL Fractured Basement Reservoir can be divided in three general topics:

1. Considerations on the fracture system that affects the Basement
2. Considerations on the adopted workflow and on the achieved results.
3. Considerations for future work.

1. Considerations on the fracture system that affects the Basement

From the analysis of the references in the literature, seismic, well data (FMI and DST data), it was possible to conclude that the Basement rock in the area of Block-A and Block-B is highly fractured. Statistical analysis of the FMI measurements allowed the identification of several fracture families, of which one – Family A – was considered to be the most common as it was found in all seven wells.

Conjugating FMI data with seismic and by applying geomechanical principles, and DFN modelling, it was possible to simulate how fractures are distributed in the basement rock and as a final product generate comparative simulated permeability and porosity graphics. These showed that fracture Family A is the one which presents the highest values of both permeability and porosity.

2. Considerations on the adopted workflow and on the achieved results

The fact that only indirect data (FMI, DST and seismic data) were used to create permeability models for the fractured Basement, lends some inaccuracy to these models, as fracture densities and apertures are underestimated due to the relation vertical-well VS sub-vertical fractures. Even though, and considering that the objective was to define a fracture family that could be intersected with a directional well, i.e. a comparison between the properties of the several fracture familes, the objective was totally achieved. If the permeability and porosity values are not accurate, the error will be in the underestimation direction which allows saying that better results than those that were predicted are expected.

3. Considerations for future work.

When dealing with Naturally Fractured Reservoirs, it is imperative to define a fracture family which presents the higher permeability index so that drilling campaigns can be planned

accordingly, in order to achieve higher production rates. This thesis proved that Family A is the best candidate, and a directional well with 30º inclination drilled in the direction of the 240º azimuth should be drilled as an alternative to the vertical wells. At the same time, and because fractured reservoirs are a system sensitive to high pressures, an underbalanced well was proposed.

APPENDIX

A. Cores

Cores represent the most important direct source of information for fractured rock analaysis. They are used to determine reservoir quality and performance by summing together the individual small-scale elements of the reservoir that can be "read" on the core. Most authors recommend that, on the first exploratory wells, the fractured reservoir section should be cored. Two types of cores can be taken: side-wall cores and whole-core samples. Whole-core samples are useful in fracture evaluation for two reasons:

1. They sample a relatively large volume of rock and consequently potentially sample more regularly-spaced reservoir fractures than side-wall cores;

2. Standard permeability analyses can be performed in three dimensions on these samples (vertical, maximum horizontal and horizontal 90 degrees to maximum horizontal permeability).

Permeability analysis, allows the calculation of the absolute permeability of a fracture (or fracture system) at surface conditions and the simulation of the permeability anisotropy that fractures cause. In addition, correlative fractured and unfractured plugs taken from the whole-core samples can be subjected to tests done in confining pressure or under a variety of mixed loading conditions that simulate burial conditions, with the objective of measuring the variation in fracture and matrix properties. Determinations of fracture permeability under confining pressure are very important because open fractures are generally higher in absolute permeability than the matrix, but also much more compressible and, therefore, reduce in permeability and porosity faster than the matrix with the application of force (Jones, 1975; Nelson and Handin, 1977; and Nelson, 1981b).

Some general procedures that should be used in coring fractured formations are:

1. Use a core barrel liner of either plastic or aluminium. It helps keep the core intact and prevents jamming.
2. Most fractured rocks are usually the hardest most brittle rocks; hence there is a tendency to weight up on the bit to maintain penetration rate. However if weight on the string is too high, extension fractures in front of the coring bit might be generated. These are then captured in the core as "centerline fractures." They will also show up in the borehole wall

on image logs (FMI, etc.), and get in the way of interpreting the real fractures. This way it is important that the driller doesn't put to much weight on the bit, and that this weight is as constant as possible throughout the coring.

3. Special handling of the core is often needed. If we are interested in natural fractures, removing the core from the barrel with a sledge hammer is not a good idea.
4. Care should also be taken during twist-off at the bottom of the core. Aggressive twist-off in breaking the core off bottom may generate helical induced fractures in the bottom of the core.
5. Coring fractured rocks should be done as continuously as possible. The longer the core, the larger recovery rates obtained.
6. In some hard rocks, some workers add the Hugel Knives to the mouth of the core barrel. These knives create the orienting scribes on the core when taking an oriented core. The idea is that the knives keep the fractured core from spinning as it enters the barrel and, therefore, prevents jamming.
7. Drillers should not trip too fast, as this often causes problems and damage the core.

A complete analysis of a core should include at least the following evaluations (Aguilera, 1993):

• Fracture types description
• Grain density
• Petrophysical parameters "m" (cementation exponent) and "n" (saturation exponent)
• Whole core porosity and permeability (at room conditions and some samples at simulated net overburden pressure)
• Routine core analysis
• Capillary pressures and relative permeabilities
• Wettability determination in a preserved core
• Imbibition recoveries if the rock proves to be water wet
• Mechanical testing (Poisson's ratio, Young' modulus, stress strain analysis, matrix and fracture compressibility)
• Thin section analysis
• SEM (scanning electron microscopy) analysis
• Epoxy impregnation
• Spectrometric gamma ray and sonic velocity
• Solubility

- Non-destructive permeability determinations with a pressure decay profile permeameter
- Core scale pressure transient analysis and microsimulation of the fractured core.

B. Drill Stem Tests

Drill Stem Test (DST) is a procedure for isolating and testing the surrounding geological formation through the drill pipe. Generally DST's main objectives are (Trilobite Testing Inc. Manual):

- To assess the well potential and hence its commerciality
- To evaluate well damage
- To evaluate the reservoir pressure and permeability and to characterize the reservoir heterogeneities
- To estimate a connected volume
- To obtain samples of the reservoir fluid, for PVT, flow assurance and process studies.

These tests are usually conducted with a downhole shut-in tool that allows the well to be opened and closed at the bottom of the hole with a surface-actuated valve (Figure B-1). One or more pressure gauges are mounted into the DST tool and are read and interpreted after the test is completed. The tool includes a surface-actuated packer that can isolate the formation from the annulus between the drillstring and the borehole wall, thereby forcing any produced fluids to enter only the drillstring. By closing in the well at the bottom, afterflow is minimized and analysis is simplified, especially for formations with low flow rates. The drillstring is sometimes filled with an inert gas, usually nitrogen, for these tests. In low-permeability formations or where the production is mostly water and the formation pressure is too low to lift water to the surface, surface production may never be observed. In these cases, the volume of fluids produced into the drillstring is calculated and an analysis can be made without obtaining surface production. Occasionally, operators may wish to avoid surface production entirely for safety or environmental reasons, and produce only that amount that can be contained in the drillstring. This is accomplished by closing the surface valve when the bottom-hole valve is opened. These tests are called closed-chamber tests.

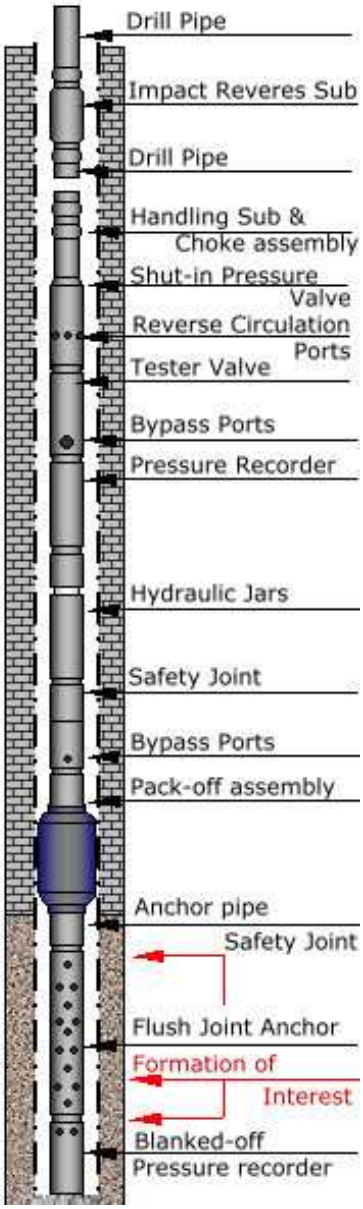

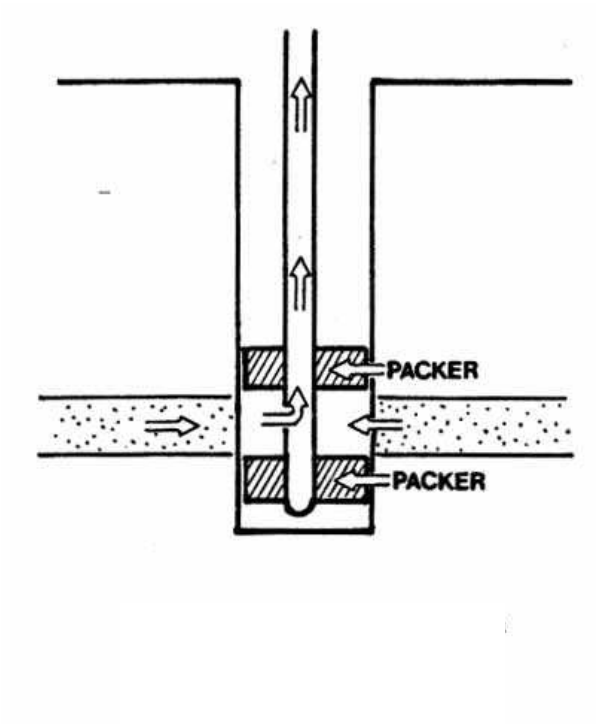

Figure B-1: The basic drill_stem test tool consists of a packer or packers, valve or ports that may be opened and closed from the surface, and two or more pressure-recording devices. (http://www.osha.gov/SLTC/etools/oilandgas/images/dst_one_packer.jpg; www.geo.wvu.edu/).

Drillstem tests are typically performed on exploration wells, and are often the key to determining whether a well has found a commercial hydrocarbon reservoir. The formation often is not cased prior to these tests, and the contents of the reservoir are frequently unknown at this point, therefore obtaining fluid samples is usually a major consideration.
The typical DST will be split into four periods, pre-flow, initial shut-in period, main-flow period and a final shut-in period (Figure B-3). Times for each test are dependent on conditions at the well site. DST's can be run at any time during the drilling operation at the current depth, or may be used to test any interval in the hole after TD has been reached. Using these data, and based on the evaluation of engineers and geologists, management can base a decision to complete the hole for potential production of oil or gas or proceed with abandonment.

Initial Flow Period: is a production period to clean up the well, and is used to remove any supercharge given to the formation due to mud infiltrating into the prospective formation during the drilling operation.
Initial Shut-In Period: this period allows the formation to recover from pressure surges caused during pre-flow. Is often referred to as "closed in for the pressure build up" and is a longer period. It allows determining the initial reservoir pressure.
Main Flow Period: a more lengthy production period designed to test the formation flow characteristics more rigorously. Flowing pressures and temperatures will be recorded. During this period surface blow is also recorded and interpreted.

Surface Blow Interpretation (Figure B-2): surface blow action is caused by the entry of fluid or gas into the empty drill string. As the fluid or gas enters the empty drill string (through the test tool) the air is displaced out of the top of the drill string. This results in a blow of air at the surface that can be measured. The procedure normally used is to place one end of the bubble hose into a 5 gallon bucket of water. The "BLOW" description is based on the level of bubbling action in the bucket of water.

Weak blow at surface indicates slow entry of recovery into the drillstem. This can be caused by several things:

a. Tight zone-low permeability
b. Plugged anchor or tool
c. Highly damaged test zone

d. Low Pressure test zone

Strong blow usually indicates that there is rapid entry into the drillstem. This indicates:

a. good zone-good permeability

b. good pressure

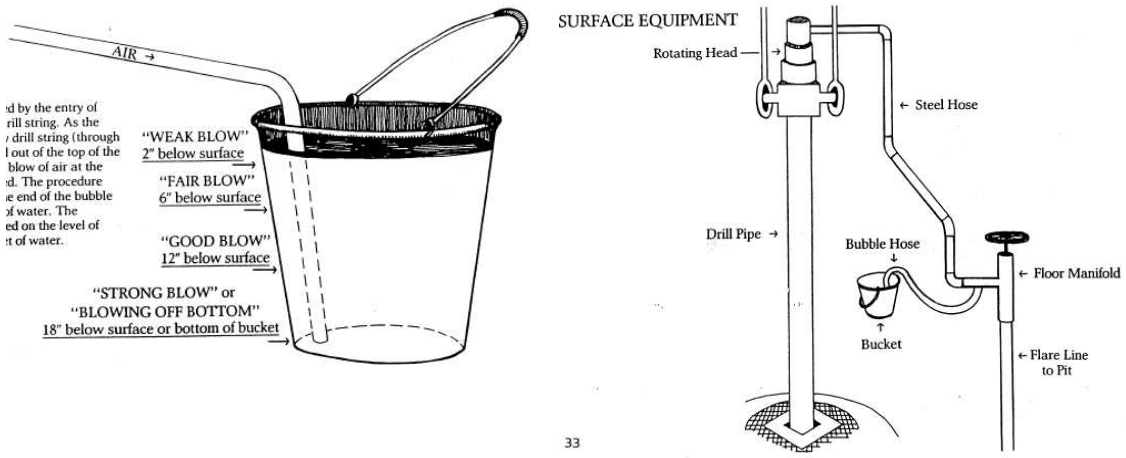

Figure B-2: surface blow equipment and blow classification. Source**:** Trilobite Testing Inc. DST guidebook

Final Shut-In: formation pressure is recorded over this period. The shape of the pressure build up curve will tell us the permeability of the formation, the degree of formation damage (likely caused during drilling operation).

As said, the drill stem testing technique, the well is controlled by a down hole shut in valve. Before the test, the well is usually partially filled with a liquid cushion designed to apply a hydrostatic pressure "B" above the valve, smaller than the formation pressure "E". When the tester valve is opened, an instantaneous drop of pressure is transmitted to the formation, and fluids from the formation start to flow into the well, it's the Initial-Flow Period ("C" to "D"). In case of liquid flow, the level rises in the production string and the backpressure due to the liquid column increases. The well is then shut-in for a pressure build-up ("D" to "E") – Initial Shut-In Period. When no flow to surface is desired, the down-hole valve is closed before the liquid level has reached the surface. If surface production is possible, the flow time is extended until the well produces at surface and the rate tends to stabilize. The DST procedure then becomes similar to that of a standard production test.

The well is then opened for the test and, due to the backpressure of the rising liquid column, the bottom-hole pressure increases (“F” to “G”). Finally, the well is shut-in for a final build up period (“G” to “H”). The “I” point is the final hydrostatic pressure.

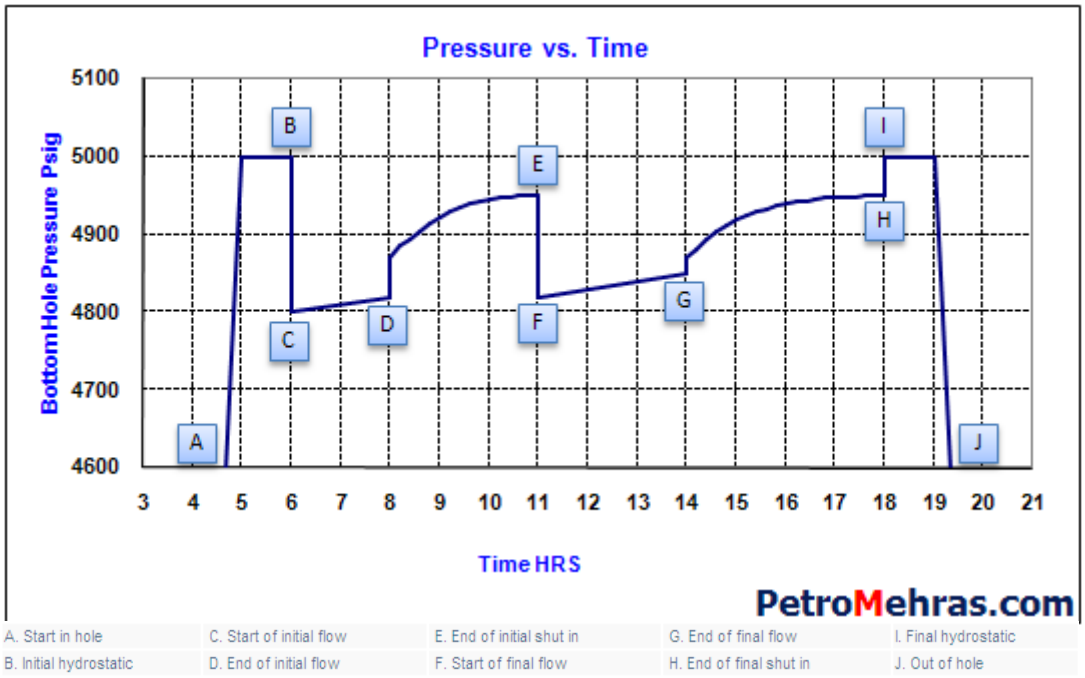

Figure B-3: standard graphic for a typical Drill Stem Test. Source**:** PetroMehras.com

The registration of the reservoir pressures, and sampled fluids in a DST, allows the engineer or geologist to take some conclusions on the reservoir and on the wellbore conditions. Some important examples are:

- Permeability
- Wellbore Damage
- Reservoir Depletion
- Reservor Barrier

Permeability: It is possible to state the relative level of formation permeability within the region of the wellbore being tested (assuming a fairly homogeneous interval). Below are three pressure graphics showing different levels of permeability (Figure B-4).

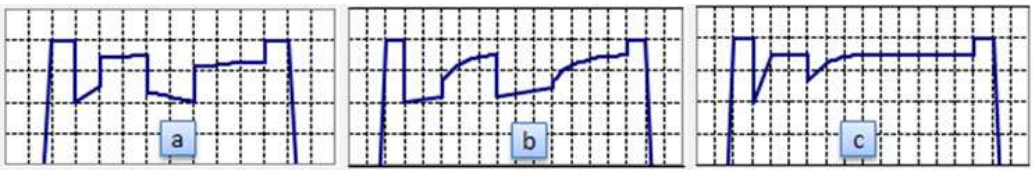

Figure B-4: DST pressure charts from three different formations. a) low permeability; b) average permeability c) high permeability. Source**:** PetroMehras.com

A) low permeability formations produce build-up curves that suggest the pressure is beginning to stabilize. They have very low pressure increases, if any, during the flow periods. There will be a weak blow at the surface, small fluid recovery and fairly low flowing pressures.

B) average permeability formations exhibit better developed build-up curves during the shut-in periods and some pressure build-up during the flow periods as fluids enter the wellbore. There should be a good blow, moderate fluid recovery, and increased pressures from one period to the next

C) high permeability formations will have high flow rate (strong blow), high flowing pressures, and rapid stabilization of pressure during build-up. The one shown here has stabilized with the flow pressure almost equal to the final shut-in pressure.

Wellbore Damage: Drillstem Tests are perhaps the best way to determine if the wellbore as suffered damage due to drilling procedures. It does not define the cause but it does estimate the presence and magnitude of damage. A low recovery on a test may be the result of damage rather than poor producing ability.

Causes of Wellbore Damage

1. Invasion of filtrate (clay content/chemical inbalance): filtrate invasion occurs when a zone has permeability and the mud system has a potential for water loss. The hydrostatic mud weight, water loss properties of the mud, and the chemical-osmotic potentials between the mud and formation determine the amount of filtrate that enters the formation.

2. Invasion of solids: solids invasion occurs when a zone has high permeability and a large pressure differential between hydrostatic and formation pressure. Drilling mud can be packed into the wellbore. The solids may be immobile when testing owing to the viscosities and pore geometries.

3. Mechanical damage: Mechanical damage is induced by the rotary drilling procedure. Often fine particles, created by the grinding of rock chips, are forced into the wellbore.

Wellbore damage DST's exhibit a weak blow at the surface and very little recovery (Figure B-5). Pressure charts indicate low flowing pressures and a sharp pressure rise after the tool is shut-in. A short radius pressure transition during build up followed by a flat pressure increase is also characteristic of a damaged wellbore. If the wellbore cleans up during the test, then there will be a change in the character of the curves (Figure B-6).

Figure B-5: DST pressure chart showing a damaged wellbore. Notice the low flowing pressure and the short radius pressure transition during build up followed by a flat pressure.

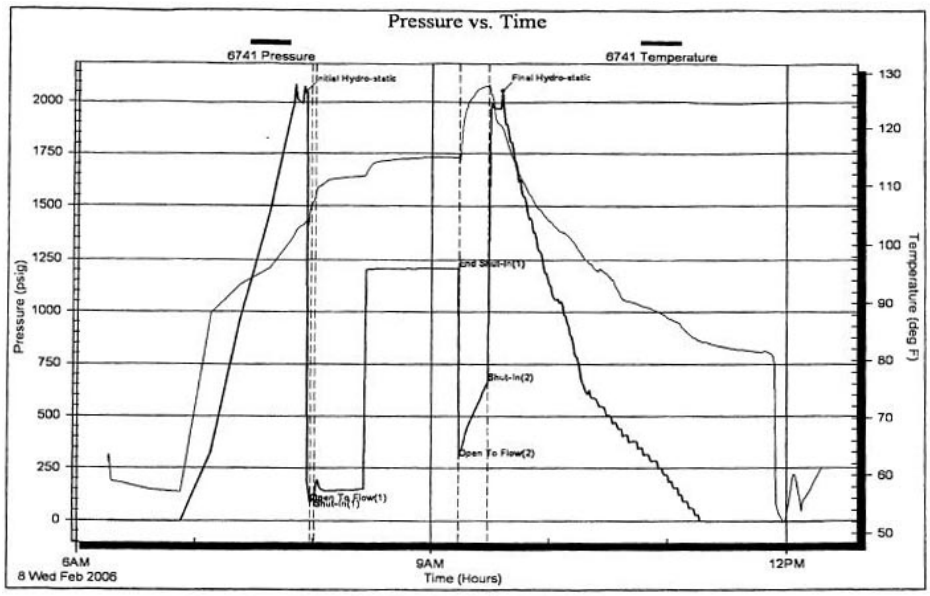

Figure B-6: DST pressure chart showing a wellbore that cleaned-up after the first flow. **Source:** Trilobite Testing Inc. DST guidebook.

Depletion: In a normal DST, a drop in pressure between the initial and final stabilized shut-in values indicates a limited of finite reservoir provided the initial value has not been affected by supercharging. The produced fluids have caused a measurable depletion ("drawdown") of the reservoir. A pressure change of 1.5% or greater is considered serious and more careful evaluation or re-testing is required. A barrier effect or nearby production may also the same effect to be recorded (Figure B-7 A).

Reservoir Barrier: Figure B-7-B is an excellent example of a decrease in pressure build-up levels between the initial and final flow periods. These are caused by a reservoir barrier or a permeability problem as opposed to depletion. The change in the slope of the build-up curve indicates a reduction in transmissibility some distance from the wellbore.

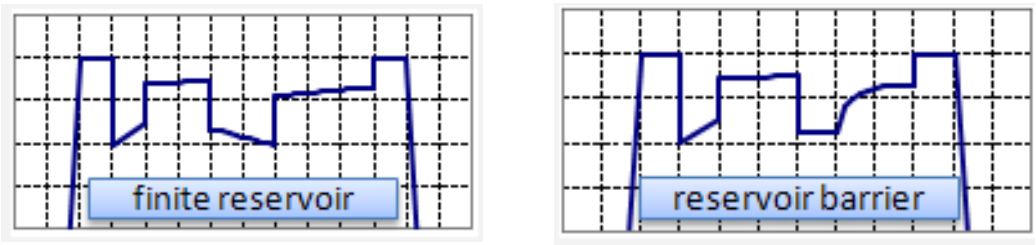

A) **B)**

Figure B-7: A) depleted reservoir. B) reservoir barrier

Examples of typical DST pressure charts:

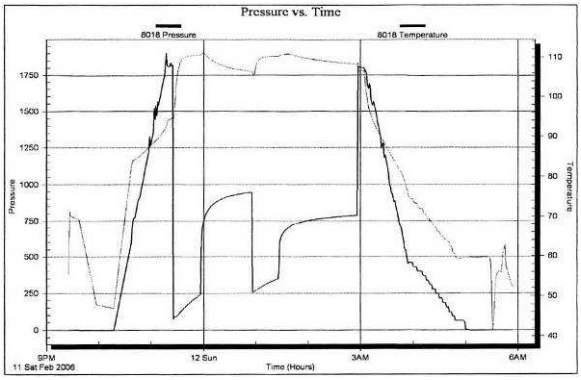

1- Limited Reservoir

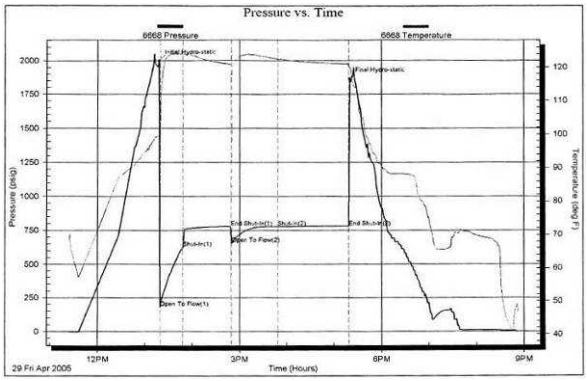

2- Flow Stabilized during final flow

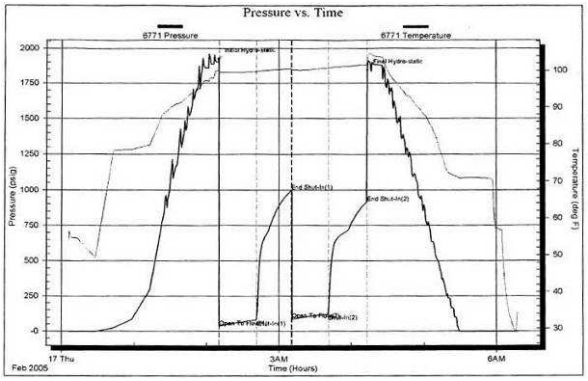

3- Two Zones in the reservoir

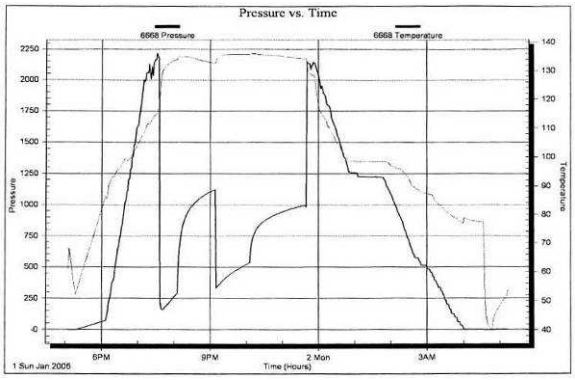

4- Barrier within radius of investigation

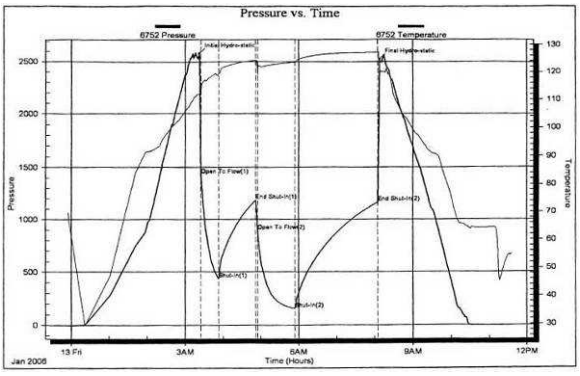

5- Depleting Gas Test

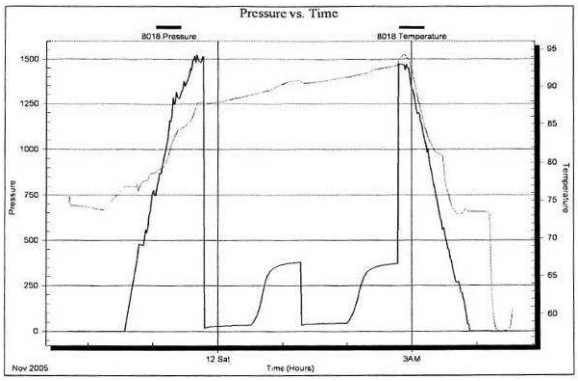

6- Depleted Pressures

Figure B-8: Typical DST graphics for different situations (Trilobite Testing Inc. DST guidebook).

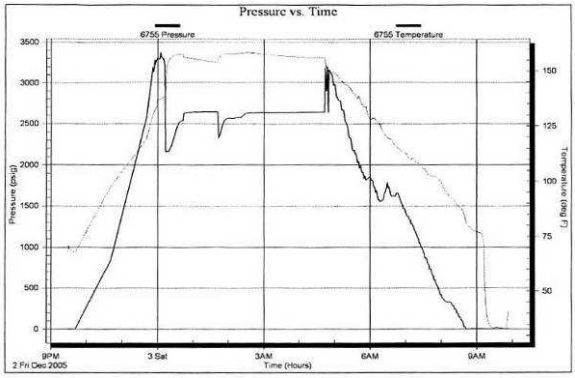

7- Excellent Permeability

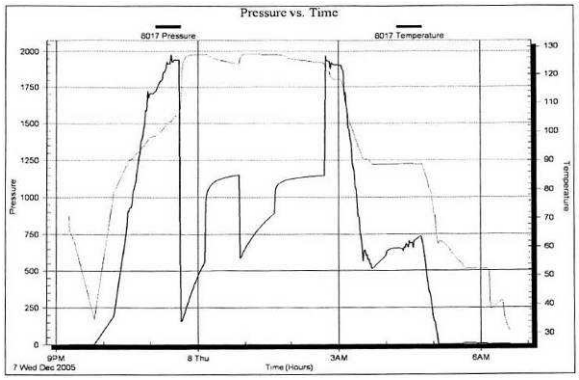

8- Good Permeability

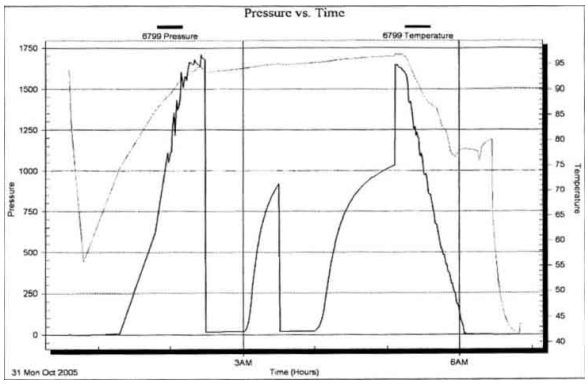

9- Low Permeability

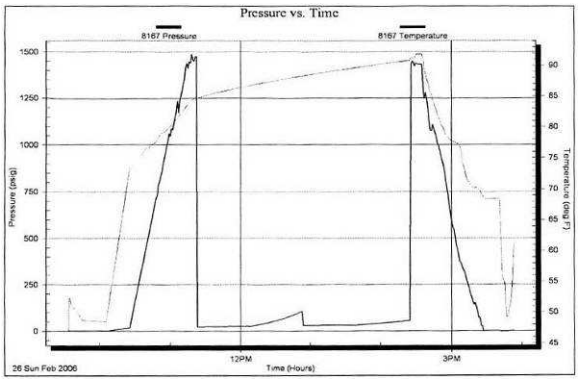

10- No permeability

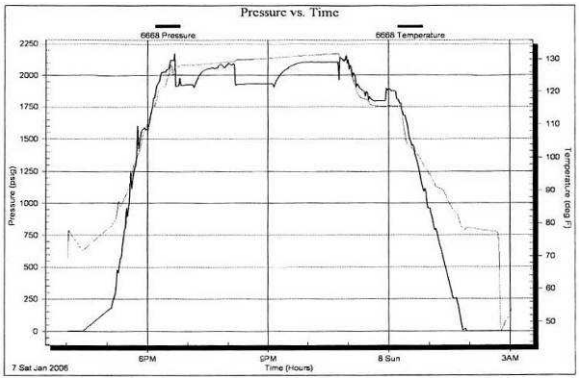

11- Hole in Pipe

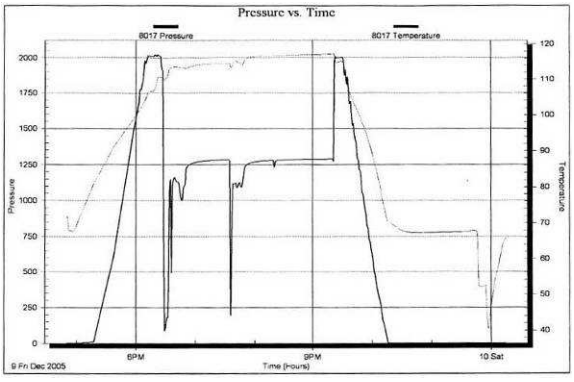

12- Severe Plugging

Figure B-8 (contd): Typical DST graphics for different situations (Trilobite Testing Inc. DST guidebook).

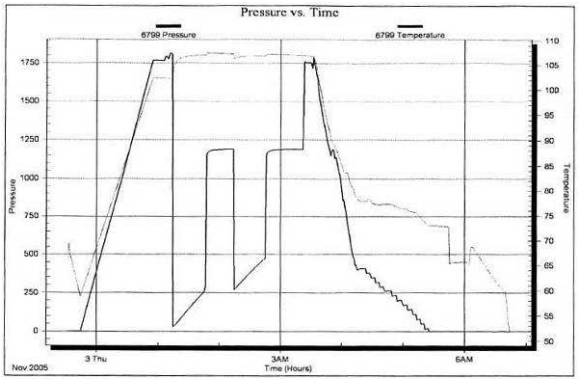

13- Wellbore damage

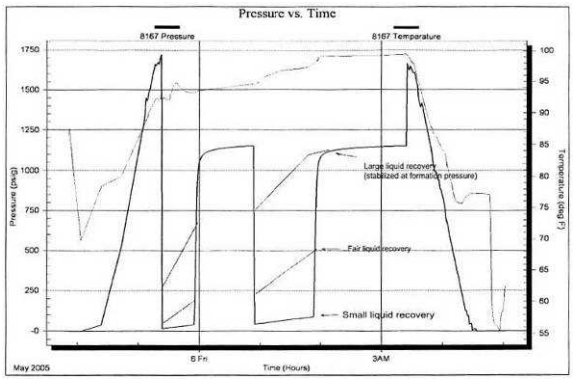

14- For liquid, the greater the increase in flow pressures, the larger the column of liquid the reservoir pressure supports

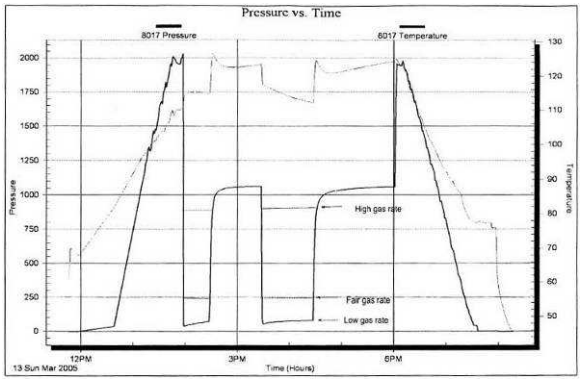

15- For gas, the higher the static pressures, the larger the gas rate. The increases in pressure reflect back-pressure from the bottom choke.

Figure B-8 (contd): Typical DST graphics for different situations (Trilobite Testing Inc. DST guidebook).

C. Borehole Images (Formation Micro Imager)

Borehole images are electronic pictures of the rocks and fluids that are found when a wellbore is drilled. Such images are made by electrical, acoustic or video devices which are lowered into the well. Images are oriented, have vertical and lateral resolution, and provide critical information such as bedding dip, fractures, faults, unconformities, paleocurrent directions, vuggy and fracture porosity. These images are best used when in conjunction with other available wellbore data such as other logs, cuttings, cores and production data. For the present purpose, only electrical borehole images are of importance.

Electrical borehole images are based on dipmeter technology that has been commercially available since the 1950s (Bigelow, 1985, Gilbreath, 1987) (Figure C-1). The recent tools are sophisticated versions of this kind of technology.

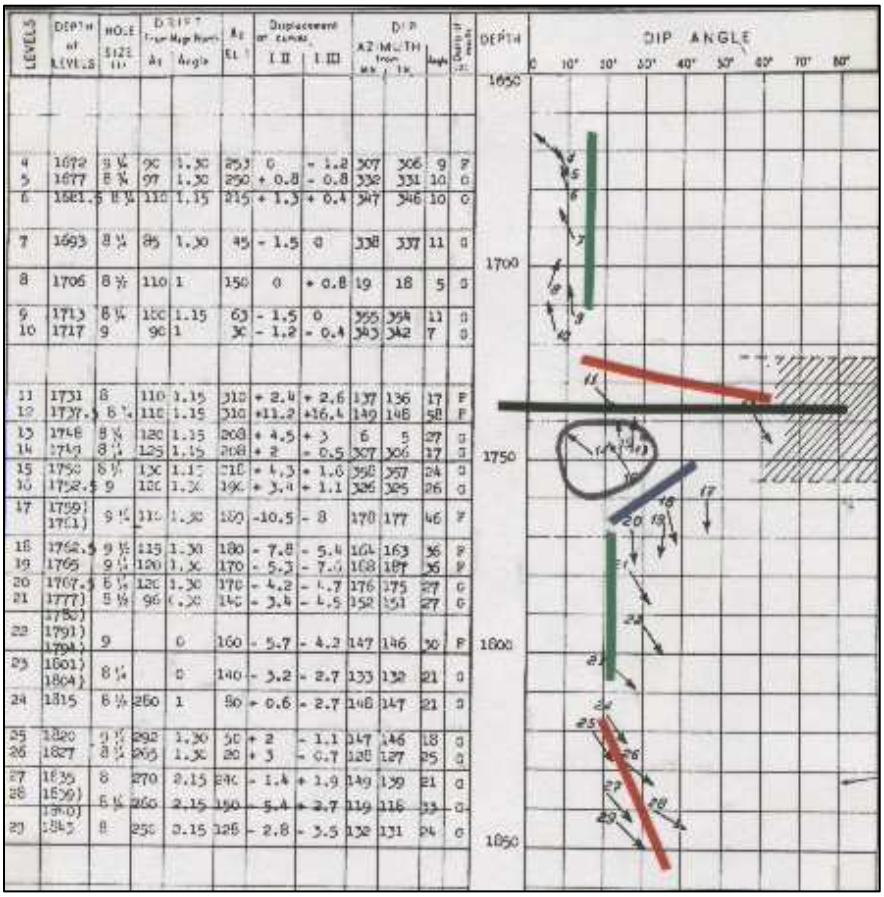

Figure C-1: Old dipmeter register chart.

Logging Routine

The modern imaging tools have microresistivity electrodes arranged around the tool on pads that are pressed against the borehole wall. The tool is first introduced in the well with the pads closed. At the start of each run, four, six or eight pads are pressed against the wall. The number of pads depends on the logging device which is being used (different companies, use different tools – Figures C-2 and C-3).

Electrical current is forced into the rock through the electrodes, and remote sensors measure the current after it interacts with the formation (Figure C-4 and C-5). Data retrieved include multiple electrode readings, calliper readings from individual pads or pairs of paids, and x-, y- and z-axis accelerometer and magnetometer readings. Borehole deviation and tool orientation (relative to pad 1) are determined by the magnetometers.

The sample rate for electrode and accelerometer data is very high (around 400 samples/), and thr areal coverage of the borehole face is a function of the width of the electrode arrays, number of pads, and borehole diameter. Generally, 40 to 80% of the borehole face is imaged, appearing the unimaged parts of as blank strips between the pads. The depth of investigation is small, usually less than 2,5 cm into the formation. Logging rate is comparable to other logs, being around 550m/h.

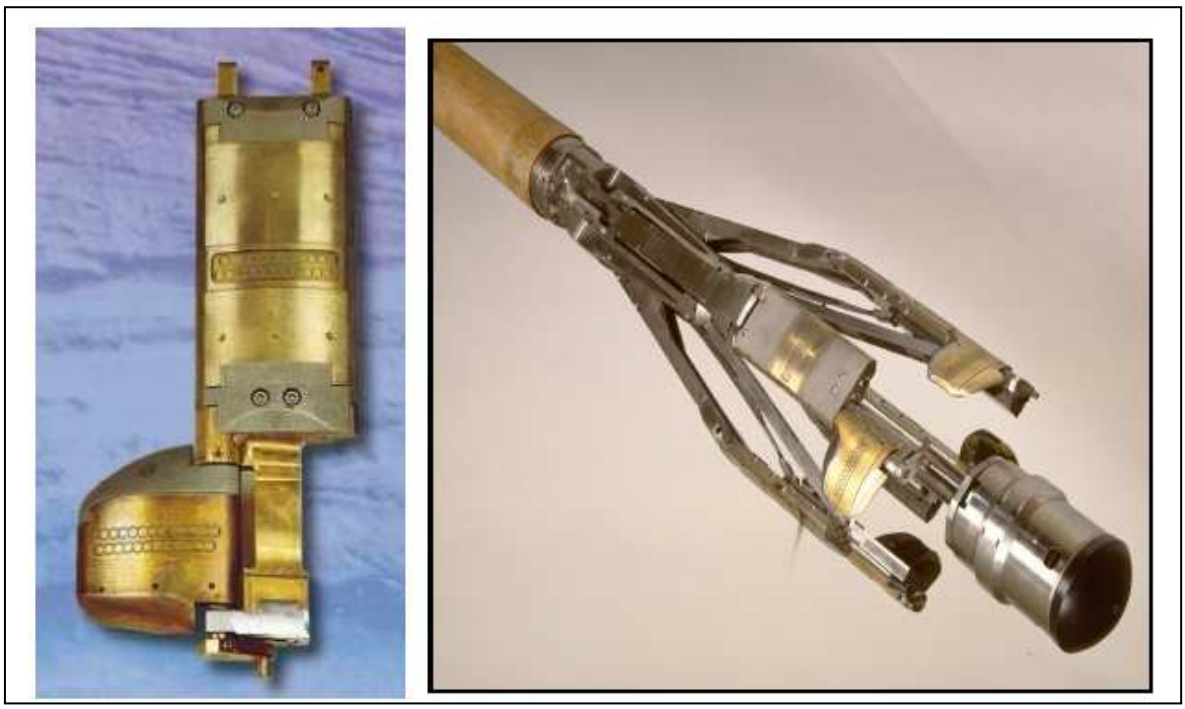

Figure C-2: Example of an e electric logging tool.

Company	Trade Name	Number of Pads	Number of Electrodes	Useful References
Halliburton	EMI (Electrical Micro Imaging Tool)	6	150	Seiler et al. (1994)
Schlumberger	FMS (Formation MicroScanner)	4	64	Ekstrom et al. (1986)
Schlumberger	FMI (Formation MicroImager)	8	192	Grace and Newberry (1998)
Baker Atlas	STAR (SimulTaneous Acoustic and Resistivity Imager)	6	144	Lacazette (1996)

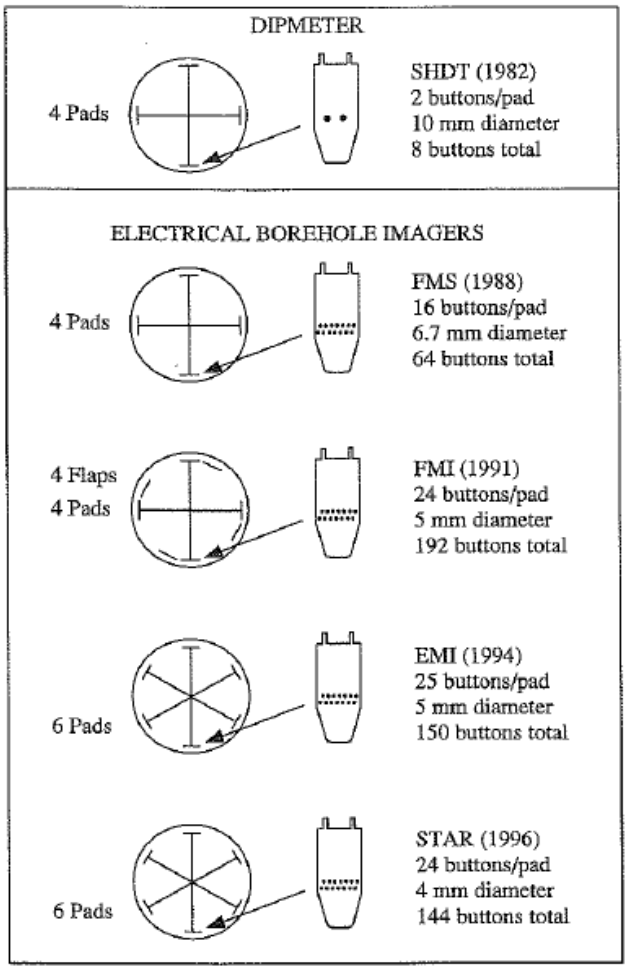

Figure C-3– tool configuration for the different logging companies. (Hurdley, 2004; Borehole Images, G. Asquish and D. Krygowski, Basic Well Log Analysis: AAPG Methods in Exploration 16. Modified from Grace and Newberry (1998).

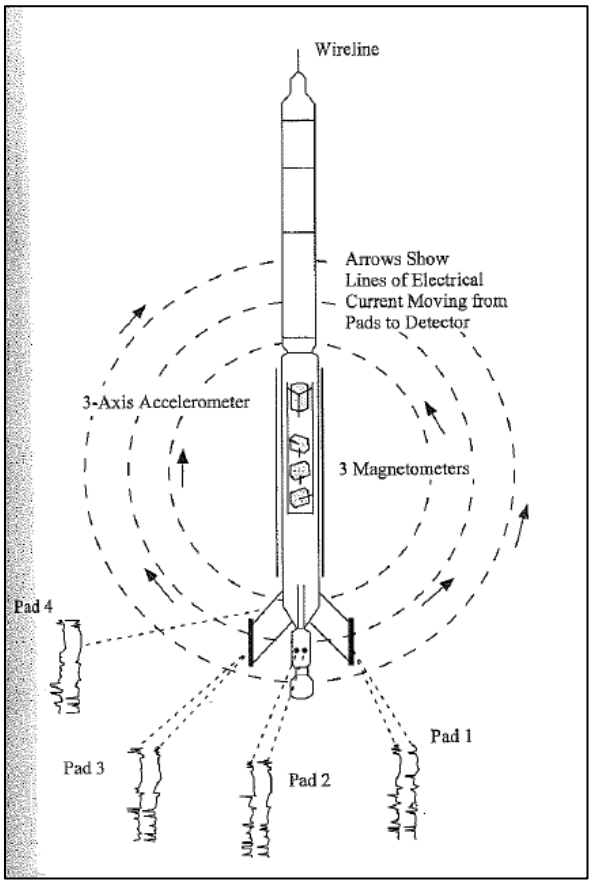

Figure C-4 – Basic principles of Stratigraphic High Resolution Dipmeter Tool from Schlumberger. Two measuring electrodes on each of four pads generate eight raw electrode traces as shown. Formation dip is computed from planes that are fit through correlative peaks and troughs on the speed-corrected electrode traces.

Hurdley, 2004; Borehole Images, *in* G. Asquish and D. Krygowski, Basic Well Log Analysis: AAPG Methods in Exploration 16. Newberry (1998), after Schlumberger (1983) and Höcker et al. (1990)

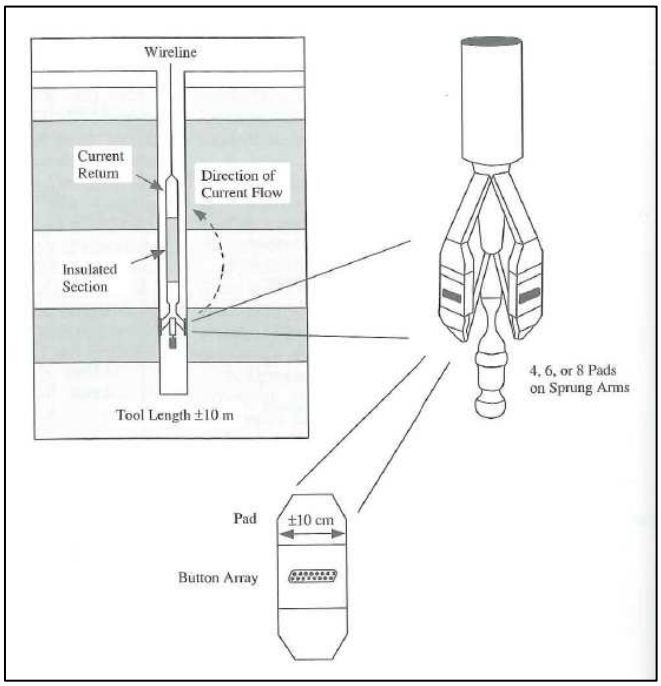

Figure C-5 - Basic elements of electrical borehole imaging tools. Electrical currents pass through button arrays into the formation. Current drop is recorded at a remote detector. Magnetometers record borehole deviation, and accelerometers speed variations. Hurdley, 2004; Borehole Images, *in* G. Asquish and D. Krygowski, Basic Well Log Analysis: AAPG Methods in Exploration 16. Newberry (1998), after Schlumberger (1983) and Höcker et al. (1990)

Data Processing

From what was said above, it is fair to conclude that a processed electrical borehole image is basically a map of rock resisitivity at the borehole face. As it is very difficult to examine borehole images in 3-D, it is common to "cut" the borehole along true north, and then unroll the cylinder until it becomes a 2D view. Planar features that intersect the cylindrical borehole will appear as sine waves in the 2D view (Figure C-6).

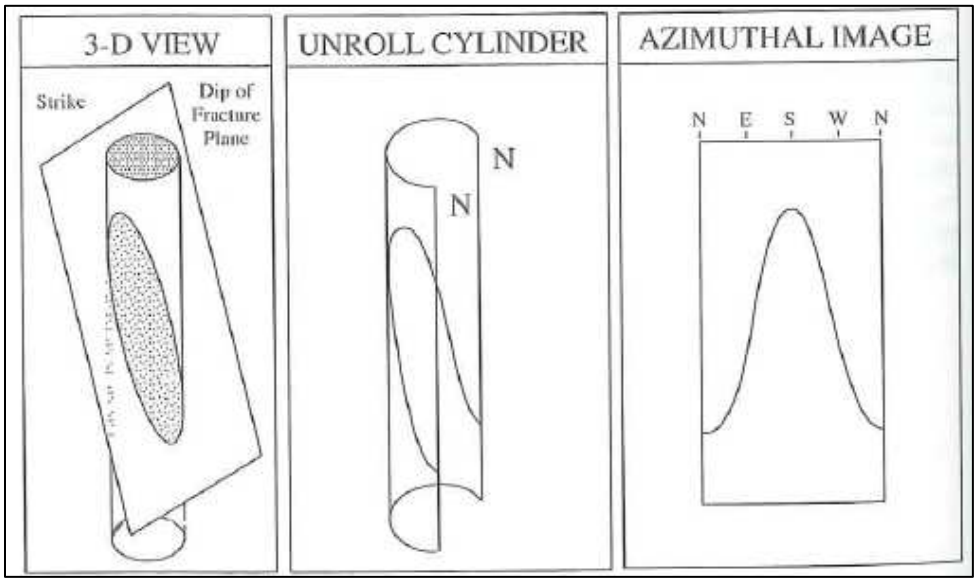

Figure C-6: Schematic diagram of a vertical cylindrical borehole intersected by a planar feature such as a steeply dipping fracture. After the cylinder correspondent to the borehole is unrolled and geo-referenced, the line of intersection becomes a sinusoidal curve which can be identified through strike and dip. Hurdley, 2004; Borehole Images, *in* G. Asquish and D. Krygowski, Basic Well Log Analysis: AAPG Methods in Exploration 16. Newberry (1998) after Schlumberger (1983) and Höcker et al. (1990)

Other processing steps that need to be operated:

- Correcting the directional data – pad 1 azimuth, which gives the tool orientation – and hole azimuth for magnetic declination.
- Accelerometer corrections to make sure that the accelerometer curve is on depth with the resistivity traces. The accelerometer accounts for differential sticking speed variations and resonant vibrations that occur as the tool moves up-hole (Figure C-7).
- Depth shifting so that rows of buttons are in line where the same slice of the borehole, perpendicular to the tool, was imaged.

After the corrections have been made, the image assigned with a colour map to different ranges of resistivity values, which are then positioned in their popper geometric position around the wellbore. Normally the colour scale ranges from black to white, and yellows and browns in the middle. By convention low-resistivity features such as shales or fluid filled fractures appear as dark colours, and high-resistivity features such as sandstones and limestones, are displayed as shades of brown, yellow and white (Figure C-8).

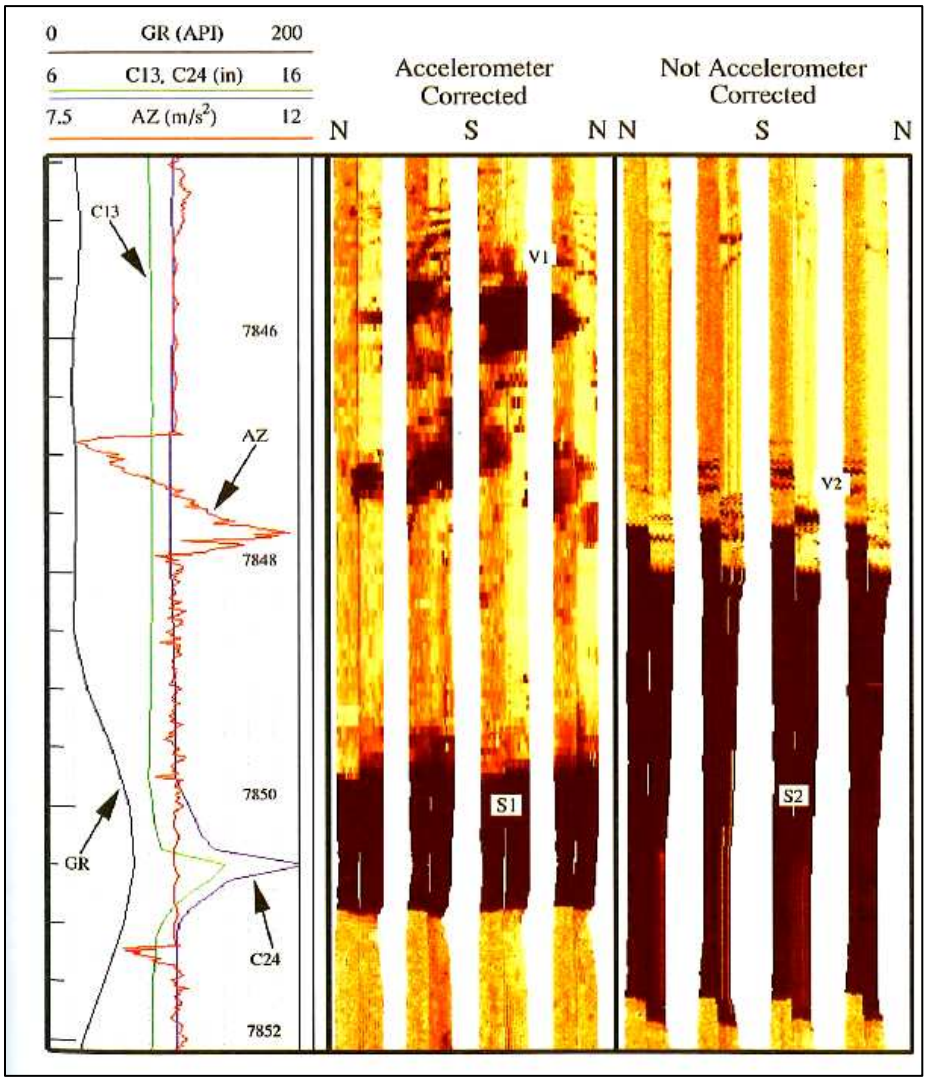

Figure C-7: Image showing a accelerometer corrected FMI log (A) and a not corrected log (B). Notice that the vugs signed with V1 at (A), appear compressed at (B), V2, due to a negative acceleration of the tool in this zone. The shale, S1 and S2, has been stretched due to an acceleration of the tool at its top. Hurdley, 2004; Borehole Images, *in* G. Asquish and D. Krygowski, Basic Well Log Analysis: AAPG Methods in Exploration 16. Newberry (1998)After Schlumberger (1983) and Höcker et al. (1990).

Figure C-8: FMI log showing the influence of the different features on the colourbar. The "P's" represent the pads. Green lines represent foliation and the blue sinusoidal curve is a fracture. Source: GALP E&P archive.

Two types of processed images can be created: static and dynamic (Figure C-10).

Static: images which have had on contrast setting applied to the entire well image. These images are useful to detect relative changes in rock resistivity along the borehole

Dynamic: dynamic images had a variable contrast applied in a moving window, providing enhanced views of features such as vugs, fractures and bed boundaries. They allow the interpreter to detect subtle features in rocks that have very low resistivities, such as shales, and very high resistivities such as carbonates and crystalline rocks.

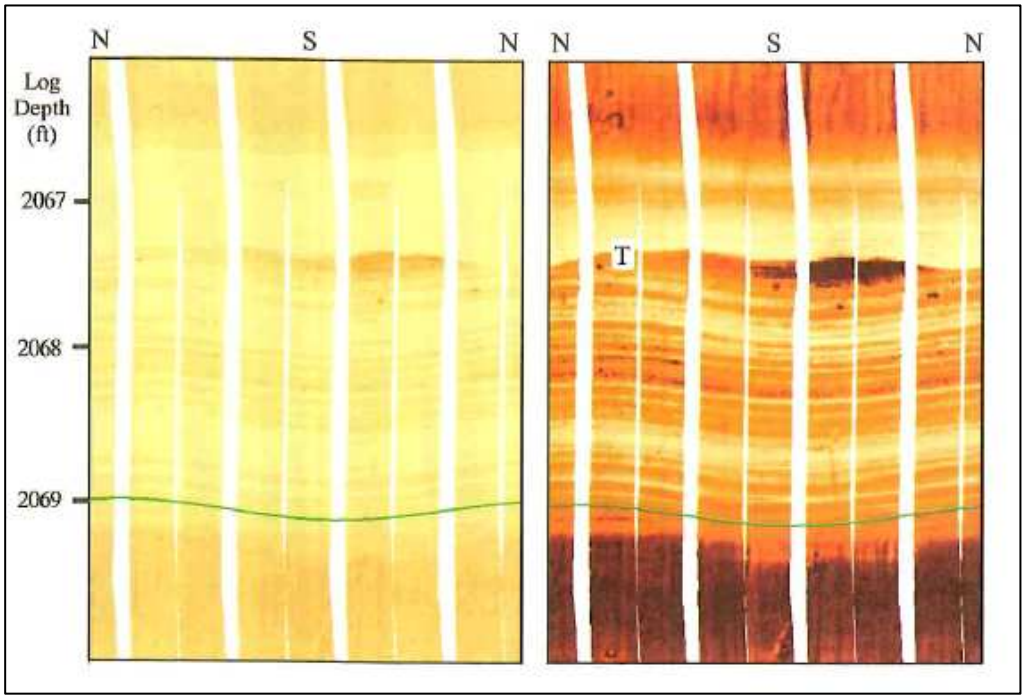

Figure C-9: Comparison between static (left) and dynamic (right) images in a sandstone. Notice that the application of a dynamic colour bar, in which the image contrast is normalized in a 5-ft moving window, sharpens the image and allows sedimentary features easier to see. T is a truncation surface, and the green sine wave is fitted to a bedding plane. Hurdley, 2004; Borehole Images, *in* G. Asquish and D. Krygowski, Basic Well Log Analysis: AAPG Methods in Exploration 16. Newberry (1998) after Schlumberger (1983) and Höcker et al. (1990).

Interpretation

The interpretation of image logs, consists in scrolling through the processed log on a computer, viewing dynamic or static images and fitting sine waves to the geological features that are considered to be of importance – bed boundaries, fractures, foliations etc. Automated dip-picking programs are available, and the interpreter can choose to edit dips already picked by various computer algorithms. The most common use of borehole images is in the area of structural interpretation, especially detecting and orienting fractures and faults. These can be identified through the following features in the image log (Figure C-11):

- Resistivity lineaments in the shape of a sine wave usually cross cutting the formation
- Wellbore breakouts
- Changes in bedding orientation

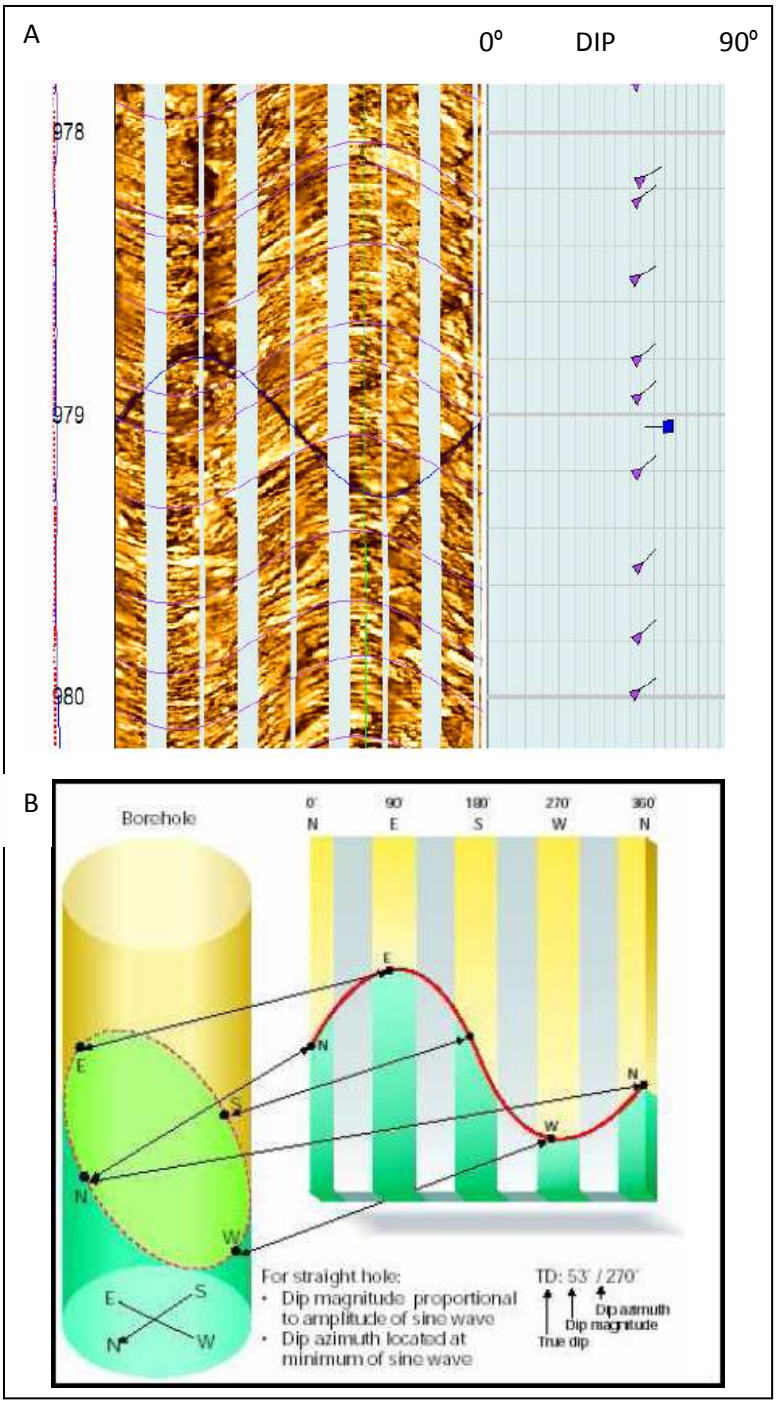

Figure C-10: Interpreted section of an image log (A) and scheme showing how the dip and dip direction of a plane is obtained by an image log interpretation software (B). After the interpreter has identified a planar feature on the log, he draws a sine curve and the software positions the corresponding marker on a scale ranging from 0º to 90º of dip which is relative to the amplitude of the sine. The dip azimuth is located at the minimum of the sine wave and given by the small trace on the marker which points towards the correct direction.

When the wells are drilled with conductive mud (this is one important principle for the image logs to work), we can use this to identify and evaluate open faults and fractures. Hence, an open fracture will appear as a dark trace because is filled with low conductivity fluid (the mud) and a closed fracture will appear as a light trace on the log (Figure C-12). Healed fractures filled with calcite, anhydrite or quartz, will appear as a resistive trace, but if they are filled with clay or shale, then the fracture will show a conductive trace (dark). Using Gamma Ray logs can help solve these situations.

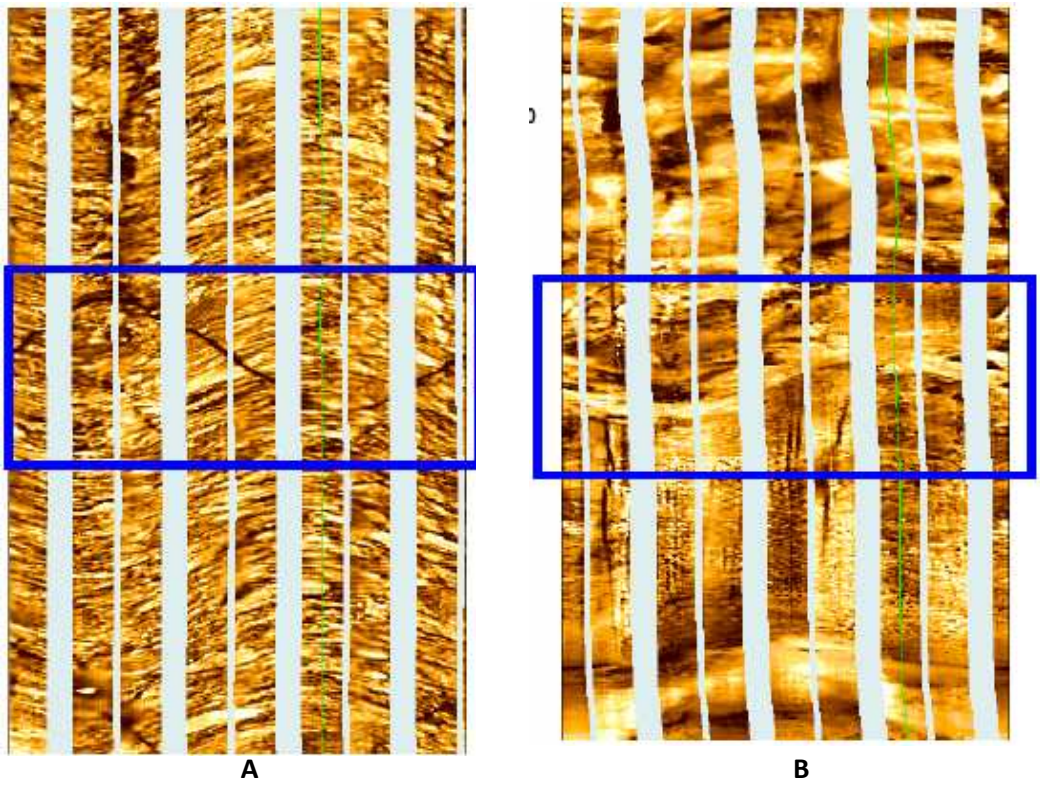

Figure C-11: section of an image log showing open (A) and closed fractures (B). **Source:** GALP E&P Archive.

Natural and induced fractures can also be differentiated (Figure C-14 and C-14):

Natural fractures: are created by the regional stress field and can occur as one or more fracture sets, each with a distinct orientation.

Induced fractures: are generated during drilling by the subsurface stress, are commonly near vertical, have a well defined strike azimuth that is perpendicular to borehole breakouts, or oval elongations of the borehole.

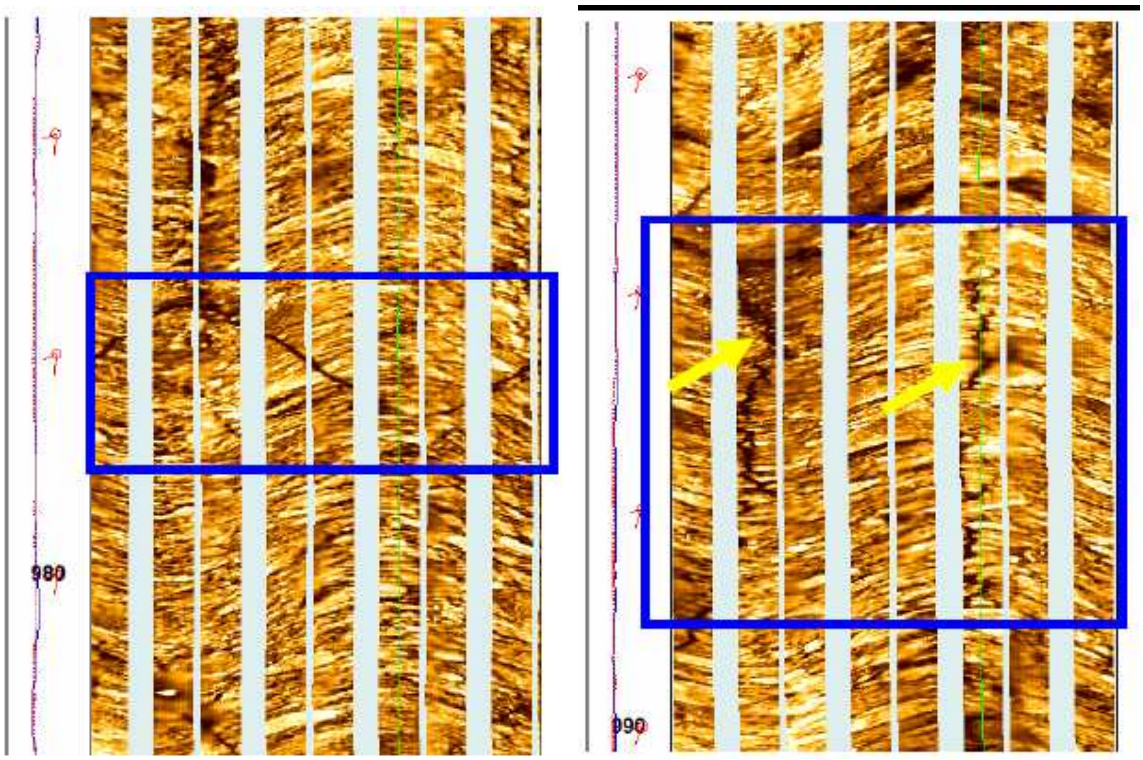

A **B**

Figure C-12: section of an image log showing natural fractures (A) and induced fractures (B).

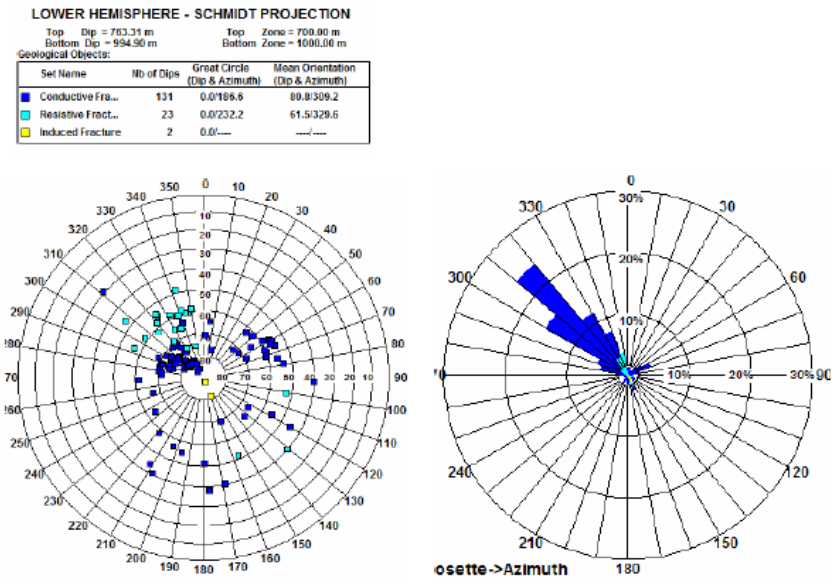

A **B**

Figure C-13: Schimdt projection (A) and Rose Diagram (B) showing natural (blue tadpoles) and induced (yellow tadpoles) fractures.

Image logs can also be used to calculate fractures permeability. In the parallel-plate model for fluid flow in fractures (Brown, 1987), permeability is proportional to the square of fracture-aperture with (Figure C-15). Present-day software already has an algorithm to make this calculation in an easy way.

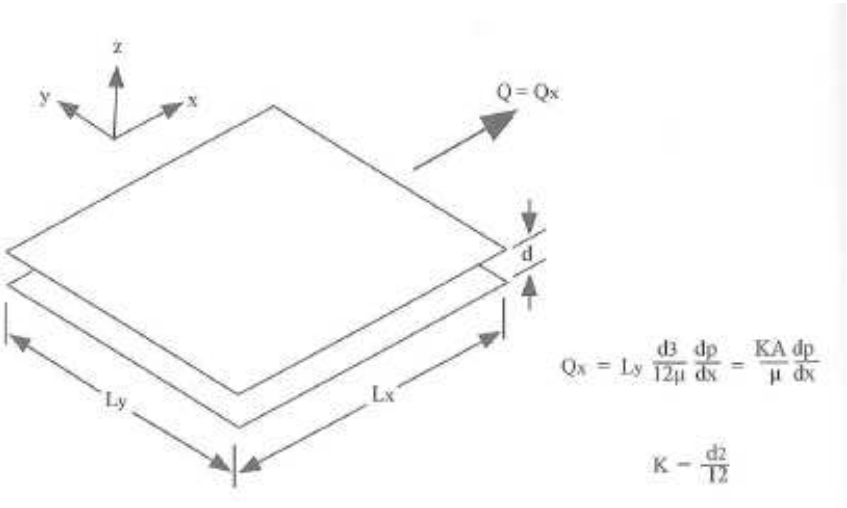

Figure C-14: simple parallel-plate model for fluid flow in a fracture. L= length; d= aperture with; Q= flow rate; p= pressure; μ= viscosity; K= permeability. The Darcy equation for linear flow (Qx), when applied to this geometry, suggests that permeability is proportional to the square of the aperture width (Hurdley, 2004; Borehole Images, *in* G. Asquish and D. Krygowski, Basic Well Log Analysis: AAPG Methods in Exploration 16; modified from Brown (1987)).

Fracture density can also be calculated using two different calculation methods:

Method 1: calculates the density of fractures within a certain unit interval along the wellbore. It is well applied in vertical wells (Figure C-16, red fractures).

Method 2: corrects the density, by counting the number of fractures of an interval along a perpendicular line to the fracture plane. This is possible to account for the wellbore inclination. (Figure C-16, blue fractures).

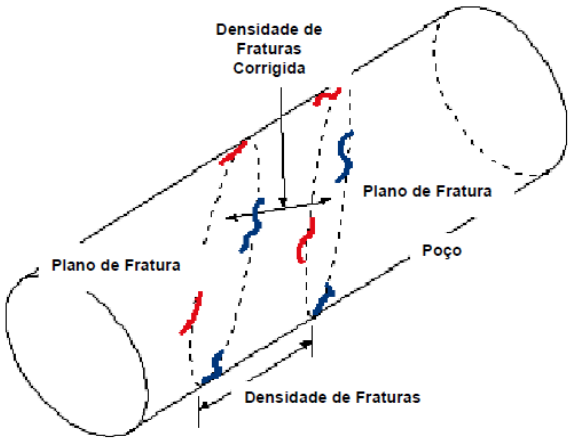

Figure C-15: scheme of a directional wellbore showing the corrected fracture density – blue fractures.

Breakouts can be used for indication of present-day *in situ* stress (Figure C-17). These breakouts when combined with the orientation of inferred natural and induced fracture sets may be related to directional permeability in the surface (Heffer and Lean, 1993). This information is important for optimizing the orientation of horizontal wells and configuring injection patterns is secondary and tertiary recovery schemes.

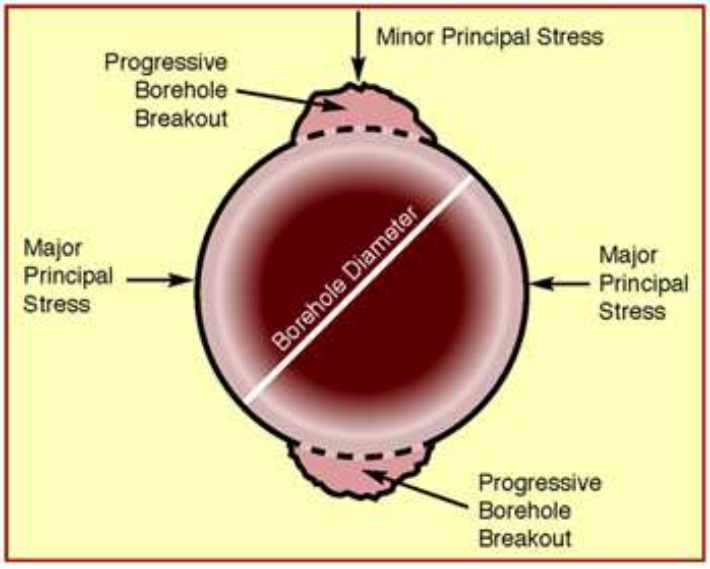

Figure C-16: Borehole breakout. From the direction of the breakout the interpreter can learn on the principal stresses operating in the region.

D. Well Cost Simulation

	Fox	Hotel-D Directional	Hotel-D.U. Directional-UBD
	$	$	$
PLANNING	**27.027,350**	**38.612,164**	**38.612,164**
Well Project	7.027,350	7.027,350	7.027,350
Rig Biding	0,000	4.684,900	4.684,900
Service Biding	0,000	4.392,094	4.392,094
Material Biding	0,000	2.507,820	2.507,820
Headquarters Support	20.000,000	20.000,000	20.000,000
LOCATION	**146.149,410**	**104.138,482**	**104.138,482**
Environmental License	10.043,530	10.043,530	10.043,530
Topographic Studies	2.576,470	2.576,470	2.576,470
Base Construction, Conductor Pipe	133.529,410	91.518,482	91.518,482
RIG	**957.385,730**	**1.302.660,155**	**1.302.660,155**
Moving to Location	0,000	0,000	30.000,000
Renting	542.647,000	687.750,000	687.750,000
Demobilizing-Transport-Mounting	414.738,730	614.910,155	614.910,155
OUTSOURCING	**338.417,550**	**423.082,221**	**423.082,221**
Drilling Fluid	21.255,880	42.910,217	42.910,217
Mudlogging	53.308,850	69.937,941	69.937,941
Solids control equipment	23.265,000	37.535,604	37.535,604
Lab	3.639,710	9.535,604	9.535,604
Specific Drilling Tools	24.624,120	29.534,706	29.534,706
Wireline Logging	85.000,000	91.407,260	91.407,260
Casing Cementing	21.599,660	21.599,660	21.599,660
Bridge Plugs	18.498,660	18.498,660	18.498,660
Accomodations	17.960,970	17.960,970	17.960,970
Transportation	69.264,710	40.661,600	40.661,600
Formation Tests	0,000	43.500,000	43.500,000
MATERIALS	**414.456,130**	**433.687,246**	**494.837,246**
Drilling Bits	35.134,000	35.134,000	35.134,000
Completion Fluids	116.923,610	105.764,360	105.764,360
Coring	0,000	0,000	0,000
Casing and Acessories	156.300,000	156.300,000	156.300,000
Cement	30.377,160	30.377,160	30.377,160
Liner	0,000	0,000	0,000
Well Heds	2.676,470	16.477,540	16.477,540
Diesel	66.003,750	81.200,000	81.200,000
Abandonment Plugs	7.041,130	8.434,186	8.434,186
UBD Elements			20.000,000
UBD Operation Cost			22.400,000
Equipment Rental			3.750,000
Others	0,000	0,000	15.000,000
HUMAN SUPERVISION	**90.615,750**	**123.903,150**	**123.903,150**
Headquarters	35.136,750	35.136,750	35.136,750
Field	55.479,000	88.766,400	88.766,400
LOGISTIC SUPPORT	**81.380,950**	**81.380,940**	**81.380,940**
Land Transportations	1.585,880	1.585,880	1.585,880
Comunications	0,000	0,000	0,000
Storage Facilities	980,390	980,390	980,390
Waste Management	74.893,100	74.893,100	74.893,100
Cuttings and Core Storage	3.921,570	3.921,570	3.921,570
Total	***2.363.747,801***	***2.883.584,012***	***2.953.906,512***

Bibliography

Aguilera, R. (1983). Exploring for Naturally Fractured Reservoirs. *SPWLA 24th Annual Logging Symposium.* SPWLA.

Aguilera, R. (2003). Geologic and Engineering Aspects of Naturally Fractured Reservoirs. *CSEG Recorder, February 2003*, 45-49.

Chagas, L. S. (1996). *Tectono-Sedimentação das Bacias do tipo Rift: Aplicação na porção emersa da Bacia de Sergipe-Alagoas.* Porto Alegre: Universidade Federal do Rio Grande do Sul.

Chan, W. (1995). *AVO in Azimuthal Anisotropic Media, Fracture Detection Using P-Wave Data and a Seismic Study of Narturally Fractured Thight Gas Reservoirs.* Palo Alto, California: Standford University.

Chiossi, N., & Sousa, D. (1996). *Estratigrafia de Sequências e Condicionamento Tectono-Climático num rift Continental: Bacia Sergipe-Alagoas.* Porto Alegre: Universidade Federal do Rio Grande do Sul.

Chopra, S. (2002). Choerence Cube and Beyond. *first break*, pp. 27-33.

Chopra, S. (2009). Interpreting Fractures through 3D Seismic Discontinuity Attributes and their Visualization. *CSEG Recorder*, pp. 5-14.

Chopra, S., & Marfut, K. J. (2007). Seismic Attributes for Fault/Fracture Characterization. *CSPG CSEG Convention.* Calgary, Alberta, Canada: CSPG/CSEG.

Chopra, S., & Marfut, K. J. (2007). Volumetric Curvature Attributes for Fault/Fracture Characterization. *first break, Vol 25, July 2007*, 35-46.

Claerbot, J. (1985). *Imaging the Earth's Interior.* Palo Alto, California: Standford University.

Cordsen, A., & Galbraith, M. (1999). Narrow VS Wide Azimuth Land 3D Seismic Surveys. *Europeean Association of Geoscientists and Engineers*.

D.Waldren, & Corrigan, A. (1995). An Engineering and Geological Review of the Problems Encountered in Simulating Naturally Fractured Reservoirs. *SPE Middle East Oil Technical Conference and Exhibition.* Bahrain: SPE.

Davison, I., & Santos, R. A. (1999). Tectonic Evolution of the Sergipano Fold Belt, NE Brazil, during the Brasiliano Orogeny. *Precambrian Research, 45*, 319-342.

D'el-Rey Silva, L. J. (1995, December). Tectonic Evolution of the Sergipano Belt, NE Brazil. *Revista Brasileira de Geociências*, pp. 315-332.

D'el-Rey Silva, L. J. (1999). Basin infilling in the southern-central part of the Sergipano Belt (NE Brazil) and implications for the evolution of Pan-African/Brasiliano cratons and Neoproterozoic sedimentary cover. *Journal of South American Earth Sciences, 12*, 453-4790.

D'el-Rey Silva, L., & McClay, K. R. (1995, Setember). Stratigraphy of the Southern Part of The Sergipano Belt, NE Brazil: Tectonic Implications. *Revista Brasileira de Geociências*, pp. 185-202.

Ehlig, C., Taha, M., Marin, H., Novoa, E., & Sanchez, O. (2000). Drilling and Completion Strategies in Naturally Fractured Reservoirs. *SPE International Petroleum Conference.* Villahermosa, Mexico: SPE.

Gutmanis, J. (2009). Basement Reservoirs - A Review of their Geological and Production Characteristics. *International Petroleum Technology Conference .* Doha, Qatar: IPTC.

iReservoir. (2009). *Fractured Reservoirs.* Retrieved August 2011, from ireservoir: www.ireservoir.com

Jon Gutmanins; Tony Bachelor - GeoScience Limited. (2010). *Hydrocarbon Production From Fractured Basement Formations - Version 9.* GeoScience Limited.

Lage, A. C., Sotomayor, G. P., Vargas, A. C., Rodrigano, R., Silva, P. R., Lira, H. L., et al. (2003). Planning, Executing and Analyzing the Productive Life of the First of Six Branches Multilateral Well Drilled Underbalanced in Brazil. *IADC/SPE Underbalanced Technology Conference and Exhibition.* Houston, Texas: SPE/IADC.

Legrand, N., Kok, J. d., Neff, P., & Clemens, T. (2010). Recovery Mechanisms and Oil Recovery from a Tight, Fractured Basement Reservoir, Yemen. *SPE Annual Technical Conference and Exhibition.* Florence, Italy: SPE.

Li, B., Guttormsen, J., Hoi, T. V., & Duc., N. V. (2004). Characterizing Permeability for the Fractured Basement Reservoirs. *SPE Asia Pacific Oil and Gas Conference.* Perth, Australia: SPE.

Long, A. S., Eivind, F., Page, C., Pramik, W., & Laurain, R. (2006). Multi-Azimuth and Wide-Azimuth Lessons for Better Seismic Imaging in Complex Settings. *AESC Conference, 2006.* Melbourne, Australia: AESC.

Mezzamo, R. F., Luvizotto, J. M., & Palagi, C. L. (April. 2001). Improved Oil Recovery in Carmópolis Field: R&D and Field Implementations. *SPE/DOE Improved Oil Recovery Symposium* (pp. 4-10). Tulsa, Oklahoma: SPE.

Murray, A., Montgomery, D., & Milne, D. (n.d.). *Structural Analysis of Highly Fractured, Heterogeneous Basement, Say'un-Masila Basin, Yemen.* Aberdeen, UK: Task Geoscience and Dove Energy.

Nawab, R., Maultzsch, S., Yuh, S., & Mouly, B. (2006). Multiazimuth Seismic to Well Tie for Fracture Characterization. *SPE International Oil&Gas Conference and Exibithion .* Beijing, China: SPE.

Nelson, R. (2001). *Geologic Analysis of Naturally Fractured Reservoirs.* Houston, Texas: Gulf Professional Publishing.

Ngoc, N. H., Quan, N. Q., Dong, N. H., & Nhi, N. D. (2011). Role of 3D Seismic Data in Prediction of High Potential Areas within Pre-Tertiary Fractured Granite Basement Reservoir in Cuu Long Basin, Vietnam Offshore. *Search and Discovery*.

OMV. (2010, August 17). Challenges in Exploring and Developing Basement Reservoirs in Sab'atayn Basin, Habban Field Case Study.

Petford, N., & McCaffrey, K. (2003). *Hydrocarbons in Crystalline Rocks.* London: Geological Society.

Rancan, C. (2009, November 2008 - May 2009). O soerguimento do domínio Macururé e a sua influência na sedimentação turbidítica no Cretáceo Superior da Sub-bacia de Sergipe, Bacia de Sergipe-Alagoas. *Boletim de Geociências - Petrobrás*, pp. 45-67.

Shirui., W., Yun, L., & Xiangyu, G. (2003). Application of Wide Azimutg Land 3D - a case history. *SEG.* Dallas: SEG.

Sircar, A. (2004). Hydrocarbon Production from Fractured Basement Formations. *Current Science, Vol. 87, nº2, July 2004*, 147-151.

Sliz, K. (2011). Fracture Imaging Using Azimuthal Prestack Depth Migration. *SPE/DGS Saudi Arabia Technical Symposium and Exhibition.* Al-Khobar, Saudi Arabia: SPE.

Souza-Lima, W. (2006, May). Evolução Tectono-Sedimentar da Bacia de Sergipe-Alagoas. *Fundação Paleontológica Phoenix*.

Souza-Lima, W. (2006, June). Litoestratigrafia e evolução Tectono-Sedimentar da Bacia de Sergipe Alagoas- o Embasamento. *Fundação Paleontológica Phoenix*.

Sugiri, O. I. (2010). *Fractured Basement Delineation Using Seismic Mult-Attributes; The MLB Field, Jambi, Indonesia.* Perth - Australia: CUT - Curtin University of Technology.

Tan, M. T., & Tap, N. Q. (2001). The Possibility of Applying Geophysical Methods to Study Fractured Basement Reservoir in the Continental Shelf of Vietnam. *Offshore Technology Conference.* Houston, Texas: OTC.

Tandom, P., N.H.Ngoc, H.D.Tjia, & Lloyd, P. (1999). Identifying and Evaluating Producing Horizons in Fractured Basement. *SPE Asia Pacific Improved Oil Recovery Conference.* Kuala Lumpur, Malaysia: SPE.

Thomas Harting, J. G. (2003). Drilling Near Balance and Completing Open Hole to Minimize Formation Damage in a Sour Gas Reservoir. *IADC/SPE Underbalanced Technology Conference and Exhibition.* Houston, Texas: IADC/SPE.

Trilobite Testing, Inc. (n.d.). *Field Guide to Drill Stem Testing and Chart Interpretation.* Houston, Texas: Trilobite Testing, Inc.

Tsvankin, I. (1997). Reflection Moveout and Parameter estimation for horizontal transverse isotropy. *Geophysics, Vol.62*, 614-629.

Unknown. (n.d.). Introduction to Underbalanced Drilling, Chapter 12. In *Unknown.* Leading Edge.

UNL, UALG, UA, & IST. (2011). *Modelling and Characterization of Fractured Reservoirs -GALP E&P Internal Report.* Lisbon.

Urreiztieta, M. d., Troussaut, X., Baradi, A., Nagaraj, G., Tresse, P., Meunier, J.-P., et al. (2007). Formation Testing Strategy Based on a Quick-Look Data Evaluation from a Fractured Basement Reservoir: A case study from Kharir Field, Yemen. *International Petroleum Conference* . Dubai, U.A.E: IPTC.

W.U.Mohriak, Bassetto, M., Mello, M., & E.A.M.Koutsoukos. (2000). Crustal Architecture, Sedimentation and Petroleum Systems in the Sergipe-Alagoas Basin, Northeast Brazil. *AAPG Memoir; Petroleum Systems of the South Atlantic Margins*, pp. 273-300.

Western Geco. (n.d.). *Multicomponent Wide-Azimuth Seismic Data for Defining Fractured Reservoirs.* Retrieved July 2011, from Schlumberger: www.slb.com